Human organoids: a model system for intestinal diseases

Humane organoids: een *in vitro* model voor darmziekten.
(met een samenvatting in het Nederlands)

Proefschrift

ter verkrijging van de graad van doctor aan de
Universiteit Utrecht op gezag van de rector
magnificus, prof.dr. G.J. van der Zwaan, ingevolge
het besluit van het college voor promoties in het
openbaar te verdedigen op donderdag 18 juni
2015 des middags te 2.30 uur.

door

Caroline Louise Wiegerinck

geboren op 28 augustus 1984
te Utrecht

Promotor: Prof.dr. E.E.S. Nieuwenhuis

Copromotor: Dr. S. Middendorp

"'Life,' said Emerson, 'consists in what a man is thinking all day.' If that be so, then my life is nothing but a big intestine. I not only think about food all day, but I dream about it at night."

- Henry Miller

HUMAN ORGANOIDS: A MODEL SYSTEM
FOR INTESTINAL DISEASES.

TABLE OF CONTENTS

CONTENTS

CONTENTS

THE LUXURY OF EATING

"Dis-moi ce que tu manges, je te dirai ce que tu es."[1]. "Der Mensch ist, was er ißt."[2]. Or modernly translated as: " You are what you eat."[3]. These phrases indicate that what you eat could influence your state of mind or physical health. The last decades the choice of food has become more abundant and increasingly important as is depicted in food trends. Not only are we able to choose between a variety of world-cuisines and exotic ingredients, but the media also feeds us with hypes such as organic food, superfoods containing antioxidants, pro-biotics and carbohydrate-free diets. Which makes it even more difficult to decide what to eat.

Sometimes, however, the question is not what we would like to eat, but rather what we can eat. Some people do not have this choice due to economical-, social status; place of birth or literally due to a physical inability to take up and digest certain foods (malabsorption), which is the case in many intestinal diseases (enteropathies).

INTRODUCTION TO INTESTINAL DISEASES

This inability to take up food, necessary to feed all the cells in the body, can range from total dysfunction in rare intestinal diseases or be confined to only one type of food, such as wheat, barley and rye in celiac disease. Also, the extent to which malabsorption occurs within one disease can differ per patient. For example, some patients have a mutation (defect in the DNA) that leads to complete abrogation of a protein and therefore loss of function, resulting in severe malabsorption. While other patients, who carry a different mutation in the same gene, might maintain a part of the protein with residual function and, thus, are able to partially take up nutrients. Occasionally, it is possible to treat these patients with supporting medication that conserves or improves the protein function, which is sometimes the case in cystic fibrosis. These diseases will be explained shortly in the next paragraphs.

Microvillus inclusion disease

An extreme example of an intestinal disease is microvillus inclusion disease (MVID), a rare enteropathy that usually presents itself in a newborn baby (congenital) with severe, watery diarrhea [4, 5]. Their intestine is unable to absorb nutrients. The only therapeutic option is feeding, often life-long, through the blood veins (parenteral feeding) with severe complications as a consequence. Common complications that arise from parental nutrition are liver failure, increased risk of infection, blood clots and, ultimately, the inability to find an accessible vein to feed over. If the latter occurs, small bowel transplantation is the only therapeutic option left.

Cystic fibrosis

Another congenital disease that could be associated with diarrhea due to malabsorption is cystic fibrosis. This congenital disease is

more known for its lung problems, where mucus, a substance that is usually watery and protects organs from bacteria, is thickened and therefore causes difficulty breathing by blocking of airways and increases risk of infections [6]. In other organs, such as the pancreas and intestine, similar pathology can be seen. The pancreas provides the intestine with enzymes that help to break down fat and other food particles. In cystic fibrosis the thick mucus induces pancreas insufficiency. The lack of pancreatic enzymes can result in fat malabsorption and therefore cause diarrhea. Frequently, persistent intestinal malabsorption, despite pancreas enzyme supplementation, exists due to other intestinal problems caused by cystic fibrosis [7, 8].

Celiac disease

In celiac disease, the inability to digest is related to intake of specific food proteins. A genetically predisposed group of patients are not capable of eating food containing wheat, barley or rye (or more specifically gluten, one of the components in these grains) without occurrence of intestinal damage, often accompanied with failure to grow, abdominal pain and/or diarrhea [9]. Currently, the only treatment for these patients is a gluten-free diet. This might sound feasible; nonetheless it has a big impact on simple daily life choices as what to eat.

All these intestinal diseases and others emphasize that to be able to eat what you choose is a luxury. This thesis will address these 3 diseases in which nutrient uptake and/or digestion are often impaired and in which a patient-specific model to study these diseases in more depth is desirable. Yet, before we get into the specifics of these diseases we first need to better understand how the healthy intestine works.

THE INTESTINE

Anatomy of the intestine

The intestine is one of the largest organs in the human body with a surface area of approximately 32 m2 caused by protrusions and invaginations, called the villi and crypts, respectively [10]. While the small intestine accommodates both villi and crypts, the large intestine is composed of only crypts. The large surface area is important for optimal uptake and digestion of nutrients and protection against pathogens. The functions of the small intestine are mainly digestion and uptake of food and consist of three segments from proximal to distal: the duodenum, the jejunum and the ileum. Posterior, the large intestine (colon) is responsible for further processing of undigested food and formation of thickened stool. The large intestine comprises the caecum, the colon -ascendens, -transversum, -descendens, the sigmoid and rectum.

To execute these different functions properly, the intestinal tract consists of four layers from the outside to the inside: the adventitia/

serosa, the muscularis externa, the submucosa and the mucosa. The most outer layer of the intestine is named the adventitia or serosa, depending on the location out/inside the peritoneum (lining of abdominal cavity) and protects the intestine from other organs. The muscularis externa comprises two muscle layers that together with the enteric nervous system control peristaltic movement of the gut and thus movement of food particles/stool. The submucosa is a connective tissue layer, which contains blood vessels, lymphatics and nerves, necessary to give oxygen to the cells and connect the intestine to the rest of the body. The mucosa consists of three different layers: a small smooth muscle layer; a lamina propria with connective tissue, blood vessels and immune cells; and the epithelium, a single cell layer on the luminal side of the gut (Figure 1) [11, 12].

The luminal epithelial cell layer performs the major functions of the intestine: food digestion, uptake of nutrients and maintaining a barrier against external pathogens such as bacteria, viruses and fungi. To absorb as many nutrients as possible, the enterocytes on the villi of the intestine have microvilli, small tiny hair-like protrusions on the apical side of the cell, also called the brush-border.

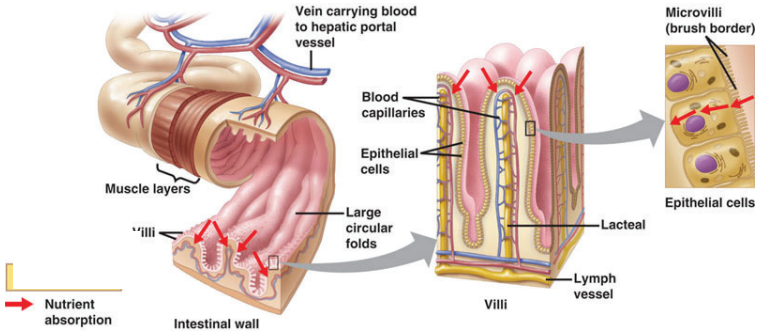

Figure 1. Overview of intestinal layers, structure and microvilli (adapted from kvhs.nbed.nb.ca/gallant/biology/small_intestine.jpg).

Intestinal cell types

The major functions of the intestine are mediated by seven differentiated cell types within the epithelial layer: enterocytes, goblet cells, enteroendocrine cells, Paneth cells, microfold (M or membranous) cells at Peyer's patches, tuft cells, and cup cells. The exact role of these last two cell types is still unresolved [13].

Enterocytes are the most common cell type in the villi of the small

intestine, and are capable of digestion and absorption of nutrients. Moreover, they have an important barrier function against pathogens and have the ability to act as antigen presenting cells [14].

The mucus producing goblet cells help to protect the intestine from infections. They are more abundant towards the colon where they also function as lubricant for the stool.

Enteroendocrine cells are scarce and these hormone-secreting cells and have many subtypes, dependent on the hormone they secrete [15]. These cells regulate mainly postprandial (after eating) secretion of gut peptides and motility [16]. M cells are secluded to Peyer's patches (the lymph nodes of the intestine) and are involved in antigen processing and interact directly with lymphocytes [17]. Lastly, Paneth cells have anti-microbial properties and reside in the bottom of small intestinal crypts, alongside intestinal stem cells [18, 19]. Located higher up in the crypt are the transit-amplifying cells that multiply former stem cells and are destined to differentiate into either the secretory or the absorptive lineage (see Figure 2: adapted from [20]).

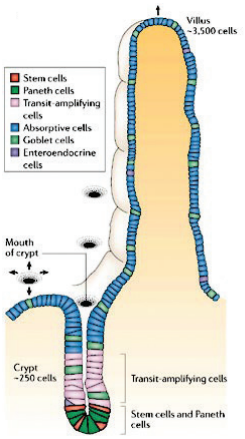

Figure 2. Epithelial cell lineages in the small intestine (adapted from [20]).

Intestinal stem cell

The properties of a true stem cell is that it can multiply itself for a long period of time and all differentiated lineages arise from these stem cells [12]. An embryonic stem cell is capable to differentiate into any cell type in the body such as a kidney, lung or brain cell. An adult stem cell on the other hand is restricted to one organ only. For example, an adult intestinal stem cell can only become one of the seven differentiated intestinal cell types, and ensures renewal of most intestinal cells every 3 to 5 days. The Clevers group provided functional evidence for an active stem cell, residing in the bottom of

the crypts, by lineage tracing of Lgr5+ columnar base crypt cells (CBC) and in *in vitro* cultures that originated from one single stem cell [21, 22]. Lineage tracing with other CBC markers, such as low-expressing Sox9-EGFP cells, support the role of these active cycling stem cells [23]. A 'sleeping' or quiescent stem cell population at the +4 position from the crypt has been mentioned in the literature as well. Proposed markers for these cells are Bmi1, Lrig1, mTert and Hopx [24-28]. Although, until now, a unique marker for these putative +4 stem cells have not been shown and some of these proposed +4 markers are also seen in the active stem cell population [29, 30]. In addition, there is increasing support that these +4 cells are only active in tissue regeneration and not in intestinal homeostasis [31, 32]. The exact nature of these +4 cells is still unclear, hence the intestinal stem cells that are referred to in this thesis will be the columnar crypt base active cycling stem cells that, among other markers, are identified by expression of Lgr5.

Crypt-villus regulation

To ensure constant renewal and maintain all the different intestinal functions two processes are tightly regulated in the intestinal epithelium: proliferation and differentiation. Proliferation ensures the growth or production of cells by multiplication of intestinal cells, this occurs mainly in the crypt. While on the other hand, differentiation drives the cells towards a specific cell type with a specialized function. For example, the main function of an absorptive enterocyte is to absorb and digest food. A controlled environment is necessary to direct cell fate into either a proliferation or differentiation state, this is regulated by multiple pathways such as bone morphogenetic protein (BMP), hedgehog and EphrinB (EPHB) pathways [33-37]. Two other important regulating pathways are Wnt and Notch signaling. Wnt signalling is active in the crypt (and absent in villi) and promotes proliferation and maintenance of stem- and Paneth cells [38-40]. Paneth cells and mesenchymal cells are known to produce Wnt. Notch signalling is also involved in stem cell maintenance and in deciding the differentiation fate of transit-amplifying cells towards absorptive lineage (Notch on) or secretory lineage (Notch off) [41, 42]. The absence of Wnt, on the other hand, promotes differentiation of cells (excluding Paneth cells), this mainly occurs in the villi of the intestine. An overview of the interaction between Wnt and Notch pathways in intestinal differentiation is given in Figure 3 (adapted from [41]).

Cell polarity

Another form of regulation exists within the epithelial cell itself: cell polarity. Polarity means having two opposite poles, in epithelial cells this translates to an apical and basolateral side, on the luminal or mesenchymal side of the cell, respectively. Intestinal cell polarity is an essential property to ensure normal function. For example, nutrient uptake, regulation of water balance and bile acid secretion all are dependent on correct polarization. Transmembrane proteins,

such as the enzyme sucrose-isomaltase, are specifically located on the apical side to digest sucrose proteins. The major components that maintain cell polarity are the extracellular matrix (such as the collagens in the lamina propria), and tight junctions proteins that connect epithelial cells on the basolateral side ([43] and Figure 4, adapted from [44]).

INTESTINAL FUNCTION IN DISEASE

In a healthy person the intestine is tightly regulated, nonetheless, in several intestinal diseases dysregulation of the epithelium can occur.

Microvillus inclusion disease

One can imagine that if one of the transporter proteins does not function properly, uptake or digestion of food could be distorted. This is the case for a severe, but rare, congenital enteropathy such as Microvillus inclusion disease (MVID) [4, 45]. As the name implicates, the microvilli are not formed properly and can accumulate in vesicles inside the enterocyte. Hence, the transporter proteins, which are normally expressed on the microvilli of the apical membrane, are dislocated intracellularly and are therefore not able to take up nutrients [46, 47]. The lack of nutrient uptake is visible in patients by watery diarrhea and dependency on intravenous feeding [5]. The disease is caused by microvillus atrophy as well as mislocalisation of the transporter proteins. In a healthy cell, newly synthesized transporter proteins are shipped in vesicles from the Golgi system to the

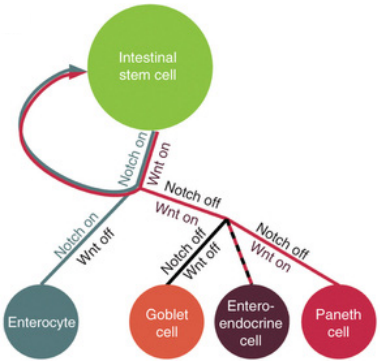

Figure 3. Notch and Wnt regulation in small intestinal cells (adapted from [41]).

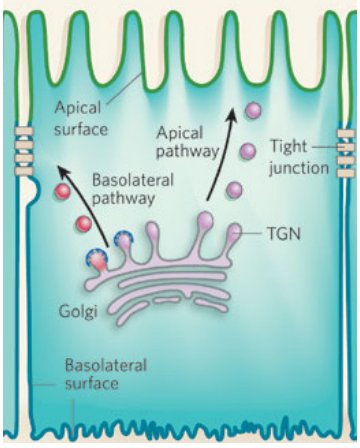

Figure 4. Polarized epithelial cell with an apical and basolateral surface. Figure adapted from [44].

apical membrane by moving over microtubules. Subsequently, vesicles reach the apical membrane, dock and fuse to the membrane and place or secrete the transporter protein onto or out of the membrane [43]. Microvillus inclusion disease is the result of aberrant transport of these apical, and recently discovered, basolateral proteins to the membrane [48, 49]. Microvillus inclusion disease is caused in 90% of the patients by mutations in the *MYO5B* gene, encoding for the myosin 5b protein [50, 51]. MYO5B is an accessory motor protein that connects these vesicles to actin. If MYO5B does not function, newly synthesized proteins are not transported properly to their desired apical location of the cell, which is then unable to absorb nutrients.

We aim to identify other genes that could cause the MVID phenotype. In addition, by understanding these diseases better, we hope to diagnose and treat patients more specifically. Currently, there is no good model that recapitulates this disease and therefore it is difficult to study the pathogenesis in more detail other than by biopsies or, more recently, siRNA CACO2 cell-lines [48, 49]. Although, CACO2 cell lines help to unravel the pathophysiology of MVID, they are not entirely representative for the *in vivo* epithelium.

Cystic fibrosis

Another disease that causes congenital diarrhea is cystic fibrosis. Cystic fibrosis is caused by a missing or misfolded transporter protein; the cystic fibrosis transmembrane regulator (CFTR), on the apical membrane of epithelial cells [6, 52]. This transporter is responsible for secreting chloride into the lumen, the negatively charged chloride attracts the positively charged sodium, and therefore water. The main manifestation in patients with cystic fibrosis is a thick mucus layer on the epithelial cells because of diminished water secretion. This thick mucus clogs the cells/ducts and therefore prevents normal functioning of many organs. Different mutations in the *CFTR* gene result in different severity of the disease and response to drugs in patients [53, 54]. However, since even patients with the same mutation respond differently to a certain drug, it is difficult to predict which drug will work for which patient [55]. A tool to advance this knowledge is if CFTR function and patient-specific drug response could be assessed in an *in vitro* model.

Celiac disease

Malabsorption may also be confined to one compound. This is the case in celiac disease, where gluten induces a specific T-cell mediated response after being presented by antigen presenting cells. This occurs only in genetically predisposed individuals with HLA-DQ2.2, 2.5 or 8 [56, 57]. Although 30% of the population has one of these HLA types, the prevalence of this disease is estimated to be 1% in Europe [58]. The role of lymphocytes in celiac disease has been extensively studied and is thought to play a big role in developing the disease [59-61]. Yet, there is more necessary to cause the disease. The literature debates the role of the epithelium in celiac

disease. Some claim that gliadin has a direct effect on epithelial cells or cell lines and is differently transported in intestinal biopsies of celiac patients [62-67]. As most studies are either executed on cell lines or whole biopsy material, it is still unclear if the epithelium is involved in celiac disease.

INTESTINAL STUDY MODEL

Many intestinal diseases have been studied in more detail in animal models, cancerous cell lines or intestinal biopsy material. Although it helped to understand a range of diseases better, the major drawbacks are that animal models and cell lines differ from the patients intestine, while patient biopsy material is often limited and has a short life-span once it is taken from the intestine. Therefore a patient-specific *in vitro* model is desirable for improved understanding, diagnostics and therapy.

Intestinal organoids

Soon after identification of the Lgr5+ stem cell, an *in vitro* model to culture these stem cells was set up for mouse and human intestinal tissue [22, 68]. To establish human intestinal organoids, crypts (which contain the stem cell) were isolated from intestinal resection material or biopsies. These crypts were embedded in matrigel (which contain collagen and laminin that are also present in the submucosa) and cultured in expansion medium (EM) containing: WNT3A, Rspondin-1 (a WNT-activating protein and ligand for Lgr5), Noggin (a BMP inhibitor), epidermal growth factor (EGF, induces intestinal cell proliferation), A83 (a TGF-beta receptor type 1 inhibitor), n-acetylcysteine, b27, nicotinamide and SB202190 (a selective inhibitor of p38 mitogen-activated protein kinase). As this medium promotes the intestinal crypt or proliferative compartment, WNT3A, nicotinamide and SB202190 were excluded to induce intestinal differentiation [68]. Since organoids represent all cell types of the intestine and are maintained by endogenous stem cell proliferation, they could serve as an appropriate model to study previously mentioned diseases.

Healthy intestine

Nonetheless, it is just as important to truly understand the healthy intestinal epithelium. How could we compare diseased tissue with healthy controls if we do not know what is normal? As the organoid model was quite recently developed at the start of this study, we aimed to understand proliferation and differentiation per specific segment of the intestine. Already from the clinic it is known that bile acids are mainly reabsorbed in the ileum, while iron is especially taken up in the first part of the intestine, the duodenum. Beuling ea. showed previously that GATA4 controls the duodenal, and HNF1-alfa the ileal segment of the intestine [69]. However, it remains elusive if this segmental specificity is maintained in the stem cell or controlled by external factors. To better understand the different segments in

the gut, both mouse and human organoids of the different small intestinal parts were studied for morphology, mRNA and protein levels.

The core of this thesis is to use organoids as a tool to better understand intestinal diseases.

THESIS OUTLINE

Chapter 2 of this thesis focuses on the healthy intestine, the intestinal stem cell and location-specific properties. In chapter 3, we report our discovery of a new gene mutation for MVID, syntaxin 3. In chapter 4 we elaborate on these STX3 patients and the function/dysfunction of their intestine. In chapter 5, we study cystic fibrosis and use organoids as a model to set up a forskolin-swelling assay that can help to predict patient-specific response on drugs. In chapter 6, we use organoids to discuss the role of the epithelium in celiac disease. At the end of this thesis we will evaluate if organoids, used as intestinal model in all chapters, truly recapitulates the *in vivo* epithelium and discuss possible applications and recommendations for this model.

1. Brillat-Savarin, J.A., Physiologie du goût; ou, méditation de gastronomie transcendante. 1825, Paris.
2. Feuerbach, L.A., Die Naturwißensschaft und die Revolution. 1850.
3. Lindlahr, V.H., You are what you eat. 1940, New York: National Nutrition Society.
4. Cutz, E., et al., Microvillus inclusion disease: an inherited defect of brush-border assembly and differentiation. N Engl J Med, 1989. 320(10): p. 646-51.
5. Ruemmele, F.M., J. Schmitz, and O. Goulet, Microvillous inclusion disease (microvillous atrophy). Orphanet J Rare Dis, 2006. 1: p. 22.
6. Ratjen, F. and G. Doring, Cystic fibrosis. Lancet, 2003. 361(9358): p. 681-9.
7. Bouquet, J., M. Sinaasappel, and H.J. Neijens, Malabsorption in cystic fibrosis: mechanisms and treatment. J Pediatr Gastroenterol Nutr, 1988. 7 Suppl 1: p. S30-5.
8. Wouthuyzen-Bakker, M., F.A. Bodewes, and H.J. Verkade, Persistent fat malabsorption in cystic fibrosis; lessons from patients and mice. J Cyst Fibros, 2011. 10(3): p. 150-8.
9. Mubarak, A., R.H. Houwen, and V.M. Wolters, Celiac disease: an overview from pathophysiology to treatment. Minerva Pediatr, 2012. 64(3): p. 271-87.
10. Helander, H.F. and L. Fandriks, Surface area of the digestive tract - revisited. Scand J Gastroenterol, 2014. 49(6): p. 681-9.
11. Gartner, L.P.H., J.L., Color atlas and text of histology. 2014. 6th edition: p. 353-354.
12. Barker, N., M. van de Wetering, and H. Clevers, The intestinal stem cell. Genes Dev, 2008. 22(14): p. 1856-64.
13. Gerbe, F., C. Legraverend, and P. Jay, The intestinal epithelium tuft cells: specification and function. Cell Mol Life Sci, 2012. 69(17): p. 2907-17.
14. Snoeck, V., B. Goddeeris, and E. Cox, The role of enterocytes in the intestinal barrier function and antigen uptake. Microbes Infect, 2005. 7(7-8): p. 997-1004.
15. Harrison, E., S. Lal, and J.T. McLaughlin, Enteroendocrine cells in gastrointestinal pathophysiology. Curr Opin Pharmacol, 2013. 13(6): p. 941-5.
16. Wu, T., et al., Gut motility and enteroendocrine secretion. Curr Opin Pharmacol, 2013. 13(6): p. 928-34.
17. Mabbott, N.A., et al., Microfold (M) cells: important immunosurveillance posts in the intestinal epithelium. Mucosal Immunol, 2013. 6(4): p. 666-77.
18. Clevers, H.C. and C.L. Bevins, Paneth cells: maestros of the small intestinal crypts. Annu Rev Physiol, 2013. 75: p. 289-311.
19. Sato, T., et al., Paneth cells constitute the niche for Lgr5 stem cells in intestinal crypts. Nature, 2011. 469(7330): p. 415-8.
20. Crosnier, C., D. Stamataki, and J. Lewis, Organizing cell renewal in the intestine: stem cells, signals and combinatorial control. Nat Rev Genet, 2006. 7(5): p. 349-59.
21. Barker, N., et al., Identification of stem cells in small intestine and colon by marker gene Lgr5. Nature, 2007. 449(7165): p. 1003-7.
22. Sato, T., et al., Single Lgr5 stem cells build crypt-villus structures in vitro without a mesenchymal niche. Nature, 2009. 459(7244): p. 262-5.
23. Van Landeghem, L., et al., Activation of two distinct Sox9-EGFP-expressing intestinal stem cell populations during crypt regeneration after irradiation. Am J Physiol Gastrointest Liver Physiol, 2012. 302(10): p. G1111-32.
24. Sangiorgi, E. and M.R. Capecchi, Bmi1 is expressed in vivo in intestinal stem cells. Nat Genet, 2008. 40(7): p. 915-20.
25. Tian, H., et al., A reserve stem cell population in small intestine renders Lgr5-positive cells dispensable. Nature, 2011. 478(7368): p. 255-9.
26. Powell, A.E., et al., The pan-ErbB negative regulator Lrig1 is an intestinal stem cell marker that functions as a tumor suppressor. Cell, 2012. 149(1): p. 146-58.
27. Montgomery, R.K., et al., Mouse telomerase reverse transcriptase (mTert) expression marks slowly cycling intestinal stem cells. Proc Natl Acad Sci U S A, 2011. 108(1): p. 179-84.
28. Takeda, N., et al., Interconversion between intestinal stem cell populations in distinct niches. Science, 2011. 334(6061): p. 1420-4.
29. Carulli, A.J., L.C. Samuelson, and S. Schnell, Unraveling intestinal stem cell behavior with models of crypt dynamics. Integr Biol (Camb), 2014. 6(3): p. 243-57.
30. Munoz, J., et al., The Lgr5 intestinal stem cell signature: robust expression of proposed quiescent '+4' cell markers. Embo j, 2012. 31(14): p. 3079-91.
31. Roth, S., et al., Paneth cells in intestinal homeostasis and tissue injury. PLoS One, 2012. 7(6): p. e38965.
32. Buczacki, S.J., et al., Intestinal label-retaining cells are secretory precursors expressing Lgr5. Nature, 2013. 495(7439): p. 65-9.
33. Haramis, A.P., et al., De novo crypt formation and juvenile polyposis on BMP inhibition in mouse intestine. Science, 2004. 303(5664): p. 1684-6.
34. He, X.C., et al., BMP signaling inhibits intestinal stem cell self-renewal through suppression of Wnt-beta-catenin signaling. Nat Genet, 2004. 36(10): p. 1117-21.
35. Madison, B.B., et al., Epithelial hedgehog signals pattern the intestinal crypt-villus axis. Development, 2005. 132(2): p. 279-89.
36. van de Wetering, M., et al., The beta-catenin/TCF-4 complex imposes a crypt progenitor phenotype on colorectal cancer cells. Cell, 2002. 111(2): p. 241-50.
37. Batlle, E., et al., Beta-catenin and TCF mediate cell positioning in the intestinal epithelium by controlling the expression of EphB/ephrinB. Cell, 2002. 111(2): p. 251-63.
38. van der Flier, L.G. and H. Clevers, Stem cells, self-renewal, and differentiation in the intestinal epithelium. Annu Rev Physiol, 2009. 71: p. 241-60.
39. Pinto, D., et al., Canonical Wnt signals are essential for

homeostasis of the intestinal epithelium. Genes Dev, 2003. 17(14): p. 1709-13.
40. Farin, H.F., J.H. Van Es, and H. Clevers, Redundant sources of Wnt regulate intestinal stem cells and promote formation of Paneth cells. Gastroenterology, 2012. 143(6): p. 1518-1529 e7.
41. Yin, X., et al., Niche-independent high-purity cultures of Lgr5+ intestinal stem cells and their progeny. Nat Methods, 2014. 11(1): p. 106-12.
42. VanDussen, K.L., et al., Notch signaling modulates proliferation and differentiation of intestinal crypt base columnar stem cells. Development, 2012. 139(3): p. 488-97.
43. Rodriguez-Boulan, E. and I.G. Macara, Organization and execution of the epithelial polarity programme. Nat Rev Mol Cell Biol, 2014. 15(4): p. 225-42.
44. Roth, M.G., Cell biology: porter and sorter. Nature, 2008. 452(7188): p. 706-7.
45. Phillips, A.D., et al., Congenital microvillous atrophy: specific diagnostic features. Arch Dis Child, 1985. 60(2): p. 135-40.
46. Reinshagen, K., et al., Pathophysiology in Microvillus inclusion disease. Z Gastroenterol, 2006. 44(8): p. 667-71.
47. Sherman, P.M., D.J. Mitchell, and E. Cutz, Neonatal enteropathies: defining the causes of protracted diarrhea of infancy. J Pediatr Gastroenterol Nutr, 2004. 38(1): p. 16-26.
48. Thoeni, C.E., et al., Microvillus inclusion disease: loss of Myosin vb disrupts intracellular traffic and cell polarity. Traffic, 2014. 15(1): p. 22-42.
49. Knowles, B.C., et al., Myosin Vb uncoupling from RAB8A and RAB11A elicits microvillus inclusion disease. J Clin Invest, 2014. 124(7): p. 2947-62.
50. Ruemmele, F.M., et al., Loss-of-function of MYO5B is the main cause of microvillus inclusion disease: 15 novel mutations and a CaCo-2 RNAi cell model. Hum Mutat, 2010. 31(5): p. 544-51.
51. Muller, T., et al., MYO5B mutations cause microvillus inclusion disease and disrupt epithelial cell polarity. Nat Genet, 2008. 40(10): p. 1163-5.
52. Rowe, S.M., S. Miller, and E.J. Sorscher, Cystic fibrosis. N Engl J Med, 2005. 352(19): p. 1992-2001.
53. McKone, E.F., C.H. Goss, and M.L. Aitken, CFTR genotype as a predictor of prognosis in cystic fibrosis. Chest, 2006. 130(5): p. 1441-7.
54. Amaral, M.D., Targeting CFTR: how to treat cystic fibrosis by CFTR-repairing therapies. Curr Drug Targets, 2011. 12(5): p. 683-93.
55. Hall, I.P., Stratified medicine: drugs meet genetics. Eur Respir Rev, 2013. 22(127): p. 53-7.
56. Mubarak, A., et al., Human leukocyte antigen DQ2.2 and celiac disease. J Pediatr Gastroenterol Nutr, 2013. 56(4): p. 428-30.
57. Jabri, B., D.D. Kasarda, and P.H. Green, Innate and adaptive immunity: the yin and yang of celiac disease. Immunol Rev, 2005. 206: p. 219-31.
58. Mustalahti, K., et al., The prevalence of celiac disease in Europe: results of a centralized, international mass screening project. Ann Med, 2010. 42(8): p. 587-95.
59. Jabri, B. and L.M. Sollid, Tissue-mediated control of immunopathology in coeliac disease. Nat Rev Immunol, 2009. 9(12): p. 858-70.
60. Vader, W., et al., The HLA-DQ2 gene dose effect in celiac disease is directly related to the magnitude and breadth of gluten-specific T cell responses. Proc Natl Acad Sci U S A, 2003. 100(21): p. 12390-5.
61. Stepniak, D. and F. Koning, Celiac disease--sandwiched between innate and adaptive immunity. Hum Immunol, 2006. 67(6): p. 460-8.
62. Lammers, K.M., et al., Gliadin induces an increase in intestinal permeability and zonulin release by binding to the chemokine receptor CXCR3. Gastroenterology, 2008. 135(1): p. 194-204 e3.
63. Maiuri, L., et al., Interleukin 15 mediates epithelial changes in celiac disease. Gastroenterology, 2000. 119(4): p. 996-1006.
64. Maiuri, L., et al., Association between innate response to gliadin and activation of pathogenic T cells in coeliac disease. Lancet, 2003. 362(9377): p. 30-7.
65. Hue, S., et al., A direct role for NKG2D/MICA interaction in villous atrophy during celiac disease. Immunity, 2004. 21(3): p. 367-77.
66. Mention, J.J., et al., Interleukin 15: a key to disrupted intraepithelial lymphocyte homeostasis and lymphomagenesis in celiac disease. Gastroenterology, 2003. 125(3): p. 730-45.
67. Lebreton, C., et al., Interactions among secretory immunoglobulin A, CD71, and transglutaminase-2 affect permeability of intestinal epithelial cells to gliadin peptides. Gastroenterology, 2012. 143(3): p. 698-707 e1-4.
68. Sato, T., et al., Long-term expansion of epithelial organoids from human colon, adenoma, adenocarcinoma, and Barrett's epithelium. Gastroenterology, 2011. 141(5): p. 1762-72.
69. Beuling, E., et al., Conditional Gata4 deletion in mice induces bile acid absorption in the proximal small intestine. Gut, 2010. 59(7): p. 888-95.

CHAPTER 2

ADULT STEM CELLS IN THE SMALL INTESTINE ARE INTRINSICALLY PROGRAMMED WITH THEIR LOCATION-SPECIFIC FUNCTION

CHAPTER 2

Sabine Middendorp, Kerstin Schneeberger*, Caroline L. Wiegerinck*, Michal Mokry, Ronald D.L. Akkerman, Simone van Wijngaarden, Hans Clevers and Edward E.S. Nieuwenhuis

*These authors contributed equally

Stem Cells 2014;32:1083-1091

ABSTRACT

Differentiation and specialisation of epithelial cells in the small intestine are regulated in two ways. First, there is differentiation along the crypt-villus axis of the intestinal stem cells into absorptive enterocytes, Paneth, goblet, tuft, enteroendocrine, or M-cells, which is mainly regulated by WNT. Second, there is specialization along the cephalocaudal axis with different absorptive and digestive functions in duodenum, jejunum and ileum that is controlled by several transcription factors such as GATA4. However, so far it is unknown whether location-specific functional properties are intrinsically programmed within stem cells or if continuous signalling from mesenchymal cells is necessary to maintain the location-specific identity of the small intestine.

Using the pure epithelial organoid technique, we show that region-specific gene expression profiles are conserved throughout long-term cultures of both mouse and human intestinal stem cells and correlated with differential Gata4 expression. Furthermore, the human organoid culture system demonstrates that *Gata4*-regulated gene expression is only allowed in absence of WNT signalling.

These data show that location-specific function is intrinsically programmed in the adult stem cells of the small intestine and that their differentiation fate is independent of location-specific extracellular signals. In light of the potential future clinical application of small intestine-derived organoids, our data imply that it is important to generate GATA4-positive and GATA4-negative cultures to regenerate all essential functions of the small intestine.

INTRODUCTION

The mammalian intestine is responsible for the absorption of dietary nutrients and water, and the excretion of waste materials. The intestine also has an important barrier function in preventing direct contact with bacteria that reside in the lumen. To facilitate these diverse functions, the intestinal surface is covered by specialized epithelial cells that can take up nutrients from the lumen, but also form a continuous lining of cells that are linked close together by tight junctions.

The intestinal epithelium is ordered into crypts of Lieberkühn that harbor the stem and Paneth cells and mainly constitute a proliferative compartment, and the villi that represent the differentiated compartment containing the enterocytes, goblet, tuft, and enteroendocrine cells. It has been shown that four signaling pathways control homeostasis of the intestinal epithelium: WNT, Notch, epidermal growth factor (EGF) and bone morphogenic protein (BMP) (reviewed in [1]). WNT and EGF signalling are active in a gradient from the bottom to the crypt-villus junction, while BMP signalling is active in the villus compartment and Notch signalling determines the differentiation toward the secretory lineage (reviewed in [2]). High expression of WNT induces stem cell survival and proliferation of transit amplifying (TA) cells, while low levels of WNT allow TA cells to fully differentiate into one of the various epithelial cell types[3].

In addition to differentiation along the crypt-villus axis, there are also structural differences along the length of the intestine, such as cell type distribution and expression of proteins with specialized functions [4-6]. These differences correlate with the functionality of the different regions of the intestine and are referred to as regional or spatial differences along the cephalocaudal axis. This structural organization is established during development and is maintained throughout adulthood [7].

The small intestine is roughly divided into three segments along the cephalocaudal axis: duodenum, jejunum and ileum [8]. In mice, the duodenum involves the proximal two centimeters directly after the gastric pylorus [8]. Its main function is the digestion and absorption of iron, calcium and water-soluble vitamins. The function of the jejunum is the digestion and uptake of nutrients, whereas the ileum absorbs residual nutrients and mediates transport of bile acids and vitamin B12 [8].

To facilitate these highly specialized functions, multiple proteins such as digestive enzymes, nutrient transporters, cytoplasmic carriers and antimicrobial peptides are differentially expressed along the cephalocaudal axis. For example, duodenal cytochrome b reductase 1 (*Cybrd1*), involved in iron metabolism, is expressed only in duodenum [9], lactase-phlorizin hydrolase (Lct) is mainly expressed in jejunum [10] and apical sodium-dependent bile acid transporter (ASBT, *Slc10a2*) in ileum [11].

It has been shown that several transcription factors, for example, GATA4 and CDX2, control the expression of genes along the cephalocaudal axis [12, 13]. As such, GATA4 is expressed in proximal small intestine where it inhibits expression of ileum-specific genes [12], whereas CDX2 is expressed throughout small and large intestine and has an important role in formation of normal intestinal identity [13, 14].

Furthermore, syngeneic and xenogeneic transplantation of intestinal tissue into murine hosts have demonstrated that donor fetal intestine retains its positional information [15-18]. However, it is not known whether the identity of the intestinal epithelium is a hard-wired program within the stem cells or if the microenvironment, such as surrounding mesenchymal cells or luminal content, provides location-specific signals to the stem cells.

Recently, we developed a method to grow intestinal epithelial tissue *in vitro* from isolated crypts of both murine [19] and human origin [20]. We characterized the functional properties of organoids that were derived from different segments of the small intestine of mice and human. We found that the functional fate of both murine and human differentiated cell types is intrinsically programmed within location-specific stem cells as specific gene expression programs are maintained in the absence of location-specific external signals from mesenchyme or microbiota.

MATERIALS AND METHODS

Mice

C57BL/6 wild type mice (6-12 weeks old) were used for experiments. The mice were specific pathogen free and maintained in an environmentally controlled facility. Experiments were approved by the local Ethical Committee. Murine small intestines were dissected and cut into three equal parts. We isolated small parts of duodenum (proximal 2 cm of the proximal part), jejunum (proximal 2-4 cm of the middle part) and ileum (distal 2-4 cm of the distal part). Each segment was opened longitudinally, washed with cold phosphate buffered saline (PBS), and further processed for crypt isolation. From other mice, similar pieces of intestinal segments were used for *ex vivo* RNA isolation and histology.

Human material

Approval for this study was obtained by the Ethics Committee of the University Medical Centre Utrecht. Duodenal biopsies were obtained by flexible gastroduodenoscopy and ileal biopsies were obtained from the terminal ileum by colonoscopy. The biopsies were macroscopically and pathologically normal.

Crypt isolation and organoid culture

Murine organoids were generated from isolated small intestinal crypts and maintained in culture as described previously [19]. Crypt isolation and culture of human intestinal cells from biopsies have been described previously [20, 21]. In short, human organoids were maintained long-term in expansion medium (EM) containing RSPO1, noggin, EGF, A83-01, nicotinamide, SB202190 and WNT3A. For induction of differentiation, cultures were maintained for 5 days in differentiation medium (DM), which is EM without nicotinamide, SB202190 and WNT3A. We used conditioned media for RSPO1 (stably transfected *RSPO1* HEK293T cells were kindly provided by Dr. C. J. Kuo, Department of Medicine, Stanford, CA), noggin and WNT3A. The medium was changed every 2-3 days and organoids were passaged 1:6 every week.

RNA isolation and qPCR

From dissected tissue or cultured organoids, RNA was isolated with the RNeasy minikit or microkit (Qiagen, Venlo, the Netherlands), respectively, and quantified by optical density. cDNA was synthesized from 1 µg of RNA by performing reverse-transcription (Invitrogen, Carlsbad, CA or iScript, Biorad, Hercules, CA). Messenger RNA (mRNA) abundances were determined by real-time PCR using validated primer pairs (Suppl. Table S1) with the SYBR Green method (Bio-Rad, Hercules, CA). Glyceraldehyde-3-phosphate dehydrogenase (*Gapdh*) or *ACTIN* mRNA abundance was used to normalize mouse or human data, respectively.

RNA sequencing

Freshly isolated villi, crypts or organoids (cultured for 12 weeks) were used for mRNA sequencing. Total RNA was isolated using Trizol LS reagent (Invitrogen). Total RNA was purified using the Poly(A)Purist MAG Kit (Life Technologies, Ghent, Belgium) and subsequently re-purified using the mRNA-ONLY Eukaryotic mRNA Isolation Kit (Epicentre, Madison, Wisconsin) to obtain full length mRNA. Sequencing libraries were constructed using the SOLiD® Total RNA-Seq Kit (Life technologies, Ghent, Belgium) and sequenced on a SOLiD 4 sequencer to produce 50-bp long reads. Reads per 1,000 base pairs of transcript per million reads sequenced (RPKM) values were calculated for all RefSeq annotated genes and quantile normalized. A location-specific gene was defined as a gene with expression >10 RPKM (crypt) or >5 RPKM (villi) in at least one part of the intestine and with >1.5-fold higher expression in a specific part compared to any other part separately in both replicates (crypt) or in single replicate (villi). The gene ontology analysis was performed using the ToppGene Suite website [22]. The mRNA-seq datasets can be accessed via GEO (http://www.ncbi.nlm.nih.gov/geo) accession number GSE53297.

Immunohistochemistry

Intestinal segments and organoids were fixed in neutral buffered formalin and sectioned. After deparaffination and dehydration, epitope

retrieval was performed by boiling for 15 minutes at 120°C in target retrieval solution pH = 6.0 (DAKO, Glostrup, Denmark). Slides were blocked for endogenous peroxidase with 3% H2O2/PBS for 20 min and blocked with 1% bovine serum albumin (BSA)/PBS for 30 min at RT. Primary antibodies were diluted in 0.05 % BSA/PBS and incubated for 1 hour at RT or o/n at 4°C. Next, slides were incubated with secondary antibody (Envision anti-Rabbit-HRP or Envision anti-mouse-HRP, DAKO) 30min at RT, with Vector-Nova Red (Vector Labs, Burlingame, CA) to develop staining and counterstained with hematoxylin. Primary antibodies were monoclonal mouse anti-human proliferating cell nuclear antigen (NCL-PCNA, Leica Biosystems, Wertzlar, Germany), polyclonal rabbit anti-human sucrose-isomaltase (SI, HPA011897, Sigma, St.Louis, MO), and polyclonal rabbit anti-human SLC10A2 (ASBT, HPA004795, Sigma). Alcian Blue - periodic acid Schiff (AB-PAS) staining was performed according to standard methods.

Statistics

Data were expressed as means ± SEM and analyzed using one-way ANOVA and Tukey's Multiple Comparison Post-Test.

RESULTS

Location-specific signatures within the murine small intestinal crypts are maintained in long-term epithelial cell cultures

To obtain a systematic overview of location-specific gene expression, we performed mRNA sequencing on crypts and villi isolated from three equal parts of the small intestine. For analysis, we listed genes that were most strongly expressed in duodenum (A), jejunum (B) and ileum (C) or in two adjacent compartments (AB, BC). Next, we generated organoids from similar crypt preparations of the three small intestinal segments and cultured them for 12 weeks. mRNA sequencing profiles of these cultures were compared to their location-specific crypt-derived (Figure 1A) and villus-derived (Figure 1B) *ex vivo* counterparts. For example, we found that from those genes that were specifically expressed in crypts or villi of duodenum, 78% or 43% of these genes was also specifically expressed in organoids derived from duodenum, respectively (Figure 1 and Table 1). Similarly, 87% versus 83% of duodenal-jejunal, 70% versus 65% of jejunal, 77% versus 73% of jejunal-ileal and 65% versus 49% of ileal crypt- versus villi-specific genes were maintained in organoids derived from their *ex vivo* counterparts, respectively (Figure 1 and Table 1).
GO analysis of the selected genes was performed (Suppl. Tables S2, S3) and showed that the location-specific crypt- or villus-derived genes are mainly involved in digestion, transport, and metabolic processes. The complete list of location-specific crypt- and villi-genes is deposited in the GEO database. In summary, we confirmed differential expression of several genes that are known to be involved in location-specific function of the small intestine, such as genes coding for the proteins ferroportin (FPN) (*Slc40a1*) in duodenum, lactase (*Lct*) in jejunum, GATA4 (*Gata4*) in duodenum-jejunum, and ASBT (*Slc10a2*) in ileum (Figure 1). These data show that crypt-derived genes were highly maintained in organoid cultures, indicating that mouse organoids are mainly crypt-based structures. However, organoids do contain differentiated cells that express villus-derived genes, albeit in low levels. As the organoids were cultured inwthe same conditions, that is, in Matrigel and in presence of EGF, noggin, and R-spondin-1, these data indicate that epithelial stem cells maintain their identity, without location-specific external signals from mesenchyme or luminal content.

To validate the mRNA sequencing data, we determined expression of several location-specific genes by quantitative reverse transcription PCR (qRT-PCR). We used small pieces (~2cm) of each compartment of the small intestine for direct *ex vivo* RNA isolation or generation of organoid cultures that were maintained short term (3 weeks) or long-term (10-12 weeks). The transcription factor GATA4 has been shown to be a key regulator of location-specific gene expression in the mouse small intestine by repressing ileum-specific genes [12, 23]. In

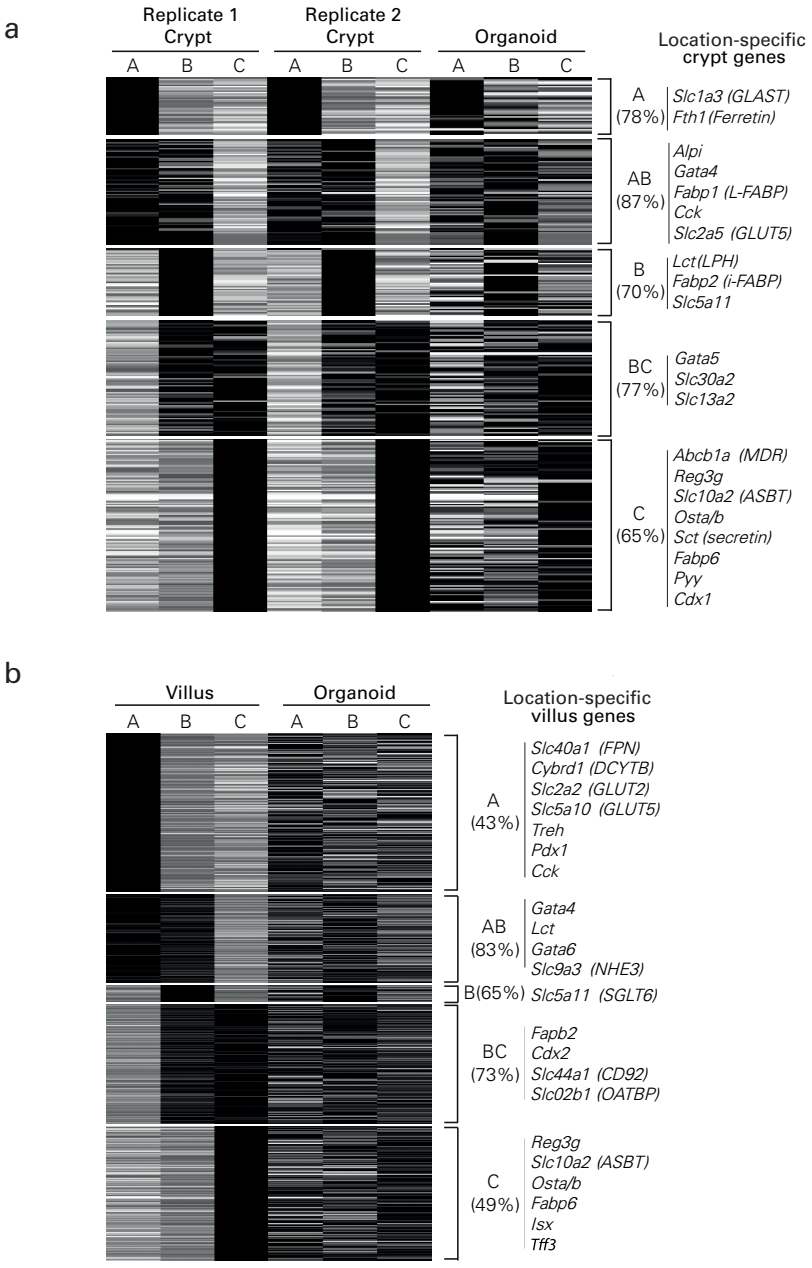

Figure 1. RNA sequencing profiles in *ex vivo* crypts, villi, and in cultured organoids derived from mouse small intestine. Intestines were divided in three equal parts, A (duodenum), B (jejunum), and C (ileum). Crypts (n = 2) and villi (n = 1) were harvested for mRNA sequencing. Part of the crypts were used for generation of long-term (12 weeks) organoid cultures (pool of n = 2). Since the absolute expression values can differ between crypts, villi, and organoids, mRNA RPKM values were normalized separately for (panel A) crypts and organoids and (panel B) villi and organoids with black as maximal expression and white as zero expression. In each compartment, genes are sorted by chromosomal location. Percentages of genes expressed in crypts (panel A) or villi (panel B) that were maintained in location-specific organoids and examples of genes are indicated per location. All mRNA-seq datasets are deposited in the GEO database.

Table 1. Number of location-specific crypt (upper panel) and villus (lower panel) genes whose expression is maintained in organoids of the ex vivo counterpart duodenum, jejunum, or ileum.

Ex vivo location	Total number of crypt genes	Organoid duodenum	Organoid jejunum	Organoid ileum
duodenum	40	31 (78%)	5 (13%)	3 (8%)
duodenum-jejunum	75	23 (31%)	42 (56%)	9 (12%)
jejunum	46	6 (13%)	32 (70%)	7 (15%)
jejunum-ileum	81	17 (21%)	24 (30%)	38 (47%)
ileum	121	23 (19%)	19 (65%)	79 (65%)

Ex vivo location	Total number of villus genes	Organoid duodenum	Organoid jejunum	Organoid ileum
duodenum	512	219 (43%)	146 (29%)	131 (26%)
duodenum-jejunum	462	174 (38%)	190 (41%)	83 (18%)
jejunum	51	10 (20%)	33 (65%)	8 (16%)
jejunum-ileum	554	153 (28%)	215 (39%)	172 (31%)
ileum	437	114 (26%)	102 (23%)	202 (46%)

Gene expression was determined by mRNA sequencing as described in Figure 1.

concordance, mRNA sequencing as well as qRT-PCR analysis confirmed that *Gata4* expression is high in duodenum and jejunum but almost absent in ileum. We found that this expression pattern was maintained in organoids that were cultured for 3 and 10-12 weeks (Figure 1 and 2A).

Duodenum-specific gene expression

The uptake of nutritional iron involves the reduction of Fe3+ into Fe2+ by ferric reductases such as CYBRD1 (encoded by *Cybrd1*) in the intestinal brush border and the subsequent transport of Fe2+ across the apical membrane of enterocytes by the divalent metal transporter 1 [9]. Iron is eventually exported across the basolateral membrane into the bloodstream via the solute carrier and Fe2+ transporter ferroportin (FPN, encoded by *Slc40a1*) [24]. Transcripts of these genes were only found in our villus-based mRNA sequencing data (Figure 1B) because they are expressed at the tips of the villi *in vivo* [9].
We determined mRNA expression levels of *Cybrd1* and *Slc40a1* by qRT-PCR and found that their expression *ex vivo* is indeed restricted to the duodenum and this cephalocaudal expression pattern remained stable in cultured organoids (Figure 2B).

Jejunum-specific gene expression

It has been shown that disaccharidases, like lactase (encoded by *Lct*) and sucrase-isomaltase (encoded by *Sis*), show the highest expression and activity in the jejunum [25]. We confirmed these expression patterns in *ex vivo* tissue and for *Lct* we also found highest expression in jejunum-derived organoid cultures, whereas the specific expression pattern of *Sis* was less obvious (Figure 2C).

Ileum-specific gene expression

The bile acid transporter ASBT (encoded by *Slc10a2*) is expressed apically on enterocytes in the ileum and can take up bile from the intestinal lumen, while organic solute transporter (OST)α/β form a pore at the basolateral side of the cell to export bile acids from the enterocytes to the blood [26]. We found by mRNA sequencing and qRT-PCR that the expression of both *Slc10a2* and *Ostb* were highly specific for the ileum, and that expression was maintained throughout organoid culture (Figure1 and 2D). We observed low *Ostb* expression in *ex vivo* jejunum, which was also reflected in the cultures. Collectively, these data show that the functional fate of mature intestinal epithelial cells is intrinsically programmed within the stem cell niches of each location and that these signatures are maintained even after long-term organoid culture where stem cells are not exposed to exogenous signals from mesenchyme or luminal content.

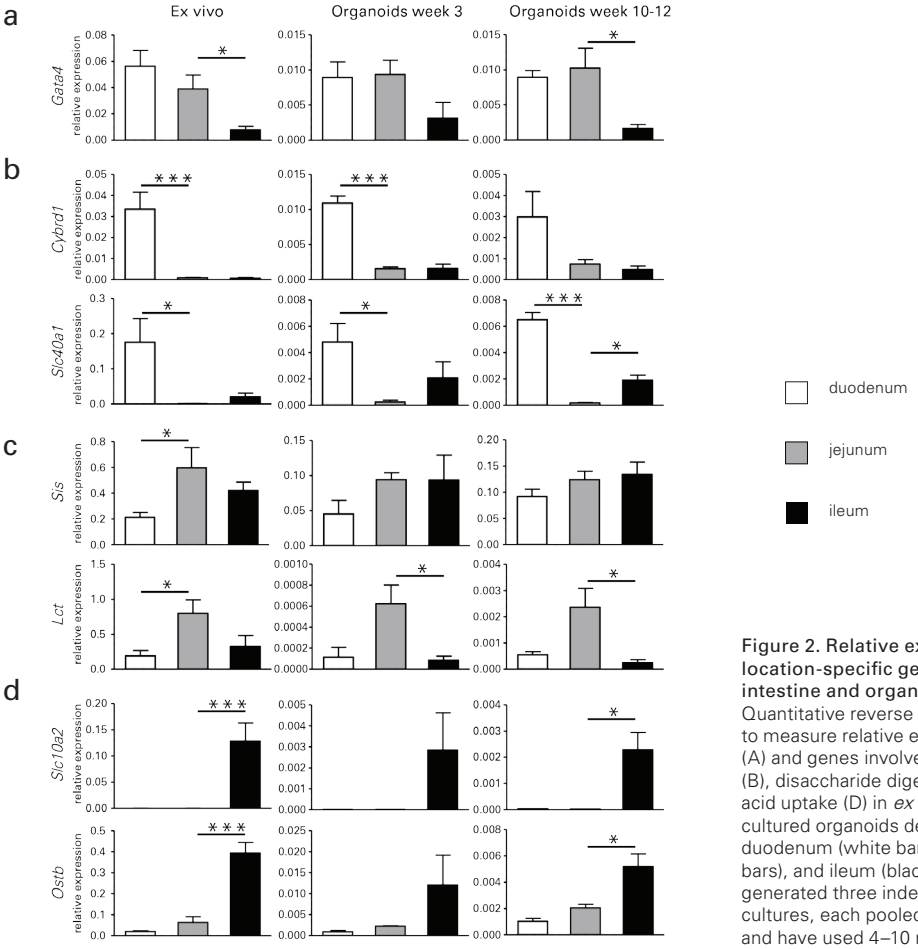

Figure 2. Relative expression of location-specific genes in murine intestine and organoid cultures. Quantitative reverse transcription PCR to measure relative expression of Gata4 (A) and genes involved in iron uptake (B), disaccharide digestion (C), and bile acid uptake (D) in *ex vivo* tissue and in cultured organoids derived from murine duodenum (white bars), jejunum (gray bars), and ileum (black bars). We have generated three independent organoid cultures, each pooled from two mice and have used 4–10 mice for *ex vivo* RNA isolation. Data were normalized to *Gapdh* housekeeping mRNA levels and are represented as means ± SEM; *, $p < .01$; and ***, $p < .005$.

Mouse organoids do not require exogenous WNT for long-term maintenance

We have shown that mouse stem cells maintain their location-specific origin during organoid culture by analyzing expression patterns of genes that are involved in location-specific functions along the cephalocaudal axis of the small intestine.

However, mouse organoids consist mainly of crypt compartments and contain only limited amounts of fully differentiated enterocytes that fulfill the location-specific function [19]. As such, the percentages of location-specific genes that were maintained in organoids were higher for crypt-derived genes compared to villus-derived genes (Figure 1 and Table 1). Furthermore, it has been shown that mouse small intestinal organoids have an intrinsic WNT gradient, which allows proliferation but limits differentiation [19], resulting in low levels of gene transcripts for the genes of interest.

By adding WNT3A-conditioned media to the location-specific mouse cultures, we show that WNT inhibits the expression of differentiation markers, such as *Sis* and *Slc10a2*, whereas the expression of *Gata4* remains unchanged

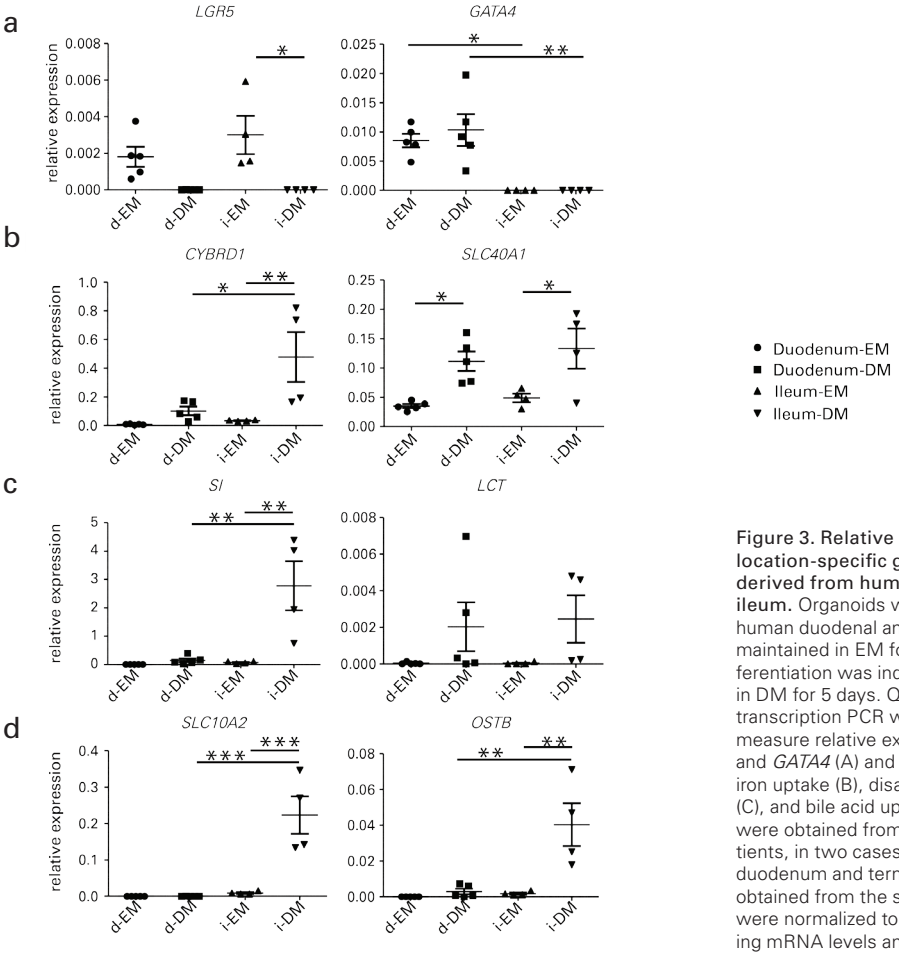

Figure 3. Relative expression of location-specific genes in organoids derived from human duodenum and ileum. Organoids were generated from human duodenal and ileal biopsies and maintained in EM for 7 weeks. Differentiation was induced by incubation in DM for 5 days. Quantitative reverse transcription PCR was performed to measure relative expression of *LGR5* and *GATA4* (A) and genes involved in iron uptake (B), disaccharide digestion (C), and bile acid uptake (D). Biopsies were obtained from four to five patients, in two cases biopsies from both duodenum and terminal ileum were obtained from the same patient. Data were normalized to *ACTIN* housekeeping mRNA levels and are represented as means ± SEM; *, $p < .05$; **, $p < .01$; and ***, $p < .005$. Abbreviations: DM, differentiation medium; EM, expansion medium.

(Suppl. Figure 1A). Morphologically, the addition of WNT results in more spherical organoids compared to the standard culture condition (Suppl. Figure 1B), an indication for induced proliferation.

Location-specific genes are induced upon differentiation of human organoid cultures

In contrast to mouse small intestinal organoids, human small intestinal organoid cultures produce little endogenous WNT. Therefore, their proliferation is dependent on exogenous WNT and differentiation is only initiated upon withdrawal of WNT [20]. Here, we use the human organoid system to delineate the effects of WNT on human location-specific small intestinal organoid cultures and show the full differentiation capacity of location-specific stem cells.

Human organoid cultures were established from crypts that were isolated from duodenal and ileal small intestinal biopsies. The organoids were maintained in so-called EM, containing WNT3A conditioned medium, which induces expansion of stem cells and repression of differentiation. We cultured the organoids for 3 (data not shown) or 7 weeks in

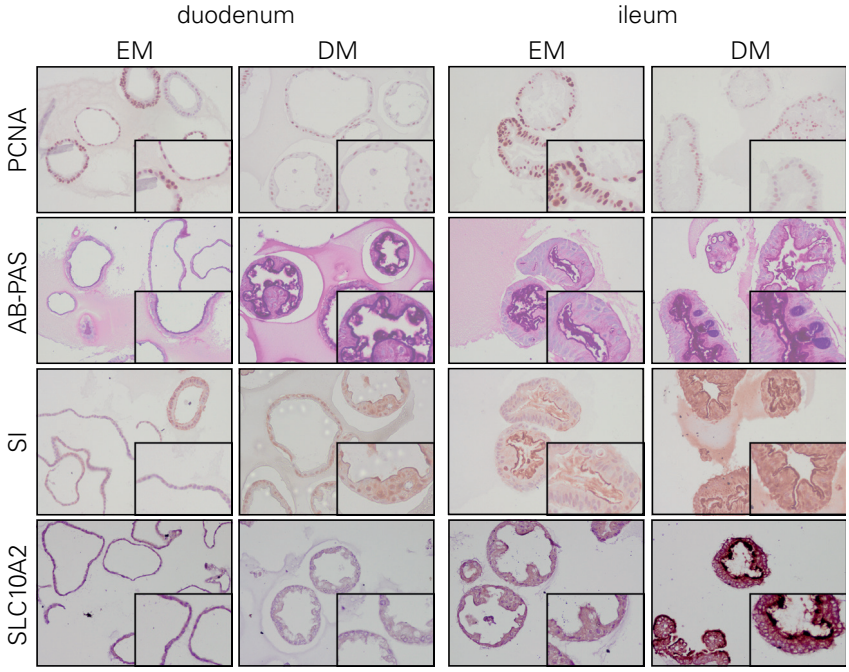

Figure 4. Immunohistochemical characterization of human organoids. Organoids were generated from human duodenal and ileal biopsies and maintained in EM for 7 weeks. Differentiation was induced by incubation in DM for 5 days. Organoids were embedded in paraffin, sectioned, and stained for PCNA, AB-PAS, SI, and SLC10A2 (ASBT). Original magnification ×20, insets ×50. Abbreviations: AB-PAS, Alcian Blue periodic acid Schiff; DM, differentiation medium; EM, expansion medium; PCNA, proliferating cell nuclear antigen; SI, sucrase-isomaltase.

EM, after which the medium was replaced by so-called DM for 5 days. DM lacks WNT3A, Nicotinamide and SB202190 in order to inhibit expansion and induce differentiation, demonstrated by the loss of *LGR5* mRNA (Figure 3A left), more dense morphology (Suppl. Figure 2) and loss of PCNA staining on immunohistochemistry (Figure 4). Incubation in DM also induced the differentiation of Goblet cells and production of glycoproteins as shown by AB-PAS staining of both duodenal and ileal organoids (Figure 4).

We confirmed *GATA4* as a specific marker for duodenum and found that the expression levels did not change in the absence of WNT3A (Figure 3A right). This was in concordance with the previously reported finding that GATA4 protein in proximal small intestine is expressed in all cells from crypt to tips of the villi [27]. We found that induction of *CYBRD1* and *SLC40A1* was equal or even higher in ileal organoids compared to duodenal organoids (Figure 3B) and that *SI* (coding for SI) expression was only induced in organoids derived from human ileum and not in duodenal organoids (Figure 3C and 4). In contrast, *LCT* was induced in both duodenum and ileum, but expression was rather low. The ileal markers *SLC10A2* and *OSTB* were highly restricted to differentiated organoids derived from ileum (Figure 3D and 4). Notably, not all of the

location-specific gene expression profiles in human intestinal organoids corresponded with the profiles in mice.

Collectively, these data show that WNT signaling inhibits expression of genes involved in the function of differentiated cells (*LCT*, *SLC10A2*) but not those that are involved in spatial patterning (*GATA4*). Furthermore, by using the organoid technique we show that location-specific stem cell fate is programmed within the stem cell niche, as the removal of WNT only induces expression of those genes that are not repressed by GATA4.

DISCUSSION

It has been shown that WNT is expressed by Paneth cells in the crypt compartments of the small intestine to enable proliferation (and inhibit differentiation) in the crypt [28, 29]. WNT signalling activity tapers off toward the crypt-villus junction, thereby reducing proliferation and inducing the differentiation into enterocytes, goblet, tuft, or enteroendocrine cells. Conversely, spatial compartmentalisation of the small intestine along the cephalocaudal axis is regulated by expression gradients of transcription factors, such as GATA4 and CDX2 [12, 13]. These transcription factors are expressed in epithelial cells and have been shown to regulate expression of genes that are involved in functional properties of differentiated enterocytes.

As such, WNT expression is regulating differentiation along the crypt–villus axis, whereas GATA4 is regulating regional specification and the linked differentiation along the cephalocaudal axis. To date, it was not known whether the expression of location-specific genes is programmed in a hard-wired fashion within the stem cells or if continuous signalling from mesenchymal cells is necessary to maintain the location-specific identity.

Using the organoid culturing technique, we now show that pure epithelial cell cultures that originated from location-specific stem cells are intrinsically programmed to differentiate into enterocytes with defined regional gene expression profiles. The organoid culture technique is based on the fact that Lgr5+ murine stem cells can be grown in laminin-rich Matrigel in the presence of the WNT-agonist and Lgr5-ligand R-spondin-1, the BMP-antagonist noggin, and EGF [2, 19]. In the presence of these extracellular signals, which are *in vivo* derived from Paneth cells and underlying mesenchyme, isolated crypts from the intestine can generate crypt-villus structures, which can be maintained in long-term culture [19]. Others have shown that mesenchymal cells are required for long-term culture of intestinal stem cells using myofibroblasts as well as stem cell niche signalling molecules to establish long-term cultures of intestine and colon [30].

Recently, it has been shown that *in vivo*, murine mesenchymal cells produce various WNT proteins [28], whereas Paneth cells produce EGF and WNT3A [31]. However, Paneth cells within organoids only produce WNT3A [28]. Endogenous Paneth cell-derived WNT3A is sufficient to maintain mouse small intestinal organoids in the presence of EGF, noggin and R-spondin-1 and allow generation of all differentiated epithelial cell types concomitant with stem cell self-renewal [28]. The addition of WNT3A to these mouse organoid cultures interferes with intestinal differentiation and yields organoids that largely consist of undifferentiated progenitors ([19] and Suppl. Figure 1).

Previously, it has been shown that intestine-specific deletion of Gata4 results in expression of Slc10a2 in the proximal intestine. As such, GATA4 is normally restricting the expression of Slc10a2 to the distal small intestine by repressing its expression in the proximal part [12].

Furthermore, reduction of GATA4 activity in the small intestine results in an induction of bile acid absorption in the proximal small intestine that is sufficient to correct bile acid malabsorption associated with ileocecal resected mice [32]. In contrast, CDX2 has been shown to be a master regulator in the posterior endoderm by

repressing the foregut differentiation program in the posterior gut [13, 33].
In the human organoid system, we demonstrate that GATA4 is expressed both under expansion and differentiation conditions, while the expression of differentiation genes, such as SLC10A2, is only induced in DM. We can explain this by the fact that EM contains WNT3-conditioned medium, which is inhibiting differentiation.

Recently, these data were supported by the finding that genetic regulatory networks and compartment-specific stem cell differences direct regional diversity in the Drosophila midgut [34, 35]. Furthermore, the GATAe transcription factor, a master regulator of midgut development, was shown to control compartment-specific gene expression along the length of the adult intestine, whereas gradients of WNT activity were shown to refine the location of boundaries [34].
As our key observation, we found differences in location-specific gene expression patterns, even though all cells were exposed to the same extracellular factors. This suggests that the cephalocaudal programming in the small intestine is not dependent on mesenchymal or niche factors, but rather on the location-specific expression of patterning genes such as Gata4.

CONCLUSION

Here, we show that adult stem cells of the small intestine are regionally specified in a cell-autonomous fashion and retain their location-specific gene expression profiles even after long-term culture. Furthermore, our data are also of importance with respect to the differentiation of intestinal tissue from induced pluripotent stem cells [36, 37]. To date, there is a generally accepted tendency to define small intestinal tissue as CDX2+, but we here show that especially the expression of GATA4 will determine the functional fate of the established cultures. Moreover, in light of the potential future clinical application of organoids, either derived from iPS cells or intestinal adult stem cells [38, 39], our data imply that it is important to generate GATA4-positive and GATA4-negative cultures to regenerate all essential functions of the small intestine.

ACKNOWLEDGMENTS

We thank Stieneke van den Brink, Hans Teunissen and Joyce Blokker for practical guidance and providing noggin- and WNT3A-conditioned media; Akifumi Ootani for providing the R-spondin-1-producing cell line; the gastroenterologists of the Wilhelmina Children's Hospital and the department of gastroenterology of the University Medical Center Utrecht for obtaining biopsies; Sylvia Brugman and Sabrina Roth for critically reading the manuscript.

1. Clevers, H., The intestinal crypt, a prototype stem cell compartment. Cell, 2013. 154(2): p. 274-84.
2. Sato, T. and H. Clevers, Growing self-organizing mini-guts from a single intestinal stem cell: mechanism and applications. Science, 2013. 340(6137): p. 1190-4.
3. van der Flier, L.G. and H. Clevers, Stem cells, self-renewal, and differentiation in the intestinal epithelium. Annu Rev Physiol, 2009. 71: p. 241-60.
4. Anderle, P., et al., Changes in the transcriptional profile of transporters in the intestine along the anterior-posterior and crypt-villus axes. BMC Genomics, 2005. 6: p. 69.
5. Bates, M.D., et al., Novel genes and functional relationships in the adult mouse gastrointestinal tract identified by microarray analysis. Gastroenterology, 2002. 122(5): p. 1467-82.
6. Comelli, E.M., et al., Biomarkers of human gastrointestinal

tract regions. Mamm Genome, 2009. 20(8): p. 516-27.
7. Shaw-Smith, C.J. and J.R. Walters, Regional expression of intestinal genes for nutrient absorption. Gut, 1997. 40(1): p. 5-8.
8. Thomson, A.B., et al., Small bowel review: Normal physiology, part 1. Dig Dis Sci, 2003. 48(8): p. 1546-64.
9. McKie, A.T., et al., An iron-regulated ferric reductase associated with the absorption of dietary iron. Science, 2001. 291(5509): p. 1755-9.
10. Krasinski, S.D., et al., Rat lactase-phlorizin hydrolase/human growth hormone transgene is expressed on small intestinal villi in transgenic mice. Gastroenterology, 1997. 113(3): p. 844-55.
11. Shneider, B.L., Intestinal bile acid transport: biology, physiology, and pathophysiology. J Pediatr Gastroenterol Nutr, 2001. 32(4): p. 407-17.
12. Bosse, T., et al., Gata4 is essential for the maintenance of jejunal-ileal identities in the adult mouse small intestine. Mol Cell Biol, 2006. 26(23): p. 9060-70.
13. Silberg, D.G., et al., Cdx1 and cdx2 expression during intestinal development. Gastroenterology, 2000. 119(4): p. 961-71.
14. Boyd, M., et al., Genome-wide analysis of CDX2 binding in intestinal epithelial cells (Caco-2). J Biol Chem. 285(33): p. 25115-25.
15. Duluc, I., et al., Fetal endoderm primarily holds the temporal and positional information required for mammalian intestinal development. J Cell Biol, 1994. 126(1): p. 211-21.
16. Ratineau, C., et al., Endoderm- and mesenchyme-dependent commitment of the differentiated epithelial cell types in the developing intestine of rat. Differentiation, 2003. 71(2): p. 163-9.
17. Rubin, D.C., et al., Use of fetal intestinal isografts from normal and transgenic mice to study the programming of positional information along the duodenal-to-colonic axis. J Biol Chem, 1992. 267(21): p. 15122-33.
18. Savidge, T.C., et al., Human intestinal development in a severe-combined immunodeficient xenograft model. Differentiation, 1995. 58(5): p. 361-71.
19. Sato, T., et al., Single Lgr5 stem cells build crypt-villus structures in vitro without a mesenchymal niche. Nature, 2009. 459(7244): p. 262-5.
20. Sato, T., et al., Long-term expansion of epithelial organoids from human colon, adenoma, adenocarcinoma, and Barrett's epithelium. Gastroenterology, 2011. 141(5): p. 1762-72.
21. Dekkers, J.F., et al., A functional CFTR assay using primary cystic fibrosis intestinal organoids. Nat Med, 2013. 19(7): p. 939-45.
22. Chen, J., et al., ToppGene Suite for gene list enrichment analysis and candidate gene prioritization. Nucleic Acids Res, 2009. 37(Web Server issue): p. W305-11.
23. Beuling, E., et al., GATA4 mediates gene repression in the mature mouse small intestine through interactions with friend of GATA (FOG) cofactors. Dev Biol, 2008. 322(1): p. 179-89.
24. Galy, B., et al., Iron regulatory proteins are essential for intestinal function and control key iron absorption molecules in the duodenum. Cell Metab, 2008. 7(1): p. 79-85.
25. Bosse, T., et al., Gata4 and Hnf1alpha are partially required for the expression of specific intestinal genes during development. Am J Physiol Gastrointest Liver Physiol, 2007. 292(5): p. G1302-14.
26. Dawson, P.A., T. Lan, and A. Rao, Bile acid transporters. J Lipid Res, 2009. 50(12): p. 2340-57.
27. Haveri, H., et al., Transcription factors GATA-4 and GATA-6 in normal and neoplastic human gastrointestinal mucosa. BMC Gastroenterol, 2008. 8: p. 9.
28. Farin, H.F., J.H. Van Es, and H. Clevers, Redundant sources of Wnt regulate intestinal stem cells and promote formation of Paneth cells. Gastroenterology, 2012. 143(6): p. 1518-1529 e7.
29. Korinek, V., et al., Depletion of epithelial stem-cell compartments in the small intestine of mice lacking Tcf-4. Nat Genet, 1998. 19(4): p. 379-83.
30. Ootani, A., et al., Sustained in vitro intestinal epithelial culture within a Wnt-dependent stem cell niche. Nat Med, 2009. 15(6): p. 701-6.
31. Sato, T., et al., Paneth cells constitute the niche for Lgr5 stem cells in intestinal crypts. Nature, 2011. 469(7330): p. 415-8.
32. Beuling, E., et al., Conditional Gata4 deletion in mice induces bile acid absorption in the proximal small intestine. Gut, 2010. 59(7): p. 888-95.
33. Gao, N., P. White, and K.H. Kaestner, Establishment of intestinal identity and epithelial-mesenchymal signaling by Cdx2. Dev Cell, 2009. 16(4): p. 588-99.
34. Buchon, N., et al., Morphological and molecular characterization of adult midgut compartmentalization in Drosophila. Cell Rep, 2013. 3(5): p. 1725-38.
35. Marianes, A. and A.C. Spradling, Physiological and stem cell compartmentalization within the Drosophila midgut. Elife, 2013. 2: p. e00886.
36. Finkbeiner, S.R. and J.R. Spence, A Gutsy Task: Generating Intestinal Tissue from Human Pluripotent Stem Cells. Dig Dis Sci, Epub ahead of print, 2013.
37. Spence, J.R., et al., Directed differentiation of human pluripotent stem cells into intestinal tissue in vitro. Nature, 2010. 470(7332): p. 105-9.
38. Howell, J.C. and J.M. Wells, Generating intestinal tissue from stem cells: potential for research and therapy. Regen Med, 2011. 6(6): p. 743-55.
39. Hynds, R.E. and A. Giangreco, Concise review: the relevance of human stem cell-derived organoid models for epithelial translational medicine. Stem Cells, 2013. 31(3): p. 417-22.

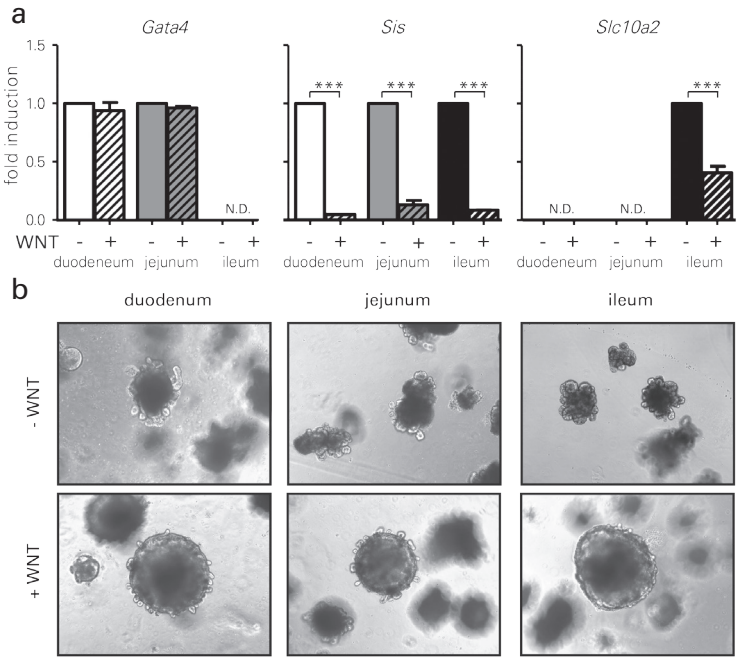

Supplementary Figure 1. Addition of WNT3A to murine organoid cultures induces proliferation and inhibits differentiation. Murine organoids derived from duodenum, jejunum and ileum were grown for 2 weeks and then incubated with or without WNT3A for 7 days. (A) qRT-PCR for *Gata4*, *Sis* (sucrase isomaltase) and *Slc10a2* (ASBT). Data from two independent experiments were normalized to Gapdh housekeeping mRNA levels and are represented as fold induction relative to cultures without WNT ± SEM; ***p < 0.005. (B) Differential interference contrast (DIC) pictures of the organoid cultures in presence or absence of WNT for 7 days after splitting. Original magnification 10x.

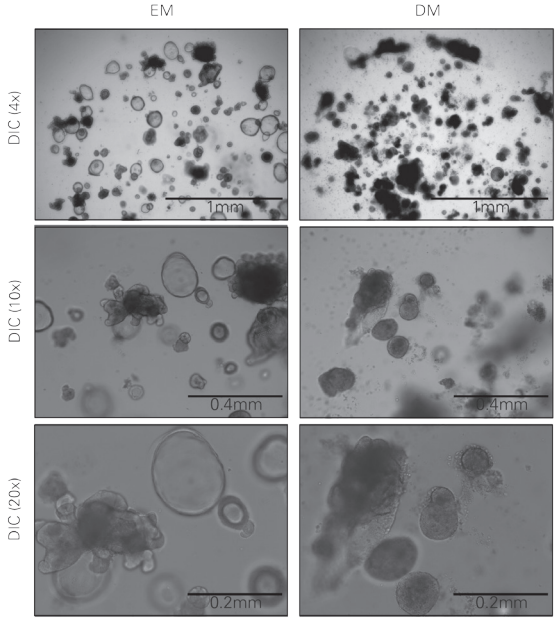

Supplementary Figure 2. Differential interference contrast (DIC) pictures from human duodenum organoid cultures. Organoids were generated from human duodenal biopsies and maintained in expansion medium (EM) for 7 weeks. Differentiation was induced by incubation in differentiation medium (DM) for 5 days.

TABLE S1. REAL TIME RT-PCR PRIMER SEQUENCES

MOUSE GENE	SEQUENCE
mGapdh-F	GCCTTCCGTGTTCCTACCC
mGapdh-R	TGCCTGCTTCACCACCTTC
mGata4-F	TTTGAGCGAGTTGGG
mGata4-R	GAATGCGGGTGTGC
mCybrd1-F	AGGCTTTTTCGTCTTTCTGCT
mCybrd1-R	GGTGGGAATGAATGGTACGAG
mSlc40a1-F	CCGGTTGGAATTTGGTGTC
mSlc40a1-R	TTCACGGATGTTGGAGTCTTT
mSis-F	CAGACCCGTAATCGTTTCC
mSis-R	AGACCTTGACATCATACAGTG
mLct-F	CAGCGATGCCCACAGGAAAG
mLct-R	ACGGAGCCCTTGACGAGAG
mSlc10a2-F	TTGCCTCTTCGTCTACACC
mSlc10a2-R	CCAAAGGAAACAGGAATAACAAG
mOstb-F	CAGCCACAAGACAAAGAAA
mOstb-R	CTGGCAGAAAGACAAGTGA

HUMAN GENE	SEQUENCE
hActin-F	CATGTACGTTGCTATCCAGGC
hActin-R	CTCCTTAATGTCACGCACGAT
hGata4-F	GCCTGGCCTGTCATCTCAC
hGata4-R	TTTGAGGAGGGAAGAGGGAA
hCybrd1-F	GGCCGTGTTTGAGAACCAC
hCybrd1-R	CTGGCGGGAATGTACTGTATG
hSlc40a1-F	TTGGCCGACTACCTGACCT
hSlc40a1-R	ACCACCAGCCCGTAGACTG
hSi-F	GGACACTGGCTTGGAGACAAC
hSi-R	TCCAGCGGGTACAGAGATGAT
hLct-F	CACGGTCGATTTCCTCTCTCT
hLct-R	AACCCAATGGTGAGCACTTG
hSlc10a2-F	TGGCCCCAAAAAGCAAA
hSlc10a2-R	AACCGTTCGGCACCTGTAC
hOstb-F	GGGGCTAAGGGGTCTAAGG
hOstb-R	CAGGGCAAGGATGGAATGA
hLgr5-F	GAATCCCCTGCCCAGTCTC
hLgr5-R	ATTGAAGGCTTCGCAAATTCT

TABLE S2. GENE ONTOLOGY OF BIOLOGICAL PROCESSES FOR LOCATION-SPECIFIC CRYPT GENES

GO NUMBER	BIOLOGICAL PROCESS	P-VALUE
GO:0007586	digestion	4.033E-12
GO:0031667	response to nutrient levels	2.168E-8
GO:0009991	response to extracellular stimulus	3.147E-8
GO:0006805	xenobiotic metabolic process	1.095E-7
GO:0071466	cellular response to xenobiotic stimulus	1.223E-7
GO:0019752	carboxylic acid metabolic process	2.904E-7
GO:0009725	response to hormone stimulus	6.091E-7
GO:0009410	response to xenobiotic stimulus	7.829E-7
GO:0043436	oxoacid metabolic process	1.089E-6
GO:0044255	cellular lipid metabolic process	1.825E-6
GO:0006082	organic acid metabolic process	1.917E-6
GO:0048545	response to steroid hormone stimulus	2.341E-6
GO:0014070	response to organic cyclic compound	3.764E-6
GO:1901615	organic hydroxy compound metabolic process	8.205E-6
GO:0033993	response to lipid	1.904E-5
GO:0006820	anion transport	2.089E-5
GO:0008202	steroid metabolic process	2.451E-5
GO:0006066	alcohol metabolic process	4.505E-5
GO:0032787	monocarboxylic acid metabolic process	5.023E-5
GO:0034284	response to monosaccharide stimulus	1.496E-4
GO:0042594	response to starvation	1.910E-4
GO:0034754	cellular hormone metabolic process	2.021E-4
GO:0009746	response to hexose stimulus	3.412E-4
GO:0051384	response to glucocorticoid stimulus	4.826E-4
GO:0050892	intestinal absorption	5.350E-4
GO:0046942	carboxylic acid transport	6.122E-4
GO:0015849	organic acid transport	6.122E-4
GO:0015711	organic anion transport	7.065E-4
GO:1901700	response to oxygen-containing compound	8.111E-4
GO:0006639	acylglycerol metabolic process	1.018E-3
GO:0031960	response to corticosteroid stimulus	1.064E-3
GO:0006638	neutral lipid metabolic process	1.116E-3
GO:0001101	response to acid	1.116E-3
GO:0071385	cellular response to glucocorticoid stimulus	1.254E-3
GO:0001523	retinoid metabolic process	1.254E-3
GO:0071384	cellular response to corticosteroid stimulus	1.472E-3
GO:0016042	lipid catabolic process	1.577E-3
GO:0010817	regulation of hormone levels	1.757E-3
GO:0006641	triglyceride metabolic process	2.920E-3
GO:0010243	response to organonitrogen compound	3.036E-3
GO:0001889	liver development	3.239E-3
GO:0006811	ion transport	3.463E-3
GO:0009743	response to carbohydrate stimulus	3.993E-3

GO:0061008	hepaticobiliary system development	4.026E-3
GO:0055114	oxidation-reduction process	4.027E-3
GO:0008610	lipid biosynthetic process	4.480E-3
GO:0022600	digestive system process	4.662E-3
GO:0016101	diterpenoid metabolic process	6.208E-3
GO:0042445	hormone metabolic process	7.614E-3
GO:0019585	glucuronate metabolic process	9.346E-3
GO:1901698	response to nitrogen compound	1.216E-2
GO:0043603	cellular amide metabolic process	1.225E-2
GO:0006063	uronic acid metabolic process	1.383E-2
GO:0046466	membrane lipid catabolic process	1.517E-2
GO:0071383	cellular response to steroid hormone stimulus	1.545E-2
GO:0015718	monocarboxylic acid transport	1.545E-2
GO:0009611	response to wounding	1.676E-2
GO:0019400	alditol metabolic process	1.923E-2
GO:0017144	drug metabolic process	1.987E-2
GO:0006631	fatty acid metabolic process	2.920E-2
GO:0006720	isoprenoid metabolic process	3.915E-2
GO:0044106	cellular amine metabolic process	4.091E-2
GO:0044242	cellular lipid catabolic process	4.531E-2

TABLE S3. GENE ONTOLOGY OF BIOLOGICAL PROCESSES FOR LOCATION-SPECIFIC VILLUS GENES

GO NUMBER	BIOLOGICAL PROCESS	P-VALUE
GO:0006082	organic acid metabolic process	7.933E-31
GO:0043436	oxoacid metabolic process	1.636E-30
GO:0019752	carboxylic acid metabolic process	1.522E-29
GO:0044255	cellular lipid metabolic process	1.067E-25
GO:0008610	lipid biosynthetic process	3.061E-21
GO:0006066	alcohol metabolic process	9.006E-21
GO:0006614	SRP-dependent cotranslational protein targeting to membrane	2.893E-19
GO:0006613	cotranslational protein targeting to membrane	7.065E-19
GO:0045047	protein targeting to ER	1.722E-18
GO:0072599	establishment of protein localization to ER	1.722E-18
GO:1901615	organic hydroxy compound metabolic process	3.207E-18
GO:0044711	single-organism biosynthetic process	8.195E-18
GO:0010035	response to inorganic substance	3.427E-17
GO:0044283	small molecule biosynthetic process	3.583E-16
GO:0070972	protein localization to endoplasmic reticulum	7.414E-16
GO:0055114	oxidation-reduction process	7.673E-16
GO:0008202	steroid metabolic process	2.551E-15
GO:0010038	response to metal ion	5.120E-15
GO:0032787	monocarboxylic acid metabolic process	5.296E-15

GO NUMBER	BIOLOGICAL PROCESS	P-VALUE
GO:0006612	protein targeting to membrane	2.663E-14
GO:0016125	sterol metabolic process	2.883E-13
GO:0002181	cytoplasmic translation	4.999E-13
GO:0006415	translational termination	6.045E-13
GO:0006413	translational initiation	9.381E-13
GO:0006639	acylglycerol metabolic process	1.221E-12
GO:0006638	neutral lipid metabolic process	1.677E-12
GO:0006641	triglyceride metabolic process	1.785E-12
GO:0006414	translational elongation	2.612E-12
GO:0016126	sterol biosynthetic process	1.131E-11
GO:0006520	cellular amino acid metabolic process	2.006E-11
GO:0044703	multi-organism reproductive process	4.520E-11
GO:0008203	cholesterol metabolic process	5.344E-11
GO:0006695	cholesterol biosynthetic process	6.539E-11
GO:0006644	phospholipid metabolic process	8.345E-11
GO:0042493	response to drug	9.466E-11
GO:0000184	nuclear-transcribed mRNA catabolic process, NMD	1.340E-10
GO:0046486	glycerolipid metabolic process	1.413E-10
GO:0009725	response to hormone stimulus	3.130E-10
GO:0022415	viral reproductive process	8.757E-10
GO:0006575	cellular modified amino acid metabolic process	1.023E-9
GO:0016129	phytosteroid biosynthetic process	1.603E-9
GO:0006631	fatty acid metabolic process	2.099E-9
GO:0006694	steroid biosynthetic process	5.969E-9
GO:0016128	phytosteroid metabolic process	5.979E-9
GO:0009991	response to extracellular stimulus	9.218E-9
GO:0019080	viral genome expression	9.640E-9
GO:0019083	viral transcription	9.640E-9
GO:1901700	response to oxygen-containing compound	1.649E-8
GO:0046394	carboxylic acid biosynthetic process	2.977E-8
GO:0016053	organic acid biosynthetic process	2.977E-8
GO:0019058	viral infectious cycle	3.577E-8
GO:0051186	cofactor metabolic process	3.717E-8
GO:0044108	cellular alcohol biosynthetic process	3.816E-8
GO:0008204	ergosterol metabolic process	3.816E-8
GO:0006696	ergosterol biosynthetic process	3.816E-8
GO:1901566	organonitrogen compound biosynthetic process	4.105E-8
GO:0031667	response to nutrient levels	4.681E-8
GO:0043603	cellular amide metabolic process	4.878E-8
GO:1901617	organic hydroxy compound biosynthetic process	8.363E-8
GO:0046165	alcohol biosynthetic process	8.942E-8
GO:0044107	cellular alcohol metabolic process	2.194E-7
GO:0006820	anion transport	2.362E-7
GO:0006732	coenzyme metabolic process	2.626E-7
GO:0006790	sulfur compound metabolic process	3.199E-7
GO:0006412	translation	3.247E-7
GO:0010243	response to organonitrogen compound	1.272E-6
GO:0006805	xenobiotic metabolic process	2.022E-6
GO:0071466	cellular response to xenobiotic stimulus	2.453E-6

GO NUMBER	BIOLOGICAL PROCESS	P-VALUE
GO:0007568	aging	2.473E-6
GO:0033993	response to lipid	3.941E-6
GO:0015711	organic anion transport	4.654E-6
GO:0009410	response to xenobiotic stimulus	4.872E-6
GO:0006518	peptide metabolic process	5.058E-6
GO:0006979	response to oxidative stress	5.674E-6
GO:0000022	mitotic spindle elongation	5.959E-6
GO:0000956	nuclear-transcribed mRNA catabolic process	6.188E-6
GO:0009607	response to biotic stimulus	6.706E-6
GO:0046460	neutral lipid biosynthetic process	7.116E-6
GO:0046463	acylglycerol biosynthetic process	7.116E-6
GO:1901698	response to nitrogen compound	7.159E-6
GO:0006576	cellular biogenic amine metabolic process	7.722E-6
GO:0051707	response to other organism	8.711E-6
GO:0051231	spindle elongation	1.130E-5
GO:0090407	organophosphate biosynthetic process	1.146E-5
GO:0009636	response to toxic substance	1.473E-5
GO:0045017	glycerolipid biosynthetic process	1.516E-5
GO:0006402	mRNA catabolic process	2.615E-5
GO:0006637	acyl-CoA metabolic process	2.896E-5
GO:0035383	thioester metabolic process	2.896E-5
GO:0043624	cellular protein complex disassembly	2.999E-5
GO:0042445	hormone metabolic process	3.849E-5
GO:0019432	triglyceride biosynthetic process	3.866E-5
GO:0046686	response to cadmium ion	4.343E-5
GO:0006665	sphingolipid metabolic process	5.245E-5
GO:0014070	response to organic cyclic compound	5.487E-5
GO:0006955	immune response	5.964E-5
GO:0015849	organic acid transport	6.265E-5
GO:0072330	monocarboxylic acid biosynthetic process	6.265E-5
GO:0046942	carboxylic acid transport	6.265E-5
GO:0006720	isoprenoid metabolic process	7.524E-5
GO:0006749	glutathione metabolic process	7.555E-5
GO:0006633	fatty acid biosynthetic process	9.789E-5
GO:0009743	response to carbohydrate stimulus	1.033E-4
GO:0006643	membrane lipid metabolic process	1.101E-4
GO:0009651	response to salt stress	1.153E-4
GO:0043241	protein complex disassembly	1.301E-4
GO:0006952	defense response	1.319E-4
GO:0006721	terpenoid metabolic process	1.346E-4
GO:0072594	establishment of protein localization to organelle	1.383E-4
GO:0046890	regulation of lipid biosynthetic process	1.419E-4
GO:0042439	ethanolamine-containing compound metabolic process	1.443E-4
GO:0016032	viral process	1.645E-4
GO:1901652	response to peptide	1.666E-4
GO:0043434	response to peptide hormone stimulus	1.701E-4
GO:0048545	response to steroid hormone stimulus	2.148E-4
GO:0044282	small molecule catabolic process	2.343E-4
GO:0044712	single-organism catabolic process	2.343E-4

GO NUMBER	BIOLOGICAL PROCESS	P-VALUE
GO:0034284	response to monosaccharide stimulus	2.595E-4
GO:0032984	macromolecular complex disassembly	2.861E-4
GO:0044764	multi-organism cellular process	2.972E-4
GO:0019216	regulation of lipid metabolic process	3.313E-4
GO:0006401	RNA catabolic process	3.561E-4
GO:0010817	regulation of hormone levels	3.638E-4
GO:0042542	response to hydrogen peroxide	3.721E-4
GO:0009308	amine metabolic process	3.779E-4
GO:0009746	response to hexose stimulus	3.870E-4
GO:0042594	response to starvation	4.713E-4
GO:0044106	cellular amine metabolic process	4.961E-4
GO:0031347	regulation of defense response	5.839E-4
GO:0001510	RNA methylation	6.277E-4
GO:0055088	lipid homeostasis	6.665E-4
GO:1901361	organic cyclic compound catabolic process	7.264E-4
GO:0019439	aromatic compound catabolic process	7.519E-4
GO:0022411	cellular component disassembly	8.249E-4
GO:0008299	isoprenoid biosynthetic process	1.036E-3
GO:0006811	ion transport	1.089E-3
GO:0016104	triterpenoid biosynthetic process	1.229E-3
GO:0019745	pentacyclic triterpenoid biosynthetic process	1.229E-3
GO:0044270	cellular nitrogen compound catabolic process	1.318E-3
GO:0046700	heterocycle catabolic process	1.609E-3
GO:0071705	nitrogen compound transport	1.619E-3
GO:0001676	long-chain fatty acid metabolic process	1.881E-3
GO:0048878	chemical homeostasis	2.205E-3
GO:0016114	terpenoid biosynthetic process	2.464E-3
GO:0031668	cellular response to extracellular stimulus	2.559E-3
GO:0016132	brassinosteroid biosynthetic process	2.611E-3
GO:0042545	cell wall modification	2.694E-3
GO:0071496	cellular response to external stimulus	2.774E-3
GO:0009664	plant-type cell wall organization	3.113E-3
GO:0006970	response to osmotic stress	3.921E-3
GO:1901565	organonitrogen compound catabolic process	4.348E-3
GO:0044242	cellular lipid catabolic process	4.743E-3
GO:1901654	response to ketone	4.764E-3
GO:0010876	lipid localization	5.257E-3
GO:0016042	lipid catabolic process	6.413E-3
GO:0007052	mitotic spindle organization	6.846E-3
GO:0097305	response to alcohol	7.776E-3
GO:0019742	pentacyclic triterpenoid metabolic process	8.330E-3
GO:0006722	triterpenoid metabolic process	8.330E-3
GO:0016131	brassinosteroid metabolic process	8.639E-3
GO:0080134	regulation of response to stress	8.858E-3
GO:0031669	cellular response to nutrient levels	9.131E-3
GO:0006084	acetyl-CoA metabolic process	9.326E-3
GO:0019748	secondary metabolic process	9.356E-3
GO:0042632	cholesterol homeostasis	9.363E-3
GO:0042953	lipoprotein transport	9.698E-3

GO NUMBER	BIOLOGICAL PROCESS	P-VALUE
GO:0000302	response to reactive oxygen species	9.902E-3
GO:0010259	multicellular organismal aging	1.009E-2
GO:0055092	sterol homeostasis	1.195E-2
GO:0010039	response to iron ion	1.243E-2
GO:0008340	determination of adult lifespan	1.266E-2
GO:0034655	nucleobase-containing compound catabolic process	1.304E-2
GO:0006672	ceramide metabolic process	1.341E-2
GO:0015718	monocarboxylic acid transport	1.390E-2
GO:0090181	regulation of cholesterol metabolic process	1.474E-2
GO:0045834	positive regulation of lipid metabolic process	1.553E-2
GO:0009617	response to bacterium	1.586E-2
GO:0008654	phospholipid biosynthetic process	1.599E-2
GO:0046464	acylglycerol catabolic process	1.692E-2
GO:0046461	neutral lipid catabolic process	1.692E-2
GO:0034599	cellular response to oxidative stress	1.694E-2
GO:0033194	response to hydroperoxide	1.812E-2
GO:0045540	regulation of cholesterol biosynthetic process	1.812E-2
GO:0006982	response to lipid hydroperoxide	2.038E-2
GO:0046503	glycerolipid catabolic process	2.097E-2
GO:0002682	regulation of immune system process	2.123E-2
GO:0044403	symbiosis, encompassing mutualism through parasitism	2.196E-2
GO:0001889	liver development	2.225E-2
GO:0006650	glycerophospholipid metabolic process	2.368E-2
GO:0044419	interspecies interaction between organisms	2.517E-2
GO:0009611	response to wounding	2.547E-2
GO:0046470	phosphatidylcholine metabolic process	2.579E-2
GO:0071248	cellular response to metal ion	2.922E-2
GO:0010044	response to aluminum ion	3.002E-2
GO:0009451	RNA modification	3.049E-2
GO:0032868	response to insulin stimulus	3.091E-2
GO:0009698	phenylpropanoid metabolic process	3.149E-2
GO:0070301	cellular response to hydrogen peroxide	3.178E-2
GO:0030148	sphingolipid biosynthetic process	3.236E-2
GO:0061008	hepaticobiliary system development	3.287E-2
GO:0007584	response to nutrient	4.131E-2
GO:0050727	regulation of inflammatory response	4.154E-2
GO:0009267	cellular response to starvation	4.521E-2
GO:0044262	cellular carbohydrate metabolic process	4.676E-2

CHAPTER 3

LOSS OF SYNTAXIN-3 CAUSES VARIANT MICRO-VILLUS INCLUSION DISEASE

Caroline L. Wiegerinck*, Andreas R. Janecke*, Kerstin Schneeberger*, Georg F. Vogel*, Désirée Y. van Haaften-Visser*, Johanna C. Escher, Rüdiger Adam, Cornelia E. Thöni, Kristian Pfaller, Alexander J. Jordan, Cleo-Aron Weis, Isaac J. Nijman, Glen R. Monroe, Peter M. van Hasselt, Ernest Cutz, Judith Klumperman, Hans Clevers, Edward E.S. Nieuwenhuis, Roderick H.J. Houwen, Gijs van Haaften, Michael W. Hess#, Lukas A. Huber#, Janneke M. Stapelbroek#, Thomas Müller# and Sabine Middendorp#

*, # These authors contributed equally

Gastroenterology 2014;147:65-68

ABSTRACT

Microvillus inclusion disease (MVID) is a disorder of intestinal epithelial differentiation characterized by life-threatening intractable diarrhea. MVID can be diagnosed based on loss of microvilli, microvillus inclusions, and accumulation of subapical vesicles. Most patients with MVID have mutations in myosin Vb that cause defects in recycling of apical vesicles. Whole-exome sequencing of DNA from patients with variant MVID showed homozygous truncating mutations in syntaxin 3 (*STX3*). STX3 is an apical receptor involved in membrane fusion of apical vesicles in enterocytes. Patient-derived organoid cultures and overexpression of truncated STX3 in Caco-2 cells recapitulated most characteristics of variant MVID. We conclude that loss of STX3 function causes variant MVID.

BRIEF REPORT

Microvillus inclusion disease (MVID) represents a form of congenital diarrhea. Patients typically present with persistent diarrhea within a few days, weeks, or months after birth, resulting in severe dehydration and metabolic acidosis. Current treatment comprises life-long total parenteral nutrition (TPN) and eventual small-bowel and/or liver transplantation [1]. The pathologic hallmarks of MVID are variable loss of brush-border microvilli, microvillus inclusions, and numerous subapical vesicles (secretory granules) in villus enterocytes [2]. In parallel, variant cases of MVID are described with milder clinical phenotypes permitting partial or complete weaning from TPN [3, 4].

Mutations in myosin Vb (*MYO5B*) have been found to cause classic MVID and our mutation detection rate exceeded 90% in more than 60 MVID patients [5, 6] (and unpublished data). MYO5B is a motor protein that facilitates protein trafficking and recycling in polarized cells by Rab11-dependent mechanisms. *MYO5B* mutations result in mislocalization of apical proteins and disrupted enterocyte polarization, leading to MVID [5, 7]. Interestingly, *MYO5B* mutations were absent in 2 referrals classified as variant MVID on the basis of clinical presentation.

Patient 1 was a 1-year-old Dutch girl born as the third child of a niece–uncle marriage, who developed watery diarrhea and severe metabolic acidosis from the second day of life. Currently, she receives daily intravenous sodium bicarbonate supplementation and is TPN-dependent but tolerates minimal enteral feeding for varying periods.

Patient 2 was an 18-month-old boy from Pakistan, the first child of a first-cousin marriage, who presented with frequent watery stools in the second week of life and several episodes of severe acidosis. The frequency of loose stools decreased after the early introduction of hydrolysate formula. Pulmonary infections occur frequently and he persistently suffers from mild acidosis, renal tubulopathy, and episodic vomiting. Despite increasing tolerance of enteral nutrition, he still requires partial parenteral nutrition and daily sodium bicarbonate supplementation for adequate growth.

Light and electron microscopy on duodenal and rectal biopsy specimens from both patients showed the histologic characteristics of MVID (Figure 1A–D and Supplementary Figure 1): accumulation of periodic acid–Schiff–positive subapical vesicles, intracellular microvillus inclusions, and variable loss of brush border. In contrast to classic MVID, we observed multiple microvilli at the basolateral membranes.

After the exclusion of *MYO5B* mutations by Sanger sequencing, we performed whole-exome sequencing—independently for patients 1 and 2—for identifying the causal gene. One single gene, *syntaxin 3* (*STX3*), harbored supposedly disease-causing mutations in both patients. We identified a homozygous nonsense mutation (c.739C>T, p.Arg247*, Ensembl COSM193004) in exon 9 and a homozygous frame-shifting 2-bp insertion (c.372_373dup, p.Arg125Leufs*7) in exon 6 of *STX3* in patients 1 and 2, respectively (Supplementary Figure 2A and B). Both mutations were confirmed by Sanger sequencing, co-segregated with the disease in the families, and were predicted to cause cellular STX3 protein depletion and truncation (Figure 1E), which was supported by Western blotting (Supplementary Figure 2C). Sanger sequencing of 5 additional MYO5B-negative MVID samples did not show *STX3* mutations.

Stable expression of truncated versions of STX3, corresponding to the patients' mutations, recapitulated all histologic hallmarks of MVID in Caco-2 cell cultures (Figure 2 and Supplementary Figure 3A–E), including a statistically significant increase of both microvillus inclusions and basolateral microvilli (Supplementary Table 1).

Disruption of cell polarity was reflected further by the formation of intercellular lumina within the cell multilayer (Figure 2 and Supplementary Figure 3C and D). Confocal laser-scanning microscopy showed mislocalization of STX3 (Supplementary Figure 3F), and Western

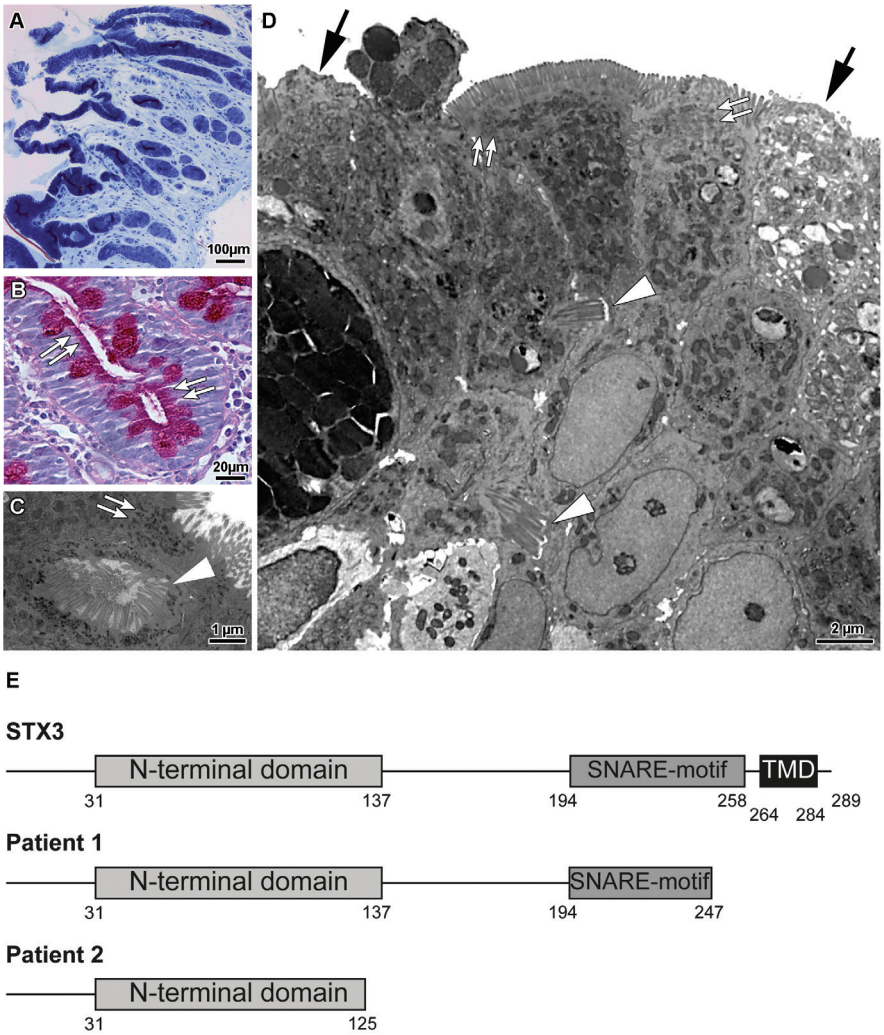

Figure 1. Histology of duodenal biopsy specimens from patients with variant MVID. (A) Toluidine blue staining shows mild focal villus atrophy. (B) Subapical accumulation of periodic acid–Schiff–positive vesicles in crypt epithelium (double arrows). (C) Secretory granules (double arrows) and microvillus inclusions (arrowhead). (D) Transmission electron microscopy shows basolateral microvilli (arrowheads), subapical vesicles (double arrows), atrophic brush border (arrows), and local cell shedding. (E) STX3 protein is predicted to be truncated in patient 1 (premature stop at Arg247) and patient 2 (2-bp insertion at Arg125 and premature stop after Arg130). TMD, transmembrane domain.

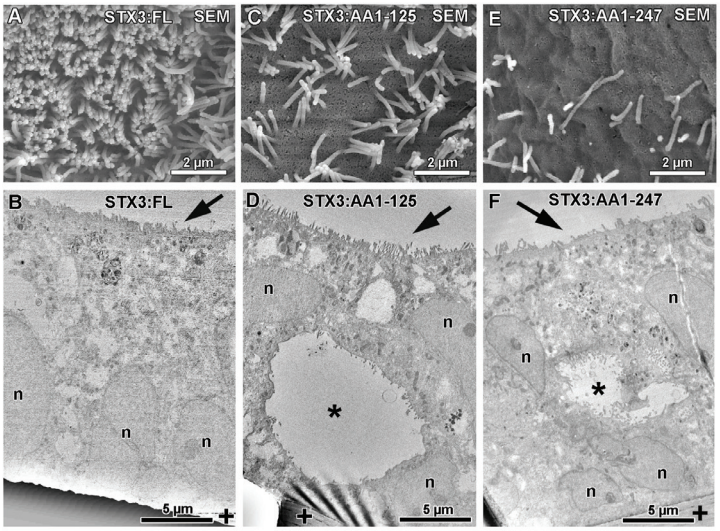

Figure 2. Scanning electron microscopy (SEM) and transmission electron microscopy of Caco-2 cells overexpressing full-length or truncated STX3 (STX3:FL, and STX3:AA1-125 or STX3:AA1-247). (A and B) Polarized monolayer with intact brush border (arrow). (C and D) Impaired brush border. Note wide intercellular lumen (asterisk) with scarce microvilli within the cell multilayer. (E and F) Cell multilayer with highly eroded brush border and intercellular lumen. n, nuclei; +, cell culture filter membrane.

blotting confirmed a reduction of endogenous STX3 levels by overexpression of truncated—but not full-length—STX3 protein (Supplementary Figure 4).
Together, these data suggest a dominant-negative effect of truncated STX3, disturbing epithelial polarity.

In addition, we used a recently established 3-dimensional culture of intestinal stem cells (organoids) [8]. Differentiated organoids from duodenal biopsy specimens of MVID patient 1 were devoid of syntaxin 3 staining and recapitulated most morphologic characteristics of the disease (Supplementary Figure 5).

The maintenance of epithelial cell function requires the establishment and continuous renewal of differentiated apical and basolateral plasma membrane domains with distinct lipid and protein compositions. STX3, an apically targeted N-ethylmaleimide-sensitive factor attachment protein receptor (SNARE) establishes and maintains polarity, which is necessary for protein trafficking, vesicle fusion, and exocytosis in intestinal, liver, kidney, and gastric parietal cells [9-11]. Target-SNAREs assemble into complexes with vesicle SNAREs, attached to recycling or biosynthetic vesicles [12]. In enterocytes, the apical SNARE complex including STX3 facilitates fusion of the target membrane and vesicles that have been trafficked into close apposition by the Rab11-regulated effector protein MYO5B [11].

Here, we have identified *STX3* mutations in 2 patients with variant MVID, in whom *MYO5B* mutations had been excluded. We were able to mimic the human MVID phenotype by overexpression of truncated STX3 *in vitro*, indicating loss of STX3 causes variant MVID. Consistent with our findings, it was reported that disruption of STX3 function or ablation of its apical targeting signal impairs delivery of apical markers *in vitro*, emphasizing syntaxin 3 is likely to act as a key regulatory SNARE in intestinal epithelium [10, 13].

Disturbed delivery of apical constituents is a common defect in both classic and variant MVID. In classic MVID, MYO5B deficiency disrupts trafficking between apical recycling endosomes and the apical membrane [14]. In variant MVID, a traffic arrest of apically destined vesicles results from STX3 loss-of-function owing to defective apical docking and exocytosis. Both classic and variant MVID enterocytes display characteristic microvillus inclusions, which might arise from the fusion of apical transport or recycling vesicles under conditions of reduced delivery to the apical plasma membrane. The appearance of microvilli at the basolateral membrane in variant MVID might result from the binding of vesicles to the basolateral syntaxin 4 protein, which is highly homologous to STX3 [13].

Interestingly, patients with mutations in the STX3 binding protein *STXBP2/Munc18-2*, causing familial hemophagocytic lymphohistiocytosis type 5, who have persistent chronic diarrhea after hematopoietic stem cell transplantation, also showed microvillus atrophy and histologic findings reminiscent of MVID [15].

In conclusion, these data provide a conceptual advance in MVID research because the newly identified causal gene *STX3* will improve the diagnosis, prognosis, genetic counseling, and prenatal screening for MVID.

ACKNOWLEDGMENTS

The authors thank members of the Clevers lab (Hubrecht Institute); The Cell Microscopy Center (University Medical Center Utrecht); B. Witting, K. Gutleben, C. Herrmann (Innsbruck), and Y. Meng Heng (Toronto) for technical assistance; and K. Biermann (Pathology, Erasmus MC) for biopsy specimens of patient 1.

1. Ruemmele FM, et al. Orphanet J Rare Dis 2006; 1: 22.
2. Sherman PM et al. J Pediatr Gastroenterol Nutr 2004; 38: 16-26.
3. Croft NM et al. J Pediatr Gastroenterol Nutr 2000; 31: 185-189.
4. Iancu TC et al. Ultrastruct Pathol 2007; 31: 173-188.
5. Muller T et al. Nat Genet 2008; 40: 1163-1165.
6. Ruemmele FM, Muller T et al. Hum Mutat 2010; 31: 544-551.
7. Szperl AM, Golachowska MR et al. J Pediatr Gastroenterol Nutr 2011; 52: 307-313.
8. Sato T et al. Nature 2009; 459: 262-265.
9. Delgrossi MH et al. J Cell Sci 1997; 110: 2207-2214.
10. Sharma N et al. J Cell Biol 2006; 173: 937-948.
11. Carmosino M et al. Biol Cell 2009; 102: 75-91.
12. Jahn R et al. Nat Rev Mol Cell Biol 2006; 7: 631-643.
13. ter Beest MB et al. Mol Biol Cell 2005; 16: 5784-5792.
14. Thoeni CE et al. Traffic 2013; 15: 22-42.
15. Stepensky P et al. Pediatr Blood Cancer 2013; 60: 1215-1222.
Author names in bold designate shared co-first authors

SUPPLEMENTARY MATERIALS AND METHODS

Human Material

All participants provided written informed consent to participate in this study according to a protocol reviewed and approved by our institutional review boards. Duodenal organoids from 3 healthy controls and patient 1 were generated from duodenal biopsy specimens obtained during duodenoscopy for diagnostic purposes. Whole blood was collected for genetic analysis. The healthy control group included patients susceptible for celiac disease or inflammatory bowel disease with normal pathology.

Whole-Exome Sequencing

Genomic DNA was isolated from whole-blood samples using standard manual or robotic procedures. Exome sequencing on patient 1 and her parents was performed as reported previously,1 with the exception that the Agilent (Santa Clara, CA) SureSelect Human All Exon 50Mb Kit V4 was used for enrichment, and sequencing was performed according to the manufacturer's protocol on the Solid5500 (Life technologies, Carlsbad, CA) sequencing platform. We obtained an average coverage of 59-, 63-, and 59-fold for the mother, father, and patient, respectively. Alignment and variant annotation was performed as reported previously.1 Filtering of rare variants (allele frequency, <0.1; seen <10 times in our in-house database consisting of exome data from 150 individuals and never seen in the homozygous state in our in-house database) with a predicted effect at the protein level for a recessive inheritance model left us with 2 variants, of which the nonsense variant in STX3 was the strongest candidate based on the literature.

The exome of patient 2 was enriched from genomic DNA using Roche-Nimblegen's SeqCap EZ Exome v2 (35-Mb capture region) Exome Enrichment Kit and sequenced using the Illumina HiSeq2000 to a median coverage of 74× according to the manufacturer's protocol, producing approximately 10 gigabases of paired-end 101-bp sequence reads by analysis with CASAVA v1.8 (Illumina, Inc). Sequencing reads were aligned to the human genome (hg19) with Burrows–Wheeler transformation. Polymerase chain reaction duplicates were removed with PICARD (available: http://picard.sourceforge.net) and single-nucleotide substitutions (SNPs), and small indels were identified with the samtools mpileup software and quality-filtered with the Genome Analysis Toolkit (Dice Holdings, New York, NY). All variants were submitted to SeattleSeq (available: http://snp.gs.washington.edu/SeattleSeqAnnotation/) for annotation, categorization into synonymous and nonsynonymous SNPs or indels, and for filtering using the data from the Single Nucleotide Polymorphism database (dbSNP137), the 1000 Genomes Project, the National Heart, Lung, and Blood Institute Exome Sequencing Project Exome Variant Server. The identified mutation was absent from an in-house database of 70 sequenced individuals. Where applicable, variants were classified by predicted protein effects with Polymorphism Phenotyping v2 (PolyPhen 2) and Scale-invariant feature transform (SIFT).

A spreadsheet-based comparison of all nonconservative and rare homozygous exomic variants of patients 1 and 2 showed a single gene, STX3, which harbored supposedly deleterious mutations in both patients.

Sanger Sequencing

The STX3 mutations from patients 1 and 2 and their parents were verified using Sanger sequencing. Exons 9 and 6 of STX3 were polymerase chain reaction–amplified in total genomic DNA isolated from peripheral blood lymphocytes of patients 1 and 2 and their parents, respectively, using intronic primers (all sequences available on request). Purified with the Exonuclease I–shrimp alkaline phosphatase enzymes (USB, Cleveland, OH), polymerase chain reaction products were sequenced bidirectionally using the BigDye Terminator v3.1 Cycle Sequencing Kit (Applied Biosystems, Foster City, CA). Fragments were separated electrophoretically on an ABI3730xl DNA Analyzer (Applied Biosystems) and analyzed with JSI SeqPilot software

(Kippenheim, Germany). Codon numbering was based on the published online amino acid and messenger RNA sequences of STX3 (available: http://www.ncbi.nlm.nih.gov.proxy.library.uu.nl/) using the first methionine as an initiation codon.

Organoid Culture

Crypts were isolated from duodenal biopsy specimens of patient 1 and 3 healthy controls and cultured as described previously.2 The organoids were maintained in expansion medium (containing epidermal growth factor, noggin, R-spondin1, WNT3A, nicotinamide, SB202190, and A83-01) and passaged weekly for 5–10 weeks. To induce differentiation, organoids were cultured in differentiation medium (which is expansion medium without SB202190, nicotinamide, and WNT3A) for 5 days.

Plasmids

Human full-length and truncated STX3 complementary DNA was polymerase chain reaction–amplified from Caco-2 complementary DNA and ligated into a pENTR4-mCitrine vector using EcoRI and XbaI restriction sites, c-terminally, and in frame with the mCitrine fluorescent protein. The fusion constructs were cloned into the lentiviral expression vector pCCL-EF1a-BlastiR-DEST using the Gateway multicloning technology (Life technologies).

Cell Culture

Caco-2 cells (American Type Culture Collection, Manassas, VA) were grown under standard conditions in Dulbecco's modified Eagle medium containing high glucose, 10% heat-inactivated fetal bovine serum, 100 U/mL penicillin, 100 µg/mL streptomycin, and 1mM sodium pyruvate. For lentiviral transduction of Caco-2 cells, Hek293LTV cells were transfected using Lipofectamine LTX (Invitrogen) with the lentiviral expression plasmids together with the vesicular stomatitis virus–G plasmid and the lentiviral gag-pol packaging vector PAX2. Forty-eight and 72 hours after transfection, the viral particle containing supernatant was harvested and directly used for Caco-2 cell infection. Six days after infection, Caco-2 cells were selected with 10 µg/mL BlasticidinS (Invitrogen). For biochemical and microscopical analyses, untreated and genetically modified Caco-2 cells were grown for 14 days on 24-mm Costar Transwell polycarbonate filters (Corning, NY). Three biological replicates from 2 independent experiments were analyzed.

Western Blotting

Western blotting after 10% sodium dodecyl sulfate–polyacrylamide gel electrophoresis and transfer onto polyvinylidene difluoride membranes (GE Healthcare, Little Chalfont, United Kingdom) of Caco-2 lysates was performed as previously described.3 Incubation with primary antibodies was performed overnight at 4°C. Blots were developed using a chemiluminescence detection system (Santa Cruz). Mouse monoclonal antitubulin (1:5000; Sigma Aldrich, Cambridge, United Kingdom), mouse monoclonal anti-enhanced green fluorescent protein (1:1000; Roche, Penzberg, Germany), and rabbit monoclonal anti–syntaxin 3 (1:1000; Abcam ab133750) were used. Secondary horseradish-peroxidase–conjugated anti-rabbit and anti-mouse antibodies (Sigma Aldrich) were used at a dilution of 1:5000.

Organoids were lysed in Laemmli buffer (0.12 mol/L Tris-HCl, pH 6.8, 4% sodium dodecyl sulfate, 20% glycerol, 0.05 µg/µL bromphenol blue, and 35 mmol/L β-mercaptoethanol) and incubated at 100°C for 5 minutes. Detection of syntaxin 3 and tubulin was performed using the Odyssey system (LI-COR, Lincoln, NE) by incubating the blots with donkey anti-rabbit IgG IRDye 680RD (926-68073; LI-COR) and donkey anti-mouse IgG IRDye 680 (926-32222; LI-COR).

Histology

Paraffin slides were generated from biopsy material and organoids. Tissues were fixed in 4% formalin overnight and 4% neutral buffered formalin for 45 minutes at room temperature, respectively. Sections (3-µm thick) were subjected to periodic acid–Schiff staining according to standard techniques. Semithin resin sections (see later) were stained with 1% toluidine blue to illustrate gross morphology of the intestinal mucosa.

Immunofluorescence and Immunohistochemistry

Duodenal biopsy specimens were embedded in Tissue-Tek optimum cutting temperature Compound and frozen at -80°C. Sections were fixed for 20 minutes in 4% PFA in phosphate-buffered saline without calcium and magnesium, and permeabilized for 5 minutes with 0.3% Triton X-100 (Sigma Aldrich). After washing with phosphate-buffered saline, slides were blocked for 1 hour at room temperature with 5% bovine serum albumin and 15% goat serum in phosphate-buffered saline. Incubation with primary antibodies was performed overnight at 4°C with rabbit monoclonal anti–syntaxin 3 (Abcam) or mouse monoclonal anti-CD10 (ImmunoTools, Germany). Alexa568 goat anti-rabbit, Alexa568 goat anti-mouse and Alexa488 phalloidin (Life technologies) were used for fluorescence and actin cytoskeleton labeling, respectively.

Caco-2 cells grown for 14 days on filters were fixed with 4% buffered paraformaldehyde solution and processed essentially as previously described.4 Briefly, fixed Caco-2 cells were permeabilized with 0.3% Triton X-100 (Sigma-Aldrich) for 30 minutes and subsequently blocked with phosphate-buffered saline containing 15% goat serum for 1 hour at room temperature. Mouse monoclonal anti-CD26/dipeptidylpeptidase IV (HBB3/775/42, obtained from the Developmental Studies Hybridoma Bank, created by the National Institute of Child Health and Human Development of the National Institutes of Health, and maintained at the Department of Biology, University of Iowa, Iowa City, IA) and rabbit monoclonal anti–syntaxin 3 (Abcam) primary antibody was incubated overnight at 4°C and labeled with secondary antibody Alexa568 goat anti-mouse and anti-rabbit (Invitrogen), respectively. Actin filaments were stained with phalloidin-Alexa568 (1:500; Invitrogen) in blocking solution for 1 hour at room temperature. Both biopsy material and Caco-2 cells were incubated with Hoechst 33342 (1:10,000; Thermo Scientific, Waltham, MA) to stain nuclei and mounted in Mowiol (Sigma-Aldrich). Epifluorescence images were recorded with an Axio Imager M1 (Carl Zeiss; Oberkochen, Germany) fluorescent microscope equipped with a charge-coupled device camera (SPOT Xplorer; Visitron Systems, Puchheim, Germany) and analyzed with ImageJ, version 1.49a software (National Institutes of Health, Bethesda, MD). Confocal image stacks were recorded with a Leica SP5 confocal fluorescence microscope (Leica Microsystems), deconvolved using Huygens Professional Deconvolution and AnalysisSoftware (Scientific Volume Imaging, Hilversum, The Netherlands), exported using Imaris 3D rendering (Bitplane AG, Zürich, Switzerland), and afterward adjusted for brightness, contrast, and pixel size in GNU Image Manipulation Program version 2.8.10 (GIMP) open source software.

Organoids were cultured for 5 days in expansion medium and fixed in 4% buffered paraformaldehyde solution for 30 minutes at room temperature. Immunofluorescent labeling was performed as described.5 Primary monoclonal antibodies used were rabbit anti-human syntaxin 3 (clone EPR8543, 1:100; Abcam) and rat anti-human α6-integrin (clone GoH3, 1:200; BD Pharmingen). Secondary antibodies used were Alexa488-conjugated goat anti-rabbit (Life Technologies) and Dylight649-conjugated goat anti-rat (Biolegend). F-actin was stained with phalloidin-Tetramethylrhodamine (TRITC) (Sigma-Aldrich). Confocal image stacks were recorded with a LSM 710 confocal fluorescent microscope (Carl Zeiss) and analyzed with Volocity software version 6.3 (Perkin Elmer).

Transmission Electron Microscopy

Intestinal biopsy specimens, organoids, and Caco-2 cell cultures were processed according to standard procedures.4 Briefly, biopsy specimens and Caco-2 cells were fixed with 4% buffered paraformaldehyde solution overnight at room temperature and organoids in 0.1 mol/L PHEM buffer (60 mmol/L 1,4-piperazinediethanesulfonic acid, 25 mmol/L HEPES, 2 mmol/L $MgCl_2$, 10 mmol/L ethylene glycol-bis(β-aminoethyl ether)-N,N,N′,N′-tetraacetic acid, pH 6.9) for 3.5 hours at room temperature and then stored in 1% paraformaldehyde in 0.1 mol/L PHEM buffer at 4°C. Before embedding, the specimens were

postfixed with 1% OsO4 (optionally followed by 1.5% K3Fe[CN]6, and subsequently 0.5% uranyl acetate). Samples then were dehydrated and embedded into Epon epoxy resin (Polysciences GmbH, Eppelheim, Germany). Ultrathin sections of 60 nm were contrasted with uranyl acetate and lead citrate.

Scanning Electron Microscopy

Caco-2 cell cultures were processed according to standard procedures.6

Morphometry and Statistics

The frequency of microvillus inclusions and sites of basolateral microvilli in Caco-2 cells, stably expressing mCitrine-STX3:FL, mCitrine-STX3:AA1-125, and mCitrine-STX3:AA1-247, was estimated by quantitative epifluorescence microscopy and transmission electron microscopy of thin sections cut perpendicularly to the cell culture surface (3 samples from 2 independent experiments, 460–650 cells per condition). The significance of differences between mCitrine-STX3:FL controls and the truncating mutations was tested using 2-sided (2-tailed) P values using the Fisher exact test. Epifluorescence microscopy was used to count the number of ring- and dot-like structures, positive either for actin or the apical marker CD26/dipeptidylpeptidase IV as compared with the cell number; thus, these structures comprised intracellular microvillus inclusions, as well as sites of basolateral microvilli. Transmission electron microscopy was used to further distinguish intracellular microvillus inclusions from sites of basolateral microvilli (Supplementary Table 1).

Supplementary Table 1. Summary of the Statistical Analyses of Caco-2 Cells With Full-Length or Truncated STX3 Expression

	Actin-rings/dots	DPPIV/CD26-rings/dots		*P* value	Intracellular microvillus inclusions		*P* value	Sites of basolateral microvilli		*P* value
STX3-FL	Mean, 0,2%	Mean, 0,4%	~ 500 cells		Mean, 0,0%	~ 460 cells		Mean, 1,5%	~ 460 cells	
STX3-AA1-125	Mean, 10,8%	Mean, 11,2%	~ 500 cells	<.0001	Mean, 1,7%	~ 650 cells	<.0038	Mean, 9,8%	~ 650 cells	<.0001
STX3-AA1-247	Mean, 10,2% Fluorescence microscopy	Mean, 8,4% Fluorescence microscopy	~ 500 cells	<.0001	Mean, 1,8% TEM	~ 500 cells	<.0039	Mean, 12,5% TEM	~ 500 cells	<.0001

TEM, transmission electron microscopy.

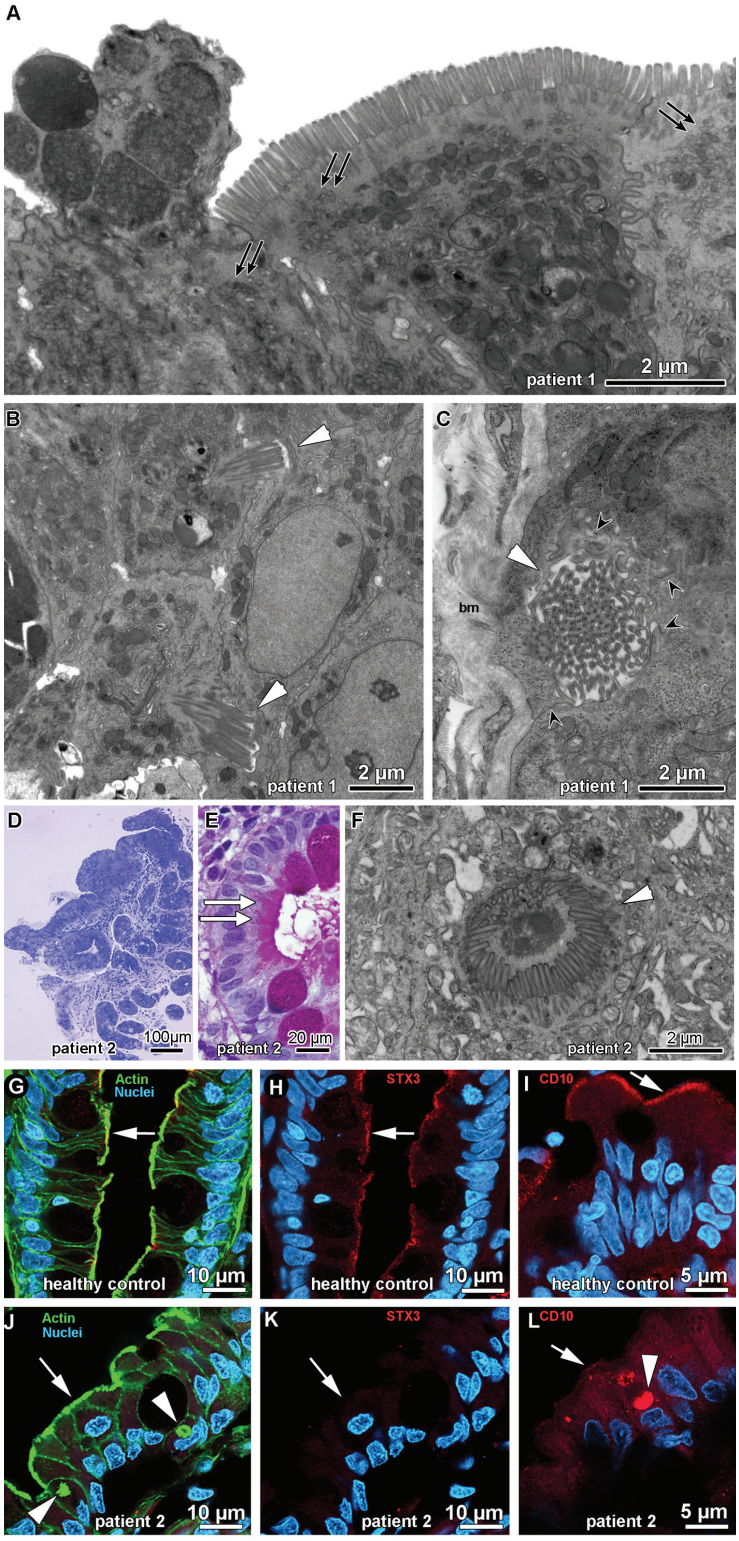

Supplementary Figure 1. (A–C) Ultrastructural details from MVID patient 1 (as described in Figure 1D). (A) Subapical vesicle accumulations, representing secretory granules (double arrows). (B) Basolateral microvilli (arrowheads). (C) Basolateral microvilli (arrowhead) (black arrowheads show cell junctions). bm, basement membrane. (D–F) Histology and transmission electron microscopy of duodenal biopsy specimens from patient 2 with variant MVID. (D) Toluidine blue staining shows mild focal villus atrophy. (E) Subapical accumulation of periodic acid–Schiff–positive vesicles in crypt epithelium (double arrows). (F) Microvillus inclusion (arrowhead). (G–L) Fluorescence microscopy showing villus epithelium of duodenal biopsy specimens from (G–I) healthy control and (J–L) MVID patient 2. Controls display proper distribution of (G) actin, (H) STX3, and (I) the apical marker CD10. Biopsy samples from patient 2 show (J) dot- and ring-like actin-rich inclusions (arrowheads), and (K) absence of STX3-staining and (L) cytoplasmic mislocalization of CD10. The apical plasma membrane is marked by arrows, microvillus inclusions are highlighted by arrowheads, and nuclei are counterstained with Hoechst dye.

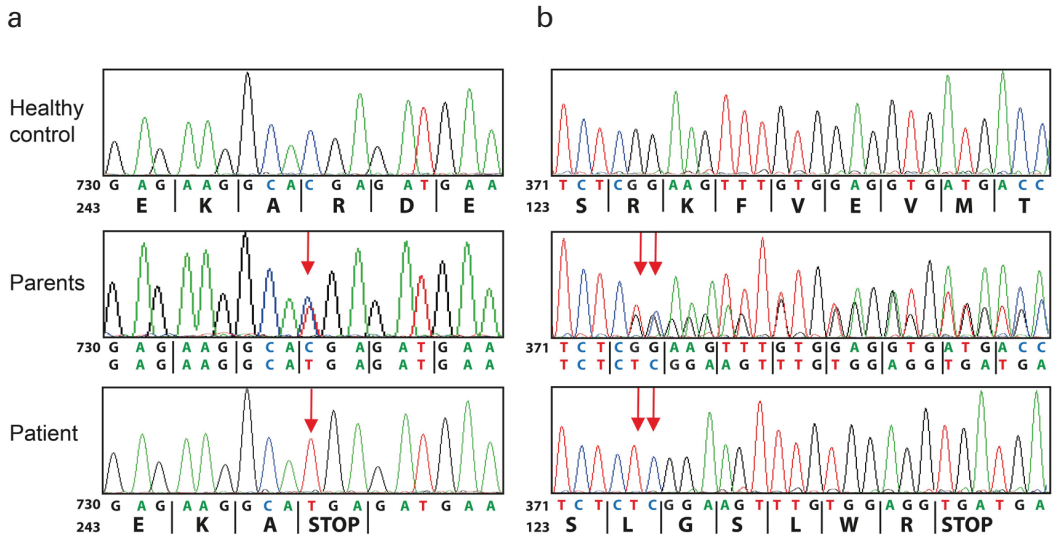

Supplementary Figure 2. Sanger sequencing of STX3 in peripheral blood of healthy controls, parents, and patients. (A) Patient 1: c.739C>T mutation leads to a premature stop at Arg247. (B) Patient 2: 2-bp insertion (c.372_373dup) leads to frameshift and premature stop after Arg130. (C) Western blot for STX3 on organoids from healthy control and patient 1 cultured in expansion medium (EM) or differentiation medium (DM). Representative of 2 samples from patient 1 and 2 controls. HC, healthy control; M, marker.

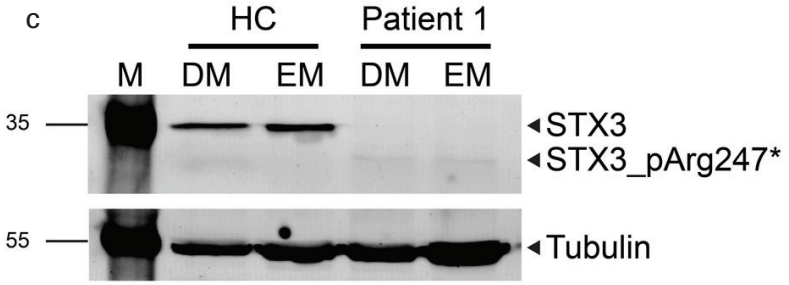

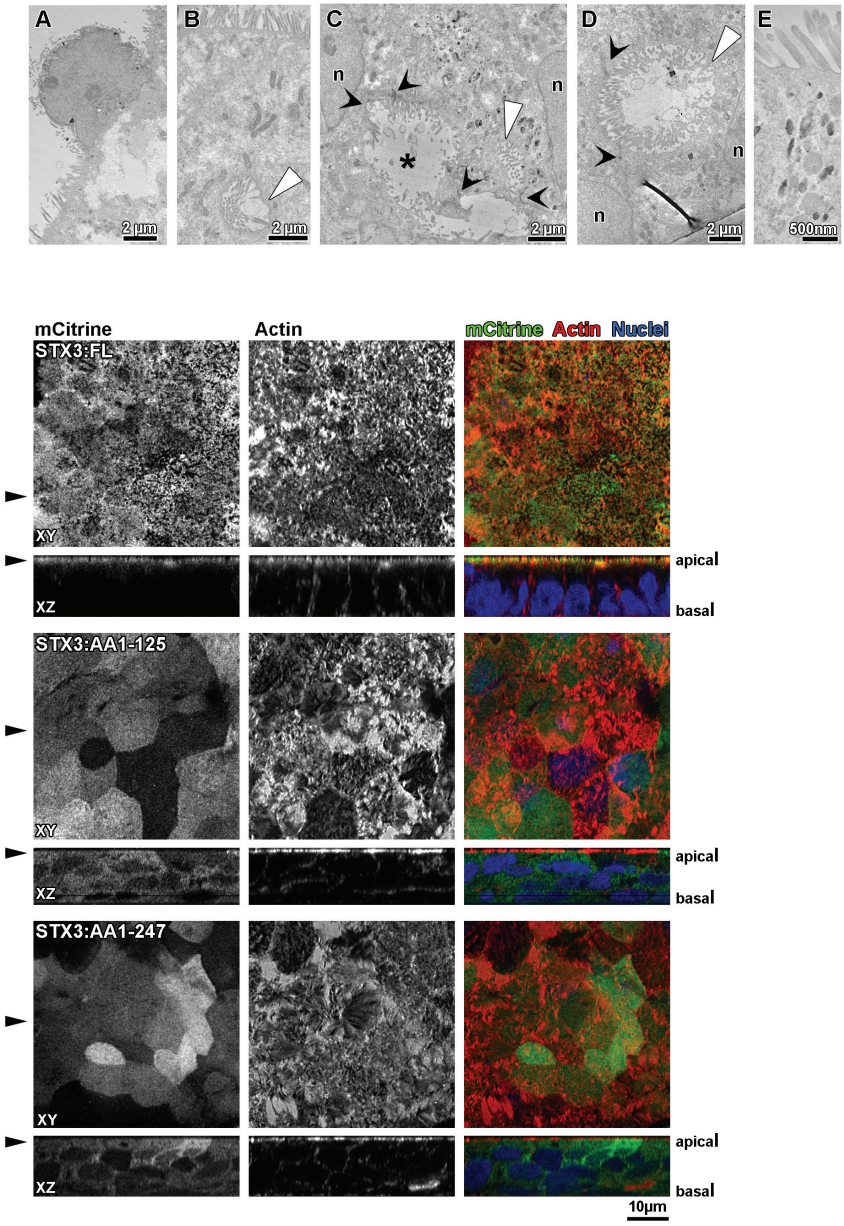

Supplementary Figure 3. (A–E) Transmission electron microscopy of Caco-2 cells stably expressing truncated STX3 (STX3:AA1-247). Cytologic details of STX3:AA1-247. (A) Denuded, shedding cell. (B) Cytoplasmic microvillus inclusion (arrowhead). (C) Pleomorphic intercellular lumen (asterisk) and associated basolateral microvilli (white arrowhead) (black arrowheads show cell junctions). (D) Basolateral microvilli (white arrowhead) (black arrowheads show cell junctions). (E) Subapical vesicles, resembling secretory granules (arrow shows plasma membrane). (F) Confocal fluorescence microscopy of Caco-2 cells, stably expressing mCitrine-STX3:FL (upper), mCitrine-STX3:AA1-125 (middle), and mCitrine-STX3:AA1-247 (lower) fusion proteins in xy and xz projections. Fluorescent signal of mCitrine (left), filamentous actin (middle), and merged channels including nuclear counterstaining (right). STX3:FL and endogenous STX3 localize strictly apically, whereas STX3:AA1-125 and STX3:AA1-247 are found throughout the cytoplasm. Expression of the truncated forms of STX3 results in multilayered growth of Caco-2 cells. Arrowheads on the left side indicate the optical section planes of xy and xz, respectively. Note the reduced apical actin signal in mCitrine-STX3:AA1-247.

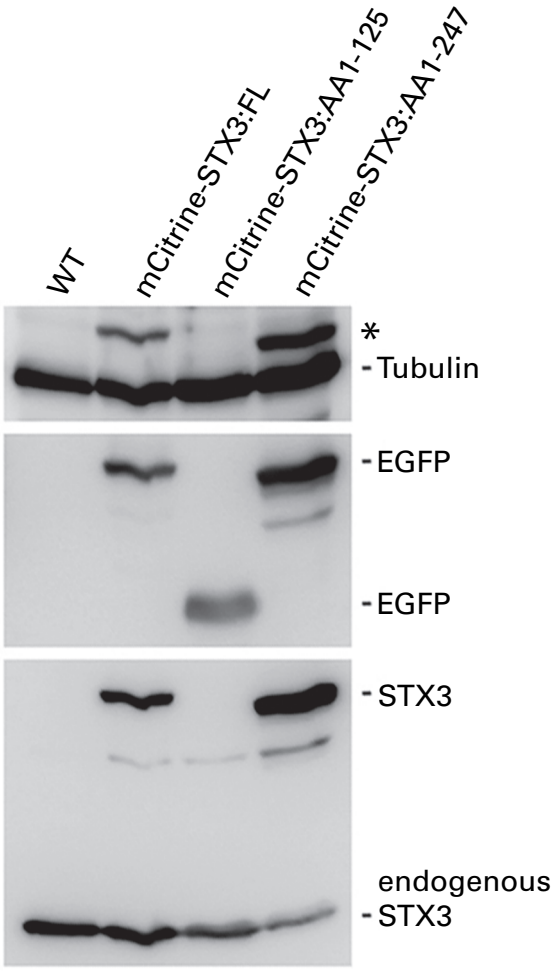

Supplementary Figure 4. Western blot illustrating the overexpression of mCitrine-STX3FL, mCitrineSTX3:AA1-125, and mCitrineSTX3:AA1-247 in Caco-2 cells, compared with untransduced cells (WT). EGFP shows the overexpression via detection of the mCitrine tag. Rabbit anti-STX3 antibody confirms overexpression of the STX3-mCitrine fusion construct (upper STX3 band) as well as endogenous STX3. Endogenous STX3 levels clearly decrease upon overexpression of STX3:AA1-25 and 1-247. Rabbit anti-STX3 antibody does not detect the short STX3:AA1-125. Tubulin was used as loading control (asterisk, unspecific band).

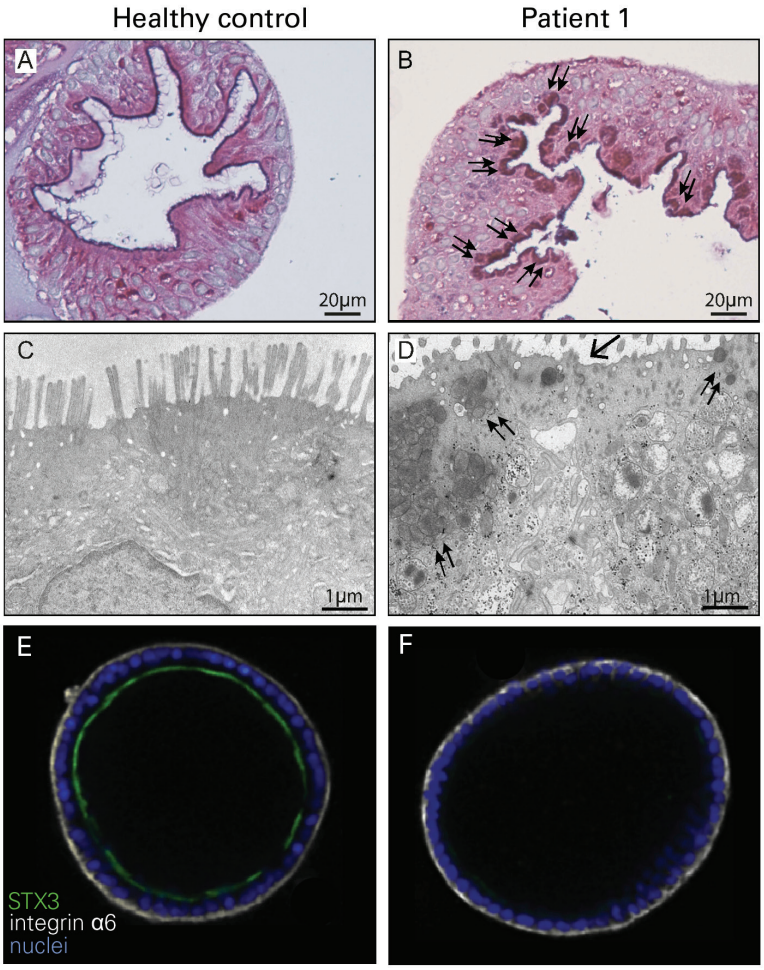

Supplementary Figure 5. Organoids derived from duodenal biopsy specimens from (A, C, and E) healthy control and (B, D, and F) patient 1 were incubated in differentiation medium for 5 days before harvesting. (A) Periodic acid–Schiff staining of apical brush border in the control sample, and (B) subapically accumulating material (double arrows) in the patient sample. Normal brush-border microvilli in (C) control sample contrast with partial loss of microvilli (arrow) and subapical accumulation of vesicles (double arrows) in (D) patient sample. (E and F) Confocal immunofluorescence microscopy shows the localization of STX3 (green) and integrin α6 (basolateral marker; white) in organoids from (E) healthy control and loss of STX3 in (F) patient 1.

CHAPTER 4

APICAL AND INTRACELLULAR TRAFFICKING PROTEINS ARE MISLOCALIZED IN ENTEROCYTES FROM SYNTAXIN 3-MUTANT PATIENTS WITH VARIANT MICROVILLUS INCLUSION DISEASE

Caroline L. Wiegerinck, Kerstin Schneeberger, Anke H.M. van Vugt, Jorik M. van Rijn, Mirjam van Aalderen, Nanda M. Verhoeven-Duif, Rüdiger Adam, Alexander Marx, Katharina Biermann, Johanna C. Escher, Edward E.S. Nieuwenhuis and Sabine Middendorp.

Manuscript in preparation

ABSTRACT

Microvillus inclusion disease (MVID) is a congenital enteropathy characterized by severe diarrhea and dependence on total parental nutrition (TPN). The disease is often caused by a loss-of-function mutation in myosin Vb (*MYO5B*), which results in defective intracellular trafficking in enterocytes and loss of cell polarity. Some patients with a milder clinical phenotype and variable periods of weaning of TPN carry mutations in syntaxin 3 (*STX3*). STX3 is a t-SNARE protein involved in fusion and exocytosis of vesicles to the apical membrane of enterocytes. However, the precise role of STX3 in the pathogenesis of MVID is unknown. Here we show that duodenum of STX3-mutant patients exhibit a disturbed cell organization with multi-layered enterocytes and presence of inclusion bodies in the cytoplasm or basolateral membrane of enterocytes. We found that apical membrane proteins, such as sucrase-isomaltase (SI), were mislocalized in biopsies and patient-derived organoids, while the basolateral proteins Na/K-ATPase and E-cadherin were localized correctly. Notably, the distribution of the intracellular trafficking protein RAB11A and lysosomes was disturbed in these patients. Our results show that STX3 is involved in apical membrane protein trafficking in human intestinal epithelial cells.

INTRODUCTION

Microvillus inclusion disease (MVID) is a severe congenital enteropathy. Patients present with failure to thrive and persistent diarrhea that results in metabolic acidosis and dehydration [1]. For survival, MVID patients need parental nutrition, which is often accompanied with severe complications, such as venal obstruction, sepsis and liver failure. Ultimately, these complications could lead to the necessity of intestinal bowel transplantation [2]. MVID is histologically characterized by villus atrophy and subapical accumulation of Periodic Acid Schiff (PAS) positive secretory-like granules. On electron microscopy, loss of microvilli and inclusion bodies lined with microvilli are identified in villus enterocytes [1, 3-8]. Immunohistochemistry on biopsies of these patients show mislocalization of apical brush border proteins such as CD10, villin-1 and sucrase isomaltase (SI) [9-12].

MVID can be classified into two types based on their clinical presentation: classic MVID, which requires total parental nutrition and a variant form, which allows variable periods of partial weaning of parental nutrition [13-16]. Classic MVID has predominantly been associated with loss-of-function mutations in myosin Vb (*MYO5B*), an accessory motor protein that facilitates vesicle trafficking on F-actin strands [17, 18]. MYO5B can bind to the small GTPase molecules RAB8A and RAB11A, which are associated with intracellular vesicle trafficking [19-21]. Previously, it has been shown that villus enterocytes of MVID patients have a disturbed cell polarity due to mislocalization of apical and basolateral proteins and intracellular trafficking proteins, such as RAB8A, RAB11A, early endosomes (EEA1) and late endosomes (LAMP2) [9-11]. In addition, it has been described that loss of MYO5B results in less stable tight junctions [9, 10].

Recently, we identified that a loss-of-function mutation in syntaxin 3 (*STX3)* was responsible for variant MVID in two patients [15]. STX3 is a target- soluble N-ethylmaleimide-sensitive factor attachment protein receptor (t-SNARE) that is involved in docking and fusion of vesicles to the apical plasma membrane [22-25]. These patients feature similar histological hallmarks as classic MVID, such as variable loss of microvilli, subapical accumulation of PAS-positive vesicles and microvillus inclusions, although we have shown that microvilli were also located on the basolateral site of enterocytes [15]. Apical brush border proteins were mislocalized intracellularly and F-actin positive inclusions were detected in MVID patient biopsies [15]. However, cell polarity and distribution of intracellular trafficking components were not yet studied in these patients. To better understand the role of STX3 in the pathogenesis of MVID, we analysed patient biopsies and generated *in vitro* patient-derived intestinal organoids from the two previously described patients with *STX3* mutations. In addition, we have grown organoids in monolayers [26] and induced differentiation to perform two functional assays: assessment of tight junction assembly by measuring trans epithelial electrical resistance (TEER) and assessment of enzymatic activity of SI at the apical membrane.

METHODS

Study approval

This study was approved by the local medical ethics committee. Written informed consent from participating families was received prior to inclusion. Additional duodenal biopsies for this study were obtained during a diagnostic endoscopy. Healthy control biopsies (n=2) were collected from patients that had an endoscopy for a suspected intestinal disease such as celiac disease, however, showed normal pathology.

Patient description and material

MVID patients included in this study have been extensively described in our previous study [15]. In short, patient 1 is a microvillus inclusion disease patient with a homozygous nonsense mutation in (c.739C>T, p.Arg247*, Ensembl COSM193004) in exon 9 of *STX3*. Patient 2 has a homozygous frame-shifting 2-bp insertion (c.372_373dup, p.Arg125Leufs*7) in exon 6 of *STX3*. Both patients presented with congenital

diarrhoea within the first two weeks after birth and have variable dependency on parental nutrition.

Cell culture

Intestinal organoids were established from isolated crypts derived from patient biopsies, as described previously [27]. In brief, biopsies were washed, incubated in EDTA for crypt detachment and isolated crypts were seeded in matrigel with expansion medium (EM) containing WNT3A, epidermal growth factor (EGF), noggin, R-spondin, A83, SB202190, nicotinamide, N-acetylcysteine and B27. Organoids were passaged weekly in a 1 to 4 ratio. For histological and functional analysis organoids were trypsinized and 2x10^5 cells were seeded in polycarbonate 0.4 µm pore-sized 24-well transwell inserts (Corning), according to an adapted protocol [26]. Organoids seeded for 2D monolayers were cultured in EM with 10 µM Rho-associated protein kinase inhibitor Y-27632 (Sigma-Aldrich) for the first day. Hereafter, organoids were cultured in normal EM medium for 7 days and then harvested or induced for differentiation with differentiation medium (DM: which is EM medium without Wnt, SB202190 and nicotinamide) for 7 days .

Immunofluorescence

Patient-derived paraffin embedded biopsies were provided by the pathology department. The organoids that were cultured in transwell inserts, were fixed in 4% PFA for 30 minutes at room temperature, dehydrated and embedded vertically into paraffin. Five µm thick sections were generated for stainings. For immunofluorescent stainings, slides were deparaffanized to distilled water, subjected to the appropriate heat-mediated antigen retrieval method, Tris/EDTA pH 9.0 or citrate pH 6.0 (DAKO) depending on the antibody used, and blocked in 15% normal goat and/or 15% horse serum in 5% BSA at 4 °C overnight.

Hereafter, slides were incubated with the primary antibody for 2 hours at room temperature, washed and incubated with the fluorescent conjugated secondary antibody for one hour at room temperature, washed in PBS, incubated with DAPI (Sigma) and mounted with Fluorsave mounting medium (Millipore). Some antibodies were labelled with the Zenon Rabbit IgG labelling kit (Life technologies) according to manufacturers protocol in order to co-stain with multiple rabbit antibodies. Stained slides were analysed on a LSM 710 confocal fluorescent microscope (Carl Zeiss) and analyzed with Volocity software version 6.3 (Perkin Elmer). Primary antibodies and dilutions used in this study are listed in Suppl. Table 2.

Cellular junction measurements and calcium-switch assay

In organoid 2D monolayers, trans-epithelial electric resistance (TEER) was measured with an epithelial volt/ohm meter (EVOM, World Precision Instruments, Inc) to measure cellular junction assembly. Ohm measurements were recalculated for cell surface per cm2. Cellular junctions were disassembled by adding 4 mM of the calcium-chelator EGTA to the cultures for 30 minutes at 37 °C. Re-assembly of junctions was induced by adding normal calcium-containing expansion medium. TEER-values were measured every 10 minutes.

Sucrose uptake assay

Sucrose uptake assay was measured adapted from previous literature [28, 29]. Concisely, transwells were preincubated in PBS at 37 °C to ensure no glucose was left in cell cultures. Hereafter, sucrose was added to the apical compartment of a transwell containing an organoid monolayer. Sucrase enzyme activity was assessed by collecting the supernatant of the apical chamber at selected time points. Sucrose is converted to glucose by the sucrase enzyme. The amount of glucose in the supernatant is measured by incubation with a glucose oxidase reagent for 1 hour at 37 °C. Oxidized glucose was measured with a Fluoroskan Ascent 2.5 with excitation and emission spectra of 544 nm and 590 nm, respectively.

RESULTS

Disturbed enterocyte architecture and pERM/Ezrin-positive inclusion bodies in

STX3-deficient patients

First, we studied the general cell architecture and cell polarity of STX3-deficient biopsies and organoids. Since we have shown previously that STX3-mutant patients show aberrancies in enterocytes located in both villi and crypts, we determined expression patterns of several proteins in both entities. Furthermore, organoid cultures were established from duodenal biopsies from STX3-mutant MVID patient 1 and 2 and maintained in expansion medium (EM) as described previously [15, 27]. For experiments, the organoids were seeded in a transwell to form a monolayer and grown in EM for a week before organoids were induced to differentiate by incubation in differentiation medium (DM) for another 7 days. TEER measurements show that monolayers that were maintained in EM for 7 days had TEERs of 90-150 Ω/cm2, which was increased to 700-1200 Ω/cm2 upon differentiation (Suppl. Fig. 1). Until day 11, TEER measurements were similar in organoid monolayers derived from patients and controls. After 11 days of culture, an increase in TEER was detected in STX3-mutant MVID patients compared to healthy controls. Collectively, the TEER measurements confirm that organoids differentiate properly when seeded in a monolayer, and can thus be used for assessment of cellular polarity.

First, we looked at the localization of two apical proteins, Ezrin and phosphorylated Ezrin/Radixin/Moesin-complex (pERM), because of their role in polarity and brush border formation. Ezrin is an apical terminal web protein that provides a platform for microvilli, is linked to the actin-cytoskeleton and is involved in localization of several apical proteins [30]. Phosphorylated Ezrin binds F-actin and is essential for well-formed brush borders of intestinal cells [31-33]. Additionally, the basolateral adherens junction E-cadherin was investigated due to its involvement in maintaining cell polarity [34].

We found that pERM and Ezrin were co-localized at the apical membrane in healthy control and MVID patient 1 and 2, suggesting that the majority of crypt and villus enterocytes maintain correct apical polarity (Figure 1AB). Nonetheless, Ezrin/pERM-positive ring structures that were not located at the apical membrane and as such presumably represent inclusion bodies or basolateral localized microvilli, were observed in villus enterocytes of MVID patient 2 (Figure 1A). In concordance, differentiated organoids of patient 2 contained pERM/Ezrin-positive rings/dots in ~5,7% of the enterocytes, whereas these were observed in only ~0,3% of enterocytes in healthy controls and patient 1 (Figure 1C and Suppl. Table 1).

Next, we determined the localisation of the adherens junction protein E-cadherin, which is confined to the basolateral membrane. Yet, in the biopsy of patient 1, the intensity of E-cadherin staining was immensely diminished compared to patient 2 and healthy controls (Figure 1AB). However, in organoids derived from patient 1, E-cadherin intensity was comparable to controls (Figure 1C), indicating that localisation of E-cadherin is not disturbed by loss of STX3.

In addition to those occasional aberrancies in apical polarity, we observed multi-layering of enterocytes in biopsies and monolayers of STX3-mutant MVID patients. We quantified multi-layering in 2D organoid cultures and found that this phenomenon was predominantly present in patient 2 (88% of cells) and less obvious in patient 1 (23% of cells), while only 12% of the cells in healthy control 2D organoids showed multi-layering (Suppl. Table 1).

Assembly and maintenance of cellular junctions is not defective in STX3-mutant patients.

Next, we assessed maintenance of cell polarity by analysing the disassembly and re-assembly of cellular junctions by means of a calcium-switch assay in organoids [23, 35-38]. Cellular junctions are necessary to provide contact between neighbouring cells and also build up the paracellular barrier of epithelia and control the paracellular transport in epithelia. They are located at the junction between the apical and basolateral membranes and are involved in maintaining epithelial cell polarity. In a calcium-switch assay, cellular junctions were

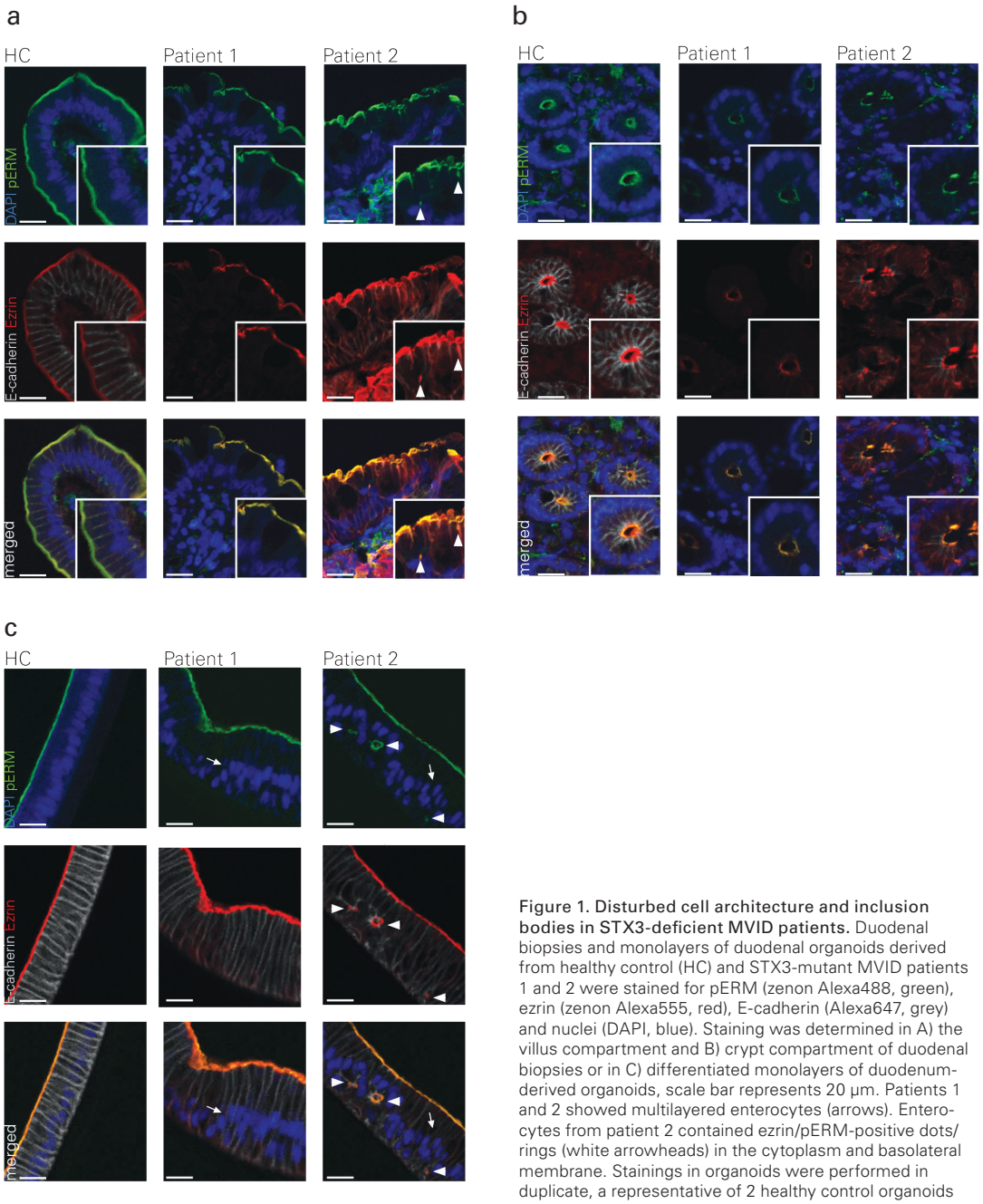

Figure 1. Disturbed cell architecture and inclusion bodies in STX3-deficient MVID patients. Duodenal biopsies and monolayers of duodenal organoids derived from healthy control (HC) and STX3-mutant MVID patients 1 and 2 were stained for pERM (zenon Alexa488, green), ezrin (zenon Alexa555, red), E-cadherin (Alexa647, grey) and nuclei (DAPI, blue). Staining was determined in A) the villus compartment and B) crypt compartment of duodenal biopsies or in C) differentiated monolayers of duodenum-derived organoids, scale bar represents 20 µm. Patients 1 and 2 showed multilayered enterocytes (arrows). Enterocytes from patient 2 contained ezrin/pERM-positive dots/rings (white arrowheads) in the cytoplasm and basolateral membrane. Stainings in organoids were performed in duplicate, a representative of 2 healthy control organoids is shown. D) Response to calcium-switch assay was equal in all organoids derived from healthy controls compared to STX3-mutant patients. The TEER measured during calcium-switch is represented as mean ± SD of 4 independent wells derived from healthy controls (n=2) or patient 1 or 2.

disassembled by calcium-depletion through ethylene glycol tetra-acetic acid (EGTA) and re-established after adding normal calcium-containing medium. Disassembly and re-assembly of cellular junctions were monitored by TEER measurements. We did not observe any difference in disassembly or re-assembly of cellular junctions in patient-derived organoids compared to controls (Figure 1D), indicating that disturbed cell polarity in STX3-mutant MVID patients was not associated with defects in cellular junctions.

Altered expression of Na/K-ATPase and SI in STX3-mutant MVID patients

Previously, it has been shown that enterocytes of classical MYO5B-mutant MVID patients have various mislocalized proteins, such as lysosome-associated membrane protein 1 (LAMP1), sucrase isomaltase (SI), RAB8A, RAB11A and Na/K-ATPase [9-11]. Therefore, we have assessed the localisation of these proteins in STX3-mutant MVID patients.
Analysis of the apical protein SI showed that SI was expressed in the subapical compartments of duodenal biopsies and patient-derived organoids and only partially co-localized with the apical protein Ezrin (Figure 2A-C). In contrast, healthy control organoids showed strict localization to the apical plasma membrane and full co-localization with Ezrin (Figure 2C). Of note, in this image we have enhanced the Ezrin signal twice as bright in patient 1 compared to patient 2 and healthy control to visualize a signal.
The basolateral marker NA/K-ATPase was shown to be both normally and abnormally distributed in different MYO5B-mutant MVID patients [9-11].
We observed normal distribution of Na/K-ATPase in the two STX3-mutant patients, although expression levels were markedly diminished in biopsies of patient 1 and 2, when compared to healthy control (Figure 2AB). In contrast, Na/K-ATPase was expressed in normal levels in patient-derived organoids and was similar to controls (Figure 2C).

STX3-deficient MVID patients show altered distribution of LAMP1

LAMP1, which marks lysosomes and normally accumulates in the subapical region, was distributed more diffusely in the cytoplasm and closer to the supranuclear region in biopsy of patient 2 (Figure 3AB), and in organoids of patient 1 and 2 (Figure 3C).
Although both, SI and LAMP1 showed altered expression in MVID patients, SI did not co-localize with the lysosomal marker LAMP1 (Figure 3A-C), indicating that SI was accumulated intracellularly but not in the lysosomal compartments.

d

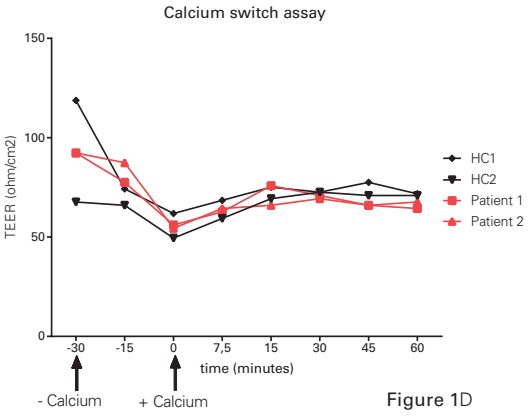

Figure 1D

Intracellular SI partially co-localizes with RAB11A but not RAB8A in STX3-deficient MVID patients

Although SI aggregates did not co-localize with LAMP1, we hypothesised that SI would co-localize with the small GTP-binding protein RAB8A or RAB11A, which regulate apical transport in intestinal cells. Subapical accumulation of apical proteins such as SI had been demonstrated previously in RAB8-deficient mice [39]. In the healthy control biopsy the apical trafficking protein RAB8 was evenly distributed in the cytoplasm of enterocytes in crypt and villi with increased expression at the apical membrane in villus enterocytes. In healthy control and in patients, RAB8A partially co-localized with the apical proteins SI and Ezrin, which was also observed in organoids (data not shown).

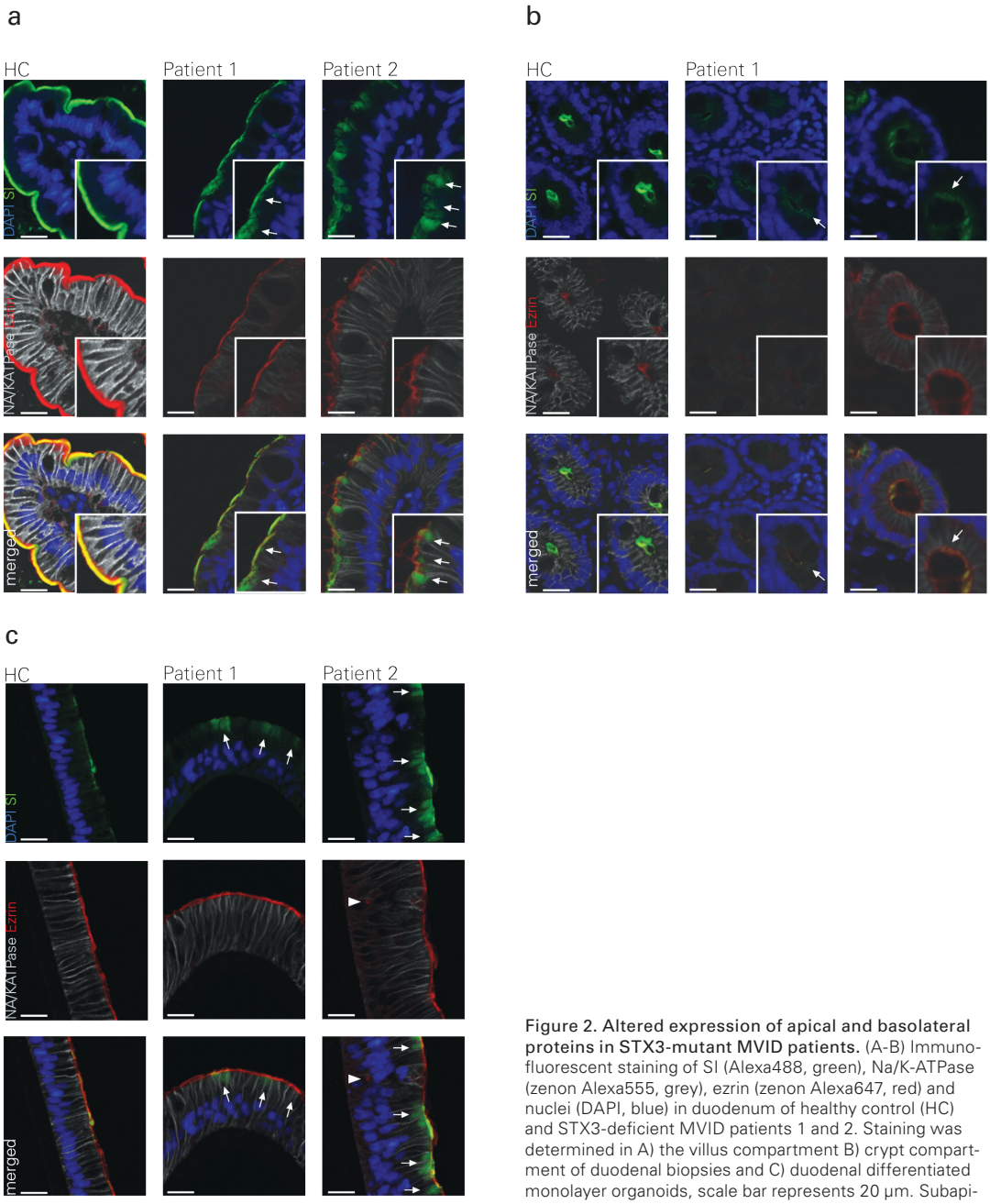

Figure 2. Altered expression of apical and basolateral proteins in STX3-mutant MVID patients. (A-B) Immunofluorescent staining of SI (Alexa488, green), Na/K-ATPase (zenon Alexa555, grey), ezrin (zenon Alexa647, red) and nuclei (DAPI, blue) in duodenum of healthy control (HC) and STX3-deficient MVID patients 1 and 2. Staining was determined in A) the villus compartment B) crypt compartment of duodenal biopsies and C) duodenal differentiated monolayer organoids, scale bar represents 20 µm. Subapical staining of SI was noted in biopsies and organoids of patient 1 and 2 (arrows). Patient 2 showed an ezrin-positive ring (white arrowhead). Note: Ezrin settings for patient 1 were adjusted to twice as bright as the healthy control and patient 2 to maintain a visible signal. Stainings in organoids were performed in duplicate, a representative of 2 healthy control organoids is shown. SI, sucrase isomaltase.

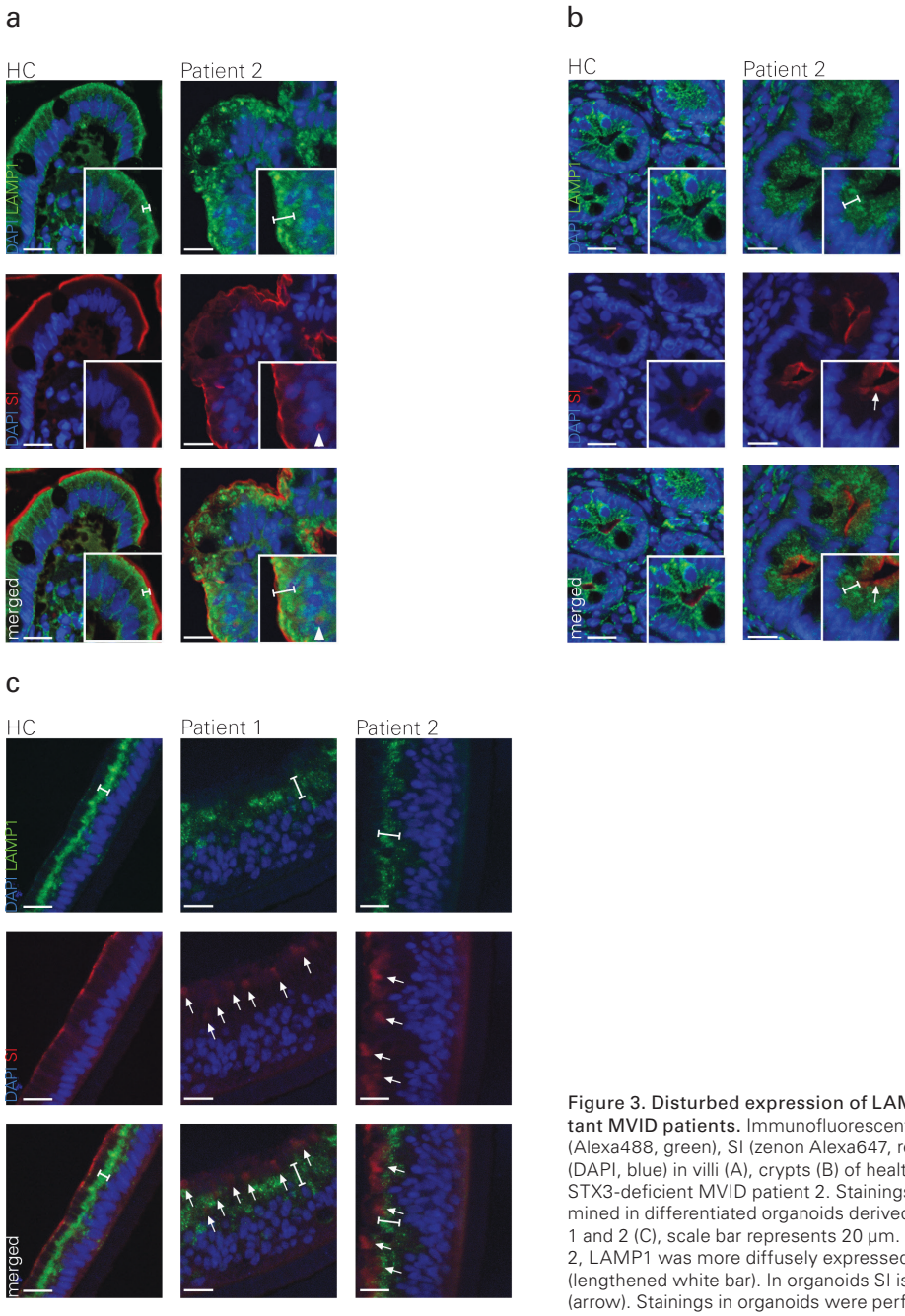

Figure 3. Disturbed expression of LAMP1 in STX3-mutant MVID patients. Immunofluorescent staining of LAMP1 (Alexa488, green), SI (zenon Alexa647, red) and nuclei (DAPI, blue) in villi (A), crypts (B) of healthy control (HC) and STX3-deficient MVID patient 2. Stainings were also determined in differentiated organoids derived from HC, patient 1 and 2 (C), scale bar represents 20 µm. In patient 1 and 2, LAMP1 was more diffusely expressed in the cytoplasm (lengthened white bar). In organoids SI is located subapically (arrow). Stainings in organoids were performed in duplicate, a representative of 2 healthy control organoids is shown. SI, sucrase isomaltase.

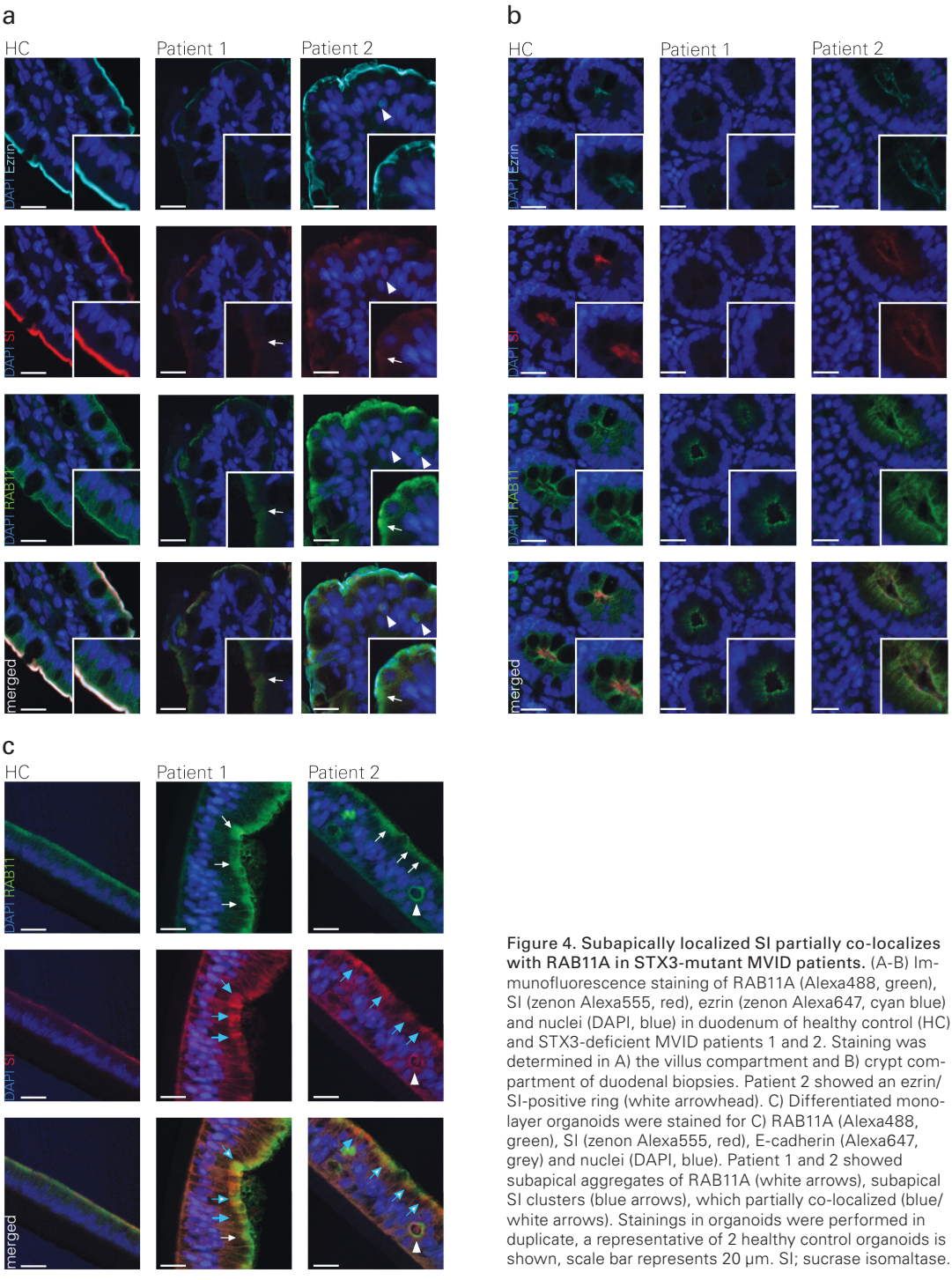

Figure 4. Subapically localized SI partially co-localizes with RAB11A in STX3-mutant MVID patients. (A-B) Immunofluorescence staining of RAB11A (Alexa488, green), SI (zenon Alexa555, red), ezrin (zenon Alexa647, cyan blue) and nuclei (DAPI, blue) in duodenum of healthy control (HC) and STX3-deficient MVID patients 1 and 2. Staining was determined in A) the villus compartment and B) crypt compartment of duodenal biopsies. Patient 2 showed an ezrin/SI-positive ring (white arrowhead). C) Differentiated monolayer organoids were stained for C) RAB11A (Alexa488, green), SI (zenon Alexa555, red), E-cadherin (Alexa647, grey) and nuclei (DAPI, blue). Patient 1 and 2 showed subapical aggregates of RAB11A (white arrows), subapical SI clusters (blue arrows), which partially co-localized (blue/white arrows). Stainings in organoids were performed in duplicate, a representative of 2 healthy control organoids is shown, scale bar represents 20 µm. SI; sucrase isomaltase.

Another small GTP-binding protein that is well known for its role in apical membrane trafficking is RAB11A. It has been shown to be involved in maintenance of apical microvilli and apical localization of STX3 [40]. SI transport to the apical membrane has been demonstrated to involve RAB11A [41]. In healthy controls, RAB11A was distributed evenly in the cytoplasm, with intensified expression at the apical border of the intestine in both crypt and villus (Figure 4AB). However, in biopsies of patient 1 and 2 RAB11A-positive clusters were noticed subapically of the plasma membrane (Figure 4AB). This phenomenon was also detected in patient-derived organoids, where RAB11A partially co-localized with subapical SI clusters (Figure 4C).
Our data suggest that STX3 is involved in localization of RAB11A and that SI is partially transported by RAB11A trafficking proteins.

Sucrase function is not affected in organoids derived from STX3-mutant MVID patients

In Figure 2A, we noticed subapically and occasionally apically located clusters of SI in STX3-mutant MVID patient-derived organoids. Additionally, STX3-mutant MVID patients partially tolerate minimal enteral feeding next to parental nutrition[15]. To determine the potentially residual enzymatic activity of SI, we investigated the function of the apical brush-border enzyme SI in organoid monolayers after adding sucrose to the apical compartment [28, 29]. To assess enzyme activity of the brush border protein SI in STX3 patients we adapted the described assay for differentiated organoids. We found no differences in SI metabolism at the apical surface of enterocytes, indicating that the low amount of SI that is expressed on the apical membrane is sufficient to digest sucrose (Suppl. Figure 2). We also depicted SI activity for undifferentiated organoids as a negative control.

DISCUSSION

MVID is clinically characterized by severe congenital diarrhea with dehydration and the inability to take up nutrients from an enteral diet. The current therapy comprises rehydration therapy and parenteral feeding [1]. Although most MVID patients carry a mutation in the *MYO5B* gene, the type of mutations associated with this gene are very heterogeneous [18, 42]. In addition, our previous data show that a variant form of MVID is caused by a mutation in *STX3* [15]. Both MYO5B and STX3 are involved in trafficking of apical proteins. Several studies have examined different MYO5B-deficient patients and indeed identified an altered distribution of apical proteins such as SI, DPPIV, RAB8 and RAB11A in intestinal biopsies [9-11]. More recently, mislocalization of basolateral proteins such as Na/K-ATPase, E-cadherin and transferrin has been demonstrated in MYO5B-mutant MVID patients [9, 10].

In this study, we assessed if similar aberrations could be identified in the MVID patients with mutations in *STX3*. We demonstrated that overall cell polarity is maintained in STX3-deficient patients, shown by apical localization of Ezrin (both native and phosphorylated form) and basolateral localization of E-cadherin and Na/K-ATPase. In addition, a calcium switch assay, which represents cellular junction assembly, did not show any differences in organoids derived from healthy controls or STX3-mutant patients. Nonetheless, we did observe an increase in intracellular pERM/Ezrin-positive rings, most evident in patient 2, which are suggestive for microvillus inclusion bodies.

Our data indicate that STX3 is involved in apical protein trafficking in human intestinal cells, which is in concordance with previous studies in Caco2 cell lines [22, 43] and Madin-Darby Canine Kidney cell lines [25]. Moreover, we observed altered distribution of the lysosomal compartment, which was also noted in MYO5B-deficient patients [9]. We found that STX3 is involved in enterocyte polarity by means of preventing multi-layering of enterocytes and localisation of some apical proteins, such as SI. Loss of function of STX3 results in formation of pERM/Ezrin-containing inclusions either in the cytoplasm or on the basolateral membranes. However, STX3 is not involved in

proper assembly of cellular junctions or localisation of the basolateral proteins E-cadherin and Na/K-ATPase.

ACKNOWLEDGMENTS

We thank the pediatric gastroenterologist of the UMC Utrecht, Erasmus MC Rotterdam and University Medical Center Mannheim for performing endoscopies and obtaining duodenal biopsies and Ans Geboers for assistance with the disaccharidase assay.

1. Ruemmele, F.M., J. Schmitz, and O. Goulet, Microvillous inclusion disease (microvillous atrophy). Orphanet J Rare Dis, 2006. 1: p. 22.
2. Ruemmele, F.M., et al., New perspectives for children with microvillous inclusion disease: early small bowel transplantation. Transplantation, 2004. 77(7): p. 1024-8.
3. Phillips, A.D., et al., Congenital microvillous atrophy: specific diagnostic features. Arch Dis Child, 1985. 60(2): p. 135-40.
4. Lake, B.D., Microvillus inclusion disease: specific diagnostic features shown by alkaline phosphatase histochemistry. J Clin Pathol, 1988. 41(8): p. 880-2.
5. Cutz, E., et al., Microvillus inclusion disease: an inherited defect of brush-border assembly and differentiation. N Engl J Med, 1989. 320(10): p. 646-51.
6. Phillips, A.D. and J. Schmitz, Familial microvillous atrophy: a clinicopathological survey of 23 cases. J Pediatr Gastroenterol Nutr, 1992. 14(4): p. 380-96.
7. Sherman, P.M., D.J. Mitchell, and E. Cutz, Neonatal enteropathies: defining the causes of protracted diarrhea of infancy. J Pediatr Gastroenterol Nutr, 2004. 38(1): p. 16-26.
8. Reinshagen, K., et al., Pathophysiology in Microvillus inclusion disease. Z Gastroenterol, 2006. 44(8): p. 667-71.
9. Thoeni, C.E., et al., Microvillus inclusion disease: loss of Myosin vb disrupts intracellular traffic and cell polarity. Traffic, 2014. 15(1): p. 22-42.
10. Knowles, B.C., et al., Myosin Vb uncoupling from RAB8A and RAB11A elicits microvillus inclusion disease. J Clin Invest, 2014. 124(7): p. 2947-62.
11. Ameen, N.A. and P.J. Salas, Microvillus inclusion disease: a genetic defect affecting apical membrane protein traffic in intestinal epithelium. Traffic, 2000. 1(1): p. 76-83.
12. Groisman, G.M., M. Amar, and E. Livne, CD10: a valuable tool for the light microscopic diagnosis of microvillous inclusion disease (familial microvillous atrophy). Am J Surg Pathol, 2002. 26(7): p. 902-7.
13. Croft, N.M., et al., Microvillous inclusion disease: an evolving condition. J Pediatr Gastroenterol Nutr, 2000. 31(2): p. 185-9.
14. Iancu, T.C., et al., Microvillous inclusion disease: ultrastructural variability. Ultrastruct Pathol, 2007. 31(3): p. 173-88.
15. Wiegerinck, C.L., et al., Loss of syntaxin 3 causes variant microvillus inclusion disease. Gastroenterology, 2014. 147(1): p. 65-68 e10.
16. Cutz, E., P.M. Sherman, and G.P. Davidson, Enteropathies associated with protracted diarrhea of infancy: clinicopathological features, cellular and molecular mechanisms. Pediatr Pathol Lab Med, 1997. 17(3): p. 335-68.
17. Golachowska, M.R., D. Hoekstra, and I.S.C. van, Recycling endosomes in apical plasma membrane domain formation and epithelial cell polarity. Trends Cell Biol, 2010. 20(10): p. 618-26.
18. Muller, T., et al., MYO5B mutations cause microvillus inclusion disease and disrupt epithelial cell polarity. Nat Genet, 2008.

40(10): p. 1163-5.
19. Hales, C.M., J.P. Vaerman, and J.R. Goldenring, Rab11 family interacting protein 2 associates with Myosin Vb and regulates plasma membrane recycling. J Biol Chem, 2002. 277(52): p. 50415-21.
20. Roland, J.T., et al., Myosin Vb interacts with Rab8a on a tubular network containing EHD1 and EHD3. Mol Biol Cell, 2007. 18(8): p. 2828-37.
21. Lapierre, L.A., et al., Myosin vb is associated with plasma membrane recycling systems. Mol Biol Cell, 2001. 12(6): p. 1843-57.
22. Delgrossi, M.H., et al., Human syntaxin 3 is localized apically in human intestinal cells. J Cell Sci, 1997. 110 (Pt 18): p. 2207-14.
23. Sharma, N., et al., Apical targeting of syntaxin 3 is essential for epithelial cell polarity. J Cell Biol, 2006. 173(6): p. 937-48.
24. ter Beest, M.B., et al., The role of syntaxins in the specificity of vesicle targeting in polarized epithelial cells. Mol Biol Cell, 2005. 16(12): p. 5784-92.
25. Low, S.H., et al., The SNARE machinery is involved in apical plasma membrane trafficking in MDCK cells. J Cell Biol, 1998. 141(7): p. 1503-13.
26. VanDussen, K.L., et al., Development of an enhanced human gastrointestinal epithelial culture system to facilitate patient-based assays. Gut, 2014.
27. Sato, T., et al., Long-term expansion of epithelial organoids from human colon, adenoma, adenocarcinoma, and Barrett's epithelium. Gastroenterology, 2011. 141(5): p. 1762-72.
28. Dahlqvist, A., Assay of intestinal disaccharidases. Anal Biochem, 1968. 22(1): p. 99-107.
29. Ferruzza, S., et al., A protocol for in situ enzyme assays to assess the differentiation of human intestinal Caco-2 cells. Toxicol In Vitro, 2012. 26(8): p. 1247-51.
30. Saotome, I., M. Curto, and A.I. McClatchey, Ezrin is essential for epithelial organization and villus morphogenesis in the developing intestine. Dev Cell, 2004. 6(6): p. 855-64.
31. ten Klooster, J.P., et al., Mst4 and Ezrin induce brush borders downstream of the Lkb1/Strad/Mo25 polarization complex. Dev Cell, 2009. 16(4): p. 551-62.
32. Morales, F.C., et al., Ezrin-radixin-moesin (ERM)-binding phosphoprotein 50 organizes ERM proteins at the apical membrane of polarized epithelia. Proc Natl Acad Sci U S A, 2004. 101(51): p. 17705-10.
33. Dhekne, H.S., et al., Myosin Vb and Rab11a regulate phosphorylation of ezrin in enterocytes. J Cell Sci, 2014. 127(Pt 5): p. 1007-17.
34. Desai, R.A., et al., Cell polarity triggered by cell-cell adhesion via E-cadherin. J Cell Sci, 2009. 122(Pt 7): p. 905-11.
35. Hurd, T.W., et al., Direct interaction of two polarity complexes implicated in epithelial tight junction assembly. Nat Cell Biol, 2003. 5(2): p. 137-42.
36. Yeh, T.Y., et al., Tankyrase recruitment to the lateral membrane in polarized epithelial cells: regulation by cell-cell contact and protein poly(ADP-ribosyl)ation. Biochem J, 2006. 399(3): p. 415-25.
37. Tokunaga, Y., et al., A novel monoclonal antibody against the second extracellular loop of occludin disrupts epithelial cell polarity. J Histochem Cytochem, 2007. 55(7): p. 735-44.
38. Balda, M.S., et al., Assembly of the tight junction: the role of diacylglycerol. J Cell Biol, 1993. 123(2): p. 293-302.
39. Sato, T., et al., The Rab8 GTPase regulates apical protein localization in intestinal cells. Nature, 2007. 448(7151): p. 366-9.
40. Knowles, B.C., et al., Rab11a regulates Syntaxin 3 localization and microvillus assembly in enterocytes. J Cell Sci, 2015.
41. Cramm-Behrens, C.I., M. Dienst, and R. Jacob, Apical cargo traverses endosomal compartments on the passage to the cell surface. Traffic, 2008. 9(12): p. 2206-20.
42. van der Velde, K.J., et al., An overview and online registry of microvillus inclusion disease patients and their MYO5B mutations. Hum Mutat, 2013. 34(12): p. 1597-605.
43. Breuza, L., J. Fransen, and A. Le Bivic, Transport and function of syntaxin 3 in human epithelial intestinal cells. Am J Physiol Cell Physiol, 2000. 279(4): p. C1239-48.

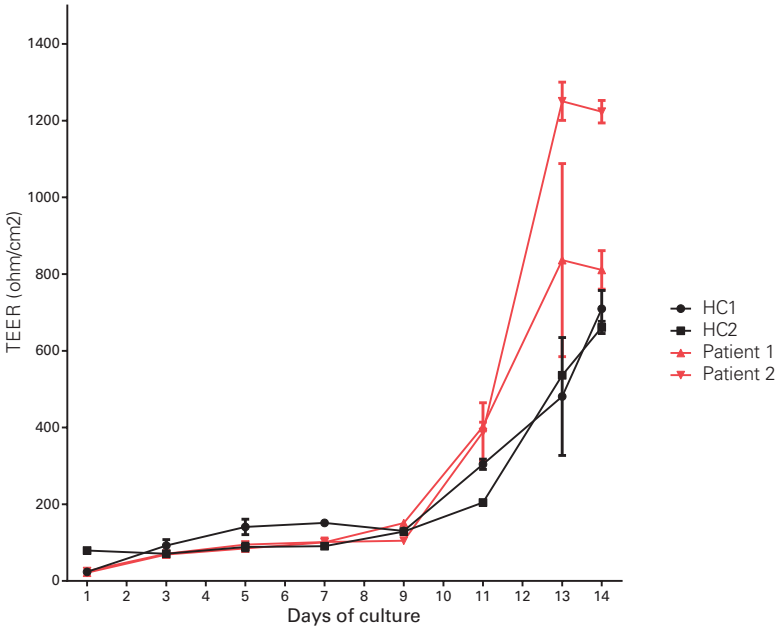

Supplementary Figure 1. TEER measurements of cultured differentiated organoids. TEER levels are represented as mean ± SD of two independent wells per healthy control (HC) or patient 1 and 2.

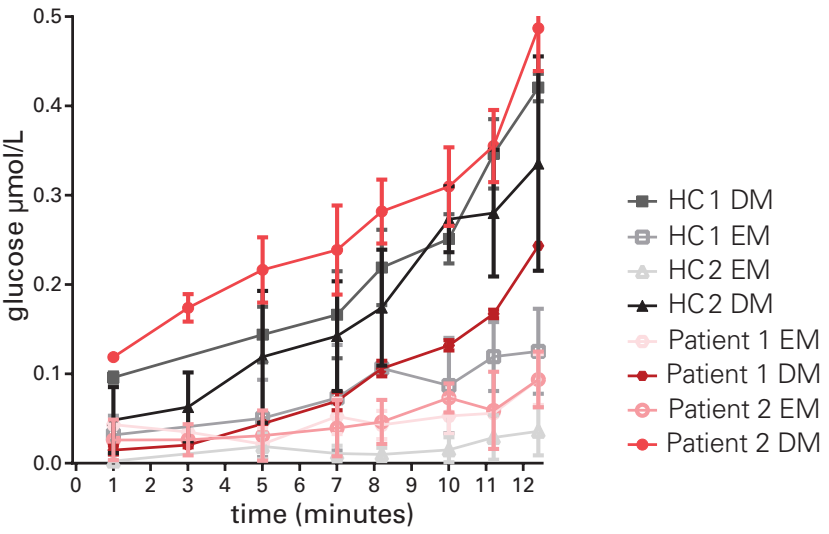

Supplementary Figure 2. Sucrase activity in cultured organoids. Sucrase activity was measured in organoids cultured in differentiation medium (DM) and expansion medium (EM). Sucrase activity is depicted as mean ± SD of two independent cultured organoid wells derived from healthy controls (HC) (n=2), patient 1 and 2.

Supplementary table 1. Summary of the statistical analysis of organoids derived from healthy control or STX3-mutant patient 1 and 2.

	% multilayer	nr of cells analyzed	*P* value	% pERM/ezrin+ rings/dots	*P* value
healthy control (n=2)	Mean, 12,1%	~ 1360 cells		Mean, 0,29%	
STX3-mutant patient 1	Mean, 23,5%	~ 725 cells	<.0001	Mean, 0,28%	NS
STX3-mutant patient 2	Mean, 88,1%	~ 1020 cells	<.0001	Mean, 5,69%	<.0001
	Fluorescence microscopy			Fluorescence microscopy	

Two healthy controls and patient 1 and 2 were analyzed for multilayered enterocytes and pERM/ezrin positive dots or rings suggestive for inclusion bodies. Experiments were performed in duplicate. P value is analyzed with fisher-exact test (2-tailed) relative to the healthy control organoids. NS = not-significant.

Supplementary table 2. Antibodies used for Immunohistochemistry and immunofluorescence

Antibody	Company	Catalogue number	Antigen retrieval	Dilution	Incubation
Anti-ezrin	Abcam	ab41672	Citrate pH6	1/100	2 hrs; RT
Anti-pERM	Cell Signalling	3149S	Citrate pH6	1/200	2 hrs; RT
Anti-Rab8a	BD	610845	Tris-EDTA pH9	1/100	2 hrs; RT
Anti-Rab11a	Invitrogen	71-5300	Citrate pH6	1/50	2 hrs; RT
Anti-Lamp1	Abcam	ab24170	Citrate pH6	1/100	2 hrs; RT
Anti-Na/K-ATPase	Millipore	05-369	Tris-EDTA pH9 or Citrate pH6	1/50	2 hrs; RT
Anti-E-cadherin-647	BD	560062	Tris-EDTA pH9 or Citrate pH6	1/50	2 hrs; RT
Anti-SI	Sigma	HPA011897	Citrate pH6	1/100	2 hrs; RT
Goat anti-rabbit Alexafluor488	Life technologies	A11070		1/400	1 hr; RT
Donkey anti-mouse Alexafluor568	Life technologies	A10037		1/400	1 hr; RT

CHAPTER 5

A FUNCTIONAL CFTR ASSAY USING PRIMARY CYSTIC FIBROSIS INTESTINAL ORGANOIDS

CHAPTER 5

Johanna F Dekkers, Caroline L Wiegerinck, Hugo R de Jonge, Inez Bronsveld, Hettie M Janssens, Karin M de Winter-de Groot, Arianne M Brandsma, Nienke W M de Jong, Marcel J C Bijvelds, Bob J Scholte, Edward E S Nieuwenhuis, Stieneke van den Brink, Hans Clevers, Cornelis K van der Ent, Sabine Middendorp and Jeffrey M Beekman

Nature Medicine 2013;19:939-945

ABSTRACT

We recently established conditions allowing for long-term expansion of epithelial organoids from intestine, recapitulating essential features of the in vivo tissue architecture. Here we apply this technology to study primary intestinal organoids of people suffering from cystic fibrosis, a disease caused by mutations in *CFTR*, encoding cystic fibrosis transmembrane conductance regulator. Forskolin induces rapid swelling of organoids derived from healthy controls or wild-type mice, but this effect is strongly reduced in organoids of subjects with cystic fibrosis or in mice carrying the Cftr F508del mutation and is absent in *Cftr*-deficient organoids. This pattern is phenocopied by CFTR-specific inhibitors. Forskolin-induced swelling of *in vitro*–expanded human control and cystic fibrosis organoids corresponds quantitatively with forskolin-induced anion currents in freshly excised *ex vivo* rectal biopsies. Function of the CFTR F508del mutant protein is restored by incubation at low temperature, as well as by CFTR-restoring compounds. This relatively simple and robust assay will facilitate diagnosis, functional studies, drug development and personalized medicine approaches in cystic fibrosis.

INTRODUCTION

CFTR functions as an anion channel and is essential for fluid and electrolyte homeostasis at the epithelial surfaces of many organs, including the lung and intestine. Cystic fibrosis is caused by mutations in the *CFTR* gene [1-3], and disease expression is highly variable between individuals (http://www.cftr2.org/). People with cystic fibrosis have a median life expectancy of approximately 40 years and accumulate viscous mucus in the pulmonary and gastrointestinal tract, which is associated with bacterial infections, aberrant inflammation and malnutrition [4]. Over 1,900 *CFTR* mutations have been identified, but the most dominant mutation (accounting for ~67% of the total mutant alleles worldwide) is a deletion of phenylalanine at position 508 (CFTR F508del) (http://www.genet.sickkids.on.ca/). This causes misfolding, endoplasmic reticulum retention and early degradation of the CFTR protein that prevents its function at the plasma membrane [5]. Other *CFTR* mutations also impair protein folding or production, gating, conductance, splicing or interactions with other proteins [6].

Current therapies for cystic fibrosis are mainly symptomatic and focus on reducing bacterial pressure and inflammation and normalizing nutrient uptake and physical growth. Multiple compounds have been identified recently that target mutation-specific defects of the CFTR protein itself [6,7]. Current clinical trials that target the basic defect aim to (i) induce premature stop codon readthrough, (ii) correct plasma membrane trafficking of CFTR (correctors) and (iii) enhance CFTR gating (potentiators). A phase 3 clinical trial has been successfully completed using the potentiator VX-770 (ivacaftor, Kalydeco) in subjects with the CFTR G551D mutation, demonstrating that mutation-specific drug targeting is feasible [8]. Combination therapy using a corrector (VX-809) and a potentiator (VX-770) is currently being assessed in a phase 2 clinical trial for subjects harboring the CFTR F508del mutation.

Although CFTR-specific drug targeting is promising, the amount of functional CFTR restoration is still limited [9-11]. In addition, subjects show variable responses to these therapies due to undefined mechanisms [8,12-14], suggesting that the ability to predict individual drug responses would facilitate clinical efficacy and drug registration. Together this indicates that development of new compounds and screening of drug efficacy at the level of the individual are urgently needed. Thus far, limited primary cell models are available to screen for compounds that restore the function of mutant CFTR proteins. When such an *in vitro* model can be further expanded to analyze the drug responses of individual subjects, it may improve drug efficacy by selecting drug-responsive subgroups.

Here we demonstrate a rapid and quantitative assay for CFTR function in a mouse and human primary intestinal culture method that was recently developed [15-17]. The culture enables intestinal stem cells to expand into closed organoids containing crypt-like structures and an internal lumen lined by differentiated cells, recapitulating the *in vivo* tissue architecture. Intestinal CFTR is predominantly expressed at the apical membrane of the crypt cells, where its activation drives the secretion of electrolytes and fluids [18-20]. We found that forskolin [21] induces a rapid swelling of both human healthy control and mouse wild-type organoids that depends completely on CFTR, as demonstrated by analysis of intestinal organoids from *Cftr*^{tm1Cam} knockout (*Cftr*$^{-/-}$) mice or individuals with cystic fibrosis. Forskolin-induced swelling by *in vitro*–expanded rectal organoids is comparable to the forskolin-induced anion currents measured in *ex vivo* human rectal biopsies. Restoration of the function of CFTR F580del mutant protein using low temperature or chemicals was easily detected by organoid-based fluid transport measurements, and responses to CFTR-restoring drugs were variable between organoids derived from different subjects homozygous for F508del. This robust assay is the first functional readout developed in human organoids, to our knowledge, and will facilitate diagnosis, functional studies, drug development and personalized medicine in cystic fibrosis.

Figure 1. Quantification of forskolin-induced mouse organoid swelling.
(a) Light microscopy analysis of organoids stimulated with forskolin or DMSO. Representative examples at the indicated time points after the start of stimulation are shown. (b) Fluorescence confocal image of a calcein green–labeled organoid with object recognition (green line) by image analysis software. (c) Representative example of a forskolin-stimulated calcein green–labeled organoid. Differential interference contrast (DIC) and fluorescence were imaged using live-cell confocal microscopy. Surface areas, expressed as percentages relative to that at t = 0 (100%), are indicated in the top-left corners. (d) The surface area relative to that at t = 0 (normalized area) of all responding individual organoids from a single well. (e) The total organoid surface area normalized to that at t = 0 from three independent wells. The average response of the individual wells is indicated in black (mean ± s.e.m.). (f) Dose-dependent increase of surface area by forskolin. Each line represents the average response from three individual wells as shown in e (mean ± s.e.m.). Scale bars (a–c), 30 μm. All results are representative of at least three independent experiments.

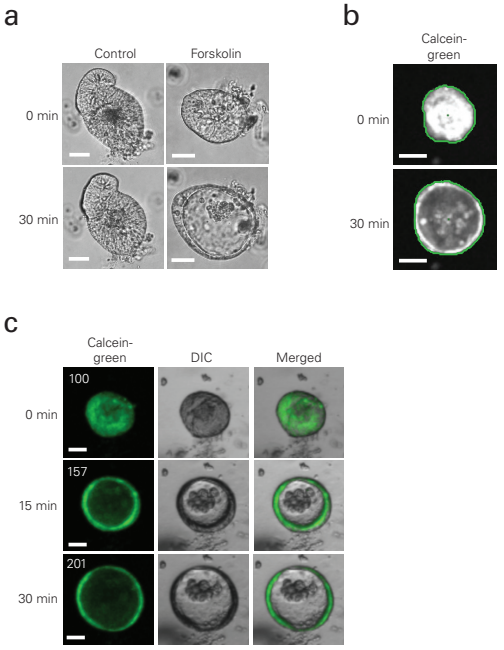

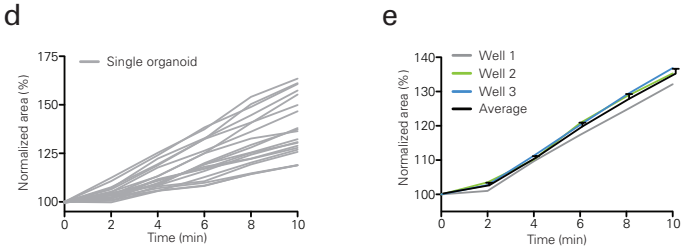

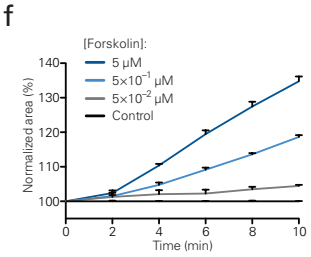

Figure 2. Forskolin-induced swelling of mouse organoids is Cftr dependent.
(a) Normalized swelling curves of forskolin-stimulated calcein green–labeled organoids preincubated with DMSO, CFTRinh-172, GlyH-101 or both CFTRinh-172 and GlyH-101 (mean ± s.e.m.). (b,c) Representative confocal microscopy images (b) and quantification of swelling (mean ± s.e.m.) (c) of calcein green–labeled *Cftr*−/− organoids and corresponding wild-type organoids in response to forskolin. Scale bars, 50 µm. (d,e) Similar to b and c but for F508del Cftr organoids (mean ± s.e.m.). Scale bars, 50 µm. (f) Forskolin-induced swelling of calcein green–labeled F508del Cftr organoids cultured for 24 h at 37 °C or 27 °C with or without CFTR inhibition (mean ± s.e.m.). (g) Normalized forskolin-induced swelling of F508del Cftr organoids pretreated for 24 h with DMSO, VRT-325, Corr-4a or both correctors with or without CFTR inhibition (mean ± s.e.m.). Note that the timescale in f and g is larger than elsewhere in the figure. All results are representative of at least three independent experiments.

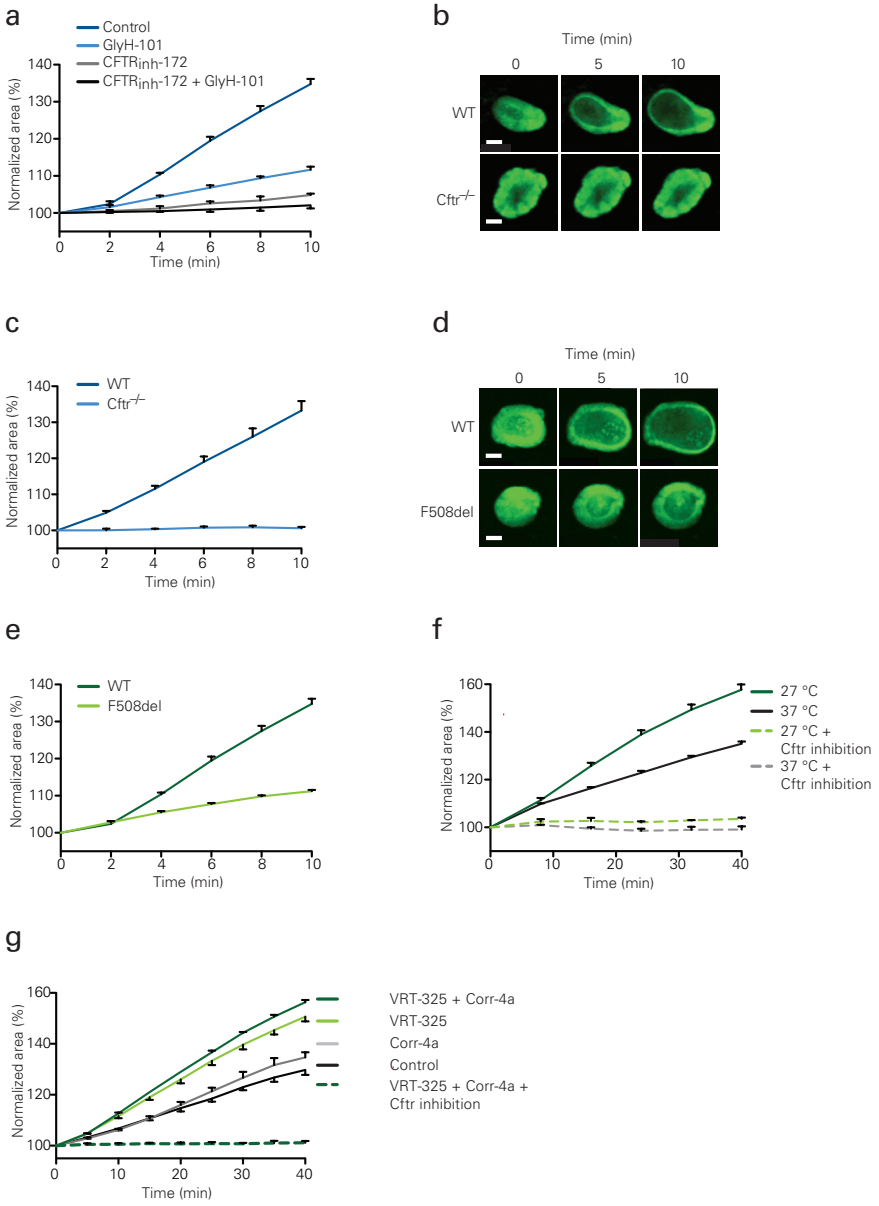

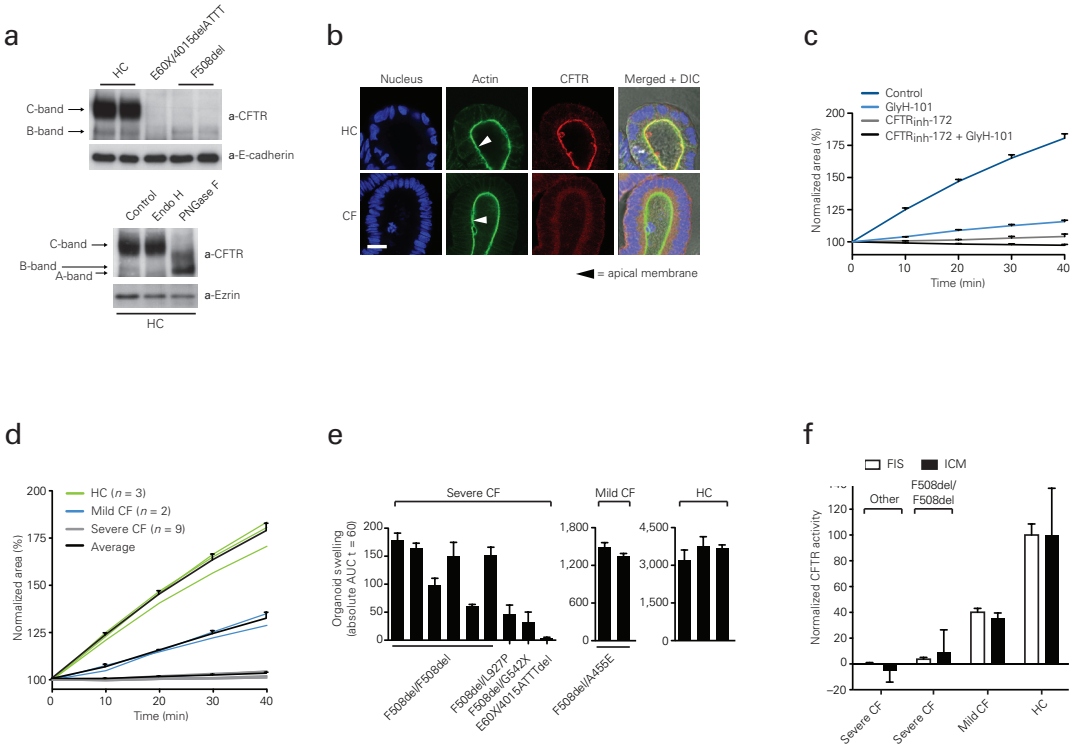

Figure 3. Forskolin-induced swelling in human organoids is CFTR dependent.
(a) Western blot analysis of CFTR and E-cadherin (loading control) expression in human rectal healthy control (HC; n = 2), E60X 4015delATTT (n = 1) and homozygous F508del CFTR (n = 2) organoids (top) and CFTR and ezrin (loading control) expression in whole-cell lysates of human rectal organoids that were either not treated (control) or treated with the deglycosylation enzyme Endo H or PNGase F (bottom). (b) CFTR detection by the monoclonal antibody to CFTR M3A7 in a healthy control and F508del CFTR organoid co-stained with phalloidin-FITC (actin) and DAPI (nucleus). DIC and fluorescence were imaged using confocal microscopy. Scale bars, 20 µm. CF, cystic fibrosis. The arrowheads indicate the apical membrane. (c) Quantification of forskolin-induced healthy control organoid swelling after preincubation with DMSO, CFTRinh-172, GlyH-101 or both CFTRinh-172 and GlyH-101 (mean ± s.e.m.). (d) Forskolin-induced swelling of rectal organoids derived from three individual healthy controls, two individuals with a mild cystic fibrosis genotype (F508del A455E) and nine individuals with a severe cystic fibrosis genotype (one individual with E60X 4015ATTTdel, one with F508del G542X, one with F508del L927P and six with F508del F508del). The average swelling in the different groups is indicated in black (mean ± s.e.m.). (e) FIS responses of organoids from healthy controls or subjects with cystic fibrosis expressed as the absolute area under the curve (AUC) calculated from the time periods shown in d (baseline = 100%, t = 60 min). Each bar represents AUC values averaged from at least three independent experiments per individual (mean ± s.e.m.). (f) Comparison of CFTR activity measured by FIS of organoids from healthy controls and subjects with cystic fibrosis or by ICMs of the corresponding rectal biopsies. ICM bars of the different indicated groups represent forskolin-induced CFTR-dependent cumulative chloride secretion (µA cm−2) relative to the average healthy control response (set at 100%). FIS bars represent FIS expressed as the AUC averaged from at least three independent experiments per individual as shown in f relative to the average healthy control response (100%). (Healthy controls, n = 3; mild cystic fibrosis, n = 2; severe cystic fibrosis (F508del F508del), n = 5; severe cystic fibrosis (other; E60X 4015ATTTdel and F508del G542X), n = 2; mean ± s.d.). All results are representative of at least three independent experiments. ICMs were performed on four rectal biopsies.

RESULTS

Quantification of forskolin-induced organoid swelling

We first assessed whether forskolin, which raises the amount of intracellular cyclic AMP (cAMP) and thereby activates CFTR, could mediate fluid secretion into the lumen of small intestinal organoids derived from wild-type mice. Using live-cell microscopy, we observed a rapid expansion of both the lumen and total organoid surface area after the addition of forskolin, whereas DMSO-treated organoids were unaffected (Fig. 1a and Supplementary Video 1). Removal of the forskolin reversed the organoid swelling (Supplementary Fig. 1a).

We then quantified these responses by automated image analysis. We found excellent cell labeling (>100 times that of the background) using calcein green, a cell-permeable dye that gains fluorescence and is retained within living cells after metabolic conversion. We quantified forskolin-induced swelling (FIS) of organoids using live-cell confocal microscopy and imaging software that calculated the relative increase in the total area of all fluorescent objects per well for each time point after the addition of forskolin (Fig. 1b,c and Supplementary Fig. 1b). The majority of the organoids responded to forskolin stimulation (Fig. 1d). Approximately 5–10% of organoids that were either very small or irregularly shaped and nonviable did not respond to forskolin (Supplementary Fig. 1c,d), but their inclusion did not affect the FIS measurements (Supplementary Fig. 1e). A time-dependent surface area increase in three independent wells showed limited variation (Fig. 1e) and a dose-dependent relationship with forskolin (Fig. 1f). We present the FIS of mouse organoids during the first 10 min, as some wild-type mouse organoids burst and collapsed during longer stimulations (Supplementary Fig. 2a–c). Together these results show that forskolin-induced organoid swelling can be quantified by automated fluorescent image analysis.

Forskolin-induced swelling of mouse organoids

High levels of *Cftr* mRNA in the organoids supported a role for Cftr in FIS (Supplementary Fig. 2d). To demonstrate that FIS is Cftr dependent, we used chemical inhibitors of CFTR [22, 23] and *Cftr*$^{-/-}$ [24] or Cftrt^{m1eur} (harboring Cftr F508del) mice [25, 26]. Preincubation (2 h) with the CFTR inhibitor $CFTR_{inh}$-172 [22] or GlyH-101 [23] reduced FIS by ~90% and ~75%, respectively, and their combination fully prevented FIS (Fig. 2a). In addition, FIS was absent in the organoids of *Cftr*$^{-/-}$ mice (Fig. 2b,c and Supplementary Video 1). Calcein green labeling was comparable in wild-type and mutant organoids, indicating that the *Cftr*$^{-/-}$ organoids were viable. Organoids of mice harboring the Cftr F508del mutation displayed low but detectable FIS (Fig. 2d,e and Supplementary Video 1) that was sensitive to $CFTR_{inh}$-172 (Fig. 2f), suggesting residual Cftr activity, as has been observed previously [25, 26]. Together these data demonstrate that FIS in mouse organoids is completely Cftr dependent.

To show that FIS can detect Cftr correction, we performed temperature-rescue experiments, which is a widely accepted method to increase the function of CFTR F508del mutant protein [27]. Misfolding of F508del CFTR is reduced at 27 °C, leading to enhanced amounts of functional CFTR at the plasma membrane. Indeed, we observed increased FIS after overnight incubation of F508del Cftr organoids at 27 °C (Fig. 2f). We next used the chemical correctors VRT-325 [28] and Corr-4a [29] to restore the function of F508del Cftr (Online Methods). Preincubation (24 h) with VRT-325 enhanced FIS, whereas preincubation with Corr-4a only slightly improved FIS, and the effect of Corr-4a was additive to that of VRT-325 (Fig. 2g). CFTR inhibitors prevented FIS after Cftr correction (Fig. 2f,g). Collectively these results demonstrate that FIS of mouse organoids can reveal functional restoration of F508del Cftr by correction approaches.

Forskolin-induced swelling of human organoids

We next assayed human intestinal organoid cultures. Using western blot analysis, we detected mature CFTR (C band, 170 kDa) and immature CFTR (B band, 130 kDa) in human

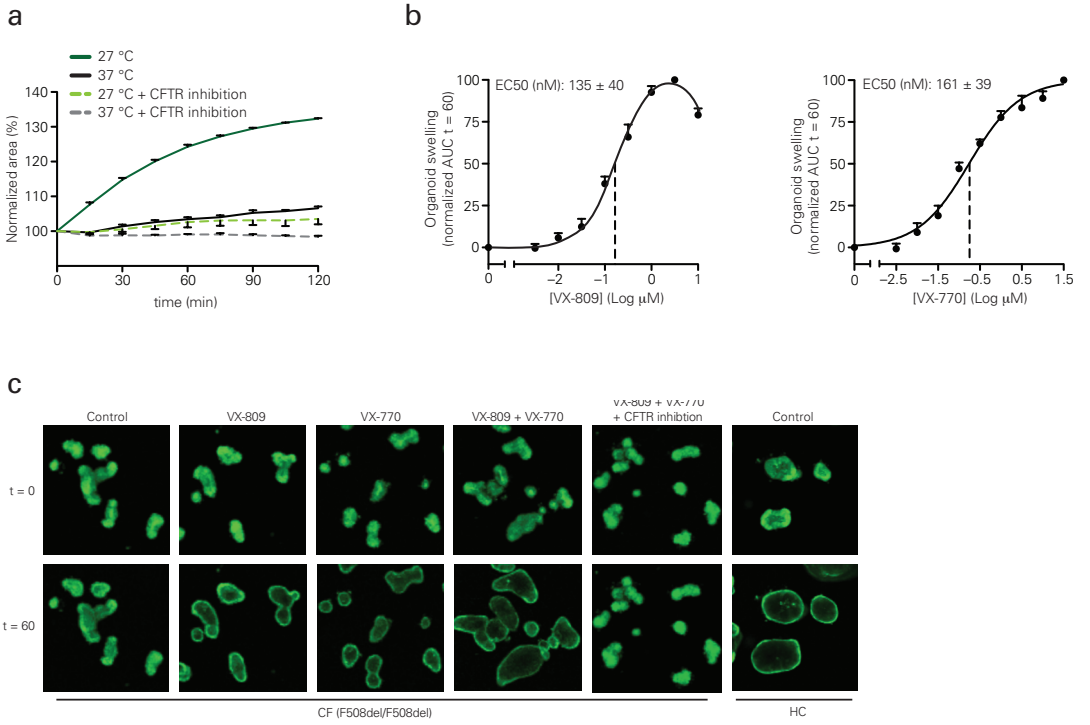

Figure 4. Chemical CFTR correction in human rectal organoids from subjects with cystic fibrosis.
(a) Normalized swelling of forskolin-induced calcein green–labeled F508del CFTR organoids cultured for 24 h at 37 °C or 27 °C with or without CFTR inhibition (mean ± s.e.m.). (b) EC50 values of F508del organoids for VX-809 or VX-770. The lines represent FIS expressed as the AUC (baseline 100%, t = 60 min) calculated from the time periods shown in d–f relative to DMSO-treated (0%) and VX-809-treated (log(0.5) μM) or VX-770-treated (log(1.5) μM) (100%) organoids (n = 6 F508del homozygous organoids; mean ± s.e.m.). (c) Representative confocal microscopy images of calcein green–labeled healthy control and F508del CFTR organoids in response to forskolin after pharmacological restoration of CFTR. Scale bars, 100 μm. (d–f) Time lapse analyses of normalized forskolin-induced swelling of F508del CFTR organoids pretreated for 24 h with DMSO, VRT-325 (10 μM), Corr-4a (10 μM) or both correctors with or without CFTR inhibition (d), with DMSO, C8 (10 μM), Corr-4a (10 μM) or both correctors with or without CFTR inhibition (e) or stimulated with the corrector VX-809 (24 h pretreatment; 3 μM), the potentiator VX-770 (simultaneously with forskolin; 3 μM) or a combined compound treatment with or without CFTR inhibition (f) (mean ± s.e.m.).

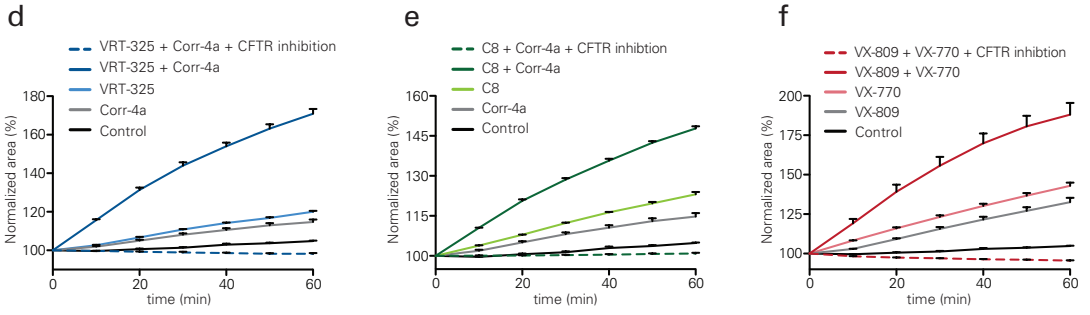

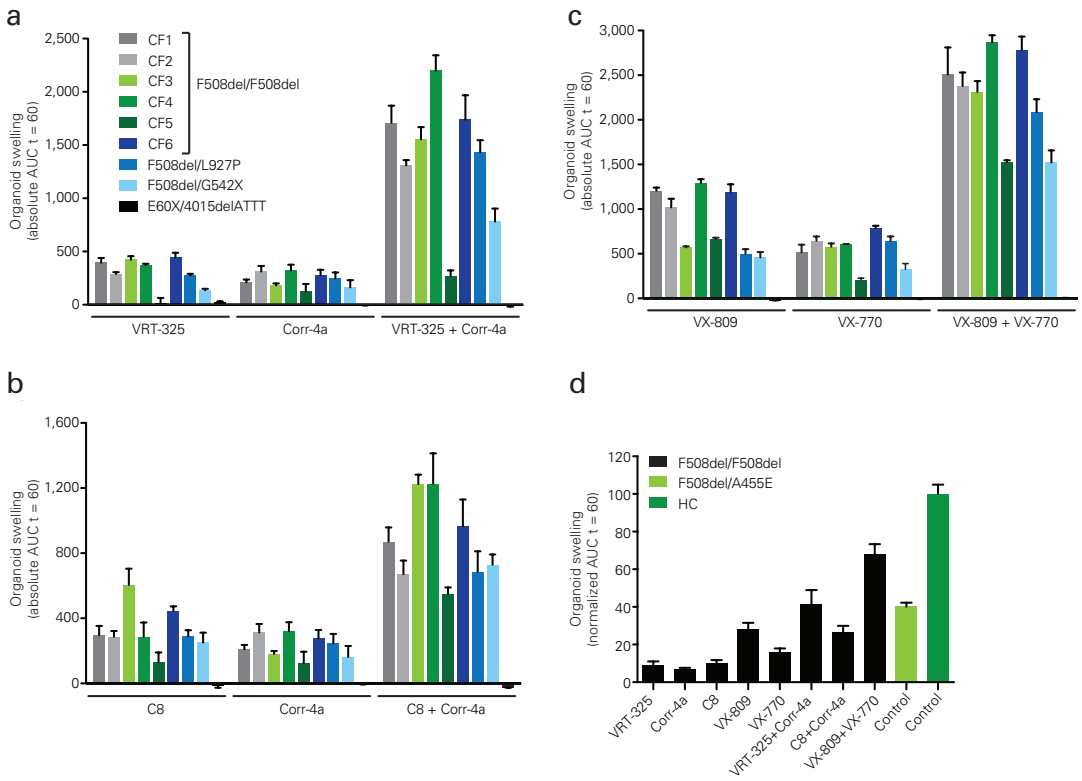

Figure 5. Differential FIS between organoids from subjects with cystic fibrosis after chemical CFTR restoration.

(a–c) Quantification of FIS in organoids derived from nine individuals with cystic fibrosis pretreated for 24 h with VRT-325 (10 μM), Corr-4a (10 μM) or both correctors (a), with C8 (10 μM), Corr-4a (10 μM) or both correctors (b) or stimulated with VX-809 (24 h pretreatment; 3 μM), VX-770 (simultaneously with forskolin; 3 μM) or both compounds (c). The bars correspond to the bars shown for the 'severe CF' group in Figure 3e. Each bar represents FIS expressed as the AUC calculated from the time periods shown in Figure 4d–f (baseline = 100%, t = 60 min) corrected for the FIS of DMSO-treated organoids and averaged from at least three independent experiments performed at weekly intervals (mean ± s.e.m.). (d) Average FIS responses of compound-treated F508del F508del organoids (n = 6 from a–c) and DMSO-treated F508del A455E organoids (n = 2) relative to the average FIS of DMSO-treated healthy control organoids (n = 3) expressed as the AUC calculated from the time periods shown inFigure 4d–f (baseline = 100%, t = 60 min; mean ± s.e.m.).

healthy control organoids, but we detected only the B band in F508del CFTR organoids (Fig. 3a). We found no CFTR B or C band in organoids carrying E60X [30] and a previously unreported allele that induces a frame shift in nucleotide-binding domain 2 (NBD2) at residue 1295 (4015delATTT). We further showed the specificity of the CFTR B and C bands using treatment with Endoglycosidase H (Endo H) and PNGase F [5], respectively. CFTR colocalized with apical actin in healthy control organoids but not F508del CFTR organoids (Fig. 3b). As observed in mouse organoids, rapid FIS of healthy control organoids was sensitive to chemical inhibition of CFTR (Fig. 3c). Human organoids showed somewhat slower kinetics compared to mouse organoids, rarely collapsed and required a longer preincubation time with CFTR inhibitors (3 h) (Fig. 3c, Supplementary Fig. 2c and Supplementary Video 2).

We analyzed FIS in a large number of intestinal organoids derived primarily from the rectum but

also from the duodenum, ileum and colon. We observed strong FIS in organoids derived from healthy control subjects (Fig. 3d and Supplementary Fig. 3a). Rectal organoids derived from individuals compound heterozygous for F508del and A455E [31], a genotype that is associated with mild cystic fibrosis [32], clearly showed reduced amounts of FIS compared to healthy control organoids (Supplementary Video 2). Subjects with severe cystic fibrosis genotypes (homozygous for F508del or compound heterozygous for F508del and L927P [33] or G542X [31]) showed much less FIS that was variable between individual subjects (Fig. 3e and Supplementary Video 2). We observed no FIS in E60X 4015delATTT organoids (Supplementary Video 2). Chemical inhibition of CFTR abolished all FIS responses of organoids from subjects with cystic fibrosis (Supplementary Fig. 3b).

FIS measurements of *in vitro*–expanded organoids derived from healthy controls or individuals with cystic fibrosis, subdivided into severe and mild genotypes, correlated tightly with forskolin-induced intestinal current measurements (ICMs) performed on rectal suction biopsies [34, 35] from which these organoids originated (Fig. 3f). Most ICM tracings of biopsies from individuals with cystic fibrosis showed residual forskolin-induced anion currents that corresponded to a quantitatively similar CFTR-dependent forskolin response in the FIS assay (Supplementary Fig. 4a–c). Together these data indicate that FIS in human organoids can accurately measure CFTR function and show that residual CFTR function in rectal organoids may differ between individuals homozygous for the CFTR F508del mutation.

CFTR restoration in cystic fibrosis organoids

We next assessed functional restoration of F508del CFTR in human organoids using either low temperature or the chemical correctors VRT-325, Corr-4a, C8 (http://cftrfolding.org) and VX-809 [36] and the potentiator VX-770 [9]. Incubation of CFTR F508del homozygous organoids at low temperature (27 °C) increased FIS (Fig. 4a). We next established dose-response curves for a single treatment of VX-809 (preincubated for 24 h) or VX-770 (added simultaneously with forskolin) in organoids from six subjects homozygous for CFTR F508del (Fig. 4b) and measured half-maximal effective concentration (EC_{50}) values of 135 ± 40 nM (mean ± s.d.) and 161 ± 39 nM for the two treatments, respectively. These dose responses are within the ranges reported in human bronchial epithelial cells [9, 36]. VX-809 combined with VX-770 induced increased FIS, which was abolished by chemical CFTR inhibition (Fig. 4c). We next assayed FIS after 24 h of preincubation with multiple correctors in F508del homozygous organoids. All correctors increased FIS, albeit with different efficacies (Fig. 4d–f, Supplementary Video 3 and Supplementary Fig. 5a). We observed that VRT-325 and Corr-4a or C8 and Corr-4a synergistically increased FIS, which was in contrast to the additive effect of VRT-325 and Corr-4a in mouse organoids (Fig. 2g). Restoration of the function of F508del CFTR by temperature and chemicals were all sensitive to CFTR inhibitors (Fig. 4a,c–f). These data indicate that FIS can reliably measure correction or potentiation of F508del CFTR.

We next studied FIS responses to a panel of CFTR-restoring drugs in rectal organoids derived from nine individuals harboring various severe CFTR mutations, including six F508del homozygous organoids. We observed different amounts of drug-induced FIS between various F508del homozygous organoids (Fig. 5a–c and Supplementary Fig. 5b). FIS was variable between organoids after incubation with single drugs, and the distribution of high and low responders was unique for a restoration approach (Fig. 5a–c). The CF5 organoid seems to be a low responder to any corrector or to VX-770 but showed an exceptionally small response to VRT-325. The CF3 and CF5 organoids showed similar responses to VX-809 but differed in their responses to C8. The measured FIS over the expected FIS (additive values of single treatment;Supplementary Fig. 6) indicated stronger synergy between VRT-325 and Corr-4a than between C8 and Corr-4a and was relatively constant between

most organoids. All F508del compound heterozygous organoids also responded to correction, but no correction or potentiation was observed in E60X 4015delATTT organoids (Fig. 5a–c). We next compared the efficacy of approaches to restore the function of F508del CFTR by comparing the amount of FIS to that in mock-treated F508del A455E organoids or healthy control organoids (Fig. 5d). This comparison indicated that VX-809 is the most potent corrector and combined treatment with VX-809 and VX-770 induced FIS beyond the amounts in F508del A455E organoids, reaching ~60% of the FIS in healthy controls. Together these results demonstrate that the potency of CFTR-targeting compounds to restore CFTR function varies widely between organoids from individuals with cystic fibrosis, including CFTR F508del homozygous organoids.

DISCUSSION

Our results collectively indicate that FIS of mouse and human intestinal organoids is CFTR dependent. Rapid FIS probably results from the near-physiological characteristics of intestinal organoids. Previous data have indicated that forskolin can increase luminal expansion in organoid-like structures grown from renal MDCK cells, colonic LIM1863 cell lines or mouse intestinal spheroids [20, 37, 38], but the larger amplitude and rate of the FIS probably results from higher CFTR expression levels in the primary tissue culture model used here.

Fluid transport measured by FIS in rectal organoids correlated to the ICMs performed on the corresponding rectal suction biopsies. The FIS assay can therefore be a valuable supplement to the electrical measurements of CFTR function currently carried out in cystic fibrosis treatment and research centers and may complement ICM data. Using ICMs and FIS, we found that most subjects harboring CFTR F508del showed some residual CFTR function, suggesting that F508del CFTR is expressed at low levels at the apical surface [39, 40]. This is also supported by the induction of FIS by the potentiator VX-770 in the absence of correctors, as was previously reported for human bronchial epithelial cells [9]. Clinical data also support low apical expression of F508del CFTR in subjects homozygous for F508del [41]. The paired FIS and ICM allows for the comparison of fluid secretion rates and ion fluxes as measured by ICM. On the basis of the geometry of organoids during FIS and the assumptions that the average organoid lumen is a sphere and the average swelling is similar in all three dimensions and is linear during an experiment, we calculated an initial fluid secretion rate of 26 ± 23 µl (mean ± s.d.) h^{-1} cm^{-2} in healthy control organoids (corresponding to an estimated current of 1.0 × 102 µA cm^{-2} on the basis of isotonic chloride secretion). When we assumed isotonic chloride secretion during ICM, we estimated that the measured currents would correspond to an approximate fluid secretion rate of 12 µl h^{-1} cm^{-2}. This rate largely exceeds the values reported previously for cysts from MDCK cells [42] and airway epithelium [43].

We demonstrate that FIS can measure functional restoration of CFTR by drugs. Notably, we observed that drug responses between organoids derived from subjects with cystic fibrosis are variable, even between CFTR F508del homozygous organoids. This raises the possibility that this *in vitro* assay may predict *in vivo* drug responsiveness of individual subjects. An ideal therapeutic model for cystic fibrosis would be to screen the effectiveness of available CFTR-restoring drugs directly after diagnosis to optimize treatment at the personal level before disease onset. Personalized medicine approaches may also facilitate the development and approval of drugs to which only subgroups of subjects respond and limit the economic risks associated with drug research. Furthermore, FIS of organoids can be used for approval of drugs in subjects that are genotypically mismatched with drugs that have been validated for a specific *CFTR* genotype. Interim phase 2 results of a current trial published on websites of the North American Cystic Fibrosis Foundation (http://www.cff.org/) and Vertex (http://www.vrtx.com/) indicate that drug responses to VX-809 and VX-770 together or to VX-770 alone14 are highly variable between subjects harboring

CFTR F508del. However, the predictive potential of organoid-based measurements of CFTR function for *in vivo* drug responsiveness remains to be established.

Individual drug responses may be predicted currently using *ex vivo* rectal biopsies [44] or primary airway tissue culture models [45]. Compared with these techniques, organoid cultures seem superior in generating large data sets from individual subjects. CFTR function analysis in organoid cultures is relatively easy, fast and robust. The organoids autodifferentiate into tissue-recapitulating structures in 96-well plates, allowing for the measurement of up to 80 organoids per well and up to 96 conditions per experiment. In this format, dose-response curves measured in triplicate for multiple drugs per individual can be easily generated at multiple culture time points, as we demonstrate here.

Using our image analysis approach, higher throughput approaches to identify new compounds that restore CFTR function may be developed. When we compare the drug responses in organoids with the limited clinical data that have been published in subjects homozygous for CFTR F508del [13, 14] (http://www.cff.org/), only the combination of VX-809 and VX-770 has been reported to improve lung function in approximately 50% of these individuals. This combination induces approximately 1.5-fold more FIS in CFTR F508del homozygous organoids as compared to untreated F508del A455E organoids and up to 60% of the FIS seen in healthy controls. It is not uncommon that treatment effects in *in vitro* models are superior to the effects measured *in vivo*, but the correction in the FIS assay also exceeds the correction in cultured human bronchial epithelium by approximately twofold [9, 36]. This might indicate that tissue-specific factors may control corrector efficacy. It is also probable that FIS rates are underestimated in healthy control organoids when CFTR expression is no longer rate limiting for FIS beyond a particular threshold by, for example, basolateral ion transport. These data suggest that new CFTR-restoring drugs may have clinical impact when FIS reaches up to ~60% of the FIS in wild-type organoids.

Two important aspects of organoid cultures render this technology highly suitable for follow-up studies. First, organoids can be greatly expanded while maintaining intact stem cell compartments during long-term culture (over 40 passages) [16]. The generation of large numbers of cells will aid cell biological and biochemical studies of CFTR-dependent cellular alterations and is a prerequisite for high-throughput screens. Second, primary cell banks from individuals with cystic fibrosis can be generated by storage of organoids in liquid nitrogen. These can be used to identify and study cellular factors associated with clinical phenotypes and would allow for the analysis of newly developed drugs at the individual level using materials that have been acquired previously.

In addition, this assay may be suitable for the development of drugs to treat secretory diarrhea, a life- threatening condition that results from CFTR hyperactivation by pathogenic toxins such as cholera toxin [46] (Supplementary Fig. 7), and for electrolyte homeostasis studies in general.

We describe a quick and robust assay for the quantification of CFTR function using a primary intestinal culture model that recapitulates essential features of the *in vivo* tissue architecture. This relatively simple assay will facilitate diagnosis, functional studies, drug development and personalized medicine approaches in cystic fibrosis.

METHODS

Mice

Cftr^{tm1Cam} knockout (*Cftr*$^{-/-}$) mice [24] were backcrossed with FVB mice, and *Cftr*^{tm1eur} (*Cftr* F508del) [25, 26] were backcrossed with C57BL/6 (F12) mice. Congenic FVB *Cftr*$^{-/-}$ mice (male) or C57BL/6 Cftr F508del mice (male and female) were used with their wild-type littermates. The mice were maintained in an environmentally controlled facility at Erasmus MC Rotterdam, and the animal

studies were approved by the Erasmus MC ethical committee.

Human material

Approval for this study was obtained by the ethics committees of the University Medical Centre Utrecht and Erasmus MC Rotterdam. Informed consent was obtained from all subjects participating in the study. Rectal organoids from healthy controls and subjects with cystic fibrosis were generated from four rectal suction biopsies after ICMs obtained (i) during standard cystic fibrosis care (one individual each harboring E60X 4015ATTTdel, F508del G542X or F508del L927P and five individuals harboring F508del F508del), (ii) for diagnostic purposes (one healthy control) or (iii) during voluntary participation in studies approved by the University Medical Center Utrecht and Erasmus MC ethics committees (two healthy controls and one individual harboring F508del F508del). Material from an individual homozygous for F508del CFTR and a healthy control was derived from proximal ileum rest sections after surgery for meconium ileus. Four duodenal biopsies were obtained from two subjects with cystic fibrosis by flexible gastroduodenoscopy to generate F508del F508del and F508del exon17del organoids. The same procedure was used to obtain four biopsies from two subjects with suspected celiac disease. The biopsies were macroscopically and pathologically normal and used to generate healthy control organoids.

Crypt isolation and organoid culture from mouse intestine

Mouse organoids were generated from isolated small intestinal crypts and maintained in culture as described previously [15]. R-spondin 1 (Rspo1)-conditioned medium (stably transfected Rspo-1 HEK293T cells were kindly provided by C.J. Kuo, Department of Medicine, Stanford, CA) was used instead of recombinant Rspo-1 and was added to the culture medium at a 1:10 dilution. *Cftr*$^{-/-}$ and Cftr F508del organoids were obtained from proximal and distal small intestinal segments, respectively. Organoids from passages 1–10 were used for confocal imaging.

Crypt isolation and organoid culture from human biopsies

Crypt isolation and culture of human intestinal cells has been described previously [16]. In short, biopsies were washed with cold complete chelation solution and incubated with 10 mM EDTA for 30 (small intestine) or 60 (rectum) min at 4 °C. The supernatant was harvested, and EDTA was washed away. Crypts were isolated by centrifugation and embedded in Matrigel (growth factor reduced, phenol free; BD bioscience) and seeded (50–200 crypts per 50 µl Matrigel per well) in 24-well plates. The Matrigel was polymerized for 10 min at 37 °C and immersed in complete culture medium consisting of advanced DMEM/F12 supplemented with penicillin and streptomycin, 10 mM HEPES, Glutamax, N2, B27 (all from Invitrogen), 1 µM N-acetylcysteine (Sigma) and the following growth factors: 50 ng ml^{-1} mouse epidermal growth factor (mEGF), 50% Wnt3a-conditioned medium (WCM) and 10% noggin-conditioned medium (NCM), 20% Rspo1-conditioned medium, 10 µM nicotinamide (Sigma), 10 nM gastrin (Sigma), 500 nM A83-01 (Tocris) and 10 µM SB202190 (Sigma). The medium was refreshed every 2–3 d, and organoids were passaged 1:4 every 7–10 d. Organoids from passages 1–10 were used for confocal live-cell imaging. For production of WCM and NCM, Wnt3a-producing L Cells (ATCC, CRL-264) were selected for high-expressing subclones, and human full-length noggin was stably transfected into HEK293T cells, respectively. Amounts and activity of the expressed factors in each batch were assessed using dot blots and luciferase reporter plasmids (TOPflash and FOPflash; Millipore) as described previously [47, 48].

Stimulation assays

Human or mouse organoids from a 7-day-old culture were seeded in a flat-bottom 96-well culture plate (Nunc) in 5 µl Matrigel commonly containing 20–80 organoids and 100 µl culture medium. One day after seeding, organoids were incubated for 60 min with 100 µl standard culture medium containing 10 µM calcein green (Invitrogen). For optimal CFTR inhibition, organoids were preincubated for 2 (mouse) or 3

h (human) with 50 µM CFTRinh-172, 50 µM GlyH-101 or their combined treatment (both from Cystic Fibrosis Foundation Therapeutics, Inc). After calcein green treatment (with or without CFTR inhibition), 5 µM forskolin was added, and organoids were directly analyzed by confocal live-cell microscopy (LSM710, Zeiss, ×5 objective). Three wells were used to study one condition, and up to 60 wells were analyzed per experiment. For CFTR correction, organoids were preincubated for 24 h with 10 µM VRT-325, 10 µM Corr-4a, 10 µM C8 (all from Cystic Fibrosis Foundation Therapeutics, Inc), 3 µM VX-809 (Selleck Chemicals LLC, Houston, USA) or combinations thereof, as indicated. For CFTR potentiation, 3 µM VX-770 (Selleck Chemicals LLC) was added simultaneously with forskolin. Dilutions of VX-809 and VX-770 were used as indicated in Figure 4b.

Quantification of organoid surface area

Forskolin-stimulated organoid swelling was automatically quantified using Volocity imaging software (Improvision). The total organoid area (xy plane) increase relative to that at t = 0 of forskolin treatment was calculated and averaged from three individual wells per condition. The AUC was calculated using Graphpad Prism.

Statistical analyses

A Kolmogorov-Smirnov test was used to test whether the ICM and FIS data were normally distributed. A paired Student's t test was used to compare FIS with or without preselection of responding organoids (Supplementary Fig. 1e). A Spearman's rank correlation test was used to correlate ICM measurements with organoid swelling (Supplementary Fig. 4c). $P < 0.05$ was considered statistically significant. All data were analyzed in SPSS statistics version 20.0 for Windows.

RNA isolation and quantitative PCR

RNA was isolated with the RNeasy minikit (Qiagen) and quantified by optical density from human duodenal organoids that were cultured for >12 weeks. cDNA was synthesized from 1 µg of RNA by performing RT-PCR (Invitrogen). From mouse small intestinal organoids that were cultured for >6 weeks, RNA was isolated using TRIzol (Invitrogen) and quantified by optical density. cDNA was generated from 500 ng using the iScript cDNA synthesis kit (Bio-Rad). mRNA levels of human *CFTR* and mouse *Cftr* were determined by quantitative real-time RT-PCR with the SYBR Green method (Bio-Rad). Glyceraldehyde-3-phosphate dehydrogenase (*GADPH*) or *β2m* mRNA abundance was used to measure cDNA input.

Western blot analysis

For CFTR protein detection, organoids from healthy controls or subjects with cystic fibrosis were lysed in Laemmli buffer supplemented with complete protease inhibitor tablets (Roche). Lysates were analyzed by SDS-PAGE and electrophoretically transferred to a polyvinylidene difluoride membrane (Millipore). The membrane was blocked with 5% milk protein in TBST (0.3% Tween, 10 mM Tris, pH 8, and 150 mM NaCl in H_2O) and probed overnight at 4 °C with a combination of the mouse monoclonal CFTR-specific antibodies 450, 570 and 596 (1:5,000, Cystic Fibrosis Folding consortium) followed by incubation with goat mouse-specific horseradish peroxidase (HRP)-conjugated secondary antibodies (1:3,000, Jackson ImmunoResearch, 115-035-146) and enhanced chemiluminescence (ECL) development. For CFTR deglycosylation, healthy control organoids were lysed in RIPA buffer (50 mM Tris, pH 8.0, 150 mM NaCl, 0.1% SDS, 0.5% sodium deoxycholate and 1% triton) supplemented with complete protease inhibitor tablets (Roche) and incubated with PNGase F and Endo H for 3 h at 33 °C (both from New England BioLabs).

Immunocytochemistry

Complete organoids from a 5-day-old culture were incubated with methanol (Sigma) for 10 min at –20 °C. Organoids were probed with the mouse monoclonal CFTR-specific antibody M3A7 (1:25, Abcam, AB4067) for 16 h at 4 °C followed by simultaneous incubation of Alexa Fluor 649–conjugated secondary antibodies (1:500, Jackson ImmunoResearch, 115-495-205) and phalloidin-FITC for 1 h at 4 °C (1:200, Sigma). Organoids were embedded in Mowiol

containing DAPI (1:10,000) and analyzed by confocal microscopy as described previously [49].

ICM

Trans-epithelial chloride secretion in human rectal suction biopsies (four per subject) was measured as described previously [34] using a recent amendment (repetitive prewashing) [35], which better accentuates forskolin-induced anion current responses by reducing basal cAMP levels. In short, the biopsies were collected in PBS on ice and directly mounted in adapted micro-Ussing chambers (aperture. 1.13 or 1.77 mm^2). After equilibration, the following compounds were added in a standardized order to the mucosal (M) or serosal (S) side of the tissue: amiloride (0.01 mM, M), to inhibit amiloride-sensitive electrogenic Na+ absorption; carbachol (0.1 mM, S), to initiate cholinergic Ca^{2+}-linked and protein kinase C–linked Cl^- secretion; DIDS (0.2 mM, M), to inhibit DIDS-sensitive, non-CFTR Cl^- channels such as the Ca^{2+}-dependent Cl^- channels; histamine (0.5 mM, S), to reactivate the Ca^{2+}-dependent secretory pathway and measure the DIDS-insensitive component of Ca^{2+}-dependent Cl^- secretion; and forskolin (0.01 mM, S), to fully activate CFTR-mediated anion secretion. Crude short circuit current values (μA) were converted to μA cm^{-2} on the basis of the surface area of the aperture.

ACKNOWLEDGMENTS

We thank K. Schneeberger for technical assistance, the Department of Pediatric Gastroenterology of the Wilhelmina Children's Hospital for performing gastroduodenoscopy to obtain intestinal biopsies, K. Tenbrock (Department of Pediatrics, Rheinisch-Westfälische Technische Hochschule (RWTH) Aachen University) and J.C. Escher (Department of Pediatric Gastroenterology, Erasmus MC–Sophia Children's Hospital) for providing intestinal rest-material, C.J. Kuo (Department of Medicine, Stanford) for providing the R-spondin 1-producing cell line, J. Riordan (Department of Biochemistry and Biophysics, University of North Carolina at Chapel Hill) for CFTR-specific monoclonal antibodies, R. Bridges (Department of Rosalind Franklin University of Medicine and Science) and Cystic Fibrosis Foundation Therapeutics for providing CFTR-restoring compounds, P.W. van Leeuwen for assistance with statistical analyses and C.B.M. ten Brink for assistance with Volocity software. This research was partly funded by a grant from the WKZ research fund (OZF-2010) and the Dutch Cystic Fibrosis society (NCFS).

1. Riordan, J. R. et al. Identification of the cystic fibrosis gene: cloning and characterization of complementary DNA. Science 245, 1066–1073 (1989).
2. Rommens, J. M. et al. Identification of the cystic fibrosis gene: chromosome walking and jumping. Science 245, 1059–1065 (1989).
3. Kerem, B. et al. Identification of the cystic fibrosis gene: genetic analysis. Science 245, 1073–1080 (1989).
4. Ratjen, F. & Döring, G. Cystic fibrosis. Lancet 361, 681–689 (2003).
5. Cheng, S. H. et al. Defective intracellular transport and processing of CFTR is the molecular basis of most cystic fibrosis. Cell 63, 827–834 (1990).
6. Riordan, J. R. CFTR function and prospects for therapy. Annu. Rev. Biochem. 77, 701–726 (2008).
7. Clancy, J. P. & Jain, M. Personalized medicine in cystic fibrosis: dawning of a new era. Am. J. Respir. Crit. Care Med. 186, 593–597 (2012).
8. Ramsey, B. W. et al. A CFTR potentiator in patients with cystic fibrosis and the G551D mutation. N. Engl. J. Med. 365, 1663–1672 (2011).
9. Van Goor, F. et al. Rescue of CF airway epithelial cell function in vitro by a CFTR potentiator, VX-770. Proc. Natl. Acad. Sci. U.S.A. 106, 18825–18830 (2009).
10. Rabeh, W. M. et al. Correction of both NBD1 energetics and domain interface is required to restore ΔF508 CFTR folding and function. Cell 148, 150–163 (2012).
11. Welch, E. M. et al. PTC124 targets genetic disorders caused by nonsense mutations. Nature 447, 87–91 (2007).
12. Sermet-Gaudelus, I. et al. Ataluren (PTC124) induces cystic fibrosis transmembrane conductance regulator protein expression and activity in children with nonsense mutation cystic fibrosis. Am. J. Respir. Crit. Care Med. 182, 1262–1272 (2010).
13. Clancy, J. P. et al. Results of a phase IIa study of VX-809, an investigational CFTR corrector compound, in subjects with cystic fibrosis homozygous for the F508del-CFTR mutation. Thorax 67, 12-18 (2011)
14. Flume, P. A. et al. Ivacaftor in subjects with cystic fibrosis who are homozygous for the F508del-CFTR mutation. Chest 142, 718–724 (2012).
15. Sato, T. et al. Single Lgr5 stem cells build crypt-villus structures in vitro without a mesenchymal niche. Nature 459, 262–265 (2009).
16. Sato, T. et al. Long-term expansion of epithelial organoids from human colon, adenoma, adenocarcinoma, and Barrett's epithelium. Gastroenterology 141, 1762-1772 (2011)
17. Sato, T. et al. Paneth cells constitute the niche for Lgr5 stem cells in intestinal crypts. Nature 469, 415–418 (2011).
18. Field, M. Intestinal ion transport and the pathophysiology of diarrhea. J. Clin. Invest. 111, 931–943 (2003).
19. Venkatasubramanian, J., Ao, M. & Rao, M. C. Ion transport in the small intestine. Curr. Opin. Gastroenterol. 26, 123–128 (2010).
20. Currid, A., Ortega, B. & Valverde, M. A. Chloride secretion in a morphologically differentiated human colonic cell line that expresses the epithelial Na+ channel. J. Physiol. (Lond.) 555, 241–250 (2004).
21. Cunningham, S. A., Worrell, R. T., Benos, D. J. & Frizzell, R. A. cAMP-stimulated ion currents in Xenopus oocytes expressing CFTR cRNA. Am. J. Physiol. 262, C783–788 (1992).
22. Thiagarajah, J. R., Song, Y., Haggie, P. M. & Verkman, A. S. A small molecule CFTR inhibitor produces cystic fibrosis-like submucosal gland fluid secretions in normal airways. FASEB J. 18, 875–877 (2004).
23. Muanprasat, C. et al. Discovery of glycine hydrazide pore-occluding CFTR inhibitors: mechanism, structure-activity analysis, and in vivo efficacy. J. Gen. Physiol. 124, 125–137 (2004).
24. Ratcliff, R. et al. Production of a severe cystic fibrosis mutation in mice by gene targeting. Nat. Genet. 4, 35–41 (1993).
25. French, P. J. et al. A delta F508 mutation in mouse cystic fibrosis transmembrane conductance regulator results in a temperature-sensitive processing defect in vivo. J. Clin. Invest. 98, 1304–1312 (1996).
26. Wilke, M. et al. Mouse models of cystic fibrosis: phenotypic analysis and research applications. J. Cyst. Fibros. 10 Suppl 2, S152–71 (2011).
27. Denning, G. M. et al. Processing of mutant cystic fibrosis transmembrane conductance regulator is temperature-sensitive. Nature 358, 761–764 (1992).
28. Loo, T. W., Bartlett, M. C. & Clarke, D. M. Rescue of DeltaF508 and other misprocessed CFTR mutants by a novel quinazoline compound. Mol. Pharm. 2, 407–413 (2005).
29. Pedemonte, N. et al. Small-molecule correctors of defective DeltaF508-CFTR cellular processing identified by high-throughput screening. J. Clin. Invest. 115, 2564–2571 (2005).
30. Strandvik, B. et al. Spectrum of mutations in the CFTR gene of patients with classical and atypical forms of cystic fibrosis from southwestern Sweden: identification of 12 novel mutations. Genet. Test. 5, 235–242 (2001).
31. Kerem, B. S. et al. Identification of mutations in regions corresponding to the two putative nucleotide (ATP)-binding folds of the cystic fibrosis gene. Proc. Natl. Acad. Sci. U.S.A. 87, 8447–8451 (1990).
32. Zielenski, J. Genotype and phenotype in cystic fibrosis. Respiration 67, 117–133 (2000).
33. Hermans, C. J., Veeze, H. J., Drexhage, V. R., Halley, D. J. & van den Ouweland, A. M. Identification of the L927P and delta L1260 mutations in the CFTR gene. Hum. Mol. Genet. 3, 1199–1200 (1994).
34. de Jonge, H. R. et al. Ex vivo CF diagnosis by intestinal current measurements (ICM) in small aperture, circulating Ussing chambers. J. Cyst. Fibros. 3 Suppl 2, 159–163 (2004).
35. De Boeck, K. et al. New clinical diagnostic procedures for cystic fibrosis in Europe. J. Cyst. Fibros. 10 Suppl 2, S53–66 (2011).
36. Van Goor, F. et al. Correction of the F508del-CFTR protein

processing defect in vitro by the investigational drug VX-809. Proc. Natl. Acad. Sci. U.S.A. 108, 18843–18848 (2011).
37. Liu, J., Walker, N. M., Cook, M. T., Ootani, A. & Clarke, L. L. Functional Cftr in crypt epithelium of organotypic enteroid cultures from murine small Intestine. Am. J. Physiol., Cell Physiol. 302, C1492-1503 (2012)
38. Li, H., Yang, W., Mendes, F., Amaral, M. D. & Sheppard, D. N. Impact of the cystic fibrosis mutation F508del-CFTR on renal cyst formation and growth. Am. J. Physiol. Renal Physiol. 303, F1176–1186 (2012).
39. Gee, H. Y., Noh, S. H., Tang, B. L., Kim, K. H. & Lee, M. G. Rescue of ΔF508-CFTR trafficking via a GRASP-dependent unconventional secretion pathway. Cell 146, 746–760 (2011).
40. Luo, Y., McDonald, K. & Hanrahan, J. W. Trafficking of immature DeltaF508-CFTR to the plasma membrane and its detection by biotinylation. Biochem. J. 419, 211–9– 2 p following 219 (2009).
41. Geborek, A. & Hjelte, L. Association between genotype and pulmonary phenotype in cystic fibrosis patients with severe mutations. J. Cyst. Fibros. 10, 187–192 (2011).
42. Sullivan, L. P., Wallace, D. P. & Grantham, J. J. Coupling of cell volume and membrane potential changes to fluid secretion in a model of renal cysts. Kidney Int. 45, 1369–1380 (1994).
43. Smith, J. J. & Welsh, M. J. Fluid and electrolyte transport by cultured human airway epithelia. J. Clin. Invest. 91, 1590–1597 (1993).
44. Roth, E. K. et al. The K+ channel opener 1-EBIO potentiates residual function of mutant CFTR in rectal biopsies from cystic fibrosis patients. PLoS ONE 6, e24445 (2011).
45. Wong, A. P. et al. Directed differentiation of human pluripotent stem cells into mature airway epithelia expressing functional CFTR protein. Nat. Biotechnol. 30, 876–882 (2012).
46. Thiagarajah, J. R. & Verkman, A. S. CFTR inhibitors for treating diarrheal disease. Clin. Pharmacol. Ther. 92, 287–290 (2012).
47. de Lau, W. et al. Lgr5 homologues associate with Wnt receptors and mediate R-spondin signalling. Nature 476, 293–297 (2011).
48. Korinek, V. et al. Constitutive transcriptional activation by a beta-catenin-Tcf complex in APC-/- colon carcinoma. Science 275, 1784–1787 (1997).
49. Beekman, J. M. et al. Syntenin-mediated regulation of Sox4 proteasomal degradation modulates transcriptional output. Oncogene 31, 2668-2679 (2012)

Supplementary Figure 1. Organoid swelling in reponse to forskolin. (a) Light microscopy analysis of wild-type mouse organoids stimulated with forskolin or DMSO. Representative examples for the indicated time points after start of stimulation are shown. The forskolin-induced swelling (FIS) of organoids was reversed upon removal of forskolin by washing. Scale bar 30 µm. (b) Examples of quantification of total organoid surface area using Volocity imaging software. A representative confocal image is shown of calcein-green-labeled rectal F508del-CFTR organoids pre-treated for 24 h with VX-809 in a well of a 96-well plate at the indicated time points of forskolin treatment. Scale bar 520 µm. (c) Percentages of forskolin responding and non-responding objects from different origin with or without drug treatment calculated from three independent experiments. (d) Representative confocal images of irregularly shaped (non-responding) or normally shaped (responding) organoids at the indicated time points of forskolin simulation. Scale bar 60 µm. (e) Quantification of FIS expressed in absolute area under the curve (AUC) calculated from time lapses as illustrated in Fig. 4d–f (baseline = 100%, t = 60 min) with or without pre-selection of responding structures. NS = not significant.

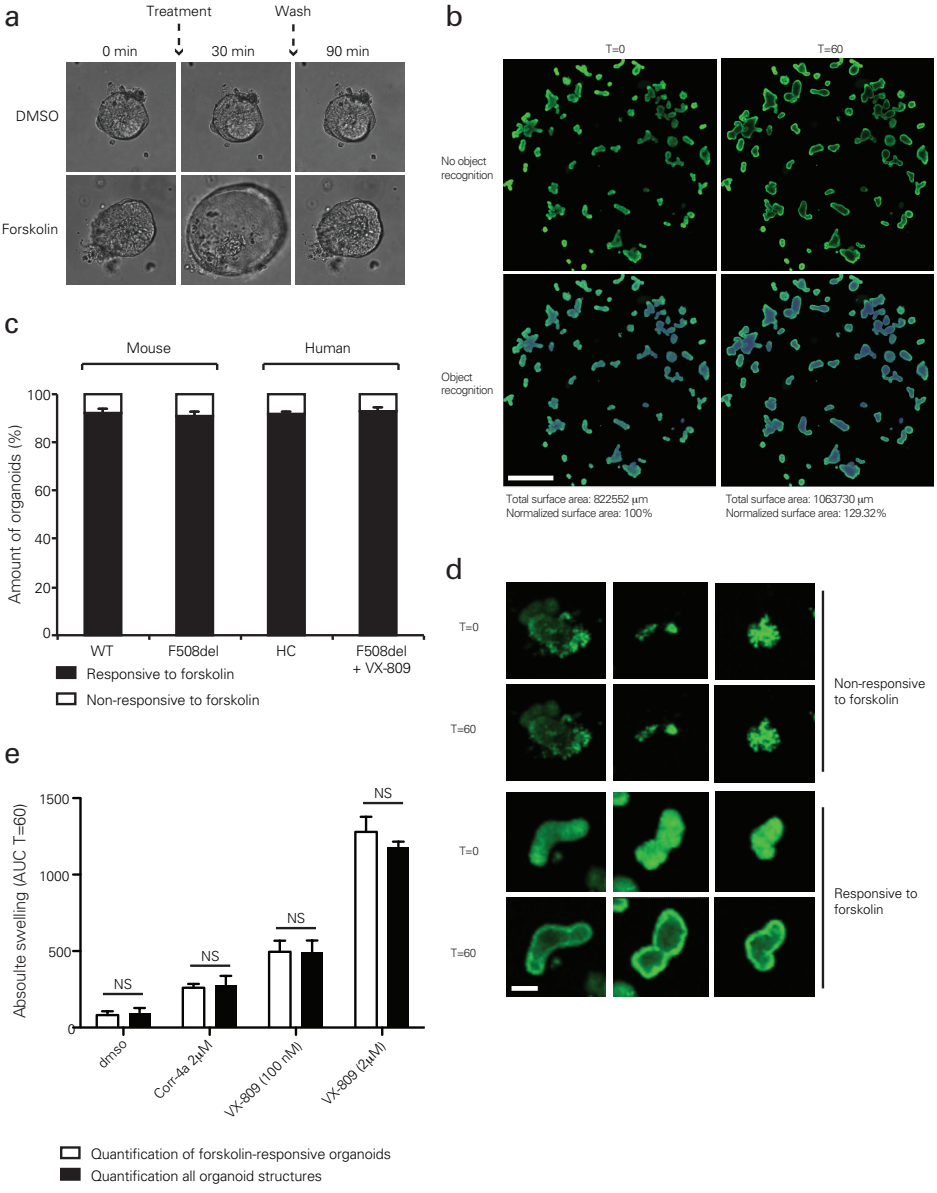

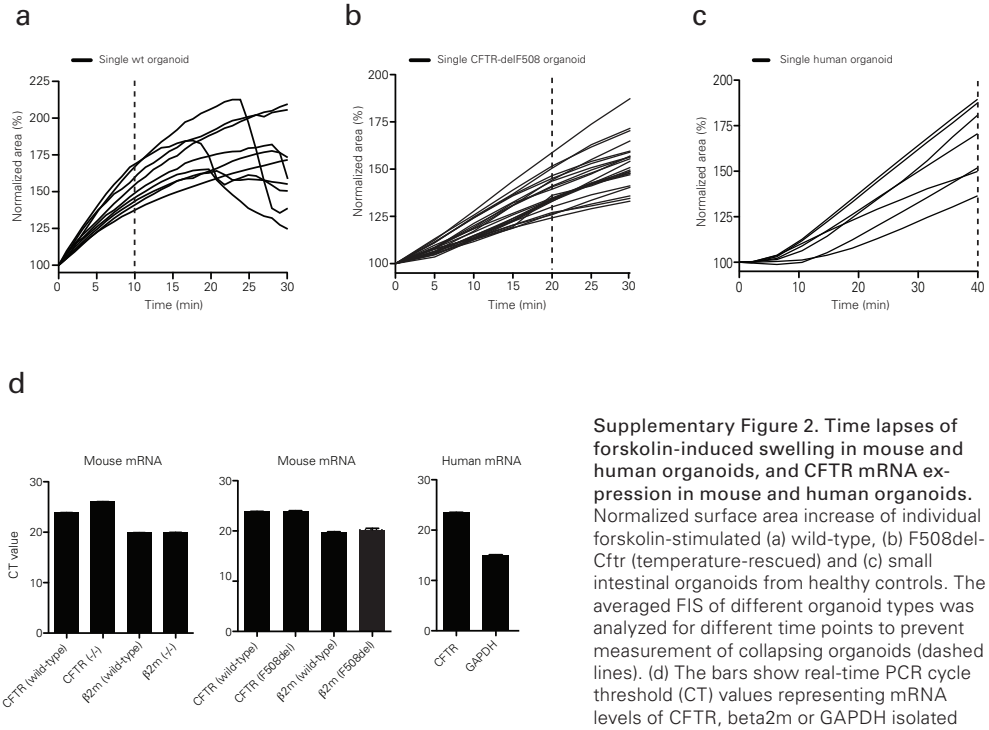

Supplementary Figure 2. Time lapses of forskolin-induced swelling in mouse and human organoids, and CFTR mRNA expression in mouse and human organoids. Normalized surface area increase of individual forskolin-stimulated (a) wild-type, (b) F508del-Cftr (temperature-rescued) and (c) small intestinal organoids from healthy controls. The averaged FIS of different organoid types was analyzed for different time points to prevent measurement of collapsing organoids (dashed lines). (d) The bars show real-time PCR cycle threshold (CT) values representing mRNA levels of CFTR, beta2m or GAPDH isolated from small intestinal F508del-Cftr (left graph) or Cftr–/– (middle graph) organoids and their corresponding wild-types, or healthy control small intestinal organoids.

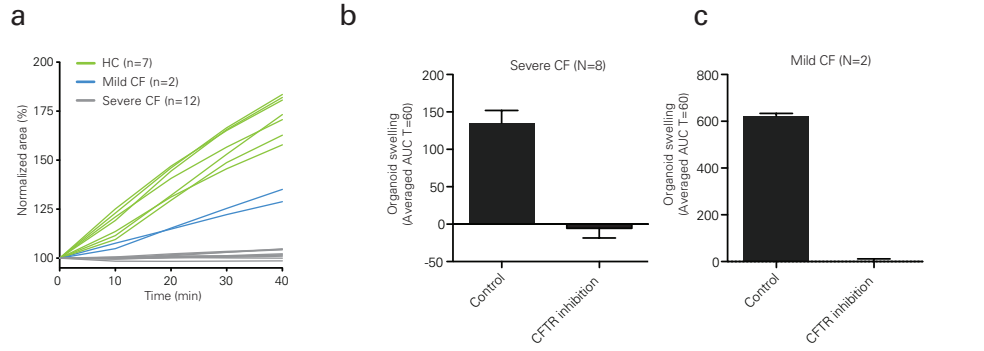

Supplementary Figure 3. Forskolin-induced swelling in organoids from healthy controls and cystic fibrosis subjects. (a) Forskolin-stimulated swelling of intestinal organoids derived from 7 individual healthy controls (HC; 2 × duodenum, 1 × ileum, 1 × colon, 3 × rectum), 2 subjects with a mild cystic fibrosis (CF) genotype (F508del/A455E; rectum) and 12 subjects with a severe cystic fibrosis genotype (duodenum: F508del/F508del and F508del/Exon17del; Ileum: F508del/F508del; rectum: 1 × E60X/4015delATTT; 1 × F508del/G542X; 1 × F508del/L927P; 6 × F508del/F508del). (b) Forskolin-induced swelling expressed in AUC calculated from time lapses of organoids area increase (baseline = 100%, t = 60) of rectal organoids with a mild or severe cystic fibrosis genotype with or without CFTR inhibition by CFTRinh-172 and GlyH-101 (severe genotype: F508del/G542X, F508del/L927P and F508del/F508del (6 ×); mild genotype: F508del/A455E n = 2); mean ± s.e.m.).

a

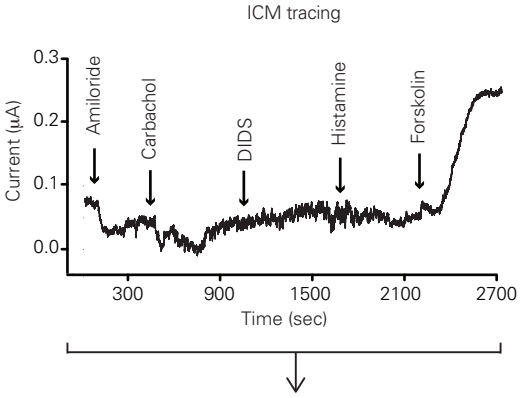

b

	Forskolin-induced swelling (AUC T=60)	SD	Forskolin-induced Cl^- secretion (µ Amp/cm^2)	SD
E60X/4015delATTT	2.63	4.56	-5.1	3.9
F508del/G542X	32.49	30.65	0.5	0.8
F508del/F508del	60.52	4.75	7	3.1
F508del/F508del	149.93	49.52	5.3	1.7
F508del/F508del	98.21	21.45	7.9	3.2
F508del/F508del	164.14	20.54	9.1	4.4
F508del/F508del	179.33	23.90	-10.1	-3.7
F508del/A455E	1494.00	118.03	14.2	4.4
F508del/A455E	1343.33	81.29	17	4.7
Healthy control	3191.33	724.50	26.3	12.8
Healthy control	3755.00	762.86	57	18.2
Healthy control	3666.75	287.97	50.1	14.5

c

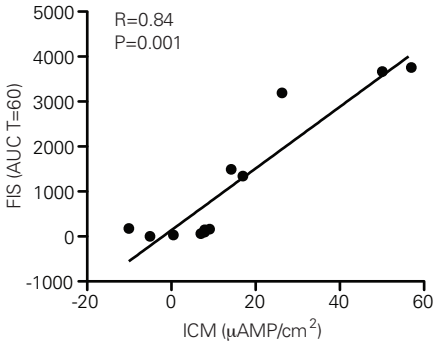

Supplementary Figure 4. Paired measurement of CFTR function by FIS or ICM. (a) Representative intestinal current measurement (ICM) tracing of F508del-CFTR rectal biopsies. (b) Overview of paired FIS and ICM responses of different individuals. FIS is expressed as absolute area under the curve (AUC) calculated from time lapses as illustrated in Fig. 4d–f (baseline = 100%, t = 60 min) and is averaged from at least three independent experiments performed with weekly interval. The ICM values represent average forskolin-induced current responses from four rectal biopsies of the same individual. (c) Correlation plot of FIS and ICM values from (b). R (= correlation coefficient) and P-value were calculated by SPSS using a Spearman's rank correlation test.

a

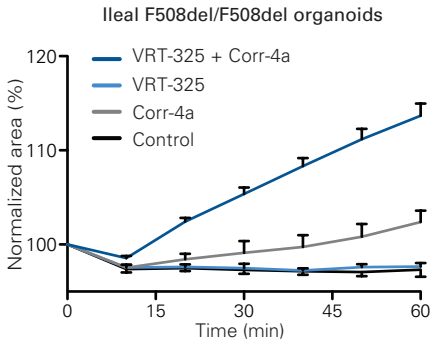

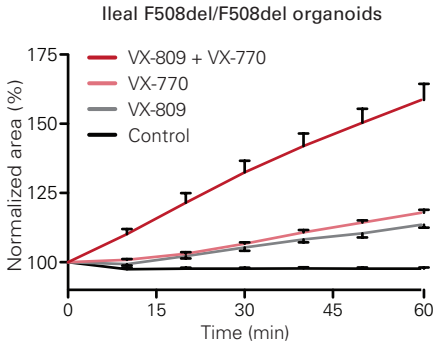

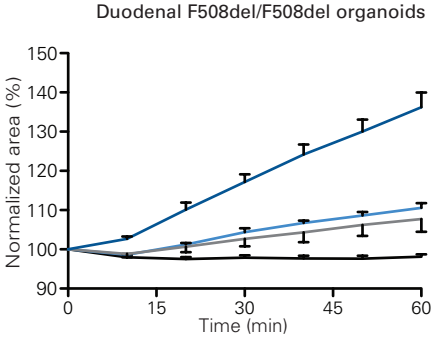

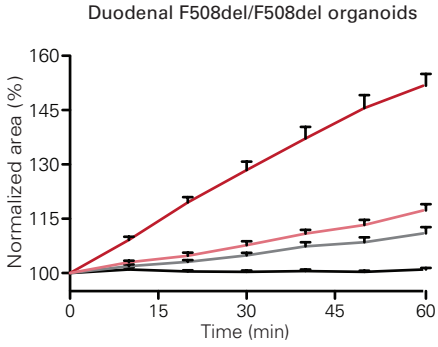

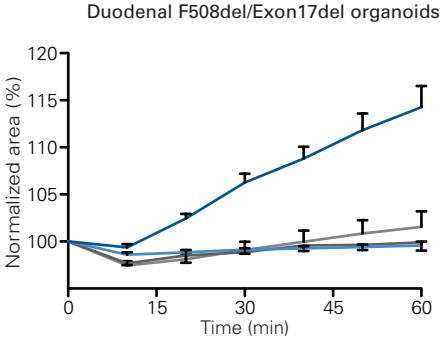

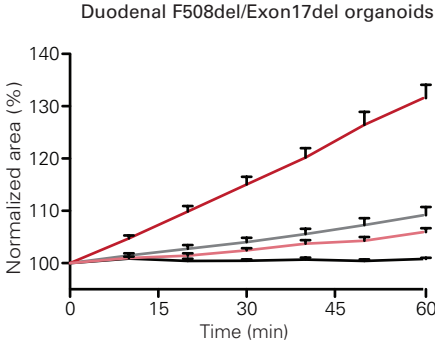

b

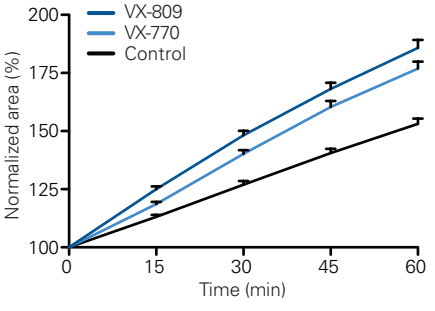

Supplementary Figure 5. Chemical CFTR correction of non-rectal intestinal or rectal F508del/A455E organoids. (a) Time lapses of normalized forskolin-induced swelling of small intestinal organoids pre-treated for 24 h with DMSO, VRT-325, Corr-4a, or both correctors or stimulated with VX-809 (24 h pre-treatment), VX-770 (simultaneous with forskolin) or their combined treatment (mean ± s.e.m.). (b) Chemical correction of rectal F508del/A455E organoids. Normalized forskolin-induced swelling of rectal F508del/A455E organoids stimulated with VX-809 (24 h pre-treatment) or VX-770 (simultaneous with forskolin) (mean ± s.e.m.).

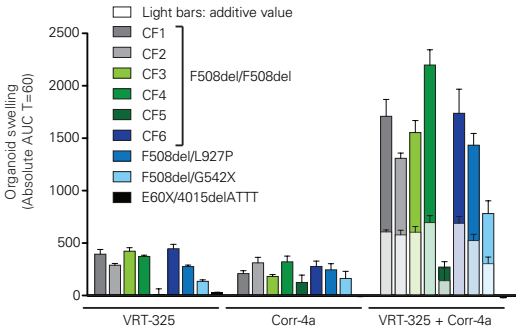

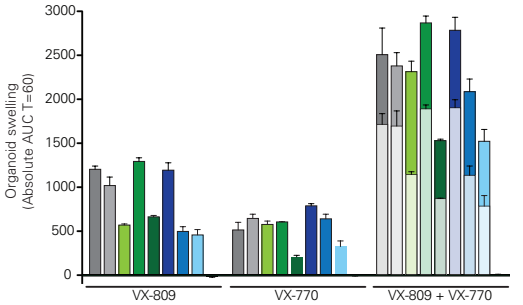

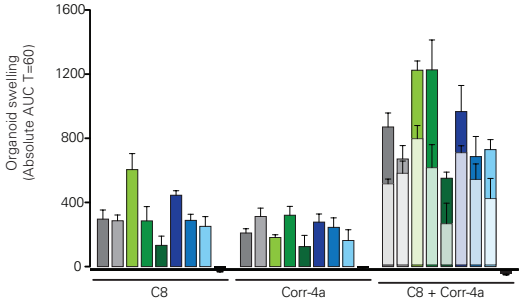

Supplementary Figure 6. Synergy between CFTR correctors. Comparison of measured responses (total bars) and additive (internal bars) responses in rectal organoids upon single or combined drug treatment as indicated in Fig. 5.

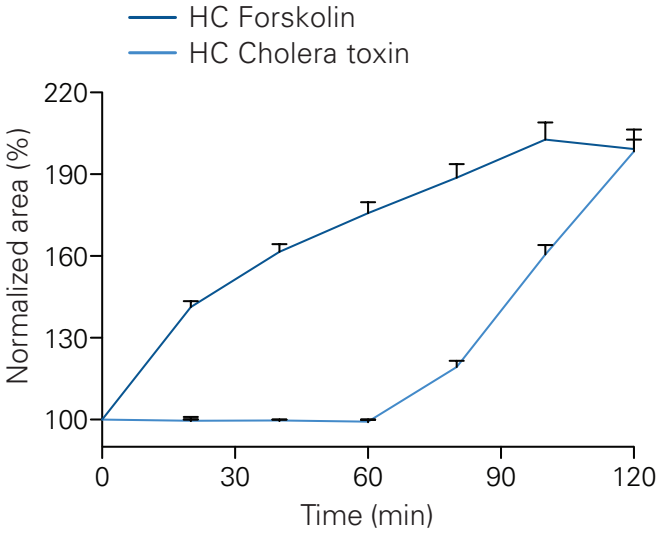

Supplementary Figure 7. Cholera toxin-induced organoid swelling in human rectal organoids is CFTR dependent. Forskolin and cholera toxin induce swelling of healthy control-derived or F508del/F508del organoids. The cholera toxin response is delayed compared to forskolin (mean ± s.e.m.) and absent in F508del/F508del organoids. Results are representative for three different experiments.

CHAPTER 6

INTESTINAL EPITHELIUM IS NOT INTRINSICALLY AFFECTED IN PATIENTS WITH CELIAC DISEASE

CHAPTER 6

Caroline L. Wiegerinck, Michal Mokry, Amani Mubarak, Marijke Groeneveld, Delia-Maria de J. Goilo, Roderick H.J. Houwen, Edward E.S. Nieuwenhuis and Sabine Middendorp

Submitted

ABSTRACT

Celiac disease is caused by an aberrant immune response to gluten in patients with genetic susceptibility. T-helper cells take center stage in the pathogenesis of the disease by recognizing gluten-derived peptides and promoting a pro-inflammatory environment, for example by inducing interferon gamma (IFNγ) production. Additionally, T-helper cells aid B-cells to produce gluten- and transglutaminase 2 (TG2)-specific antibodies and increased serum levels of TG2-antibodies are indicative for active celiac disease. Nonetheless, enterocytes might also be involved in celiac disease, since enterocytes from patients with celiac disease show alterations in gene expression, such as increased expression levels of IFNγ-responsive genes and *TGM2*, the gene encoding TG2. However, it is not known if these enterocytic changes are programmed intrinsically, induced directly by the antigen or indirectly by external factors. Therefore, we have generated epithelial organoid cultures from patients with celiac disease and healthy individuals and compared mRNA expression profiles after long-term culture with their respective biopsies. Our data show that differentially expressed genes in biopsies from patients with celiac disease were normalized upon long-term culture compared to controls. However, these genes were similarly induced in both healthy and celiac organoids upon stimulation with either IFNγ or retinoic acid (RA), a metabolite of vitamin A, which has been shown to have a critical role in the induction of intestinal regulatory responses [1-3]. In conclusion, our data suggest that the intestinal epithelium of patients with celiac disease is not intrinsically different from healthy control epithelium. Despite the fact that the intestinal epithelium might not have a primary role in celiac disease, patient-specific organoids could provide a useful model for understanding epithelial transport of gliadins or for co-culturing with immune cells to better comprehend celiac disease pathophysiology.

INTRODUCTION

Celiac disease is an immune-mediated disorder caused by an abnormal inflammatory response to gluten in genetically susceptible patients. The prevalence of the disease is estimated to be ~1% in Europe [4]. In a small percentage of the people carrying the celiac disease-associated DQ2 or DQ8 HLA types, the ingestion of mainly wheat gluten leads to massive small-bowel mucosal inflammation, crypt hyperplasia, villous atrophy and clinical symptoms, such as failure to grow, abdominal pain and/or malabsorption problems. Other secondary symptoms, such as fatigue, vitamin deficiency and anemia are also commonly reported [5, 6]. The only current therapy that reverses this phenotype is a gluten free diet (GFD). Although a small group of patients suffers from refractory celiac disease and maintain their symptoms despite refraining from gluten [7-9].

Gluten is a protein found in wheat and contains the 'toxic' gliadin [10]. Barley and rye have similar prolamins, hordeins and secalins, which are able to elicit the same response [11]. These storage proteins are highly enriched in the amino acids proline and glutamine. Due to resistance of proline to digestion by intestinal proteases [12], long fragments remain undigested in the intestinal lumen. It was suggested that these fragments are transported to the lamina propria due to increased intestinal permeability [13], although more recent studies show evidence of epithelial transcytosis as the main mechanism [14-16]. Subsequently, glutamine is deamidated (converted to glutamate) by TG2 and negatively charged, which increases binding affinity with the HLA-DQ2/8 molecules that are present on antigen presenting cells [17, 18]. Gliadin fragments are presented to T-helper cells, which help to create a pro-inflammatory environment, after surpassing a minimal threshold of antigen presentation [19]. The pro-inflammatory environment, marked by high IFNγ levels [20], is important for two reasons. First, IFNγ increases expression of HLA-DQ molecules, therefore enhancing T-cell recognition of gluten peptides [21]. Second, IFNγ induces cytotoxic T-cell activation that promotes intestinal damage [22]. This in turn increases release and activation of TG2 and thus improves deamidation and sustains antigen presentation of gluten peptides [23]. Moreover, T-helper cells promote B cell differentiation into plasma cells [24], which produce TG2 antibodies, one of the main serum markers for celiac disease [6, 25]. The discovery of gluten-specific T-helper cells that were only present in celiac patients explains the major role of these cells in the development of celiac disease [26, 27].

The haplotype HLA-DQ2 and/or HLA-DQ8 that is associated with celiac disease is present in ~30% of the population. However, only ~1% of the people develop celiac disease [4]. This suggests that other factors than HLA and gluten-specific T cells must be involved in developing celiac disease. One of the factors that is suggested and debated in literature is the intestinal epithelium. Although it seems quite unlikely that the intestinal epithelium plays a role in the pathogenesis of this clearly immune-mediated disease, the epithelium is an important barrier between gliadin peptides in the intestinal lumen and the T-helper cells in the lamina propria. Moreover, several studies have shown that enterocytes of patients with celiac disease show aberrant expression of several genes in biopsies or in response to gliadin challenge.

One study revealed an increased expression of interleukin 15 (IL15) in enterocytes, even after eight years of GFD [28]. Another study showed increased crypt enterocyte proliferation in biopsy samples of GFD-treated celiac patients [29] and suggests that this is an intrinsic property of celiac enterocytes. Furthermore, gliadin and its p31-49 derived peptide were shown to induce *in vitro* protein expression of MICA, a type of MHC class I molecule, in intestinal epithelial cells from celiac patients on GFD [30]. Interferon regulatory factor-1 (IRF1) and signal transducer and activator of transcription 1 (STAT1), both IFNγ-responsive genes, were upregulated in both lamina propria cells and epithelium upon *in vitro* gliadin exposure in active and GFD-treated celiac patients [31].

Although these and other studies have shown that enterocytes of celiac patients are affected, the majority of these studies were performed on whole biopsies or with freshly isolated enterocytes from biopsies. In this way, it is not possible to determine if these effects are programmed intrinsically, caused by an aberrant response to antigen or are induced by environmental factors, such as cytokines.

As such, it is to our knowledge not yet established whether the enterocytic alterations in intestinal epithelial cells of patients with celiac disease are primary or secondary effects. We hypothesized that the reported enterocytic alterations are secondary effects mediated by inflammatory cytokines such as IFNγ and RA, which have been shown to upregulate the gene encoding TG2, TGM2, one of the major initiators of celiac disease [32-37]. We addressed this hypothesis by establishing pure epithelial cell cultures, so-called organoids, from both celiac patients and healthy control subjects with the same HLA-DQ haplotype. We determined if the expression of epithelial genes, which were up- or down regulated in biopsy material of celiac patients, were maintained after long-term culture in absence or presence of IFNγ and RA.

METHODS

Patient material

Duodenal biopsy material was obtained from patients with a positive HLA-DQ2.5 genotype who were suspected for celiac disease. All participants (and/or parents) were informed about the study and signed written informed consent. The study protocol was examined and approved by the local medical ethics committee of the University Medical Centre Utrecht. Biopsy material was utilized for real-time polymerase chain reaction (RT-PCR) or organoid establishment. Healthy control subjects (5 female, 1 male, median age 5 years old, range 3-9 years) were selected on serum immunoglobulin A (IgA) anti-tissue transglutaminase antibodies (IgA-TG2) of 0 U/ml, combined with a Marsch criteria of 0 and no other pathologic features on histology. Celiac disease patients (4 female, 1 male, median age 12 years old, range 4-15 years) had a minimum of Marsch 3a criteria on histology and elevated serum levels of IgA- endomysial antibodies and IgA-TG2.

Organoid culture

Crypts were isolated from patients' biopsies and cultured as described previously [38]. Duodenal organoids were cultured in expansion medium (containing WNT3A, epidermal growth factor, noggin, R-spondin1, A83-01, N-actylcysteine, B27, SB202190 and nicotinamide) and passaged weekly. Per experiment, organoids (passages varied from 6-14) were cultured with one batch of expansion medium. Differentiation was induced in cultures that were grown in expansion medium for 2 days, followed by 5 days in differentiation medium (expansion medium without WNT3A, nicotinamide and SB202190). For stimulation IFNγ (eBioscience, 1000 IU/ml dissolved in DMSO) was added to the culture medium for 48 hours before harvesting. Retinoic acid (Sigma, 15 μM in DMSO) was added to the organoids 5 hours before harvesting. Unstimulated organoids were treated with similar amount of DMSO as vehicle control. Organoids were photographed with an EVOS-microscope, representative pictures of healthy and celiac organoids are depicted in Supplementary Figure 2.

RNA isolation, mRNA sequencing and real-time PCR

RNA isolation, mRNA sequencing and real-time PCR was performed as described previously [39]. The mRNA sequencing data were analyzed using R with the DESeq package [40]. For real-time PCR data were Data were analyzed in GraphPad Prism, expressed as median, and analyzed for significant differences using the Mann Whitney test. $P < 0.05$ was considered statistically significant. Supplementary Table 2 shows an overview of the primers we have used. *ACTIN* mRNA abundance was used to normalize the data.

RESULTS

Literature about differentially expressed genes

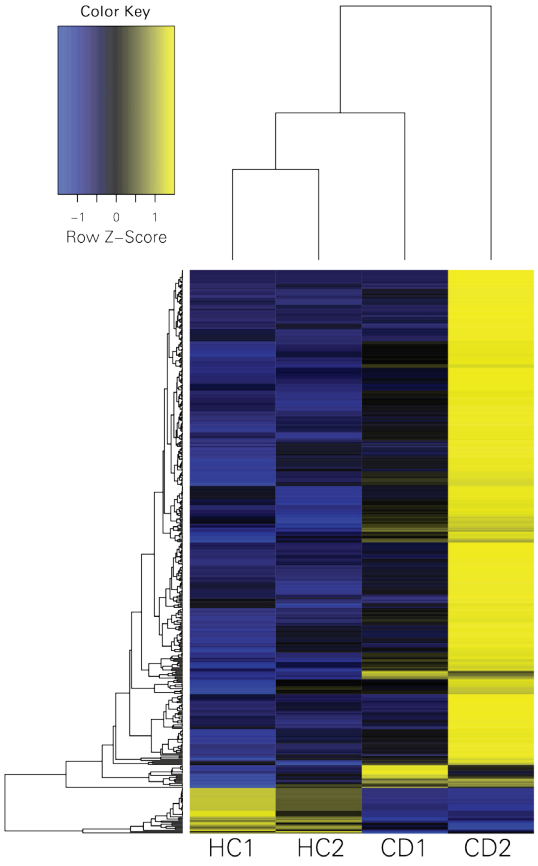

Figure 1. Differential gene expression in biopsies of celiac patients compared to healthy controls. mRNA sequencing was performed on biopsies derived from healthy controls (n=2) and celiac patients (n=2). Yellow indicates maximal expression and blue indicates zero expression. In each compartment, genes are sorted by chromosomal location.

in celiac disease is extensive and sometimes contradictory [23, 31, 41-51]. Therefore, we first performed mRNA sequencing on a selection of duodenal biopsies of celiac patients and healthy controls. Two biopsies per group were sequenced and all differentially expressed genes with >0.6 fold difference and a p-value <0.05 were selected, resulting in a list of 450 genes (Figure 1A and Suppl. Table 1), from which 300 genes were unique values and 150 duplicates. Of these 450 genes, 34 genes were downregulated in celiac biopsies (Suppl. Table 1A) and 416 genes were upregulated in celiac biopsies (Suppl. Table 1B). Notably, CD3 gene expression, a lymphocyte marker, was significantly upregulated in celiac biopsies, which was in agreement with Marsch 3 criteria.

We cross-checked our list of candidate genes with literature to select previously identified genes that were shown to be different in celiac patients compared to controls [23, 31, 41-46, 52, 53]. From our list, 25 genes were identified in other studies, from which ten correlated with the literature and were upregulated in celiac patients. In contrast, we have found 12 genes that were negatively correlated with literature [42, 45]. For example, FABP1 and GSTA1 were both found downregulated in celiac patients by proteomics [45], while they were upregulated in our biopsies. Additionally, three genes were shown to be contradictory in different studies: *DEFA6*, *MUC2* and *FBP1* [47-49, 51], of which we found *FBP1* and *MUC2* to be upregulated in our cohort of celiac patients. One explanation for these discrepancies could be that the studies were performed in adults, while our study is performed in children. Previously, discrepancies between adult and pediatric celiac patients have been described [54, 55]. Nonetheless, our data did correlate with one of the adult studies [41], therefore a heterogeneous celiac population is a more probable explanation for these discrepancies.

We have focused on genes that were differentially expressed in epithelial cells and were in concordance (ten genes) and contradictory (two genes) with previous literature. From this list of 12 genes, we selected eight genes for further validation by real-time PCR. One of the selected genes is *TGM2*, since it is the most prominent marker for celiac disease and is increased in biopsies from patients with celiac disease [6, 23, 56]. Ezrin-Radixin-Moesin-Binding Phosphoprotein 50 (EBP50), which is encoded by *SLC9A3R1*, was selected as an important member of the protein complexes that form the brush border of epithelial cells [44, 57, 58]. More importantly, EPB50 was shown to bind to TG2 and as such may have an important role in celiac disease [59]. And

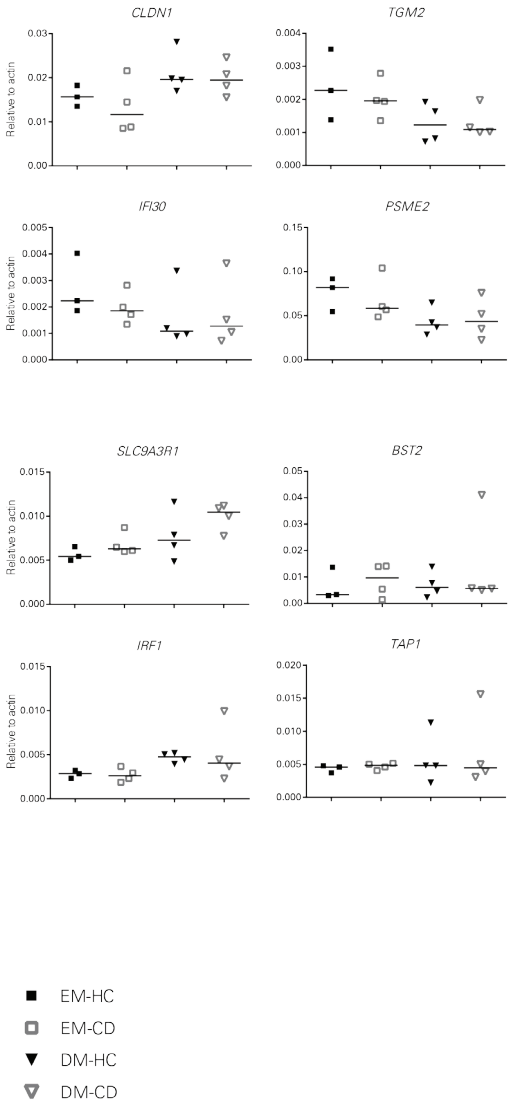

Figure 2. Similar mRNA expression in epithelial cultures derived from celiac patients and healthy controls. Relative expression of differentially expressed genes in organoids derived from healthy controls (n=3) and celiac patients (n=4). Organoids were generated from human duodenal biopsies and maintained in EM for a minimum of 6 weeks. Differentiation was induced by incubation in DM for 5 days. Quantitative reverse transcription PCR was performed to measure relative expression of the mentioned genes. Data were normalized to *ACTIN* housekeeping mRNA levels and are represented as median; *, $p<0.05$. HC, healthy control; CD, celiac disease; DM, differentiation medium; EM, expansion medium.

although not described in literature, the tight junction protein claudin 1, encoded by *CLDN1*, was clearly downregulated in celiac biopsies in our study and was therefore selected for further analysis. Isolated enterocytes of celiac patients expressed levels of bone marrow stromal cell antigen 2 (*BST2*) and therefore added to our list of candidate genes [41]. Next to these epithelial-specific genes, we added several IFNγ-responsive genes to our list of candidate genes: Proteasome activator complex subunit 2 (*PSME2*), IFNγ inducible protein 30 (*IFI30*), transporter 1-ATP-binding cassette (*TAP1*) and IFNγ regulatory factor 1 (*IRF1*) [31, 43].

mRNA sequencing data showed that these selected genes were indeed differentially expressed in biopsies from celiac patients compared to controls (Figure 1a).

Next, we determined expression of our selection of genes in organoids, which were derived from four celiac patients and four healthy controls and were cultured for a minimum of six weeks. Before analysis, proliferation and differentiation status were assessed by light microscopy, and real-time PCR. Light microscopy did not reveal macroscopic differences between healthy and celiac organoids (Suppl. Figure 1A). We determined mRNA expression of LGR5 as a marker for crypt-like organoids (cultured in expansion medium, EM) and sucrase-isomaltase (SI) for villus-like organoids (cultured in differentiation medium, DM). As such, *LGR5* is expressed in EM and lost upon differentiation, while *SI* was not detected in EM and was upregulated in DM (Suppl. Figure 1B). As expected, the expression levels of *LGR5* and *SI* were similar between celiac organoids and controls, indicating that both organoid cultures behaved identical in terms of proliferation and differentiation.

Furthermore, the expression levels of the selected set of genes, which were differentially expressed in *ex vivo* biopsies, showed no significant differences between healthy and celiac derived organoids after long-term culturing (Figure 2). These data indicate that the

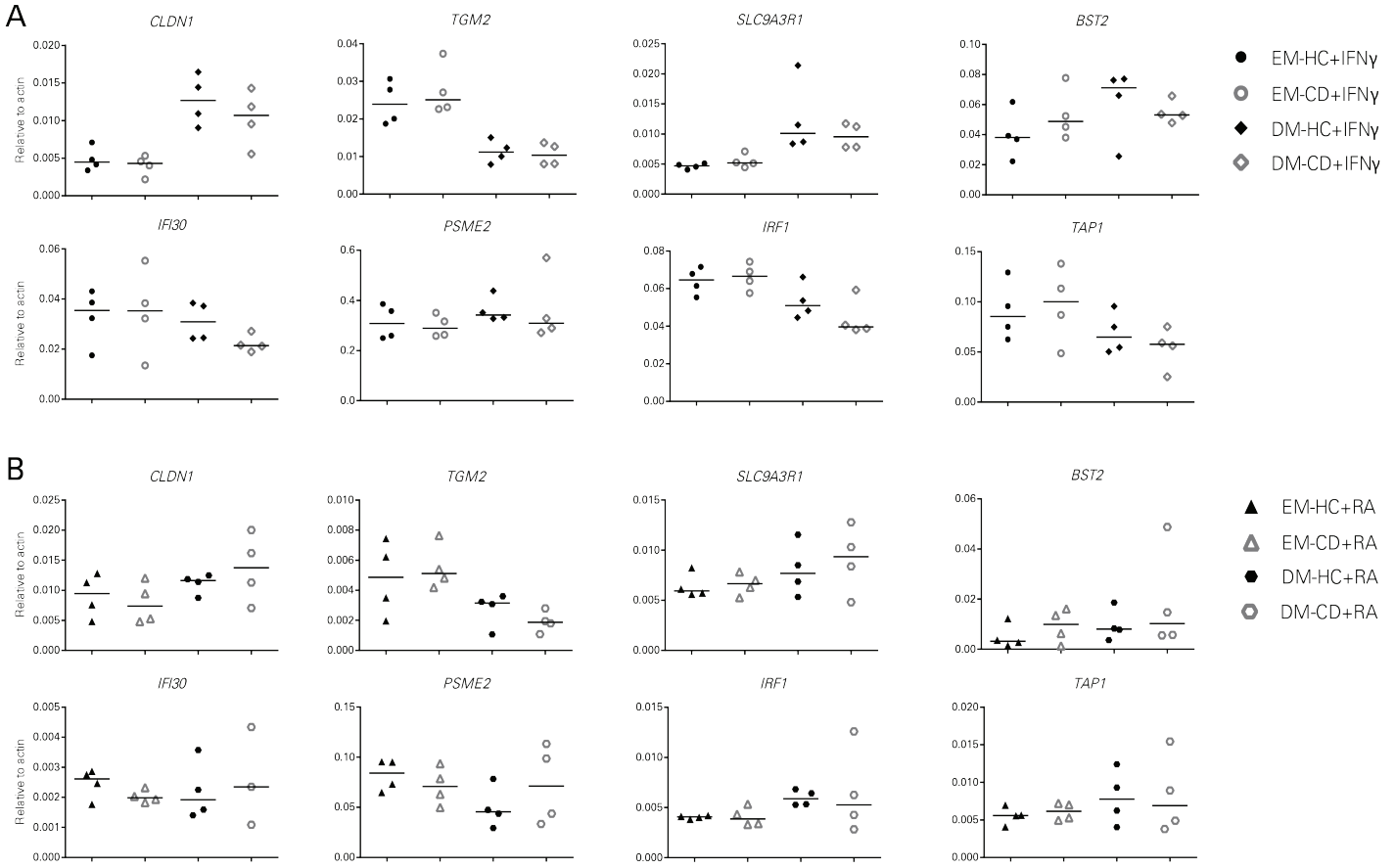

Figure 3. Organoids from celiac patients respond similarly to IFNγ and RA as healthy controls.
Relative expression of differentially expressed genes in organoids stimulated with IFNγ (A) or RA (B). Organoids were derived from duodenal biopsies from healthy controls (n=4) and celiac patients (n=4) and maintained in EM for a minimum of 6 weeks. Differentiation was induced by incubation in DM for 5 days. Organoids were either stimulated with 1000 IU/ml IFNγ for 48 hours (A) or with 15 μM RA for 5 hours (B) before harvesting. Quantitative reverse transcription PCR was performed to measure relative gene expression. Data were normalized to ACTIN housekeeping mRNA levels and are represented as median; *, $p<0.05$. HC, healthy control; CD, celiac disease; DM, differentiation medium; EM, expansion medium, IFNγ, interferon gamma; RA, retinoic acid.

differentially expressed genes in biopsies are not intrinsically programmed in epithelial cells and normalize upon long-term culture.

To assess if the differences in biopsies were dependent on changes in the external environment, we stimulated the organoids with IFNγ, the main active cytokine in celiac disease. First, the efficiency of IFNγ stimulation was validated by analysis of the expression levels of the IFNγ-responsive genes *PSME2*, *IFI30*, *TAP1* and *IRF1*. As expected, these genes were significantly upregulated in organoids that were incubated with 1000 IU/ml IFNγ compared to vehicle control (Suppl. Figure 2A), indicating sufficient response to IFNγ.

Second, we determined expression levels of our selection of genes that were differentially expressed in celiac biopsies. We found that most genes, including *TGM2*, were upregulated upon IFNγ stimulation, while *CLDN1* was downregulated (Figure 3A). However, gene expression levels did not differ between the samples, indicating that both healthy and celiac organoids respond similarly to IFNγ.

Next, we assessed the response of organoids to exogenous RA, one of the other main mediators of celiac disease. Previously, it has been shown that RA induces the activity of *TGM2* in Caco-2 cells [34]. In concordance, we detected increased levels of *TGM2* after 5 hours of RA exposure (Suppl. Figure 2B). Again, no significant differences were observed between organoids from celiac patients and controls after RA stimulation (Figure 3B), strengthening our hypothesis that epithelial changes in celiac disease are caused by exogenous stimulants.

In conclusion, we did not find any differences in gene expression in organoids derived from patients with celiac disease or healthy controls. Furthermore, stimulation with either IFNγ or RA resulted in similar induction of gene expression in both celiac and healthy organoids. Our data indicate that epithelial cells derived from patients with celiac disease, at least for the selected genes, are not intrinsically different and response similarly to the external stimuli IFNγ and RA.

We conclude that differentially expressed genes in biopsies from patients with celiac disease are probably caused by the inflammatory microenvironment in the lamina propria, consisting of e.g. IFNγ and RA, which are produced by activated immune cells upon recognition of deamidated gliadin.

DISCUSSION

In the pathophysiology of celiac disease, a leading role has been attributed to lymphocytes in response to gluten in genetically susceptible patients [22, 60]. Yet, our current knowledge does not clarify why some genetically susceptible patients do not develop celiac disease, suggesting other factors could be involved. One of these factors mentioned in the literature is the intestinal epithelium, although, its role in celiac disease is debated [29, 60-62]. Recently, a pure epithelial intestinal model was established [63], we used this model to assess if the epithelium from patients with celiac disease is intrinsically different from controls.

In this study, we compared gene expression in *ex vivo* biopsies and long-term epithelial cell cultures derived from patients with celiac disease compared to healthy controls. We found 450 genes that were differentially expressed in biopsies from celiac patients. From this list of genes, we selected eight genes on basis of epithelial specificity and complementary results in literature-based evidence, which renders them as potential candidate genes that could have a primary role in the epithelial component of celiac disease. However, we did not detect differences in mRNA expression of these nine genes in organoids derived from patients or controls. In addition, stimulation with either IFNγ or RA resulted in similar induction of these genes in both celiac and control organoids.

One of the limitations of this study is that our gene selection was primarily based on mRNA sequencing of only two biopsies per group. To

prevent selecting coincidentally up- or down regulated genes in celiac biopsies, we cross-checked all differentially expressed genes with known literature to select the most promising epithelial derived candidates genes. Obviously, our strict selection does not exclude the possibility that other genes might play a role in epithelial cells of celiac disease patients.

Although we cannot discard the epithelium from having a prominent role in celiac disease based on detailed analysis of only eight genes, we think it will be unlikely that other genes will show differential expression in organoids. This assumption is supported by the systematic analysis of genetic loci associated with celiac disease and open chromatin regions from more than 350 human tissue/cell samples (Mokry et al. submitted). While the open chromatin regions from immune cells are enriched around the celiac disease susceptibility loci, open chromatin from intestines does not show any enrichment (Suppl. Figure 3).

Our findings indicate that epithelial cells from patients with celiac disease are not intrinsically different from healthy controls. However, to strengthen this negative finding, further studies are needed in a larger number of patients. Although we suggest that epithelial differences in celiac patients are induced by exogenous factors and probably not caused by intrinsic defects, the organoid model could still be useful to assess gliadin transport in a model that resembles the *in vivo* epithelium. Additionally, co-culture studies could be performed to clarify the pathogenesis of celiac disease by studying the interaction of the epithelium with other cells, such as gliadin-specific T-cells, dendritic cells or fibroblasts.

ACKNOWLEDGMENTS

We thank the gastroenterologists of the Wilhelmina Children's Hospital for obtaining biopsies and René Eijkemans from the Julius Center of the UMC Utrecht for statistical advice.

1. Coombes, J.L., et al., A functionally specialized population of mucosal CD103+ DCs induces Foxp3+ regulatory T cells via a TGF-beta and retinoic acid-dependent mechanism. J Exp Med, 2007. 204(8): p. 1757-64.
2. Mora, J.R., M. Iwata, and U.H. von Andrian, Vitamin effects on the immune system: vitamins A and D take centre stage. Nat Rev Immunol, 2008. 8(9): p. 685-98.
3. Mucida, D., et al., Reciprocal TH17 and regulatory T cell differentiation mediated by retinoic acid. Science, 2007. 317(5835): p. 256-60.
4. Mustalahti, K., et al., The prevalence of celiac disease in Europe: results of a centralized, international mass screening project. Ann Med, 2010. 42(8): p. 587-95.
5. Mubarak, A., R.H. Houwen, and V.M. Wolters, Celiac disease: an overview from pathophysiology to treatment. Minerva Pediatr, 2012. 64(3): p. 271-87.
6. Husby, S., et al., European Society for Pediatric Gastroenterology, Hepatology, and Nutrition guidelines for the diagnosis of coeliac disease. J Pediatr Gastroenterol Nutr, 2012. 54(1): p. 136-60.
7. Leffler, D.A., et al., A randomized, double-blind study of larazotide acetate to prevent the activation of celiac disease during gluten challenge. Am J Gastroenterol, 2012. 107(10): p. 1554-62.
8. Abdulkarim, A.S., et al., Etiology of nonresponsive celiac disease: results of a systematic approach. Am J Gastroenterol, 2002. 97(8): p. 2016-21.
9. Roshan, B., et al., The incidence and clinical spectrum of refractory celiac disease in a north american referral center. Am J Gastroenterol, 2011. 106(5): p. 923-8.
10. Dicke, W.K., H.A. Weijers, and J.H. Van De Kamer, Coeliac disease. II. The presence in wheat of a factor having a deleterious effect in cases of coeliac disease. Acta Paediatr, 1953. 42(1): p. 34-42.
11. Di Sabatino, A. and G.R. Corazza, Coeliac disease. Lancet, 2009. 373(9673): p. 1480-93.
12. Wieser, H., Chemistry of gluten proteins. Food Microbiol, 2007. 24(2): p. 115-9.
13. Lammers, K.M., et al., Gliadin induces an increase in intestinal permeability and zonulin release by binding to the chemokine receptor CXCR3. Gastroenterology, 2008. 135(1): p. 194-204.e3.
14. Schumann, M., et al., Mechanisms of epithelial translocation of the alpha(2)-gliadin-33mer in coeliac sprue. Gut, 2008. 57(6): p. 747-54.
15. Lebreton, C., et al., Interactions among secretory immunoglobulin A, CD71, and transglutaminase-2 affect permeability of intestinal epithelial cells to gliadin peptides. Gastroenterology, 2012. 143(3): p. 698-707.e1-4.
16. Matysiak-Budnik, T., et al., Alterations of the intestinal transport and processing of gliadin peptides in celiac disease. Gastroenterology, 2003. 125(3): p. 696-707.

17. Molberg, O., et al., Tissue transglutaminase selectively modifies gliadin peptides that are recognized by gut-derived T cells in celiac disease. Nat Med, 1998. 4(6): p. 713-7.
18. van de Wal, Y., et al., Selective deamidation by tissue transglutaminase strongly enhances gliadin-specific T cell reactivity. J Immunol, 1998. 161(4): p. 1585-8.
19. Vader, W., et al., The HLA-DQ2 gene dose effect in celiac disease is directly related to the magnitude and breadth of gluten-specific T cell responses. Proc Natl Acad Sci U S A, 2003. 100(21): p. 12390-5.
20. Nilsen, E.M., et al., Gluten induces an intestinal cytokine response strongly dominated by interferon gamma in patients with celiac disease. Gastroenterology, 1998. 115(3): p. 551-63.
21. Tjon, J.M., J. van Bergen, and F. Koning, Celiac disease: how complicated can it get? Immunogenetics, 2010. 62(10): p. 641-51.
22. Jabri, B. and L.M. Sollid, Tissue-mediated control of immunopathology in coeliac disease. Nat Rev Immunol, 2009. 9(12): p. 858-70.
23. Esposito, C., et al., Expression and enzymatic activity of small intestinal tissue transglutaminase in celiac disease. Am J Gastroenterol, 2003. 98(8): p. 1813-20.
24. Sollid, L.M., et al., Autoantibodies in coeliac disease: tissue transglutaminase--guilt by association? Gut, 1997. 41(6): p. 851-2.
25. Dieterich, W., et al., Identification of tissue transglutaminase as the autoantigen of celiac disease. Nat Med, 1997. 3(7): p. 797-801.
26. Lundin, K.E., et al., Gliadin-specific, HLA-DQ(alpha 1*0501,beta 1*0201) restricted T cells isolated from the small intestinal mucosa of celiac disease patients. J Exp Med, 1993. 178(1): p. 187-96.
27. Lundin, K.E., et al., T cells from the small intestinal mucosa of a DR4, DQ7/DR4, DQ8 celiac disease patient preferentially recognize gliadin when presented by DQ8. Hum Immunol, 1994. 41(4): p. 285-91.
28. Mention, J.-J., et al., Interleukin 15: a key to disrupted intraepithelial lymphocyte homeostasis and lymphomagenesis in celiac disease. Gastroenterology, 2003. 125(3): p. 730-745.
29. Nanayakkara, M., et al., Enterocyte proliferation and signaling are constitutively altered in celiac disease. PLoS One, 2013. 8(10): p. e76006.
30. Hue, S., et al., A direct role for NKG2D/MICA interaction in villous atrophy during celiac disease. Immunity, 2004. 21(3): p. 367-77.
31. Salvati, V.M., et al., Enhanced expression of interferon regulatory factor-1 in the mucosa of children with celiac disease. Pediatr Res, 2003. 54(3): p. 312-8.
32. DePaolo, R.W., et al., Co-adjuvant effects of retinoic acid and IL-15 induce inflammatory immunity to dietary antigens. Nature, 2011. 471(7337): p. 220-4.
33. Hall, J.A., et al., The role of retinoic acid in tolerance and immunity. Immunity, 2011. 35(1): p. 13-22.
34. Rauhavirta, T., et al., Epithelial transport and deamidation of gliadin peptides: a role for coeliac disease patient immunoglobulin A. Clin Exp Immunol, 2011. 164(1): p. 127-36.
35. Piacentini, M., et al., In vivo and in vitro induction of 'tissue' transglutaminase in rat hepatocytes by retinoic acid. Biochim Biophys Acta, 1992. 1135(2): p. 171-9.
36. Diraimondo, T.R., C. Klock, and C. Khosla, Interferon-gamma activates transglutaminase 2 via a phosphatidylinositol-3-kinase-dependent pathway: implications for celiac sprue therapy. J Pharmacol Exp Ther, 2012. 341(1): p. 104-14.
37. Abadie, V. and B. Jabri, IL-15: a central regulator of celiac disease immunopathology. Immunol Rev, 2014. 260(1): p. 221-34.
38. Dekkers, J.F., et al., A functional CFTR assay using primary cystic fibrosis intestinal organoids. Nat Med, 2013. 19(7): p. 939-45.
39. Middendorp, S., et al., Adult stem cells in the small intestine are intrinsically programmed with their location-specific function. Stem Cells, 2014. 32(5): p. 1083-91.
40. Anders, S. and W. Huber, Differential expression analysis for sequence count data. Genome Biol, 2010. 11(10): p. R106.
41. Bracken, S., et al., Altered gene expression in highly purified enterocytes from patients with active coeliac disease. BMC Genomics, 2008. 9: p. 377.
42. Juuti-Uusitalo, K., et al., cDNA microarray analysis of gene expression in coeliac disease jejunal biopsy samples. J Autoimmun, 2004. 22(3): p. 249-65.
43. Brottveit, M., et al., Mucosal cytokine response after short-term gluten challenge in celiac disease and non-celiac gluten sensitivity. Am J Gastroenterol, 2013. 108(5): p. 842-50.
44. Diosdado, B., A microarray screen for novel candidate genes in coeliac disease pathogenesis. Gut, 2004. 53(7): p. 944-951.
45. Simula, M.P., et al., PPAR signaling pathway and cancer-related proteins are involved in celiac disease-associated tissue damage. Mol Med, 2010. 16(5-6): p. 199-209.
46. Ostensson, M., et al., A possible mechanism behind autoimmune disorders discovered by genome-wide linkage and association analysis in celiac disease. PLoS One, 2013. 8(8): p. e70174.
47. Forsberg, G., et al., Presence of bacteria and innate immunity of intestinal epithelium in childhood celiac disease. Am J Gastroenterol, 2004. 99(5): p. 894-904.
48. Capuano, M., et al., MicroRNA-449a overexpression, reduced NOTCH1 signals and scarce goblet cells characterize the small intestine of celiac patients. PLoS One, 2011. 6(12): p. e29094.
49. Di Sabatino, A., et al., Distribution, proliferation, and function of Paneth cells in uncomplicated and complicated adult celiac disease. Am J Clin Pathol, 2008. 130(1): p. 34-42.
50. Taha, A.S., et al., Natural antibiotic expression in celiac disease--correlation with villous atrophy and response to a gluten-free diet. Dig Dis Sci, 2005. 50(4): p. 791-5.
51. Vordenbaumen, S., et al., Defensin-mRNA expression in the upper gastrointestinal tract is modulated in children with celiac disease and Helicobacter pylori-positive gastritis. J Pediatr

Gastroenterol Nutr, 2010. 50(6): p. 596-600.
52. Juuti-Uusitalo, K., et al., Gluten affects epithelial differentiation-associated genes in small intestinal mucosa of coeliac patients. Clin Exp Immunol, 2007. 150(2): p. 294-305.
53. Planas, R., et al., Regenerating gene Ialpha is a biomarker for diagnosis and monitoring of celiac disease: a preliminary study. Transl Res, 2011. 158(3): p. 140-5.
54. Rodrigo-Saez, L., et al., Differences between pediatric and adult celiac disease. Rev Esp Enferm Dig, 2011. 103(5): p. 238-44.
55. Nistal, E., et al., Differences of small intestinal bacteria populations in adults and children with/without celiac disease: effect of age, gluten diet, and disease. Inflamm Bowel Dis, 2012. 18(4): p. 649-56.
56. Donaldson, M.R., et al., Strongly positive tissue transglutaminase antibodies are associated with Marsh 3 histopathology in adult and pediatric celiac disease. J Clin Gastroenterol, 2008. 42(3): p. 256-60.
57. Diosdado, B., et al., A microarray screen for novel candidate genes in coeliac disease pathogenesis. Gut, 2004. 53(7): p. 944-51.
58. Crawley, S.W., M.S. Mooseker, and M.J. Tyska, Shaping the intestinal brush border. J Cell Biol, 2014. 207(4): p. 441-51.
59. Kristensen, A.R., J. Gsponer, and L.J. Foster, A high-throughput approach for measuring temporal changes in the interactome. Nat Methods, 2012. 9(9): p. 907-9.
60. Koning, F., Pathophysiology of celiac disease. J Pediatr Gastroenterol Nutr, 2014. 59 Suppl 1: p. S1-4.
61. Barone, M.V., R. Troncone, and S. Auricchio, Gliadin peptides as triggers of the proliferative and stress/innate immune response of the celiac small intestinal mucosa. Int J Mol Sci, 2014. 15(11): p. 20518-37.
62. Jabri, B., D.D. Kasarda, and P.H. Green, Innate and adaptive immunity: the yin and yang of celiac disease. Immunol Rev, 2005. 206: p. 219-31.
63. Sato, T., et al., Long-term expansion of epithelial organoids from human colon, adenoma, adenocarcinoma, and Barrett's epithelium. Gastroenterology, 2011. 141(5): p. 1762-72.

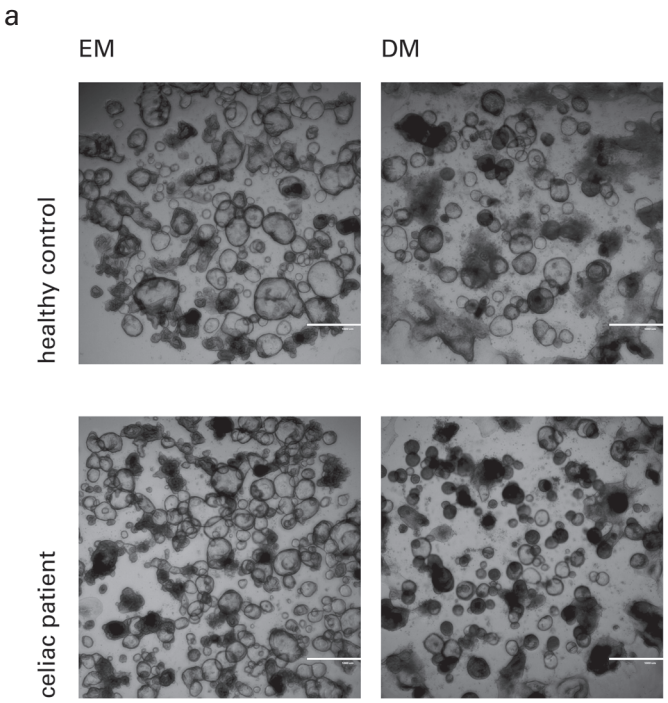

Suppl. Figure 1. Morphology and validation of organoid culture. Organoids derived from patients with celiac disease or healthy controls. were cultured for 7 days in EM or 2 days in EM, followed by 5 days in DM to induce differentiation. (A) Representative pictures by bright field microscopy showed similar morphology. (B) Relative expression of the stem cell marker *LGR5* and the differentiation marker *SI* were validated by real time PCR. Data were normalized to *ACTIN* housekeeping mRNA levels and are represented as median; *, $p<0.05$. HC, healthy control; CD, celiac disease; DM, differentiation medium; EM, expansion medium, *SI*: sucrase isomaltase.

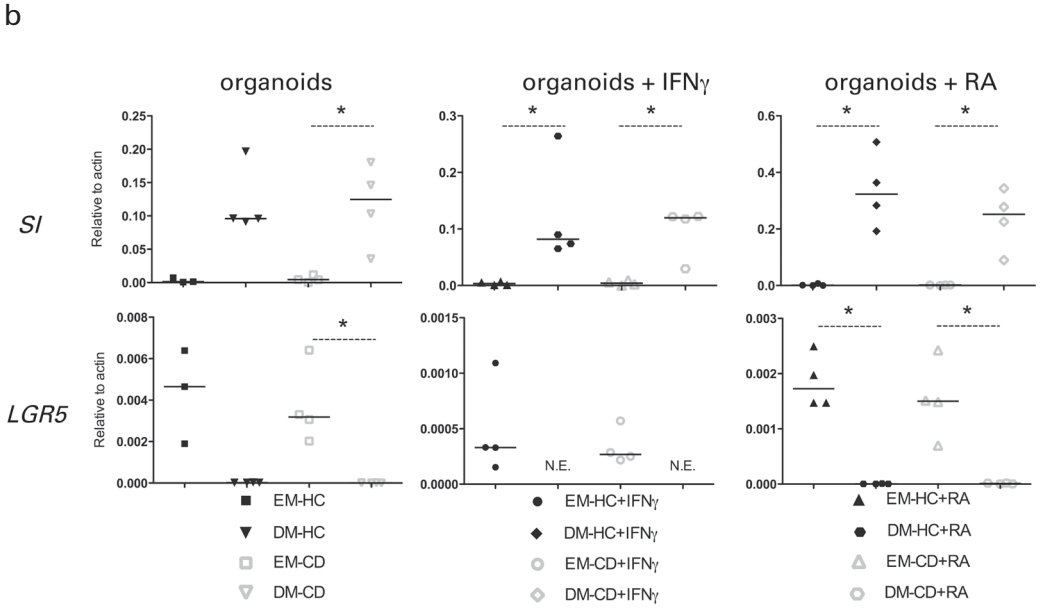

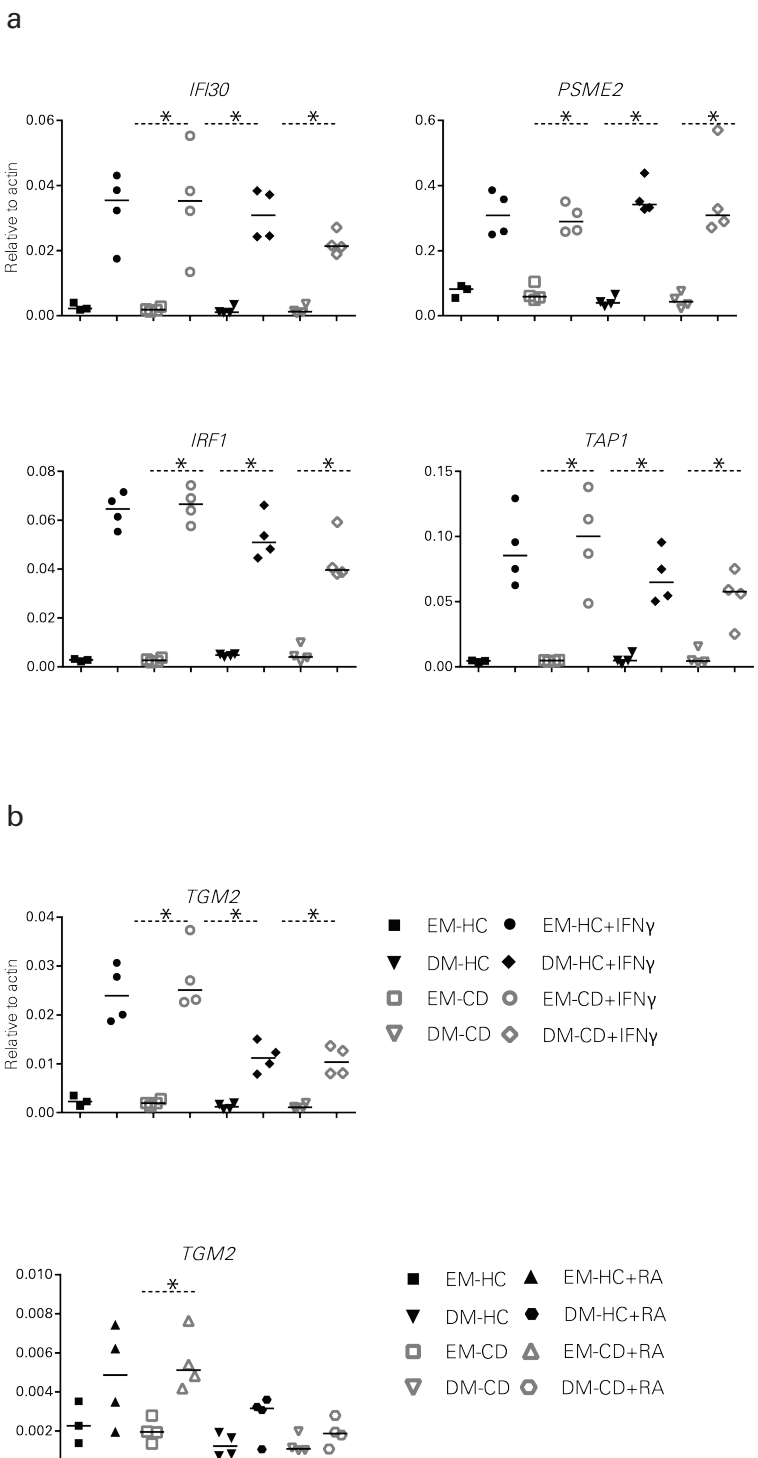

Suppl. Figure 2. Validation of IFNγ and RA stimulation. Organoids from celiac patients (n=4) and healthy controls (n=3-4) were maintained in EM for a minimum of 6 weeks before differentiation was induced by incubation in DM for 5 days. Organoids were stimulated with 1000 IU/ml IFNγ for 48 hours or 15 μM RA for 5 hours. Quantitative reverse transcription PCR was performed to determine relative expression of (A) IFNγ upon stimulation with IFNγ and (B) *TGM2* in response to IFNγ and RA. Data were normalized to *ACTIN* housekeeping mRNA levels and are represented as median; *, $p<0.05$. DM, differentiation medium; EM, expansion medium, IFNγ, interferon gamma; RA, retinoic acid.

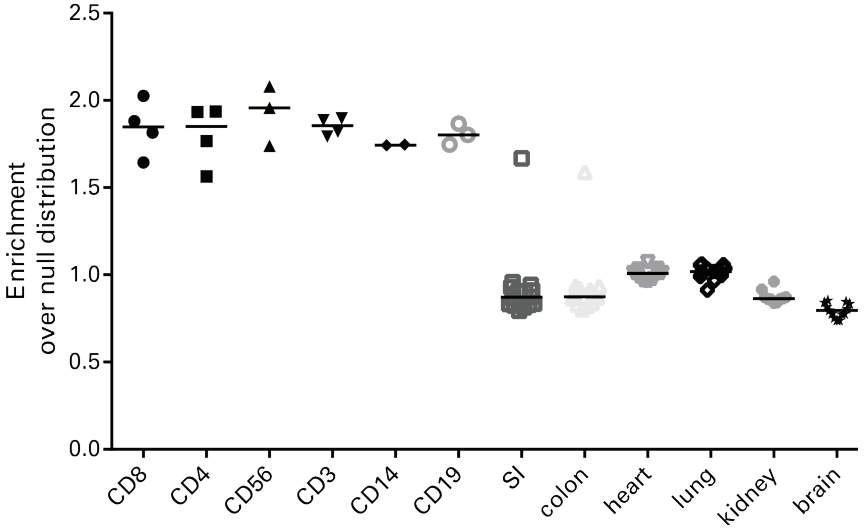

Suppl figure 3. Enrichment of open chromatin near susceptible celiac loci (PMID: 20190752) compared to random loci.
Open chromatin data was derived from Roadmap Epigenomics project (PMID: 20944595).
SI: small intestine.

TABLE S1A. DOWNREGULATED GENES IN CELIAC BIOPSIES VERSUS HEALTHY CONTROLS (HC:CD, FOLD DIFFERENCE >0.6, P-VALUE<0.05)

GENE NAME	REF SEQ ID	BASE MEAN	LOG 2 FOLD CHANGE	P-VALUE
DEFA6	NM_001926	128,4276246	1,746763924	2,17E+07
DMD	NM_004015	2607,710783	1,184388062	5,18E+09
DMD	NM_004017	2607,710783	1,184388062	5,18E+09
DMD	NM_004016	2607,572888	1,184646927	5,15E+09
DMD	NM_004018	2607,572888	1,184646927	5,15E+09
DMD	NM_000109	2606,971184	1,184972955	5,15E+09
DMD	NM_004006	2606,971184	1,184972955	5,15E+09
DMD	NM_004007	2606,971184	1,184972955	5,15E+09
DMD	NM_004009	2606,971184	1,184972955	5,15E+09
DMD	NM_004010	2606,971184	1,184972955	5,15E+09
DMD	NM_004011	2606,833288	1,185232054	5,13E+09
DMD	NM_004012	2606,833288	1,185232054	5,13E+09
DMD	NM_004013	2606,833288	1,185232054	5,13E+09
DMD	NM_004014	2606,833288	1,185232054	5,13E+09
DMD	NM_004021	2606,695393	1,185491182	5,10E+09
DMD	NM_004022	2606,695393	1,185491182	5,10E+09
DMD	NM_004020	2605,907015	1,185406836	5,09E+09
DMD	NM_004023	2606,094361	1,18583781	5,06E+09
SNORD15B	NR_000025	39,16445838	1,384782926	0,000345146
DEFA5	NM_021010	308,1899342	1,010798407	0,002914297
SNORA71D	NR_003018	11,3814428	1,157478121	0,003453154
WT1	NM_000378	29,41354841	1,064492894	0,00735111
WT1	NM_024424	29,41354841	1,064492894	0,00735111
WT1	NM_024425	29,41354841	1,064492894	0,00735111
WT1	NM_024426	29,41354841	1,064492894	0,00735111
RDH11	NM_016026	678,1996438	0,91083822	0,009591172
SNORD47	NR_002746	7,250865409	0,964688529	0,00998523
SNORA42	NR_002974	23,5481408	0,945146958	0,018036504
ATP8B2	NM_001005855	6,524410479	0,801643234	0,025280459
IFT52	NM_016004	18,16336173	0,837264965	0,037444912
SNORD99	NR_003077	10,62731604	0,807986087	0,037561667
SNORD22	NR_000008	16,25565294	0,819587652	0,041950343
CLDN1	NM_021101	43,09541754	0,75005009	0,045540448
SNORD104	NR_004380	13,60626878	0,791428552	0,048459957

TABLE S1B. UPREGULATED GENES IN CELIAC BIOPSIES VERSUS HEALTHY CONTROLS (HC:CD, FOLD DIFFERENCE >0.6, P-VALUE<0.05)

GENE NAME	REF SEQ ID	BASE MEAN	LOG 2 FOLD CHANGE	P-VALUE
MIR663	NR_030386	79,37511813	-2,065036087	7,06E+05
MUC2	NM_002457	111,3645623	-2,199009411	7,19E+05
REG1A	NM_002909	461,7864496	-1,661249651	6,67E+08
HLA-DRB1	NM_002124	240,4458219	-1,674603488	8,35E+08
KIAA0355	NM_014686	102,3821265	-1,48691689	1,14E+09
FLJ40852	NR_015392	62,54817083	-1,538030999	3,94E+09
PSMB9	NM_002800	172,9208646	-1,528165511	5,20E+09
PSMB9	NM_148954	170,0001768	-1,505431174	6,85E+09
IGJ	NM_144646	578,401747	-1,180705519	7,99E+09
BST2	NM_004335	47,85093216	-1,463142079	0,000276203
PTPRCAP	NM_005608	39,1873713	-1,422142131	0,000377224
TAP1	NM_000593	234,10286	-1,243594009	0,000620952
SDF2L1	NM_022044	72,55998927	-1,338961372	0,000667364
HLA-DRB5	NM_002125	69,28718119	-1,327468476	0,000713899
PSME2	NM_002818	410,7813959	-1,231732047	0,000829528
FABP1	NM_001443	1251,555744	-1,191256611	0,000863105
AURKAIP1	NM_001127229	227,2457185	-1,188129521	0,001258054
AURKAIP1	NM_017900	226,1667655	-1,183046261	0,001294839
AURKAIP1	NM_001127230	225,1772863	-1,178901846	0,001349081
IFI30	NM_006332	189,403705	-1,1712111	0,001353169
NLRC5	NM_032206	72,91394556	-1,209367872	0,001538967
HLA-DMB	NM_002118	75,04020877	-1,202646422	0,001898867
NUDT22	NM_032344	77,24526797	-1,151346992	0,002014824
HLA-F	NM_001098478	204,2269045	-1,137139237	0,002096559
AMN	NM_030943	213,2775667	-1,145842127	0,002133928
NKG7	NM_005601	15,31819671	-1,178870401	0,002270012
CCK	NM_000729	47,32567623	-1,226560626	0,002303905
GBP1	NM_002053	19,40026996	-1,220870268	0,002449269
BLVRB	NM_000713	233,7219922	-1,06794651	0,002463491
NUDT22	NM_001128612	75,18322018	-1,127874031	0,002568784
HRASLS2	NM_017878	40,10425921	-1,205117159	0,002788689
SLC43A2	NM_152346	131,9542305	-1,126316881	0,002908376
C22orf15	NM_182520	8,850193329	-1,079490379	0,003167383
ALKBH7	NM_032306	116,764103	-1,080937167	0,003200776
PSMB10	NM_002801	235,4495025	-1,080849828	0,003254339
SLC27A4	NM_005094	342,6400838	-1,052671063	0,003677861
RNASEK	NM_001004333	325,3559845	-1,011721532	0,003685192
GHRL	NM_001134941	15,14264973	-1,136969141	0,003754705
GHRL	NM_016362	15,14264973	-1,136969141	0,003754705
GHRL	NR_024132	15,14264973	-1,136969141	0,003754705
GHRL	NR_024133	15,14264973	-1,136969141	0,003754705
GHRL	NR_024134	15,14264973	-1,136969141	0,003754705
GHRL	NR_024135	15,14264973	-1,136969141	0,003754705

GENE NAME	REF SEQ ID	BASE MEAN	LOG 2 FOLD CHANGE	P-VALUE
GHRL	NR_024136	15,14264973	-1,136969141	0,003754705
GHRL	NR_024137	15,14264973	-1,136969141	0,003754705
GHRL	NR_024138	15,14264973	-1,136969141	0,003754705
FABP2	NM_000134	89,59343919	-1,045148918	0,003773429
HLA-B	NM_005514	2689,136766	-1,035103393	0,004007125
CGREF1	NM_001166240	145,6165729	-1,068352338	0,004072817
SLC6A19	NM_001003841	358,6586126	-1,061854349	0,004110366
CGREF1	NM_001166241	146,6578744	-1,062481716	0,004290946
HLA-F	NM_018950	259,4190014	-1,050907306	0,004307529
GHRL	NM_001134946	9,394718969	-1,0612318	0,00453321
SCT	NM_021920	25,03084341	-1,137981504	0,004630788
NDUFS6	NM_004553	193,9035794	-1,044700996	0,004845492
PPP1R16A	NM_032902	227,3675912	-0,946711955	0,004915227
NUDT22	NM_001128613	63,18321328	-1,06582848	0,004997966
IRF1	NM_002198	148,5548279	-1,018807014	0,005030754
GAST	NM_000805	11,26977773	-1,053117221	0,005069619
FGL2	NM_006682	27,50962172	-1,122875888	0,005104986
TMEM82	NM_001013641	127,7336503	-1,08289613	0,005319502
SIDT2	NM_001040455	114,9423119	-1,016726439	0,005514222
IFI27	NM_001130080	544,5891326	-0,95532038	0,005524316
IFI27	NM_005532	544,5891326	-0,95532038	0,005524316
NDUFA3	NM_004542	240,7511147	-1,030936875	0,005593201
C6orf108	NM_006443	191,6533495	-0,973978804	0,005593902
ETV7	NM_016135	29,69076629	-1,104818706	0,005630541
C6orf108	NM_199184	192,5873507	-0,973656697	0,005653097
HLA-F	NM_001098479	247,7237387	-1,016717451	0,005675419
SCRN2	NM_001145023	62,93333348	-1,046140061	0,005873613
CIDEB	NM_014430	300,0903269	-0,977165044	0,005909735
KHK	NM_000221	441,2007387	-0,95981458	0,005940052
SULT1A2	NM_001054	99,89096188	-1,076471632	0,005949136
COMTD1	NM_144589	83,58520006	-1,048517825	0,006011323
IL32	NM_001012632	1122,523218	-0,924639255	0,006030893
CIDEC	NM_022094	287,5434263	-0,985741049	0,006273514
ZG16	NM_152338	175,4046045	-1,04086402	0,00634012
ATP5D	NM_001687	399,0074907	-0,942513492	0,006654882
SCRN2	NM_138355	62,43825795	-1,031578995	0,006723378
COX6A1	NM_004373	448,3885093	-0,996798003	0,006747485
DERL3	NM_198440	56,18042599	-1,006837608	0,00674795
ATP5EP2	NR_002162	45,14932811	-1,071051789	0,006812371
KHK	NM_006488	417,5457498	-0,946803531	0,006829549
IL32	NM_001012631	1168,754127	-0,911803437	0,006842914
ADA	NM_000022	684,2982842	-0,932396851	0,006919477
DERL3	NM_001002862	53,66229794	-1,012325532	0,006930041
C4orf12	NR_015359	114,4670496	-1,024807968	0,007032032
ACOT7	NM_181865	119,4376789	-1,000154782	0,007079105
MGC29506	NM_016459	44,6253314	-1,009443864	0,007156889
IL32	NM_001012634	1065,864273	-0,899171792	0,007217725
ATP5D	NM_001001975	365,6334124	-0,938862507	0,007290196

GENE NAME	REF SEQ ID	BASE MEAN	LOG 2 FOLD CHANGE	P-VALUE
IL32	NM_001012636	1078,045282	-0,898568256	0,007350192
IL32	NM_004221	1118,274882	-0,897850705	0,007424834
PYCARD	NM_145182	80,23503003	-0,978896815	0,00743007
IL32	NM_001012718	1119,208883	-0,897849551	0,00744202
ATPIF1	NM_178190	129,068325	-0,986602876	0,007453424
IL32	NM_001012633	1093,690578	-0,896410778	0,00771614
ATPIF1	NM_016311	127,6964265	-0,98271119	0,007765096
GNA11	NM_002067	160,2358547	-0,923646548	0,007827404
LAG3	NM_002286	8,115651608	-1,015296909	0,007836871
IL32	NM_001012635	1017,407408	-0,881495417	0,008016601
NAT8B	NM_016347	44,6848478	-1,053455182	0,008089475
COQ4	NM_016035	142,5707522	-0,966075543	0,008279048
NDUFB7	NM_004146	301,9934527	-0,86798732	0,008529425
EPN1	NM_001130072	822,5842559	-0,897823512	0,00866705
NLRP6	NM_138329	50,93490829	-1,039896888	0,008679454
VAMP5	NM_006634	46,24379569	-1,036685532	0,008696866
GHRLOS	NR_004431	9,632858428	-1,007073131	0,008762618
GHRLOS	NR_024145	9,632858428	-1,007073131	0,008762618
GHRLOS	NR_024146	9,632858428	-1,007073131	0,008762618
ACOT7	NM_181864	115,9159591	-0,972636358	0,008847564
C4orf3	NM_001001701	138,2368026	-0,970670874	0,008891558
PSMB8	NM_148919	172,9275977	-0,959577632	0,008948247
PSTPIP1	NM_003978	44,47932909	-1,000773761	0,009096961
ID1	NM_002165	73,23246573	-1,013098447	0,009286437
EPN1	NM_013333	814,7880746	-0,890475386	0,009406471
ID1	NM_181353	76,44109961	-1,007058049	0,009443933
MST1	NM_020998	38,96921467	-1,041186497	0,009698337
MYO1A	NM_005379	756,4964601	-0,920882261	0,00977393
ACOT7	NM_181866	115,9411984	-0,960260747	0,009853159
ITGAL	NM_002209	10,37245781	-1,00216799	0,009905884
C14orf176	NM_001146683	212,4432714	-0,921046151	0,009989272
PSMB8	NM_004159	164,4147031	-0,942842873	0,010102952
MPP1	NM_001166462	75,40230597	-0,93946199	0,010401896
MPP1	NM_002436	75,40230597	-0,93946199	0,010401896
ITGAL	NM_001114380	10,23456233	-0,992665935	0,010568211
SLC39A5	NM_001135195	321,3674037	-0,924899926	0,010807329
C20orf114	NM_033197	23,18778191	-1,025577537	0,010904737
CDC42EP5	NM_145057	366,1101453	-0,883543285	0,011205293
C19orf21	NM_173481	1748,758699	-0,847825864	0,011323286
MPP1	NM_001166461	75,04512592	-0,929946979	0,011393127
EPN1	NM_001130071	810,3758754	-0,866463112	0,011610568
GPR172B	NM_001104577	77,20301487	-0,966036489	0,011733322
LTK	NM_001135685	21,85219114	-1,013110927	0,011815195
GHRL	NM_001134944	12,44124654	-0,972582797	0,011820793
GHRL	NM_001134945	12,44124654	-0,972582797	0,011820793
SLC39A5	NM_173596	319,6164844	-0,909185131	0,011974682
DLEC1	NM_007335	33,42675423	-1,012112125	0,01197842
DLEC1	NM_007337	33,42675423	-1,012112125	0,01197842

GENE NAME	REF SEQ ID	BASE MEAN	LOG 2 FOLD CHANGE	P-VALUE
CPNE5	NM_020939	8,710614562	-0,967653137	0,012093179
GPR172B	NM_017986	76,78932844	-0,960248073	0,012207671
GHRLOS	NR_024144	9,275678375	-0,953925225	0,012208802
MYH14	NM_024729	1334,524737	-0,845131104	0,012301309
VTRNA1-1	NR_026703	43,27092698	-0,971007021	0,01246861
ADH1C	NM_000669	96,30954187	-0,870653783	0,012514442
SULT1A1	NM_177534	157,7506708	-0,862167817	0,012545217
MYH14	NM_001145809	1337,717915	-0,842032427	0,012604857
MYH14	NM_001077186	1337,442124	-0,841753306	0,012626899
NDUFA11	NM_175614	254,1715756	-0,882438317	0,012667077
HLA-E	NM_005516	561,8694168	-0,874410144	0,012757257
HRCT1	NM_001039792	9,607975713	-0,942249702	0,012791169
C2	NM_000063	45,86544681	-0,97079881	0,013004905
NDUFA13	NM_015965	521,6525749	-0,894876737	0,013078414
ACOT7	NM_007274	120,2015886	-0,916889043	0,013210661
SULT1A1	NM_177530	156,7854025	-0,853791005	0,013270584
BAIAP2L2	NM_025045	330,3377443	-0,906761601	0,013296947
SLC23A3	NM_144712	19,11813584	-0,996264338	0,013438563
NDUFS7	NM_024407	187,5343187	-0,910711173	0,01354214
ACP2	NM_001610	149,5394805	-0,858734019	0,013706755
C14orf2	NM_004894	415,5552084	-0,885755213	0,013909714
MPP1	NM_001166460	73,72267752	-0,903816059	0,013996813
C14orf2	NM_001127393	418,8186484	-0,885084602	0,014045429
NEU4	NM_080741	24,31818363	-0,974705978	0,01407354
CHCHD10	NM_213720	308,5253526	-0,891855697	0,014234116
PYCARD	NM_013258	88,41809893	-0,893939538	0,014383715
HCLS1	NM_005335	19,06400167	-0,985668447	0,014463648
RGS11	NM_003834	44,98927868	-0,976417891	0,014676083
RGS11	NM_183337	44,98927868	-0,976417891	0,014676083
SLC25A22	NM_024698	98,31771763	-0,911713232	0,014734207
RASAL3	NM_022904	7,984497079	-0,902748097	0,014975464
CD3D	NM_000732	7,634373299	-0,863901132	0,01503498
LTK	NM_002344	23,74373257	-0,978135528	0,015134214
LTK	NM_206961	23,74373257	-0,978135528	0,015134214
EIF3K	NM_013234	407,0453248	-0,813237253	0,015379978
TMUB1	NM_031434	133,8010252	-0,902167976	0,015466015
C2	NM_001145903	41,17931449	-0,955567418	0,015759389
DAK	NM_015533	515,0154156	-0,84631984	0,015767071
COX8A	NM_004074	926,6530237	-0,827350944	0,015918432
OSTalpha	NM_152672	80,29966236	-0,907846844	0,016162037
CHRNB2	NM_000748	19,87119293	-0,966257256	0,016191788
APOBEC1	NM_001644	50,97771903	-0,946665388	0,016321519
ABCD1	NM_000033	41,98953072	-0,939010579	0,016696941
SULT1A1	NM_001055	158,8824725	-0,825271129	0,016799451
SULT1A1	NM_177529	158,8824725	-0,825271129	0,016799451
XDH	NM_000379	75,40369097	-0,8909492	0,016812601
CD3D	NM_001040651	7,358582342	-0,845143882	0,01685446
CIITA	NM_000246	30,52828076	-0,962256691	0,016965452

GENE NAME	REF SEQ ID	BASE MEAN	LOG 2 FOLD CHANGE	P-VALUE
MUPCDH	NM_031264	1391,839695	-0,842325541	0,017235459
REEP6	NM_138393	661,7468689	-0,81723092	0,017662661
TGM2	NM_004613	68,87340836	-0,861973901	0,017789799
ATP5L2	NM_001165877	24,73424019	-0,953437087	0,017810693
MRPS24	NM_032014	157,7271127	-0,838994734	0,017851692
MUPCDH	NM_021924	1605,883795	-0,835278097	0,017875936
CD3E	NM_000733	25,33966007	-0,95255918	0,017962305
LOC96610	NR_027293	33,65113053	-0,920630513	0,018063711
GPA33	NM_005814	428,8843387	-0,806339525	0,018251323
RAB4B	NM_016154	71,93033251	-0,873360745	0,018278089
DHDH	NM_014475	23,83083418	-0,945854024	0,018327589
DDTL	NM_001084393	105,3178323	-0,875064587	0,018608349
ODF3B	NM_001014440	13,48991756	-0,932605032	0,018737096
TMUB1	NM_001136044	130,6358136	-0,876546742	0,018760365
DDT	NM_001084392	105,1799369	-0,873493474	0,018798685
DDT	NM_001355	105,1799369	-0,873493474	0,018798685
HBB	NM_000518	9,852499563	-0,893771029	0,018871188
SNCA	NM_000345	18,21604939	-0,943008881	0,019261128
TFF2	NM_005423	1311,956132	-0,78320997	0,019976876
BCL3	NM_005178	128,9986131	-0,823671086	0,019998706
DHRS11	NM_024308	606,3596589	-0,747928624	0,020210158
SLC2A5	NM_001135585	57,02466438	-0,920206978	0,020541104
HN1	NM_001002033	596,1099434	-0,773689279	0,020611542
IL17RC	NM_032732	59,08947292	-0,854635354	0,020631947
GSTA1	NM_145740	110,7739043	-0,85574075	0,020639801
IL2RB	NM_000878	15,50560056	-0,919126339	0,020857886
HN1	NM_001002032	595,7527633	-0,772279208	0,020927386
HN1	NM_016185	595,7527633	-0,772279208	0,020927386
SNCA	NM_001146055	18,07815391	-0,930254966	0,020932529
HSD11B2	NM_000196	41,65588962	-0,906069006	0,021287341
ANXA2P3	NR_001446	100,2862453	-0,899858277	0,021292837
OGFR	NM_007346	97,94551728	-0,853711176	0,021521691
PDX1	NM_000209	559,1074187	-0,694290589	0,022222016
NDUFB9	NM_005005	357,4768255	-0,781379655	0,022351765
TM6SF2	NM_001001524	295,9754634	-0,809953474	0,022459095
C14orf73	NM_001077594	15,17263134	-0,909401815	0,022578237
BAX	NR_027882	101,3441198	-0,811441923	0,022938506
SLC39A4	NM_017767	465,4723949	-0,802877282	0,023062021
GIP	NM_004123	21,29525327	-0,913723069	0,023151293
BAX	NM_138761	101,2062243	-0,809578408	0,023218047
RABAC1	NM_006423	149,8731437	-0,815093875	0,023288675
CLDN5	NM_001130861	11,54963914	-0,884230145	0,023434604
CLDN5	NM_003277	11,54963914	-0,884230145	0,023434604
TBX10	NM_005995	24,63941043	-0,912486212	0,023572589
SHD	NM_020209	13,22323976	-0,894040901	0,023797322
VAMP8	NM_003761	523,8215035	-0,796203132	0,023920231
SPINK4	NM_014471	50,94310955	-0,87070616	0,024031719
SOD1	NM_000454	504,6456492	-0,743181562	0,024065367

GENE NAME	REF SEQ ID	BASE MEAN	LOG 2 FOLD CHANGE	P-VALUE
MRPL41	NM_032477	129,5137758	-0,85269108	0,024318577
C6orf203	NM_001142468	56,93641842	-0,863091854	0,024489175
C6orf203	NM_001142470	56,93641842	-0,863091854	0,024489175
IL17RC	NM_153461	59,79713331	-0,828845703	0,024556993
ZFP36	NM_003407	201,1752935	-0,801782987	0,024587587
MGST3	NM_004528	457,1397118	-0,753590253	0,024696091
HLA-A	NM_002116	4365,173822	-0,770157286	0,024735661
TLCD2	NM_001164407	70,87497882	-0,821499817	0,024939543
AADAC	NM_001086	47,18593784	-0,867236162	0,024954526
MGAM	NM_004668	63,4194366	-0,854611944	0,025011968
IL17RC	NM_153460	59,65923783	-0,825653896	0,025087969
EDF1	NM_153200	166,8519544	-0,809829708	0,025261895
LOC150197	NR_026919	4,268018879	-0,747283183	0,025300567
RECQL5	NM_004259	64,82667475	-0,85737488	0,025398333
ACY1	NM_000666	801,5249107	-0,774560922	0,025414961
AQP3	NM_004925	142,4986923	-0,807514925	0,025471821
POU2AF1	NM_006235	16,50148117	-0,899256202	0,025525211
GZMA	NM_006144	8,72980897	-0,800162701	0,025950115
HSD3B7	NM_025193	59,81422753	-0,82478708	0,026079724
ARHGDIA	NM_004309	1498,439663	-0,738854782	0,026095128
SLC9A3R1	NM_004252	1076,802693	-0,718898723	0,026116187
ACADS	NM_000017	169,8484352	-0,77823048	0,026122178
PECAM1	NM_000442	8,441921114	-0,850722763	0,026238311
GNG7	NM_052847	4,381031641	-0,7386058	0,026277288
SNCA	NM_001146054	18,32267776	-0,890451509	0,027091648
SNCA	NM_007308	18,32267776	-0,890451509	0,027091648
ID3	NM_002167	41,40332436	-0,884525341	0,027094794
SLC23A3	NM_001144889	21,44391892	-0,889568158	0,027235231
SLC23A3	NM_001144890	21,44391892	-0,889568158	0,027235231
SLC39A4	NM_130849	464,8136122	-0,778985202	0,027845958
ATP5L	NM_006476	462,8535387	-0,751912622	0,028061314
SEPX1	NM_016332	100,3186894	-0,777387002	0,028133958
NDUFA1	NM_004541	266,8595204	-0,797595819	0,028455517
TRIM21	NM_003141	58,09560588	-0,81486646	0,028462277
LSP1	NM_002339	26,16167491	-0,879648999	0,02856618
LMF2	NM_033200	104,1196158	-0,743974309	0,028738082
MOGAT3	NM_178176	87,64763231	-0,832933568	0,029074704
ABCG5	NM_022436	22,07859026	-0,879261263	0,029129337
TMEM25	NM_001144036	41,91758506	-0,824394399	0,029389629
TUBB2A	NM_001069	63,1379161	-0,848246077	0,029998457
ITFG3	NM_032039	590,2652631	-0,75709656	0,030323454
ETFB	NM_001985	281,5799431	-0,778285237	0,030427866
MLN	NM_001040109	29,37031088	-0,869887824	0,030752371
MLN	NM_002418	29,37031088	-0,869887824	0,030752371
SLC37A4	NM_001164278	214,3756991	-0,755679904	0,030828033
C19orf77	NM_001136503	1960,27423	-0,759606602	0,030855852
ABI3	NM_001135186	14,27226941	-0,840469967	0,030892831
C17orf89	NM_001086521	25,67766784	-0,869631757	0,030933067

GENE NAME	REF SEQ ID	BASE MEAN	LOG 2 FOLD CHANGE	P-VALUE
LTBP3	NM_001164266	36,89579806	-0,843686652	0,030974018
LTBP3	NM_021070	36,89579806	-0,843686652	0,030974018
HSD3B7	NM_001142777	59,29426928	-0,804313025	0,031196133
UQCR	NM_006830	264,367871	-0,744243591	0,031225262
GALM	NM_138801	116,1267955	-0,711177145	0,031449788
CCDC72	NM_015933	15,84799619	-0,863225655	0,031655218
PRR13	NM_018457	336,8321275	-0,706475288	0,031791745
TREH	NM_007180	108,3177422	-0,824404554	0,031995941
TYMP	NM_001113756	124,8311492	-0,785140358	0,032562488
PRR13	NM_001005354	336,4749475	-0,704071001	0,03256722
C19orf33	NM_033520	165,3875359	-0,770875809	0,032629532
SLC37A4	NM_001164280	208,5433372	-0,752265472	0,032837931
SLC37A4	NM_001467	208,5433372	-0,752265472	0,032837931
UBE2L6	NM_198183	190,2176485	-0,723549396	0,033011011
PRDX2	NM_005809	616,8643199	-0,689422585	0,033036589
LOC100271831	NR_027081	191,4394602	-0,748459004	0,033073399
PNKD	NM_001077399	75,28806598	-0,760615362	0,033280604
L TBP3	NM_001130144	37,41611287	-0,832285973	0,033302847
UBE2L6	NM_004223	192,3543857	-0,721560945	0,033470241
SLC22A18	NM_002555	421,6960066	-0,733709626	0,033470974
DBP	NM_001352	84,87183595	-0,815386145	0,033829007
HSD3B7	NM_001142778	57,12626501	-0,793080897	0,034012043
PRSS8	NM_002773	861,9719648	-0,717149724	0,034032338
SLC37A4	NM_001164277	222,8755678	-0,734796915	0,034249582
TYMP	NM_001113755	126,0792648	-0,771387732	0,034272917
TYMP	NM_001953	123,2712332	-0,769012817	0,034752485
DNPEP	NM_012100	217,2807509	-0,713430864	0,034879536
CTSZ	NM_001336	413,0278304	-0,736832189	0,034931719
SLC22A18	NM_183233	419,4153462	-0,727972251	0,03502508
NDUFA7	NM_005001	99,52562568	-0,736140056	0,035123924
YIF1B	NM_033557	221,7844576	-0,727307814	0,035171634
FAM128A	NM_001085365	37,32827903	-0,828739736	0,035451881
ACAA1	NM_001607	303,4221022	-0,700905835	0,035476626
S100A16	NM_080388	1324,172631	-0,663633828	0,035765237
PLEC1	NM_201378	536,4221154	-0,717102104	0,036039976
PLEC1	NM_201382	535,8705335	-0,715628205	0,036350907
BAX	NM_138764	89,29296245	-0,754262399	0,03641267
PLEC1	NM_201380	537,943708	-0,713257306	0,036525333
YIF1B	NM_001039672	221,289382	-0,722810988	0,036543412
YIF1B	NM_001039673	221,289382	-0,722810988	0,036543412
YIF1B	NM_001145463	221,289382	-0,722810988	0,036543412
HYI	NM_031207	63,54595037	-0,815695651	0,036859904
PLEC1	NM_201381	535,5133534	-0,714040411	0,036907108
SNORA63	NR_002586	9,224860301	-0,774527989	0,036918364
PLEC1	NM_201383	534,9617715	-0,712562138	0,037225727
DNASE1	NM_005223	170,8419379	-0,792873892	0,037258393
ACAA1	NR_024024	297,5897404	-0,697730528	0,037379823
DGKQ	NM_001347	91,86734399	-0,759242516	0,037499156

GENE NAME	REF SEQ ID	BASE MEAN	LOG 2 FOLD CHANGE	P-VALUE
YIF1B	NM_001039671	221,890414	-0,719695323	0,037502567
YIF1B	NM_001145461	221,890414	-0,719695323	0,037502567
CHST5	NM_024533	111,6033902	-0,758730622	0,037565772
YIF1B	NM_001145462	221,7525186	-0,718808089	0,03769943
PRR5	NM_001017530	89,03810237	-0,731797618	0,037752763
UBL5	NM_001048241	158,5375172	-0,774460634	0,037788404
PLEC1	NM_201384	541,1267873	-0,710749424	0,037828803
NR2F6	NM_005234	171,9771588	-0,679007812	0,037842839
PLEC1	NM_201379	536,8792241	-0,710684381	0,037870203
COX7A2	NM_001865	271,0912374	-0,680683187	0,037882445
COX7A2	NR_029466	271,0912374	-0,680683187	0,037882445
PLEC1	NM_000445	535,6694319	-0,709556986	0,038045658
SHBG	NR_027462	8,530723043	-0,766111862	0,038320929
SHBG	NR_027463	8,530723043	-0,766111862	0,038320929
LSP1	NM_001013253	25,25291295	-0,832665089	0,038442428
LSP1	NM_001013254	25,25291295	-0,832665089	0,038442428
LSP1	NM_001013255	25,25291295	-0,832665089	0,038442428
SLC7A9	NM_014270	118,8171224	-0,769494983	0,038457735
C19orf69	NM_001130514	41,98623165	-0,820998831	0,038493103
LOC440957	NM_001124767	51,87851283	-0,784585504	0,038493311
HLA-C	NM_002117	3270,464124	-0,703290468	0,038580755
SNORA55	NR_002983	13,33587176	-0,8158076	0,03863322
COL6A2	NM_058175	19,55407781	-0,829867082	0,039251238
UBL5	NM_024292	159,658864	-0,767857705	0,039521128
ETFB	NM_001014763	248,9922438	-0,737501891	0,040104133
RPL36AL	NM_001001	108,8470474	-0,793891981	0,040139339
MYL4	NM_001002841	5,784553817	-0,699046997	0,040392128
MYL4	NM_002476	5,784553817	-0,699046997	0,040392128
PCSK1N	NM_013271	16,48770815	-0,815404005	0,040412566
COL6A2	NM_058174	19,41618233	-0,823364031	0,040808982
CARD16	NM_052889	8,610768375	-0,764238897	0,040812272
SLC7A9	NM_001126335	115,4393259	-0,759923147	0,04084781
HNRNPM	NM_031203	65,47582807	-0,744852177	0,040850078
UCRC	NM_013387	458,918762	-0,70620437	0,041318602
POLD4	NM_021173	410,9879241	-0,682442469	0,041405864
AKR7A3	NM_012067	383,3707474	-0,735940124	0,041628652
C10orf54	NM_022153	179,3906751	-0,716775824	0,041959017
FCGBP	NM_003890	155,982618	-0,744556326	0,04212283
POLR2L	NM_021128	248,1788812	-0,696436199	0,042206002
RPPH1	NR_002312	283,346006	-0,648247967	0,04221697
PRR5	NM_001017529	82,58956749	-0,714500078	0,042387827
EDF1	NM_003792	265,6947123	-0,728042076	0,042698786
ACAA1	NM_001130410	209,6849843	-0,716588241	0,042707346
CD6	NM_006725	10,14647352	-0,777774334	0,042923008
C2CD2L	NM_014807	106,0038289	-0,714753815	0,043082755
CARD16	NM_001017534	8,472872897	-0,754270897	0,04321563
FAM128B	NM_025029	63,18238385	-0,769134107	0,043413744
MDK	NM_002391	454,3004459	-0,697629042	0,043419479

GENE NAME	REF SEQ ID	BASE MEAN	LOG 2 FOLD CHANGE	P-VALUE
MDK	NM_001012334	459,0989191	-0,698093041	0,043521842
MDK	NM_001012333	454,1625504	-0,697194353	0,043527676
COL6A2	NM_001849	41,24024996	-0,812137163	0,043570583
SLC37A4	NM_001164279	191,0250828	-0,722129324	0,04379916
UCRC	NM_001003684	476,560227	-0,692403195	0,043894141
PRR5	NM_015366	90,5112733	-0,706580615	0,044583237
ATPIF1	NM_178191	175,8857533	-0,698261652	0,044757258
SCAND1	NM_016558	99,90777507	-0,741811084	0,044866255
IL2RG	NM_000206	139,4046068	-0,678021779	0,045270462
FAM132A	NM_001014980	15,61021329	-0,789364771	0,045637727
PRR5	NM_181333	85,29741334	-0,699753692	0,045734299
NDUFB8	NM_005004	295,1793274	-0,66826924	0,04574883
TRIM56	NM_030961	49,06640874	-0,751259531	0,045926361
SCAND1	NM_033630	85,38819685	-0,751241304	0,046075059
C5orf56	NM_001013717	3,49715239	-0,632456332	0,046089935
CPS1	NM_001122634	60,52667357	-0,74466188	0,046106709
TIMM8B	NM_012459	75,92878728	-0,732310717	0,04642166
SELENBP1	NM_003944	145,5820157	-0,684839534	0,046815006
CHD5	NM_015557	4,781236177	-0,623937387	0,046975704
C17orf61	NM_152766	232,5587622	-0,670572457	0,047052009
NDUFAB1	NM_005003	169,8534696	-0,689873834	0,047548459
HNRNPM	NM_005968	70,40045641	-0,714826292	0,047615827
LDHD	NM_153486	20,82238996	-0,795358682	0,047653106
SCNN1D	NM_001130413	11,97579606	-0,785699172	0,047781585
PRAP1	NM_145202	1454,240211	-0,69484946	0,048050988
C1QC	NM_001114101	139,0289125	-0,737133924	0,048185318
C1QC	NM_172369	139,0289125	-0,737133924	0,048185318
CLDN15	NM_014343	667,9883797	-0,674836933	0,048228284
GMPPA	NM_205847	103,4574778	-0,701067747	0,04886007
ABCC6	NM_001171	30,33091012	-0,777167777	0,049032605
NUCB1	NM_006184	748,3385753	-0,644015366	0,049346111
TXNDC17	NM_032731	87,99840679	-0,753180151	0,04957105
VAMP2	NM_014232	136,3786195	-0,696132137	0,049587329
LAT	NM_001014989	8,667274756	-0,722048015	0,049617351
FBP1	NM_001127628	535,2167324	-0,667076736	0,049649649
NUDT16	NM_152395	39,08838676	-0,749404498	0,049698038
SELM	NM_080430	33,26744991	-0,770686367	0,049997768

TABLE S2. REAL TIME RT-PCR PRIMER SEQUENCES

GENE		SEQUENCE (5′ -> 3′)	REFERENCE	PRIMERBANK ID
ACTB	Forward:	CTGGAACGGTGAAGGTGACA	Designed with	
	Reverse:	AAGGGACTTCCTGTAACAATGCA	OLIGO-6 program	
DEFA6	Forward:	CTGAGCCACTCCAAGCTGAG	primerbank #, ^	315434256c1
	Reverse:	GTTGAGCCCAAAGCTCTAAGAC		
PSME2	Forward:	GCAAGAGGACTCCCTCAATGT	primerbank #, ^	30410791c1
	Reverse:	CTTCTGGCTTAACCAGGGCA		
TAP1	Forward:	CGCCTCACTGACTGGATTCTA	primerbank #, ^	53759115c3
	Reverse:	TCTGTTGGAAAAACTCCGTCTC		
IFI30	Forward:	TCCAATGCACCGCTTGTCAAT	primerbank #, ^	29826337c2
	Reverse:	ACCTTGTTGAATTTGCACTCCTC		
SLC9A3R1	Forward:	GGCTGGCAACGAAAATGAGC	primerbank #, ^	381214354c1
	Reverse:	TGTCGCTGTGCAGGTTGAAG		
TGM2	Forward:	GAGGAGCTGGTCTTAGAGAGG	primerbank #, ^	39777596c1
	Reverse:	CGGTCACGACACTGAAGGTG		
BST2	Forward:	CACACTGTGATGGCCCTAATG	primerbank #, ^	7262372c1
	Reverse:	GTCCGCGATTCTCACGCTT		
IRF	Forward:	AGAGCAAGGCCAAGAGGAAGTCAT	*	
	Reverse:	ACTGTGTAGCTGCTGTGGTCATCA		
CLDN1	Forward:	TGCAGGTCTGGCTATTTTA	Designed with	
	Reverse:	AGCCTGACCAAATTCGTA	OLIGO-6 program	
MUC2	Forward:	CAGGCCGGAGGAAGGAA	Designed with	
	Reverse:	GGTGGTGGGGAGGGTGAT	OLIGO-6 program	

A. Spandidos, X. Wang, H.Wang and B. Seed: PrimerBank: a resource of human and mouse PCR primer pairs for gene expression detection and quantification. Nucl. Acids Res. 2010 38:D792-9.

^ X. Wang and B. Seed: A PCR primer bank for quantitative gene expression analysis. Nucleic Acids Research 2003 31(24): e154; pp.1-8.

* A.J. Stoppelenburg, J.H. von Hegedus, R. Huis in 't Veld, L. Bont and M. Boes: Defective control of vitamin D receptor-mediated epithelial STAT1 signaling predisposes to severe respiratory syncytial virus bronchiolitis. J. of Pathol. 2014 232:57-64.

THE ORGANOID

The noun 'organoid' broadly means resembling an organ (see box 1; from Lancaster & Knoblich, Science 2014[1]). Although, after reading this thesis, we assume the term organoid is now well-known, some Japanese manga anime fans associate this term with something entirely different: a fictional mechanical creature that fights and protect the people that command it. Still, both organoids might share some similarities: can they both protect people? In our case, increase knowledge about intestinal diseases to prevent or treat diseases? And can they be commanded/manipulated by people for good use?

The aim of this thesis was to use organoids as a model for intestinal diseases. The biggest question is how valuable these organoids are for patients, doctors and scientists. To evaluate this, we have to address the following questions: are there other intestinal models available? Do the organoids genuinely recapitulate the *in vivo* intestine? For which applications could organoids be useful? And what future research could be conducted and recommended from a clinical point of view? In short: how valuable are these organoids as intestinal disease models and what clinical potential do they have?

Box 1 (from Lancaster and Knoblich, Science, 2014)[1]
Defining organoids.

ORGANOID n. Resembling an organ.

This implies:
1. Multiple organ-specific cell types

2. Capable of recapitulating some specific function of the organ (eg. excretion, filtration, neural activity, contraction)

3. Grouped together and spatially organized similar to an organ
Organoid formation recapitulates both major processes of self-organization during development: cell sorting out and spatially restricted lineage commitment

Definition:
A collection of organ-specific cell types that develops from stem cells or organ progenitors and self-organizes through cell sorting and spatially restricted lineage commitment in a manner similar to in vivo.

INTESTINAL MODELS: WHICH OTHER MODELS EXIST?

To evaluate the use of organoids as an intestinal *in vitro* model, it is essential to have an overview of the currently used models to study the intestine. These models could roughly be divided into three categories: a) *in vivo* models (in a living organism); b) *ex vivo* models (outside a living organism for a short period of time); c) *in vitro*

models (cells/tissue cultured in a dish). *In vivo* models encompass animal models, such as mice or pigs, which are beneficial for studying disease pathophysiology and determining the role of certain genes or cells within a living organism. The major downside of animal models is the fact that they are not human and therefore these data are not always translatable to patients. Other models that are also considered to represent *in vivo* are cultured cells that are transplanted back into an organism. For example, intestinal organoids derived from embryonic or pluripotent stem cells that have been transplanted into the kidney capsule of mice or engraftment of small intestinal organoids into the colon [2, 3]. Both studies show that intestinal organoids maintain their cell types and function in an *in vivo* model.

The main source of *ex vivo* tissue is the intestinal biopsy; helpful in the diagnosis and understanding of pathology of many intestinal diseases. Biopsies are often directly fixed after endoscopy, which preserves the *in vivo* architecture. It is also possible to mount biopsies immediately into an Ussing chamber to detect and quantify transport and barrier functions. However, epithelial cells do not survive for a long time outside the body [4]. The downside of using intestinal biopsies is the limited availability of material and limited survival of the cells when not immediately fixed for pathology.

Next to *in vivo* and *ex vivo* models, there are also several *in vitro* models to study intestinal cells, which are summarized in Table 1 (adapted from [5]).

Organ	Cellular input	Culture format	Refs*
Small intestine	Cell line (for example, Caco-2)	2D culture	[11, 12]
	Organ slice	Mechanically supported	[4, 11]
	Tissue organoid	3D-embedded culture	[12-16]
	Stem cell organoid (LGR5+)	3D-embedded culture	[9, 10, 13]
	Stem cell organoid (iPS cells)	3D-embedded culture	[14]
Colon	Organ slice	Mechanically supported	[11, 20]
	Tissue organoid	3D-embedded culture	[3, 10, 15-17]
	Stem cell organoid (LGR5+)	3D-embedded culture	[3, 10]

Table 1: Cellular and molecular techniques for three-dimensional culture
*Where possible, the original reference for the approach is included and is supplemented with additional recent references that highlight major technical advances. 3D, three-dimensional; iPS, induced pluripotent stem; LGR5, Leucine-rich repeat-containing G protein-coupled receptor 5.

Cell lines such as Caco2, derived from human colon carcinoma, have been extensively used for pharmacological and absorption studies, as they can be differentiated towards an enterocyte-like state [6-8]. Recently, stem cell organoid cultures derived from embryonic, pluripotent or intestinal adult stem cells have been reported. The adult stem cell intestinal organoid technique was developed by the Clevers group in 2009. Organoids are derived from intestinal crypts that contain the Lgr5-expressing stem cells and Paneth cells [9, 10]. In this thesis, we have used the adult stem cell-derived organoid *in vitro* model to study intestinal disease. However, the question that remains is how well these human organoids recapitulate the *in vivo* intestine. To answer this, we will evaluate different aspects of the organoids, such as culture conditions, the pure epithelial properties, functional properties and their role in complex intestinal diseases.

DO ORGANOIDS RECAPITULATE THE IN VIVO INTESTINE? CULTURE CONDITIONS

A good *in vitro* model needs to resemble the *in vivo* organ as much as possible. Essential for this is that culture conditions approximate the *in vivo* signals. The intestine is an organ with plasticity as stem cells specialize to certain cell types depending on the signals they receive. The crypts, containing the stem cells, are cultured in medium with several growth factors to maintain stemness. For example, Wnt and the Wnt-agonist R-spondin maintain crypt cells and the BMP-inhibitor Noggin inhibits differentiation. A small change in medium composition is already able to drive the cell fate to a different direction. In the human intestinal organoid model, one can drive stem cells into differentiation by withdrawal of Wnt, SB202190 and nicotinamide.[10] Furthermore, differentiation into purely enterocytes is achieved by adding extra compounds, such as valproic acid (VPA) and Wnt-inhibitor IWP-2 to the medium [18]. And incubation with RANKL will induce differentiation into M-cells, a cell-type that is normally only situated in the epithelial sheet overlaying Peyer's patches in the intestine [19].

Organoids are cultured in matrigel to provide them with an extracellular matrix, consisting of collagens and laminins that resemble the *in vivo* basal lamina. The extracellular matrix helps the epithelial cells to maintain their apical to basal cell polarity, both in matrigel or when cultured on transwells ([10, 20] and this thesis chapter 3 and 4), where the basolateral side is directed towards the matrigel. Overall, the culture conditions seem to reflect the *in vivo* situation, however, caution must be maintained, as the selected growth factors might not be sufficient for exact modeling of the *in vivo* intestine.
As the culture system relies on medium that comprises multiple growth factors, including several conditioned media, batches should be well monitored to achieve stable culture conditions.

ORGANOIDS: EPITHELIAL CELL CULTURES

While we are addressing the human organoids as a model for intestinal diseases, one has to bear in mind that the organoids are only in part representing the intestine. The adult stem cells in the crypt are epithelial cells, indicating that the organoid model system falls short on interactions with other cells such as fibroblasts, lymphocytes or glial cells. In complex intestinal diseases, such as inflammatory bowel disease, often multiple cell types are involved in the pathogenesis of the disease and therefore this disease might not be well represented in this model.

On the other hand, organoids provide an excellent model for intestinal diseases that are based on epithelial defects such as microvillus inclusion disease. The histological phenotype found in biopsies from patients with microvillus inclusion disease is retained in biopsy derived organoid cultures (chapter 3 and 4 of this thesis).

FUNCTIONAL PROPERTIES OF ORGANOIDS

Not only is the histological phenotype maintained in organoids, also the functional phenotype of intestinal organoids is preserved, as demonstrated in organoids derived from patients with cystic fibrosis (CF) in chapter 5. Intestinal organoids from CF patients show reduced organoid swelling in response to forskolin, which activates the CFTR channel through cAMP, compared to healthy controls. This indicates that CFTR function/dysfunction is still represented in these organoids.

In conclusion, intestinal organoids at least partially recapitulate the intestine of patients (this thesis), which has been confirmed by others as well [21]. As such, organoids are patient-specific *in vitro* models of disease, which is by far not achieved by *in vitro* colon cancer-derived cell models such as Caco2 cells.

COMPLEX INTESTINAL DISEASES

In complex intestinal diseases, where the pathogenesis is dependent on multiple cell types within the intestine, such as inflammatory bowel disease (IBD), the organoid *in vitro* model will not suffice to mimic all aspects of the disease. Nonetheless, organoids could be helpful to elucidate the role of the epithelium in these multifactorial diseases, since they enable the study of the epithelium of these diseased patients without interference from other non-epithelial cells.

In this thesis we used organoids from celiac patients and healthy controls to test our hypothesis that the differential expression of genes in biopsies of celiac patients are not intrinsically programmed in the epithelial cells (chapter 6). Similar studies could be performed for other multifactorial diseases, such as inflammatory bowel disease, to clarify the role of the epithelium in these diseases. In

addition, co-culture studies of organoids with fibroblast or lymphocytes could shed on light on their direct effect on the epithelium.

Beyond the use of organoids as an *in vitro* model of disease, they are also helpful to study healthy epithelial intestine. For this purpose organoids were used to identify if location-specific intestinal properties, such as bile acid uptake in ileum and iron uptake in duodenum, are imprinted in the epithelial stem cells (chapter 2). Understanding the healthy and diseased epithelium is necessary to advance our knowledge on pathogenesis of intestinal diseases.

APPLICATION OF ORGANOIDS

The value of organoids does not solely rely on recapitulating the diseased/healthy epithelial intestine to improve our comprehension of intestinal diseases. Additionally, this model could aid in diagnostics and therapy for patients suffering from intestinal diseases.

ORGANOIDS AS A PATIENT-SPECIFIC DISEASE MODEL FOR DIAGNOSTIC PURPOSES

To date, diagnosis of many intestinal diseases is often based on either the pathological analysis of biopsies or genetic make-up of the patient. For most diseases this suffices for an accurate diagnosis, nonetheless the measure of intestinal function or dysfunction is more difficult in this manner. Here organoids could assist in assessing patient-specific functional properties of epithelial cells, as is applied in cystic fibrosis patients (chapter 5). Patients with rare congenital enteropathies would also benefit from better functional studies, since the mutations found in for example myo5b are very heterogenous and could affect patients and thus treatment differently [22]. A mutation in a certain domain will have a different effect on the phenotype of microvillus inclusion disease patients, which is also evident in phenotypic analysis of two STX3-deficient patients (chapter 3).

In addition, organoids could play a role in improved diagnosis of rare congenital enteropathies. Intestinal biopsies are often difficult to obtain from these newborns, while correct diagnosis depends almost entirely on histology. If biopsies are unsatisfactory, endoscopy has to be repeated and accurate diagnosis, and therefore therapy might be delayed. Organoids provide almost unlimited material and could be used to understand diseases and determine multiple intestinal functions. Congenital enteropathies have been categorized in four groups: 1) defects in absorption or transport of nutrients and electrolytes; 2) defects in enterocyte differentiation and polarization; 3) defects in enteroendocrine differentiation; and 4) dysregulation of the intestinal immune response [23, 24]. It would be desirable to have a set of functional *in vitro* tests that could quickly identify the functional defects and determine the category of disease.
Furthermore, organoids could be used as a model for diagnosis and

even for testing tailor-made medicine, as is currently being done for patients with CF (chapter 5). Eventually, this could lead to an improved understanding of the pathogenic mechanism and, hopefully, patient-specific drug development.

THE ROLE OF ORGANOIDS IN TREATMENT STRATEGIES

Testing patient-specific drug response in organoids has already been shown for patients with cystic fibrosis (chapter 5 this thesis). Currently, this assay is used in clinical trials to assess if *in vitro* drug response is in concordance with the patient's response *in vivo*. Preliminary data show that a patient with a unique CFTR mutation responded well to the drug that showed the most optimal *in vitro* response (Dekkers ea, unpublished).
Taking into account that in some congenital enteropathies partial uptake of nutrients is possible, specific dietary conditions could also be tested *in vitro* and could help in development of a personalized diet.

Recently, Schwank et al. showed that it is possible to repair a single-gene mutation by CRISPR/CAS9 genome editing in organoids of a CFTR patient, resulting in full recovery of CFTR function [25, 26]. This opens up possibilities for gene editing in patients with single-gene diseases. However, the corrected cells still need to be delivered to the right location. In case of intestinal diseases, one would have to transplant gene-edited intestinal cells into the intestine of patients. The ability to repair the intestine and, possibly transplant the repaired intestinal cells into a patient sounds incredible. Although colon organoids were successfully transplanted in dextran sulfate sodium (DSS) induced colitis in mice, to date no successful method for transplanting the small intestine has been shown. Even if this will work in mice, it will be challenging to have everything approved for clinical practice and scaled up in such a way that the patient benefits. It was estimated that at least 20% of the intestinal surface should be replaced to become independent of total parental nutrition in microvillus inclusion disease. If you add up the cost, work and sensible outcome of transplanting organoids, currently the burden still outweighs the benefits and small intestinal transplantation is the preferred and only treatment option in case of failure of venal access for nutrition. An overview of possible applications of stem cells for clinical purposes is given in Figure 1 [1].

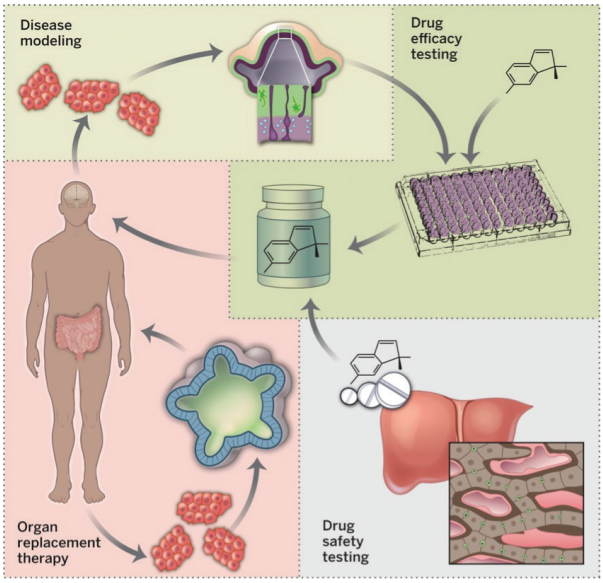

Figure 1.
Possible applications of organoids
(adapted from [1])

CONCLUSION

Organoid cultures at least partially represent the *in vivo* epithelium of a patient quite well, as shown in both functional and histological studies. In addition, mesenchymal or other cells present in a biopsy are not surviving in the epithelial culture conditions, therefore resulting in a simplified model of the intestine. As the culture system relies on medium that comprises multiple growth factors, including several conditioned media, media batches should be well monitored. Nonetheless, it is a useful tool to study intestinal diseases, improve diagnosis and eventually test various treatment regimes for patients suffering from intestinal diseases. Does this imply that we should make organoids of every patient with intestinal disease that visits the clinic? In my opinion, organoids should only be established from a select group of patients, since organoids remain an expensive and laborious *in vitro* model. However, patients with rare intestinal monogenetic traits, a pure epithelial defect and/or expensive, inefficient current treatments, such as is the case in patients with cystic fibrosis and congenital enteropathies, could benefit immensely from organoids as diagnostic or therapeutic tool.

1. Lancaster, M.A. and J.A. Knoblich, Organogenesis in a dish: modeling development and disease using organoid technologies. Science, 2014. 345(6194): p. 1247125.
2. Watson, C.L., et al., An in vivo model of human small intestine using pluripotent stem cells. Nat Med, 2014. 20(11): p. 1310-4.
3. Yui, S., et al., Functional engraftment of colon epithelium expanded in vitro from a single adult Lgr5(+) stem cell. Nat Med, 2012. 18(4): p. 618-23.
4. Browning, T.H. and J.S. Trier, Organ culture of mucosal biopsies of human small intestine. J Clin Invest, 1969. 48(8): p. 1423-32.
5. Shamir, E.R. and A.J. Ewald, Three-dimensional organotypic culture: experimental models of mammalian biology and disease. Nat Rev Mol Cell Biol, 2014. 15(10): p. 647-64.
6. Fogh, J.a.T., G., New human tumor cell lines. In Human Tumor Cells in vitro. 1975, New York: Plenum Publishing Corp.
7. Pinto, M.R.-L., S; Appay, M.D.; Kedinger, M.; Triadou, N; Dussaulx, E; Lacroix, B; Simon-Assmann, P; Haffen, K; Fogh, J. and Zweibaum A., Enterocyte-like differentiation and polarization of the human colon carcinoma cell line Caco-2 in culture. Biol. Cell, 1983. 47: p. 323-330.
8. Hidalgo, I.J., T.J. Raub, and R.T. Borchardt, Characterization of the human colon carcinoma cell line (Caco-2) as a model system for intestinal epithelial permeability. Gastroenterology, 1989. 96(3): p. 736-49.
9. Sato, T., et al., Single Lgr5 stem cells build crypt-villus structures in vitro without a mesenchymal niche. Nature, 2009. 459(7244): p. 262-5.
10. Sato, T., et al., Long-term expansion of epithelial organoids from human colon, adenoma, adenocarcinoma, and Barrett's epithelium. Gastroenterology, 2011. 141(5): p. 1762-72.
11. Jaffe, A.B., et al., Cdc42 controls spindle orientation to position the apical surface during epithelial morphogenesis. J Cell Biol, 2008. 183(4): p. 625-33.
12. Magudia, K., A. Lahoz, and A. Hall, K-Ras and B-Raf oncogenes inhibit colon epithelial polarity establishment through up-regulation of c-myc. J Cell Biol, 2012. 198(2): p. 185-94.
13. Sato, T., et al., Paneth cells constitute the niche for Lgr5 stem cells in intestinal crypts. Nature, 2011. 469(7330): p. 415-8.
14. Spence, J.R., et al., Directed differentiation of human pluripotent stem cells into intestinal tissue in vitro. Nature, 2011. 470(7332): p. 105-9.
15. Ootani, A., et al., Sustained in vitro intestinal epithelial culture within a Wnt-dependent stem cell niche. Nat Med, 2009. 15(6): p. 701-6.
16. Kovbasnjuk, O., et al., Human enteroids: preclinical models of non-inflammatory diarrhea. Stem Cell Res Ther, 2013. 4 Suppl 1: p. S3.
17. Li, X., et al., Oncogenic transformation of diverse gastrointestinal tissues in primary organoid culture. Nat Med, 2014. 20(7): p. 769-77.
18. Yin, X., et al., Niche-independent high-purity cultures of Lgr5+ intestinal stem cells and their progeny. Nat Methods, 2014. 11(1): p. 106-12.
19. de Lau, W., et al., Peyer's patch M cells derived from Lgr5(+) stem cells require SpiB and are induced by RankL in cultured "miniguts". Mol Cell Biol, 2012. 32(18): p. 3639-47.
20. VanDussen, K.L., et al., Development of an enhanced human gastrointestinal epithelial culture system to facilitate patient-based assays. Gut, 2014.
21. Bigorgne, A.E., et al., TTC7A mutations disrupt intestinal epithelial apicobasal polarity. J Clin Invest, 2014. 124(1): p. 328-37.
22. van der Velde, K.J., et al., An overview and online registry of microvillus inclusion disease patients and their MYO5B mutations. Hum Mutat, 2013. 34(12): p. 1597-605.
23. Berni Canani, R., et al., Congenital diarrheal disorders: improved understanding of gene defects is leading to advances in intestinal physiology and clinical management. J Pediatr Gastroenterol Nutr, 2010. 50(4): p. 360-6.
24. Terrin, G., et al., Congenital diarrheal disorders: an updated diagnostic approach. Int J Mol Sci, 2012. 13(4): p. 4168-85.
25. Schwank, G., et al., Functional repair of CFTR by CRISPR/Cas9 in intestinal stem cell organoids of cystic fibrosis patients. Cell Stem Cell, 2013. 13(6): p. 653-8.
26. Koo, B.K., et al., Controlled gene expression in primary Lgr5 organoid cultures. Nat Methods, 2012. 9(1): p. 81-3.

CHAPTER 8

SUMMARY / SAMENVATTING

DANKWOORD / ACKNOWLEDGEMENTS

CURRICULUM VITAE

LIST OF PUBLICATIONS

SUMMARY CHAPTER 1 - GENERAL INTRODUCTION

You are what you eat. A common saying that indicates that your physical or mental state can be influenced by your choice of food. Unfortunately, not all people have the luxury to choose what to eat; this can be related to place of birth, social, economic state, or the physical inability of the diseased intestine to take up certain food. A cell layer, the epithelium, covers the intestine, and harbors the main functions of the intestine: uptake, digestion of food, and a barrier against unwanted guests from outside the body. The intestinal epithelium consists of protrusions (villi) and invaginations (crypts) and all cells are renewed every four to five days. This renewal is possible because the stem cell, residing in the crypt, multiplies and produces all specialized epithelial cells. The group of Hans Clevers discovered a method to isolate these crypts, including the stem cells, and by adding growth factors, they were able to maintain these cells in a culture dish for weeks. These mini-intestines, which are grown in the lab, are called organoids and can be made from a small part (biopsy) of the intestine from a patient. The aim of this thesis was to make these organoids from patients with intestinal diseases, and to see if they recapitulate the patient's intestine and are a useful model for studying intestinal diseases.

Je bent wat je eet. Deze bekende uitspraak geeft aan dat je fysieke of mentale staat kan worden beïnvloed door je keuze van voedsel. Helaas heeft niet iedereen de luxe om te kiezen wat men wil eten vanwege geboorteplaats, sociale-, economische status, of door een darmziekte waardoor het fysiek onmogelijk is om bepaalde voedingsstoffen op te nemen of te verteren. De darm is bedekt door een cellaag, het epitheel, die de belangrijkste functies van de darm uitvoert zoals vertering en opname van voedsel. Ook beschermt deze darmlaag tegen ongewenste gasten van buitenaf. Darmepitheel bestaat uit uitstulpingen (villi) of instulpingen (crypten) en alle cellen worden bijna elke vier tot vijf dagen vernieuwd. Dit is mogelijk doordat de darmstamcel, die zich in de crypten bevindt, zich steeds blijft vermenigvuldigen en allerlei gespecialiseerde darmcellen kan maken. De groep van Hans Clevers heeft een methode ontdekt om deze crypten, die de stamcellen bevatten, weken lang te kunnen kweken in een plastic schaaltje in het lab. Dit kunnen ze doen doordat ze bepaalde groeifactoren aan de kweek toevoegen. Deze mini-darmpjes, ook wel organoids genoemd, kunnen worden gemaakt van een klein stukje darmweefsel (biopt) van patiënten. Het doel van dit proefschrift was om met behulp van deze methode mini-darmpjes van patiënten met verschillende darmziekten te maken, te bestuderen of dit de echte situatie nabootst, en dit te gebruiken als ziektemodel van de darm.

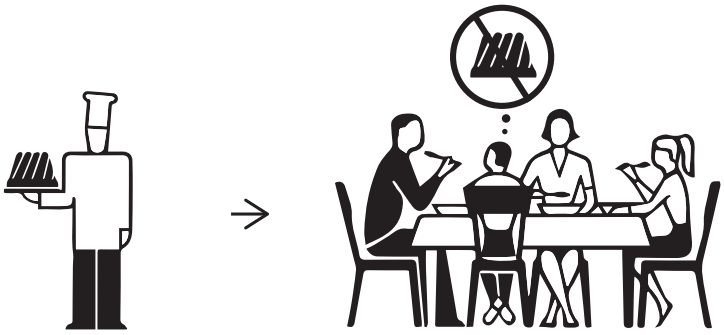

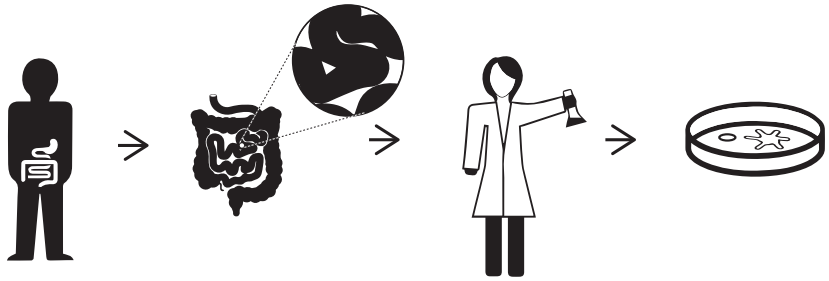

SUMMARY CHAPTER 2 – ADULT STEM CELLS IN THE SMALL INTESTINE ARE INTRINSICALLY PROGRAMMED WITH THEIR LOCATION-SPECIFIC FUNCTION

We first inspected the organoids in healthy intestines. The small intestine, which mainly digests and takes up nutrients, can be divided in three parts: the duodenum, the jejunum and the ileum. Each part has its own function such as; uptake of iron in the duodenum, milk in the jejunum, and bile acids/salts that help digestion in the intestine, are reabsorbed in the last part of the small intestine, the ileum, and returned to the liver. We were wondering if these functions are specific for the stem cell of each part, or if these functions were influenced by external factors such as the cells around the intestine. To answer this question we made organoids from these three different parts of the intestine, from both mice and human intestine, and studied if these functional properties were maintained over time (~10 weeks of culture). We noticed that organoids (containing the stem cells) from the duodenum remained specific for iron uptake and continued to be different from jejunal and ileal organoids. This confirms that each segment in the small intestine has its own specific stem cell that keeps its own functional properties.

Eerst hebben we gekeken naar gezonde organoids. De dunne darm, die met name voeding verteert en opneemt, kan opgedeeld worden in drie delen: het duodenum, het jejunum en het ileum. Elk deel heeft zijn eigen functie, zo wordt in het duodenum met name ijzer opgenomen, in het jejunum melk, en in het laatste stukje van de dunne darm, het ileum galzouten (die helpen bij het verteren van voedsel en die worden weer teruggegeven aan de lever). We vroegen ons af of deze functies intrinsiek zijn ingebed in de stam cel uit dit segment of dat deze functies aangestuurd worden door externe factoren zoals andere cellen rondom de darm. Om deze vraag te kunnen beantwoorden hebben we organoids gemaakt van alle drie de delen, van zowel muizen als mensen darm, en hebben we bekeken of deze eigenschappen nog steeds in de stamcellen zaten na deze ~10 weken te kweken in het lab. We zagen dat organoids uit het eerste deel van de dunne darm, het duodenum, nog steeds hun functie voor ijzeropname behielden en niet de functies van het jejunum of het ileum overnamen. Dit bevestigt dat elk deel van de dunne darm een eigen specifieke stamcel heeft, met zijn eigen functies.

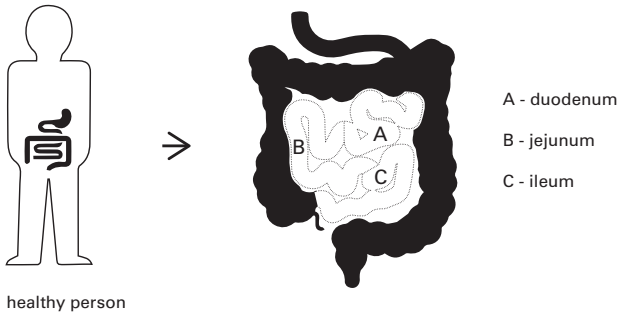
A - duodenum
B - jejunum
C - ileum
healthy person
B
A
C

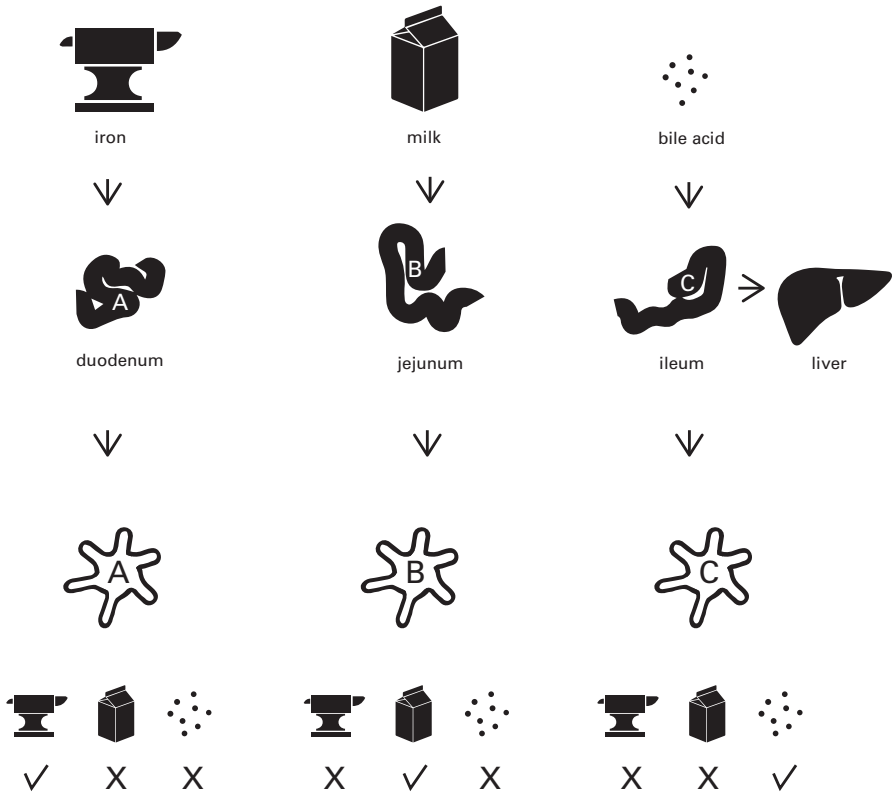
iron
milk
bile acid
A
B
C
duodenum
jejunum
ileum
liver
A
B
C
✓ X X
X ✓ X
X X ✓

SUMMARY CHAPTER 3 - LOSS OF SYNTAXIN 3 CAUSES VARIANT MICROVILLUS INCLUSION DISEASE

A severe, but rare, disease in which the intestine hardly functions at all is microvillus inclusion disease. This disease manifests itself in the first three months of life with diarrhea and total dependency on tube feeding. 90% of these children have a mutation in the *MYO5B* gene (part of the DNA). In this chapter we identified that a mutation in another gene Syntaxin 3 (*STX3*) also caused this disease. Two patients with microvillus inclusion disease had mutations in *STX3*, and cell lines, in which the same mutations were inserted, also showed the same diseased phenotype. Furthermore, organoids, made from the intestine of one of these patients, recapitulated the pathology that was present in patient's biopsies. This implies that organoids could be useful as a model to study this disease.

Een ernstige, maar zeldzame, ziekte waarbij de darm nauwelijks functioneert is microvillus inclusion disease. Deze ziekte presenteert zich in de eerste drie maanden van het leven met diarree en totale afhankelijkheid van voeding via een infuus. 90% van deze kinderen heeft een mutatie in het *MYO5B* gen (deel van het DNA). In dit hoofdstuk hebben wij een nieuwe mutatie ontdekt in een ander gen, Syntaxin 3 (*STX3*), die ook deze ziekte kan veroorzaken. Twee patiënten met microvillus inclusion disease hadden een mutatie in *STX3*, ook zagen we dat, als we dezelfde mutaties in een cellijn inbrachten, die cellen ook hetzelfde zieke fenotype lieten zien. Organoids gemaakt van de darm van één van deze patiënten lieten ook dezelfde afwijkingen zien als de darmbiopten. Kortom, organoids lijken een goed model te zijn om deze ziekte te kunnen bestuderen.

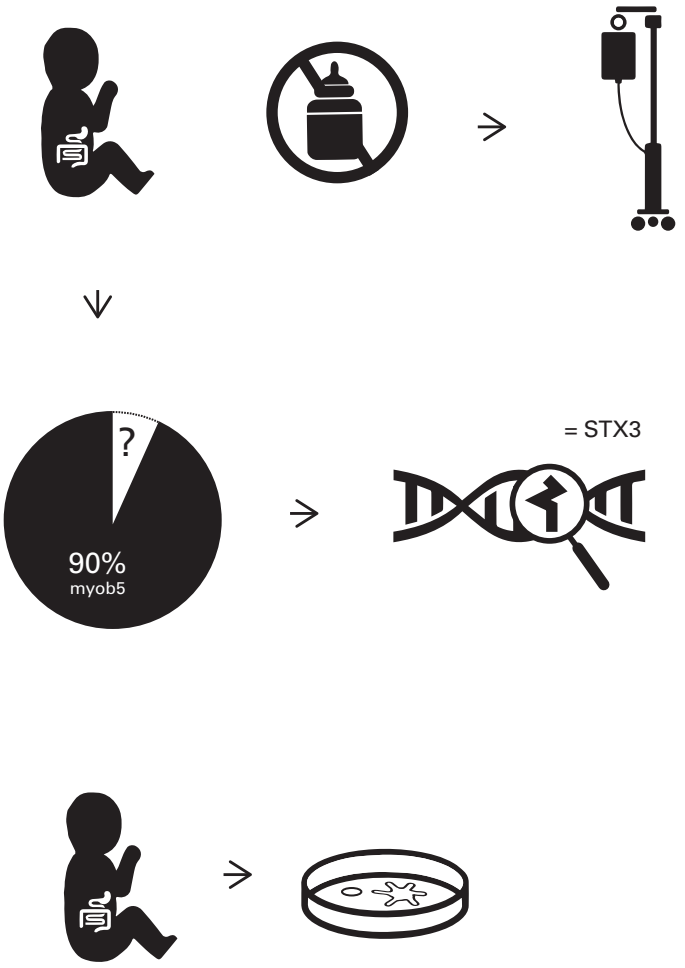
?
90%
myob5
= STX3

SUMMARY CHAPTER 4 - APICAL AND INTRACELLULAR TRAFFICKING PROTEINS ARE MISLOCALIZED IN ENTEROCYTES FROM SYNTAXIN 3-MUTANT PATIENTS WITH VARIANT MICROVILLUS INCLUSION DISEASE

In this chapter we looked more in depth at the function of Syntaxin 3, *STX3*, in patients with microvillus inclusion disease. In this disease one cell type in the intestine is especially affected: the enterocyte. This cell main function is to digest and take up nutrients with small hair-like protrusions on the villi, called microvilli. Uptake of nutrients is possible because there are enzymes/proteins located on the luminal side of the intestine on these microvilli. For example sugar can be digested by the enzyme sucrase-isomaltase (SI) on the apical (luminal) side of the cell and transferred to the blood on the basolateral side. We know these patients have difficulties in taking up food that is why they are dependent on tube feeding. STX3 is known for directing these enzymes/proteins to the membrane of the cell. We studied if these enzymes or proteins, in these *STX3* mutant patients, were still localized correctly. We noticed that in organoids and biopsies from these patients some apical proteins were maintained on the apical side, while others were mislocalized and accumulated just under the cell membrane. Other proteins, that were supposed to be on the basolateral side, remained at the right location in these patients.

In dit hoofdstuk hebben we meer in de diepte gekeken naar de functie van Syntaxin 3, *STX3*, in patiënten met microvillus inclusion disease. Bij deze ziekte is met name één type darmcel aangedaan: de enterocyt. De voornaamste functie van deze cel is vertering en opname van voeding in de darm door middel van kleine haarachtige uitstulpingen op de villi, ook wel microvilli genoemd. Opname van voedsel is mogelijk doordat er op deze microvilli eiwitten/enzymen zitten die contact maken met voedsel en dit kunnen opnemen in de cel. Zo wordt suiker klein geknipt door het enzym sucrase-isomaltase (SI) op de apicale (of luminale) zijde van de cel. De geknipte suiker wordt vervolgens opgenomen door andere eiwitten op de celmembraan en uiteindelijk doorgegeven aan het bloed via de basolaterale zijde. We weten dat deze patiënten moeite hebben met het verteren en opnamen van voedsel, dit is de reden dat ze voeding via een infuus krijgen. STX3 is bekend als een eiwit dat ervoor zorgt dat enzymen en eiwitten op de celmembraan terecht komen. We zagen dat in organoids en biopten van deze patiënten sommige apicale eiwitten op de goede plek zaten, terwijl andere ophoopten onder de celmembraan. Eiwitten die op de basolaterale zijde moesten zitten, zaten wel op de goede plek bij deze patiënten.

microvillus inclusion disease

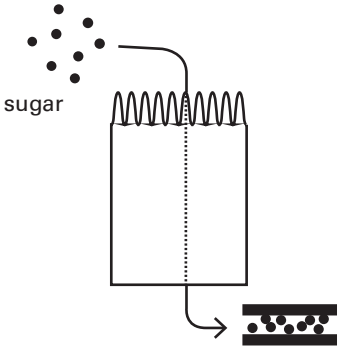

healthy situation

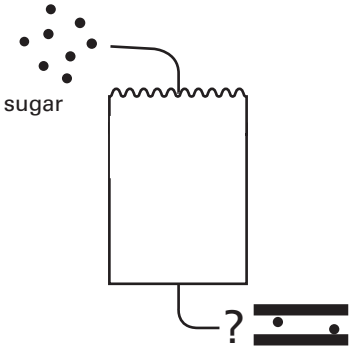

microvillus inclusion disease

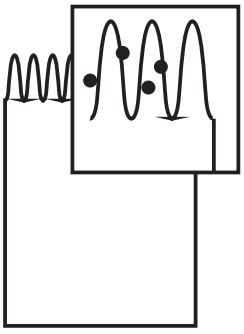

healthy situation

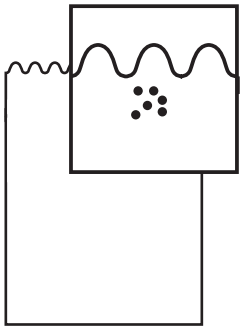

microvillus inclusion disease

SUMMARY CHAPTER 5 - A FUNCTIONAL CFTR ASSAY USING PRIMARY CYSTIC FIBROSIS INTESTINAL ORGANOIDS

Another rare disease is cystic fibrosis. In this disease mainly the lungs are affected, often in combination with the pancreas and the intestine. These organs are clogged with thick mucus, often accompanied by infections. The main cause of this disease is a mutation in the cystic fibrosis transmembrane conductance regulator (*CFTR*) gene, a chloride channel that moves water to the luminal side. In a healthy situation this channel helps in making a thin watery layer of mucus that protects organs from infections. In cystic fibrosis the mucus layer is thick instead of watery. If you add Forskolin, a drug that activates the CFTR channel, to organoids, water moves into the lumen, resulting in swelling of organoids. In organoids from a cystic fibrosis patient, CFTR does not function, therefore no swelling occurs. However, if you add Forskolin in combination with the right drug to an organoid of a cystic fibrosis patient, the CFTR channel will become activated and swelling will occur. The choice of drug and response to it varies per mutation and patient. The organoid model can help in predicting a patient-specific response to a drug by adding different drug combinations to the organoid, and observe if swelling occurs. As these drugs are very expensive and it usually takes weeks before we know if the medicine works in a patient, organoids could be a useful tool to select the right drug for each patient.

Een andere zeldzame ziekte is taaislijmziekte, ook wel cystic fibrosis genoemd. Bij deze ziekte zijn met name de longen aangedaan, vaak in combinatie met andere organen, zoals de alvleesklier en de darm. Deze organen raken verstopt door dik taai slijm en dit gaat vaak gepaard met ontsteking van deze weefsels. De oorzaak van deze ziekte is een mutatie in het cystic fibrosis transmembrane conductance regulator (*CFTR*) gen, een chloride kanaal dat water naar het lumen van organen beweegt. In een gezonde situatie zorgt dit kanaal ervoor dat er een dun waterig laagje slijm op de organen ligt die bescherming biedt tegen onstekingen. Bij taaislijmziekte is deze slijmlaag juist taai in plaats van waterig. Als je Forskolin, een stof die het CFTR kanaal activeert, aan de organoids toevoegt zie je bij gezonde organoids het lumen opzwellen. In organoids van een patiënt met taaislijmziekte, waarbij het CFTR kanaal het niet doet, zwelt het lumen niet. Echter als je, naast Forskolin, ook het goede medicijn toevoegt aan de organoids van een patiënt met taaislijmziekte kan er wel zwelling van de organoids ontstaan. Of een patiënt wel/niet reageert op bepaalde medicatie is afhankelijk van het type mutatie in het *CFTR* gen, dit kan per patiënt verschillen. Om te voorspellen welk medicijn wel of niet werkt kan een patiënt-specifieke organoid gestimuleerd worden met Forskolin en verschillende medicijn combinaties. De mate van zwelling geeft hier bij aan of het medicijn wel of niet aanslaat. Deze medicijnen zijn erg duur en het effect ervan in de patiënt is pas op lange termijn te beoordelen. Organoids zouden daarom een mooi model zijn om het gepaste medicijn te selecteren voor een patiënt.

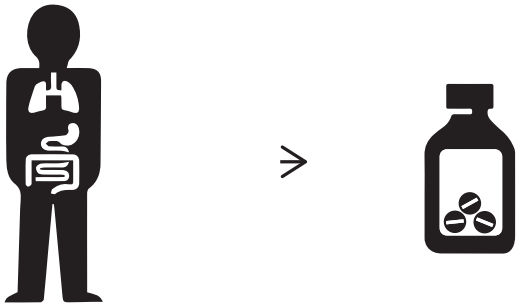

cystic fibrosis

medicine A or B?

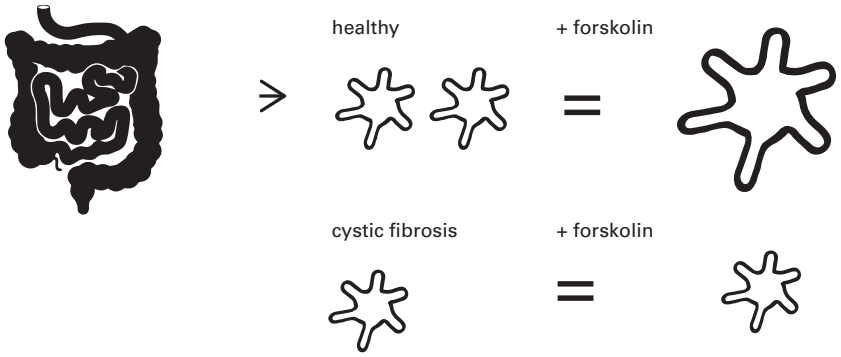

SUMMARY CHAPTER 6 - INTESTINAL EPITHELIUM IS NOT INTRINSICALLY AFFECTED IN PATIENTS WITH CELIAC DISEASE

There is a specific intestinal disease, celiac disease, where patients cannot eat a specific type of food such as: gluten. This protein is found in wheat, barley and rye. We know that a certain genetic make-up predisposes people for celiac disease, in combination with a gluten-containing diet, and causes immune cells to become active. The immune cells, located under the intestinal epithelium, make antibodies that damage the intestine. Although 30% of the population has this genetic make-up, only 1% is affected by gluten. That means additional factors play a role, one of these factors could be the intestinal epithelium. To dissect if the epithelium of celiac patients might be different from healthy intestines, we made organoids from both groups. In intestinal biopsies differences in expression of epithelial genes were seen. However, after a few weeks of culturing only the epithelium, organoids derived from healthy and celiac patients did not differ. Even after stimulating the organoids with a protein that induces inflammation in cells, both groups responded similarly. This implicates that the intestinal epithelium of celiac patients does not intrinsically differ from healthy controls.

Er is een specifieke darmziekte, coeliakie, waarbij patiënten met name een bepaald type voedsel niet goed kunnen verdragen: gluten. Dit eiwit zit in tarwe, gerst en rogge. We weten dat deze ziekte alleen voorkomt bij mensen met een bepaalde combinatie van genen die, samen met gluten, ervoor zorgen dat afweercellen geactiveerd worden. Deze afweercellen, die net onder het darmepitheel zitten, maken antistoffen die het darmepitheel beschadigen. Alhoewel deze genencombinatie bij 30% van de bevolking voorkomt, krijgt slechts 1% van de bevolking coeliakie. Dit betekent dat er meer factoren zijn die ervoor zorgen dat mensen coeliakie ontwikkelen, het darmepitheel zou hierbij een rol kunnen spelen. Om te onderzoeken of het darmepitheel van coeliakiepatiënten anders is dan dat van gezonde personen hebben wij van beide groepen organoids gemaakt. In darmbiopten zien we verschillen in expressie van bepaalde epitheelgenen. Echter, na het kweken van alleen het darmepitheel, zijn de organoids van patiënten en gezonde personen niet verschillend. Ook na stimulatie van de organoids met een eiwit dat celontsteking activeert, reageren beide groepen hetzelfde. Dit impliceert dat het darmepitheel van coeliakie patiënten niet intrinsiek anders is dan van gezonde personen.

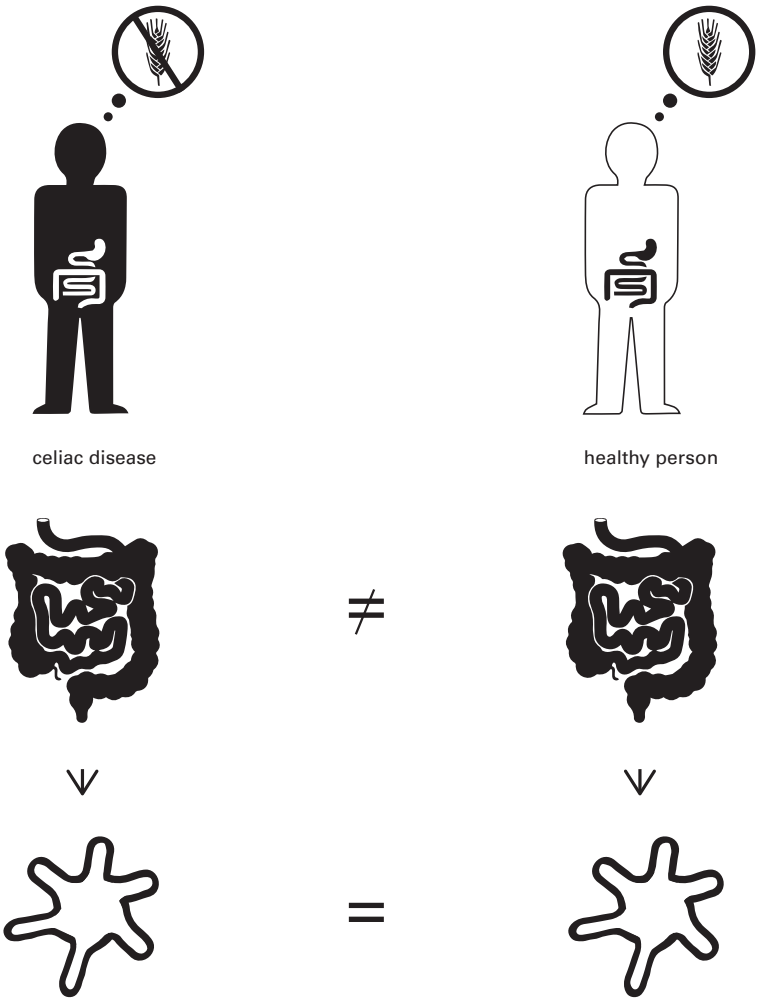
celiac disease
healthy person
≠
=

DANKWOORD

Wie is Carl Sagan? Misschien kent u hem, misschien niet, ik schaar mijzelf in ieder geval tot de laatste categorie. Toch kom ik zijn naam in verschillende proefschriften tegen, zelfs met verschillende quotes over de wetenschap in algemene zin. Ik veronderstel daarom dat hij vast een bekende mannelijke wetenschapper is. Dit kan ik alleen doen op basis van een aantal aannames: a) hij is hoogstwaarschijnlijk een man (vanwege zijn voornaam) b) hij doet uitspraken over de wetenschap en is daardoor mogelijk zelf een wetenschapper, en c) het feit dat hij in proefschriften wordt geciteerd betekend dat hij vast populair is. Toch wil ik een bevestiging hiervan en begin ik met een simpele search op Google met de zoekterm: “Carl Sagan”. Daarbij stuit ik op deze foto:

Subjectief gezien zou hij zowel een acteur van de serie Love Boat als een populaire wetenschapper kunnen zijn. Objectief zie ik een aantal andere dingen: dat er bij google ongeveer 12.800.000 resultaten verschijnen in slechts 0,29 seconden. Hij leefde van 1934 tot 1996; was astronoom en is drie keer gehuwd geweest. Zijn grootste wetenschappelijke bijdrage was het ontdekken dat de planeet Venus een temperatuur van 500 °C heeft. Hij is, echter, vooral bekend vanwege zijn zoektocht naar buitenaardse wezens. Voor zijn project SETI (Search for Extra-Terrestrial Intelligence) heeft hij 70 wetenschappers een petitie kunnen laten ondertekenen, waaronder 7 nobelprijs winnaars, die werd gepubliceerd in Science. Ook heeft hij de eerste boodschappen de ruimte in gestuurd die te begrijpen zouden zijn voor elke vorm van buitenaards leven. Zijn grote bekendheid heeft hij verworven door het televisieprogramma Cosmos, waarin hij in begrijpelijke taal allerlei dingen over het heelal uitlegde.

Nu neem ik aan dat mijn collega's hem niet direct van die tv-programma's kennen, gezien hun leeftijden. Mogelijk kennen ze hem nog van zijn science-fiction boeken. Alleen bij verder onderzoek zie ik dat hij ook makkelijk te vinden is bij Google met de termen "science" en "quote". De eerste site laat al snel vele uitspraken van Carl Sagan zien, tussen andere beroemdheden zoals Kant, Einstein en Hawking. De quotes van Carl Sagan variëren van "Absence of evidence is not evidence of absence" tot "If you wish to make an apple pie from scratch, you must first invent the universe." Na deze korte studie kunnen we concluderen dat hij inderdaad een bekende mannelijke wetenschapper is. Toch zijn er enkele kanttekeningen bij deze studie te plaatsen. De definities voor wetenschapper, bekend en man zijn niet goed uitgelegd. Als bronnen zijn met name Wikipedia en Google gebruikt. Bovendien belicht deze studie maar enkele kanten van Carl Sagan en is dus vrij summier.

Dit is onderzoek in een notendop. Je hebt een onderzoeksvraag, stelt een hypothese, onderzoekt met een bepaalde methode of dit klopt of niet. Hierna wordt een conclusie getrokken, de beperkingen van de studie besproken, besproken hoe deze bevindingen overeen komen/tegenstrijdig zijn met de huidige literatuur. Soms worden er dan nog suggesties gegeven voor aanvullend onderzoek dat in de toekomst gedaan zou kunnen worden. Simpel zou je zeggen, alleen dan moet je nog proberen dit onderzoek in een goed blad te kunnen publiceren. Dit is het moment dat het echt moeilijk wordt, zeker voor dit stuk omdat er geen nieuwe bevindingen zijn. Dit betekent dat dit onderzoek buiten de scoop van bijna alle bladen valt. Heel misschien valt het nog te publiceren in een studentenblaadje of de buurtkrant, maar om te voorkomen dat dit stuk echt in de prullenbak belandt, publiceer ik het voor de zekerheid maar zelf, in mijn eigen proefschrift.

Dat dit proefschrift hopelijk van iets meer kwaliteit is dan bovenstaande studie, heb ik gelukkig te danken aan heel veel andere mensen die ik bij deze graag zou willen bedanken.

Dat ik niet een heel hoofdstuk heb gewijd aan Carl Sagan heb ik onder andere te danken aan mijn promotor Edward Nieuwenhuis. Edward, dank je voor het helpen met de focus in mijn PhD. Ik kon rustig met vijf ideeën bij jou naar binnen lopen en weer met één naar buiten gaan. Ik heb vooral geleerd van jou dat je beter iets kleins heel goed kan uitzoeken dan iets groots half, de basis van goed onderzoek. Wat was het fijn om af en toe uit te kunnen zoomen van het onderzoek, kleine tegenvallers te kunnen relativeren, en daarnaast ook andere dingen dan werk te kunnen bespreken. Hopelijk zien we elkaar in Colombia en kunnen we in de toekomst nog eens samenwerken.

Behalve de grote lijnen, heb je ook iemand nodig die de kleine lijnen bewaakt en zorgt dat je de juiste controles meeneemt zoals Sabine Middendorp, mijn co-promotor. Sabine van jou heb ik met name de praktische kant van het onderzoek geleerd. Het zal vast niet altijd

makkelijk voor je geweest zijn om een arts in te moeten wijden in de wetenschap. Vanaf de eerste week heb ik al op het lab mogen staan en daar ben ik je zeer dankbaar voor. Door verschillende technieken te leren kon ik een beter beeld krijgen van de mogelijkheden en alles was ook mogelijk. Elk voorstel kon worden uitgevoerd, met vaak de nodige fouten, maar dat was misschien wel de beste manier om het te leren. Je hebt me veel vrijheid en zelfstandigheid gegeven en je was altijd bereikbaar voor overleg. Dank ook voor het doorploegen van teksten in de laatste fase. Ik ben heel benieuwd naar het verdere onderzoek wat jullie gaan doen.

Daarnaast wil ik de mensen in mijn begeleidingscommissie bedanken voor hun input in de laatste fase van mijn PhD: Roderick Houwen, Marianne Boes en Joost Frenkel. Roderick, dankzij jouw contacten is het STX3 stuk zo mooi geworden. Je was altijd betrokken door kritisch mee te denken over het onderzoek. Je bent *to the point* en dat is prettig om mee te werken. Marianne en Joost ook jullie brachten het onderzoek steeds terug naar de vraagstelling en dachten kritisch mee over wat wel of niet relevant zou zijn voor de stukken in de resterende tijd. Ontzettend leuk dat jullie in mijn commissie willen deelnemen.

Ook in de commissie, Berent Prakken. De rust die jij uitstraalt en de helderheid waarmee je onderzoek vertaalt vanuit de bench naar bedside zijn inspirerend. Ik zal niet vergeten om in de toekomst ook vraagstellingen vanuit patiëntengroepen mee te nemen bij het opzetten van onderzoek. Prof. Dr. P.D. Siersema, dank voor het kritisch lezen van mijn proefschrift, dankzij uw afdeling heb ik ook vele volwassen patienten van de MDL kunnen includeren. Prof. Dr. J.T.A. Knape dank voor het willen voorzitten van mijn promotie.

Hankje, dank voor je betrokkenheid bij mijn onderzoek. Jij belde/mailde mij bij elke mogelijke patiënt en alles was altijd goed geregeld in Rotterdam. Ook dankzij jouw inzet hebben we de STX3 stukken kunnen doen. Leuk om naast Edward, ook jou te leren kennen en geweldig dat je straks als professor bij mijn verdediging aanwezig bent.

Frits Koning, heel veel dank voor jouw adviezen omtrent coeliakie onderzoek. Dat het epitheel geen rol speelt in coeliakie voorspelde jij al vanaf het eerste moment. Ik zal de TCR ontwikkelingen in coeliakie in de gaten blijven houden.

Dear Thomas Müller, it has been an honor to work with you, the great Myo5b man, and your group, on STX3. Thank you for coming all the way to the Netherlands for my defense, I promise there will be a good party afterwards.

Hans Clevers, dank je voor jouw ondersteuning en die van de rest van je groep bij al het organoidwerk. Dankzij jullie hulp konden wij ook met deze techniek werken en heb ik wekelijks de kans gehad om

top-science van dichtbij te zien. Everybody from the Hubrecht group thank you for four years of inspiration, input, help and hard-core science including Rob, Mark, Wim, Stieneke, Joyce, Karin, Henner, Gerald, Sina, Valentina and everyone else.

Valentina and Ruben it was great to be able to work together, I wish the best for both of you in, respectively, the editor and the epigenetics field. Desiree dank voor je bijdrage aan STX3 en gezellige koffies. Amani dank voor al je coeliakiekennis, vriendschap en oprechtheid. Fantastisch dat je nu in opleiding bent, hopelijk worden we in de toekomst weer collega's. De afdeling metabole diagnostiek voor hun gastvrijheid om daar de disaccharidase assay te leren, in het bijzonder veel dank aan Nanda Verhoeven, Mirjam van Aalderen en Ans Geboers.

Dan wil ik met name alle patiënten en families bedanken die mee hebben gewerkt aan dit onderzoek, zonder jullie vertrouwen en deelname was dit proefschrift niet mogelijk geweest.

Ook veel dank aan alle kindergastroenterologen die geholpen hebben bij inclusie en biopten in het WKZ: Roderick, Victorien, Freddy, Sarah, Janneke, Anemone, Cathelijne en Renske. Behalve jullie hulp bij inclusies was het erg leuk om iets mee te krijgen van jullie mooie vak, praktische inzichten en humor. Graag wil ik ook alle anesthesisten, OK-personeel en assistenten bedanken voor hun hulp en goede sfeer. Ik ben alle gastroenterologen van het UMC dankbaar voor het kunnen includeren en biopteren van hun patiënten voor het onderzoek, in het bijzonder Herma Fidder, Bas Oldenburg, Karel van Erpecum, de hele dagbehandeling, Janneke ten Brink en de secretaresses die altijd hielpen met inclusie en bloedafnames. Beth en Petra dank voor alle hulp bij METC-amendementen en contracten.

Ook ben ik de kindergastroenterologen en onderzoeksmensen uit andere ziekenhuizen dankbaar die mee hielpen met het materiaal of uitbreiden van de STEM-studie, in het bijzonder: Henkjan Verkade, Edmond Rings, Els Roelofs, Marc Benninga, Merit Tabbers, Luisa Mearin, Yvonne Wijkhuizen, Barbara de Koning, Jessie Hulst, Barbara Sibbles, Katharina Biermann en Merel van Pieterson.

Dear Rüdiger Adam thank you for your hospitality and quick communication about the patient in Mannheim.

Dank ook aan alle overige co-authors voor hun bijdrage bij de stukken. Daarnaast ben ik de rest van de Nieuwenhuisgroep dankbaar voor alle wetenschappelijke input en gezelligheid. Kerstin, trouwe maat, wat had ik toch zonder jou gemoeten. Ik heb veel van je geleerd als wetenschapper, maar ben vooral blij dat ik een dierbare vriendin erbij heb gekregen. Wat een feest dat wij samen, zij aan zij, deze drei+een jaar konden beleven: successen, failures, koffies, samenwerken, burgers eten, yoga (in die volgorde), reisverhalen, Vancouver, Berlijn en als hoogtepunt onze Husky-tour. We hebben

nog heel veel samen te beleven, wie weet is onze volgende trip in Colombia. Ik ben heel benieuwd naar je volgende stap. Michal, thanks for your positive and relaxed view on everything and your great sense of humor. Sylvia, de rechtvaardige gangmaker en doe-het-zelver, ontzettend fijn dat ik tenminste 3 jaar met je heb kunnen samenwerken (en dansen). Simone, Hans en Anke van jullie alledrie heb ik het belang van precisie geleerd, alledrie een andere aanpak, maar jullie waren altijd bereid om mee te denken en geduld op te brengen voor iemand die het liefst snel resultaat heeft. Ook was het fijn om na 2 jaar enkele dokters in de groep te krijgen en niet zomaar dokters maar leading ladies: Sabine F, Caroline en Janneke. Sabine, dank voor je onuitputtelijke enthousiasme, je bent een mooi voorbeeld van iemand die alles kan combineren met een glimlach en hart voor de zaak heeft, heel inspirerend. Caroline, jij stond altijd klaar om bij te springen, zelfs in een kerstweekend voor Wnt maken, terwijl je al druk genoeg was, dank daarvoor. Janneke, wat leuk om met jou samen te werken en zelfs varkensorganoids te maken. Ik wens je veel succes in Eindhoven en dank voor al je steun gedurende mijn PhD en etentjes in Jerusalem. Claartje, de efficiënte onderzoekster en dokter, hopelijk worden we nog collega's in de toekomst. Jorik, dank voor het overnemen van onze projecten, heel veel succes de komende tijd. Ook studenten: Charlotte, dank voor al je hulp bij het IBD project, je inzet, inzicht en spontaniteit. Imre, Layla, Delia, Ronald, Tim, Sin, Lotte, Susanne en overige studenten in het lab, jullie zijn de jonge wetenschappers die ons scherp en enthousiast houden. Susanna dank voor het regelen van alle afspraken en extra zaken rondom de PhD en heel veel succes bij je nieuwe baan.

Niet alleen je directe groep maar ook de grotere groep, eerst CMCI, later LTI, helpen je verder in het onderzoek en voegen vooral veel toe met sparren over allerlei andere dingen dan onderzoek. De Boesers: Ewoud, Thijs, Robert, Arjan S, Annick, Friederike, Lotte en Willemijn. Dank voor alle nespressotalks, gitaarles, (soms ongevraagde) adviezen, hulp, gezelligheid, sticky toffee cakes, koe-bel concerten, Gent en Israel trips. Helmut Trekking en Willy succes met de laatste loodjes, ik kijk uit naar jullie promoties. U-dancers: Maud, Colin, Nina, na de verhuizing kwamen jullie gelukkig toch nog af en toe voor een borrel langs. Maud dank ook voor je FACS tips. Prakkers: Evelien, Theo, Femke, Gerdien, Genoveva, Arjan B, Judith, Sytze, Nienke, Alessandra, Felicitas, Annemieke, Lieke, Ellen, Yvonne, Henk, Bas, Maja, David en Marloes. Dank voor alle leuke borrels, etentjes en pubquizen. De spills van het lab: Lieneke, Rianne, Sigrid, Jenny en Mark. Dank voor alle organisatie zodat het lab goed loopt, jullie hulp en organisatie van goede voetbalgames, etentjes, Derk-dansjes, scherpe humor en relativeringsvermogen. Barbara and Sjors thanks for keeping up the histolab. De Beekmangroep: Jeffrey, Florijn, Dominique, Annelotte, Jennifer, Lodewijk en Evelien, het was fijn om met jullie te kunnen sparren over organoids en letterlijk hulp in nood te krijgen bij het zoveelste mediumprobleem. Florijn en Jeff, dank dat ik mee kon werken aan een mooi stuk met CF organoids, hier heb ik veel van geleerd. Een PhD is niks zonder gezellige kamergenoten:

flexers, Kerstin, Sylvia, Gerdien, Evelien, Willemijn, Sanne, Annemieke, Sandra, Luuk, Florijn, Nadia, Elena, Chiara, Pieter. En nog meer mensen uit andere groepen die wetenschappelijk input of gezelligheid gaven: Kim, Alsya, Tessa, Emmerik, Rina, Sarita, Jorg, Saskia, Yvonne, Erica, Angela, Julia, Hilde, Michiel, Nienke en nog vele anderen van het CMCI en LTI. Ook zijn er mensen die je op late uren inspireren, Achmed, heel veel dank voor alle gesprekken over politiek, Egypte, je kinderen, je bent voor mij een groot voorbeeld die door hard werken zich inzet voor de volgende generatie. Ik weet zeker dat je kinderen een fantastische toekomst dankzij jou krijgen en dat er vast een mooie nieuwe banenkans in het verschiet ligt. Bade, succes met alle drukte thuis en dank voor mijn schone kamer, lab en aanspraak in de avond.

Verder wil ik ook de mensen bedanken voor andere samenwerkingen die niet in dit boekje voorkomen: Carolijn voor het IBD project, Wentao en Peter voor de aanraking met varken en kat organoids.

In addition I would like to thank everybody from the Grand lab for making me enthusiastic about basic science in the first place. De kinderartsen en collega's van Tergooiziekenhuizen voor het mij enthousiasmeren voor het vak kindergeneeskunde. Clairetje, wat een feest dat je mee wilt buigen als paranimf op de dag van mijn promotie. Naast studiematen, oud-collega's, jaargenoot, ben je vooral een heel goede vriendin die ik graag naast me zie staan bij dit moment.

Overigens ben ik mijn andere vrienden die alles goed te weten relativeren en klaar stonden buiten werktijden voor leuke dingen ook dankbaar: Eddy, Emma, Linde, Lieke, Laura, Soof, Jos, Claar, Frederique, Rosanne, Mariette, Neel, Maria, Claire L, Claire S, Klaus & co. Ook mijn medische familie Sophie, Melanie en Maarten die altijd geinteresseerd bleven ondanks specialistische termen.

Lieve familie, pappa, mamma, Nils, Lisa, Roland, Nina, lieve Marie, maar ook mijn schoonfamilie, Kees, Monika en Niels dank dat jullie altijd voor mij klaar stonden en voor alle mooie momenten met jullie de afgelopen jaren, waarbij de komst van Marie toch wel een van de hoogtepunten was.

Lieve Sven, dank voor je hulp bij het mooi maken van dit boekje, je liefde en al je vrolijkheid. Elke dag is weer een feest met jou en ik kijk heel erg uit naar ons buitenland avontuur met zijn tweeën.

LIST OF PUBLICATIONS

Wiegerinck CL*, Janecke AR*, Schneeberger K*, Vogel GF*, van Haaften-Visser DY*, Escher JC, Adam R, Thöni CE, Pfaller K, Jordan AJ, Weis CA, Nijman IJ, Monroe GR, van Hasselt PM, Cutz E, Klumperman J, Clevers H, Nieuwenhuis EE, Houwen RH, van Haaften G, Hess MW^, Huber LA^, Stapelbroek JM^, Müller T^, Middendorp S^. Loss of syntaxin 3 causes variant microvillus inclusion disease. Gastroenterology. 2014 Jul;147(1):65-68.e10. Note: * & ^ Authors share authorship.

Middendorp S, Schneeberger K*, Wiegerinck CL*, Mokry M, Akkerman RD, van Wijngaarden S, Clevers H, Nieuwenhuis EE. Adult stem cells in the small intestine are intrinsically programmed with their location-specific function. Stem Cells. 2014 May;32(5):1083-91. Note:* Authors share authorship.

Mokry M, Middendorp S, Wiegerinck CL, Witte M, Teunissen H, Meddens CA, Cuppen E, Clevers H, Nieuwenhuis EE. Many inflammatory bowel disease risk loci include regions that regulate gene expression in immune cells and the intestinal epithelium. Gastroenterology. 2014 Apr;146(4):1040-7.

Dekkers JF, Wiegerinck CL, de Jonge HR, Bronsveld I, Janssens HM, de Winter-de Groot KM, Brandsma AM, de Jong NW, Bijvelds MJ, Scholte BJ, Nieuwenhuis EE, van den Brink S, Clevers H, van der Ent CK, Middendorp S, Beekman JM. A functional CFTR assay using primary cystic fibrosis intestinal organoids. Nature Medicine. 2013 Jul;19(7):939-45.

Wiegerinck CL, Lasham CA, Straver B. Klinisch redeneren in de praktijk: Een puber met pijn op de borst. Praktische pediatrie. Volume 3, Hematologie, August 2011. Dutch

SUBMITTED/IN PREPARATION

Wiegerinck CL, Schneeberger K, van Vugt AHM, van Rijn JM, van Aalderen M, Verhoeven-Duif NM, Adam R, Marx A, Biermann K, Escher JC, Nieuwenhuis EES, Middendorp S. Apical and intracellular trafficking proteins are mislocalized in enterocytes from syntaxin 3-mutant patients with variant microvillus inclusion disease. Manuscript in preparation.

Wiegerinck CL, Mokry M, Mubarak A, Groeneveld M, de J. Golio DM, Houwen RHJ, Nieuwenhuis EES, Middendorp S. Intestinal epithelium is not intrinsically affected in patients with celiac disease. Submitted

CURRICULUM VITAE

Caroline Louise Wiegerinck
born on 28 August 1984, Utrecht, the Netherlands

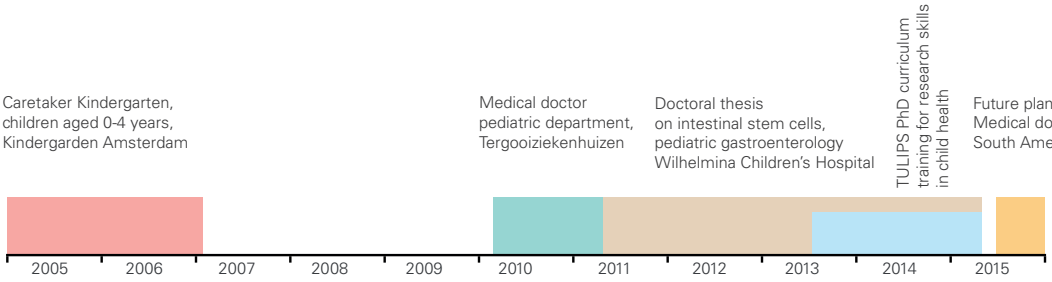

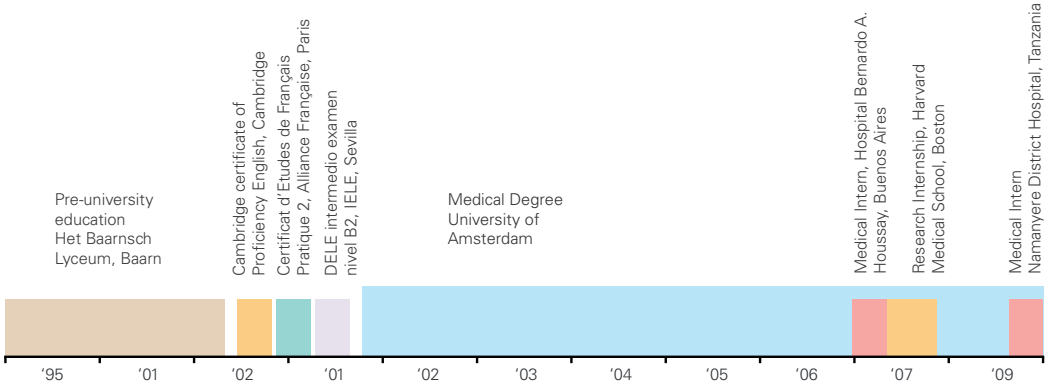

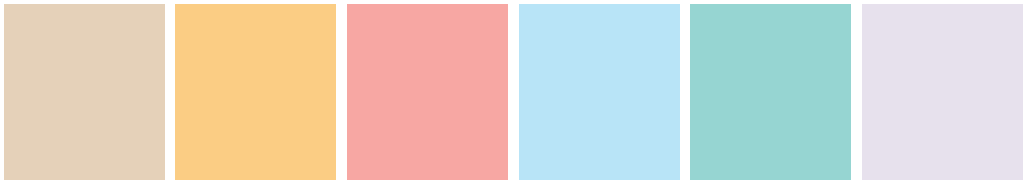

HUMAN ORGANOIDS: A MODEL SYSTEM FOR INTESTINAL DISEASES.

18 juni 2015

ISBN: 978-90-393-6368-3

Grafisch ontwerp/Graphic design:
Sven Hoogerheide

Drukwerk/Print:
CPI Wöhrmann

Uitgever/Publisher:
Universiteit Utrecht

Deze publicatie is mogelijk gemaakt door / This publication is made possible by: